LEVEL (2)

AFWAL-TR-80-2092
ESL-TR-80-46
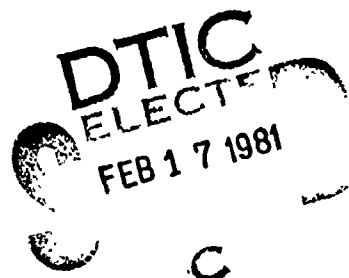
AD A095057

EVALUATION OF FUEL CHARACTER EFFECTS ON J79 SMOKELESS COMBUSTOR

GENERAL ELECTRIC COMPANY
AIRCRAFT ENGINE BUSINESS GROUP
TECHNOLOGY PROGRAMS AND
PERFORMANCE TECHNOLOGY DEPARTMENT
CINCINNATI, OHIO 45215

November 1980

DTIC
ELECT
FEB 1 7 1981

C

TECHNICAL REPORT AFWAL-TR-80-2092, ESL-TR-80-46

Final Report for Period July 1979 - June 1980

Approved for public release; distribution unlimited.

AERO PROPULSION LABORATORY
AIR FORCE WRIGHT AERONAUTICAL LABORATORIES
AIR FORCE SYSTEMS COMMAND
WRIGHT-PATTERSON AIR FORCE BASE, OHIO 45433

81 2 17 041

JEFFREY S. STUTRUD
Fuels Branch
Fuels and Lubrication Division

ARTHUR V. CHURCHILL
Chief, Fuels Branch
Fuels and Lubrication Division

FOR THE COMMANDER

ROBERT D. SHERRILL, Chief
Fuels and Lubrication Division
Aero Propulsion Laboratory

REPORT DOCUMENTATION PAGE

READ INSTRUCTIONS
BEFORE COMPLETING FORM

1. REPORT NUMBER AFWAL-TR-80-2092, ESL-TR-80-46	2. GOVT ACCESSION NO. AD-A095057	3. RECIPIENT'S CATALOG NUMBER

4. TITLE (and Subtitle)

EVALUATION OF FUEL CHARACTER EFFECTS ON J79 SMOKELESS COMBUSTOR

5. TYPE OF REPORT & PERIOD COVERED

Final Technical Report
7/1/79 through 6/1/80

6. PERFORMING ORG. REPORT NUMBER

R80AEG618

7. AUTHOR(s)

C.C. Gleason, T.L. Oller, M.W. Shayeson and M.J. Kenworthy

8. CONTRACT OR GRANT NUMBER(s)

F33615-79-C-2033

9. PERFORMING ORGANIZATION NAME AND ADDRESS

General Electric Company
Aircraft Engine Group
Cincinnati, Ohio 45215

10. PROGRAM ELEMENT, PROJECT, TASK AREA & WORK UNIT NUMBERS

62203F
3048-05-98

11. CONTROLLING OFFICE NAME AND ADDRESS

Aero Propulsion Laboratory (AFWAL/POSF)
Air Force Wright Aeronautical Laboratories (AFSC)
Wright-Patterson AFB, Ohio 45433

12. REPORT DATE

November 1980

13. NUMBER OF PAGES

178

14. MONITORING AGENCY NAME & ADDRESS(if different from Controlling Office)

15. SECURITY CLASS. (of this report)

Unclassified

15a. DECLASSIFICATION/DOWNGRADING SCHEDULE

16. DISTRIBUTION STATEMENT (of this Report)

Approved for public release; distribution unlimited.

17. DISTRIBUTION STATEMENT (of the abstract entered in Block 20, if different from Report)

18. SUPPLEMENTARY NOTES

Partial funding and technical support in the area of the measurement and analysis of gaseous emissions and smoke data were provided by the Environmental Sciences Branch of the Environics Division in the Research and Development Directorate of HQ Air Force Engineering and Services Center.

19. KEY WORDS (Continue on reverse side if necessary and identify by block number)

Fuels
Alternate Fuels
Gas Turbine Combustion
Exhaust Emissions

J79 Engine Combustor

20. ABSTRACT (Continue on reverse side if necessary and identify by block number)

Results of a program to determine the effects of broad variations in fuel properties on the performance, emissions, and durability of the J79-17C turbojet engine combustion system are presented. Thirteen different fuels were tested, covering a range of hydrogen contents, aromatic types, boiling ranges, and viscosities.

DD FORM 1473 EDITION OF 1 NOV 65 IS OBSOLETE
1 JAN 73

Block 20 (Continued)

At high power operating conditions, fuel hydrogen content was found to be a very significant fuel property with respect to liner temperature, flame radiation, smoke, and NO_x emission levels.

At idle and cruise operating conditions, CO and HC emission levels were found to be dependent on both fuel hydrogen content and relative spray droplet size.

At cold day ground start conditions lightoff correlated with the relative fuel droplet size.

Altitude relight limits at low flight Mach numbers were fuel dependent and also correlated with the relative fuel droplet size.

Combustor liner life analyses, based on the test data, yielded relative life predictions of 1.00, 0.93, 0.83, and 0.73 for fuel hydrogen contents of 14.5, 14.0, 13.0, and 12.0 percent, respectively.

High temperature cyclic fuel nozzle fouling tests revealed significant effects of fuel quality and operating temperature on nozzle life. The results correlated with laboratory thermal stability ratings of the fuels.

PREFACE

iii

TABLE OF CONTENTS

TABLE CF CONTENTS (Concluded)

LIST OF ILLUSTRATIONS

LIST OF ILLUSTRATIONS (Continued)

LIST OF ILLUSTRATIONS (Continued)

LIST OF ILLUSTRATIONS (Concluded)

LIST OF TABLES

LIST OF TABLES (Continued)

LIST OF TABLES (Concluded)

NOMENCLATURE

Symbol		Units
A	Area	cm^2, mm^2
CO	Carbon monoxide	---
CO_2	Carbon dioxide	---
CWALF	Clockwise aft looking forward	---
EI	Pollutant emission index	g pollutant/kg fuel
H	Fuel hydrogen content (mass fraction)	%
HC	Hydrocarbon (calculated as CH_4)	---
N	Fuel naphthalene content (volume fraction)	%
JFTOT	Jet Fuel Thermal Oxidation Tester	---
NO_x	Total oxides of nitrogen ($=NO+NO_2$, calculated as NO_2)	---
Q	Heat of combustion (net)	MJ/kg
S	Combustor operating severity parameter	---
SMD	Sauter mean diameter	---
SN	Smoke number (by ARP #1256)	---
T	Temperature	K
V	Velocity	m/s
W	Mass flow rate	g/s, kg/s
X	Exhaust gas pollutant concentration	mg pollutant/kg air
b	Curve fit equation intercept	---
f	Fuel/air ratio	g fuel/kg air
h	Absolute humidity	g H20/kg air
k	Arbitrary constant	---

NOMENCLATURE (Concluded)

Symbol		Units
m	Curve fit equation slope	---
n	Hydrogen-to-carbon atom ratio	---
$\dot{q}$	Heat flux	kW/m^2
r	Curve fit correlation coefficient	---
x	Independent variable	---
y	Dependent variable	---
ΔP	Pressure drop	mPa
ΔT	Temperature rise	K
η	Combustion efficiency	%
ν	Kinematic viscosity	mm^2/s
ρ	Density	kg/m^3
σ	Surface tension	mN/m
$\phi(f)$	Fuel/air ratio function (Figure 35)	

Subscripts

3	Compressor exit station (Combustor inlet)
4	Combustor exit station
8	Engine exit station
c	Combustor
e	Effective
f	Fuel
m	Metered
r	Reference
st	Stoichiometric
L	Liner (metal)
gs	Gas sample
TC	Thermal (Thermocouple)
s	Sample
avg	Average
max	Maximum
OGV	Compressor outlet guide vane
TND	Turbine nozzle diaphragm

SECTION I

SUMMARY

The purpose of this program was to determine by combustor rig tests and
data analyses, the effects of fuel property variations on the performance, ex-
haust emission and durability characteristics of the General Electric J79-17C
(low smoke, long life) engine combustion system, and compare the results to
those previously obtained in similar tests of the J79-17A (in use, high smoke)
and F101 (advanced low smoke) combustion systems. Thirteen refined and
blended fuels, which incorporated systematic variations in hydrogen content
(11.9 to 14.5 weight percent) aromatic type (monocyclic or dicyclic), initial
boiling point (298 to 409 K by gas chromatograph), final boiling point (554 to
646 K also by gas chromatograph), kinematic viscosity (0.90 to 3.27 mm^2/s at
294.3 K) and thermal stability breakpoint (518 to 598 K by JFTOT), were eval-
uated in: (a) 14 high pressure/temperature combustor performance/emissions/
durability tests; (b) 14 low pressure/temperature combustor cold-day ground
start/altitude relight tests; and, (c) 7 high temperature cyclic fuel nozzle
fouling tests.

At high engine power operating conditions, (takeoff and supersonic dash),
fuel hydrogen content was found to be a very significant fuel property with
respect to smoke, oxides of nitrogen (NO_x), liner temperature, and flame radia-
tion levels. Each of these parameters increased with decreasing fuel hydrogen
content. Dicyclic aromatics tended to cause somewhat higher smoke levels, but
no other discernable effect of any other fuel property was found. Carbon
monoxide (CO) and unburned hydrocarbon (HC) emission levels were so low at
these operating conditions that no trend with fuel properties could be de-
tected.

At engine ground idle and subsonic cruise conditions, the same strong
effects of fuel hydrogen content on smoke levels was evident, but NO_x levels
became virtually independent of any fuel property. Emission levels of CO
and HC were found to be jointly dependent on fuel hydrogen content and rela-
tive fuel spray droplet size calculated from fuel viscosity, density and
surface tension.

Combustor exit temperature profile and pattern factor (in high pressure
tests) were essentially independent of fuel type, but a sensitivity to liner
thermocouple installations was found.

In cold day ground start tests (to 239 K), lightoff was obtained with
all fuels. At standard day conditions, lightoff fuel/air ratio was indepen-
dent of fuel type, but at lower temperatures, the lightoff fuel/air ratio
increased with the less volatile more viscous fuels and correlated with the
relative spray droplet size.

Altitude relight test results were similarly dependent upon ambient
temperature and fuel properties. At low flight Mach numbers, where fuel and

1

air temperatures are low, relight altitude limits correlated with the relative spray droplet size. At high flight Mach numbers where fuel and air temperature are elevated, relight altitude limits were nearly independent of fuel type.

High temperature cyclic fuel nozzle tests with JP-8 and No. 2 diesel fuels revealed significant effects of fuel type and operating conditions on nozzle fouling rates. Nozzle life was correlated with fuel temperature and fuel breakpoint (by JFTOT).

Combustor liner life analyses, based on the test data, were conducted. These analyses resulted in relative life predictions of 1.00, 0.93, 0.83, and 0.74 for fuel hydrogen contents of 14.5, 14.0, 13.0 and 12.0, respectively. Turbine system life is not predicted to change for any fuels with properties within the matrix tested.

The fuel property effects observed in these tests of the J79-17C combustion system are generally similar to those previously determined for the J79-17A (in use, high smoke) and F101 (advanced, low smoke) combustion systems, except for relative combustor liner life predictions. Because of the high front end cooling effectiveness, the J79-17C combustor life is predicted to be significantly less sensitive to fuel hydrogen content than are the other two combustor designs.

SECTION II

INTRODUCTION

For more than 25 years, the primary fuel for USAF gas-turbine-powered aircraft has been JP-4, a wide-cut distillate with excellent combustion characteristics and low-temperature capability. Typically, its heating value has been over 43.5 MJ/kg (18,700 Btu/lb), its freezing point below 219 K (-65° F), and its aromatic content quite low, around 11 percent by volume. A prime consideration in the definition of JP-4 was that during wartime a large percentage of domestic crude oil could be converted into this product with minimum delay and minimum impact on other major users of petroleum products.

Conversion from high volatility JP-4 to lower voilatility JP-8, which is similar to commercial Jet A-1, as the primary USAF aircraft turbine fuel has been under consideration since 1968. The strong motives for the change are NATO standardization and reduced combat vulnerability.

Domestic crude oil production peaked in 1971 and has been steadily declining since that time, while demand has continued to increase. Thus, particularly since 1973, the cost and availability of high-grade aircraft turbine fuels have drastically changed. These considerations have spurred efforts to determine the extent to which current USAF fuel specifications can be broadened to increase the yield from available petroleum crudes and, ultimately, to permit production from other sources such as coal, oil shale, and tar sands.

As a result of the current and projected fuel situation, the USAF has established an aviation turbine fuel technology program to identify JP-4 and/or JP-8 fuel specifications which:

1. Allow usage of key world-wide resources to assure availability

2. Minimize the total cost of aircraft system operation

3. Avoid sacrifices of engine performance, flight safety, or environmental impact.

Engine, airframe, logistic, and fuel processing data are being acquired to establish these specifications. This report contributes to the needed data base by describing the effects of fuel property variations on the General Electric J79-17C engine main combustion system with respect to performance, exhaust emissions, and durability. Similar programs, based on the General Electric J79-17A and F101 engines and the Detroit Diesel Allison TF41 and high Mach engines have been previously conducted (References 1, 2, 3, and 4). Collectively, these programs provide representative data for the engine classes that are expected to be in substantial use by the USAF in the 1980's.

This report summarizes the results of a 9-month, 3-task program which was conducted to identify which fuel properties are important to J79-17C (low-smoke, long life) engine combustor operation and quantitatively relate fuel property variations to combustor performance, emission characteristics, and durability characteristics. Also, wherever possible, these results have been compared to those previously obtained for the JP79-17A (high smoke, in-use) and F101 (advanced, low smoke) engine combustion systems in order to illustrate how fuel property sensitivity is affected by combustor design features and/or engine cycles.

Thirteen test fuels provided by the USAF were utilized. Descriptions and properties of these fuels are presented in Section III. In Task I of the program, test planning and preparations were made, based on use of the J79 engine combustion system components and operating characteristics described in Section IV, and on the three test rigs and procedures described in Section V. In Task II of the program, 35 tests (14 high pressure/temperature combustor performance/emissions/durability tests, 14 low pressure/temperature combustor cold-day ground start/altitude relight tests, and 7 high temperature fuel nozzle fouling tests) were conducted. These are summarized in Section VI-A. In Task III of the program these test data were analyzed to establish the fuel property correlations also presented in Section VI-A and to establish the engine system life predictions presented in Section VI-B. Finally, these results are compared in Section VI-C to those previously obtained, and conclusions and recommendations drawn from these tests and analyses are summarized in Section VII.

SECTION III

TEST FUEL DESCRIPTION

A. General Description

Thirteen test fuels were supplied by the USAF for combustion system
evaluation in this program. The fuels included a current JP-4, a current
JP-8, and a No. 2 diesel. The blends were made up by the USAF to achieve
three different levels of hydrogen content: 12, 13, and about 14 percent
by weight. Two different types of aromatics were used to reduce the hydrogen
content of the base fuels: a monocyclic aromatic (xylene bottoms), and a
dicyclic aromatic described by the supplier as "2040 solvent" (a naphthalene
concentrate). A third blend component, used to increase the final boiling
point and the viscosity of two blends, is described as a Mineral Seal Oil,
a predominantly (90 percent) paraffinic white oil.

The rationale for the selection of this test fuel matrix was to span sys-
tematically the possible future variations in key properties that might be dic-
tated by availability, cost, the change from JP-4 to JP-8 as the prime USAF
aviation turbine fuel, and the use of nonpetroleum sources for jet fuel pro-
duction. The No. 2 diesel was selected to approximate the Experimental Referee
Broad Specification (ERBS) aviation turbine fuel that evolved in the NASA-Lewis
workshop on Jet Aircraft Hydrocarbon Fuel Technology (Reference 5).

B. Physical and Chemical Properties

As before, all fuel property data were provided to General Electric by
the USAF from either their own in-house or contracted (Monsanto Research Cor-
poration) laboratory tests. Key fuel properties are summarized in Table 1,
and additional detailed data are presented in Appendix A.

5

Table 1. Summary of Test Fuel Properties.

Fuel Blend Number	Fuel Components Base Fuel	Fuel Components Blend Component	Hydrogen,(1) Wt. % (NMR D3701)	Aromatics, Volume % (Mass Spec., D2789-71) Monocyclic	Dicyclic	Total	Density kg/m³ @ 294.3 K	Kinematic Viscosity mm²/s @ 294.3 K	Surface Tension, mN/m @ 294.3 K	Simulated Distillation, Temp. (K) @ % Recovered (Gas Chrom. D2887) 0.5	10	50	90	99.5	Thermal Stability,(1,2) Breakpoint, K (JFTOT, D3241)
1A	JP-4	---	14.48	9.5	0.5	10.0	755.7	0.955	23.28	298	366	433	510	554	538
2A1	JP-8	---	13.94	11.3	1.9	13.2	809.6	2.230	27.08	401	463	504	545	579	598
3A	JP-8	Seal Oil	13.92	11.0	1.8	12.8	810.4	2.450	26.56	401	462	505	562	628	593
4A	JP-8	Solvent	11.90	16.9	22.0	38.9	858.9	2.130	27.77	406	463	503	540	577	570
5A	JP-8	Xylene	13.02	29.7	1.6	31.3	821.9	1.690	27.80	409	438	488	536	575	583
6A	JP-8	Xylene	12.04	51.4	0.8	52.2	831.4	1.240	27.82	353	429	450	527	574	573
7A	JP-8	Solvent	12.93	14.1	11.9	26.0	833.3	2.170	27.00	409	462	501	539	576	560
8A	JP-4	Solvent	11.94	17.2	24.5	41.7	830.9	1.210	24.59	307	376	481	528	575	538
9A	JP-4	Solvent	12.95	14.0	13.7	27.7	799.0	1.070	23.62	303	369	460	526	573	537
10A	JP-4	Xylene	12.08	53.1	0.4	53.5	811.0	0.900	24.81	304	379	441	494	578	543
11A	JP-4	Xylene	12.96	34.9	0.4	35.3	787.8	0.910	24.73	305	374	439	505	562	576
12A	JP-4	Xylene & Seal Oil	13.99	14.9	0.5	15.4	771.2	1.110	24.20	301	371	451	574	619	553
13A1	DF2	---	12.91	14.1	7.5	21.6	843.4	3.270	28.60	405	470	529	591	646	533

(1)Data determined by USAF, other listed data determined by Monsanto Research Corporation.
(2)Data determined on retained samples, other data listed in Table A-4.

SECTION IV

J79 ENGINE AND COMBUSTION SYSTEM DESCRIPTION

A. Overall Engine Description

The J79 engine is a lightweight, high-thrust, axial-flow turbojet engine with variable afterburner thrust. This engine was originally qualified in 1956, and since that time various models with improved life and thrust have been developed. The model currently in use by the USAF, the J79-17A, was the reference engine for the previous fuel character effects program (Reference 1). A later model, the J79-17C, which incorporates a low-smoke long-life combustion system, is the reference engine for this fuel character effects program.

An overall view of the J79 engine is presented in Figure 1. The J79 has a 17-stage compressor in which the inlet guide vanes and the first six stator stages are variable. The compressor pressure ratio is approximately 13.4:1. The combustion system is cannular with ten individual combustion liner assemblies. The turbine has an air-cooled first-stage stator, and a three-stage uncooled rotor that is coupled directly to the compressor. The engine rotor is supported by three main bearings. The afterburner is fully modulating with a three-ring "V" gutter flameholder. Afterburner thrust modulation is accomplished by means of fuel flow scheduling and actuation of the variable area, converging-diverging type exhaust nozzle.

B. Combustion System Description

The J79 engine employs a cannular combustion system which consists of ten individual combustion liner assemblies located between inner and outer combustion casings forming an annular passage. An exploded view of the system with the various components, including the compressor rear frame and the turbine first stage nozzle is shown in Figure 2.

A pictorial view of a combustion liner assembly is shown in Figure 3, and a flowpath is shown in Figure 4. Each combustor (or "can") consists of three parts which are riveted together to form an assembly. The key feature of the low-smoke long-life J79-17C combustor is a completely redesigned, shortened, inner liner shown in Figure 5. This part is a machined ring shell which has continuous film cooling slots in the cylindrical portion of the liner, and an impingement cooling manifold coupled with cooling slots in the dome transition section. Combustion air is introduced through a swirl cup, a secondary co-swirler and bellmouthed thimbles (4 in ignition cans, 6 in non-ignition cans) in the dome transition region. The rear liner is a sheet metal shell having punched cooling louvers and dilution thimble holes. The outer liner is an air-flow guide to assure proper flow distribution to the inner and aft liners. In an engine assembly, two of the combustors are provided with spark ignitors for starting. Adjacent combustors are joined near the forward ends by cross ignition tubes to allow propagation of the flame from the combustors with a spark ignitor to the other combustors. The liners are each positioned and held in

7
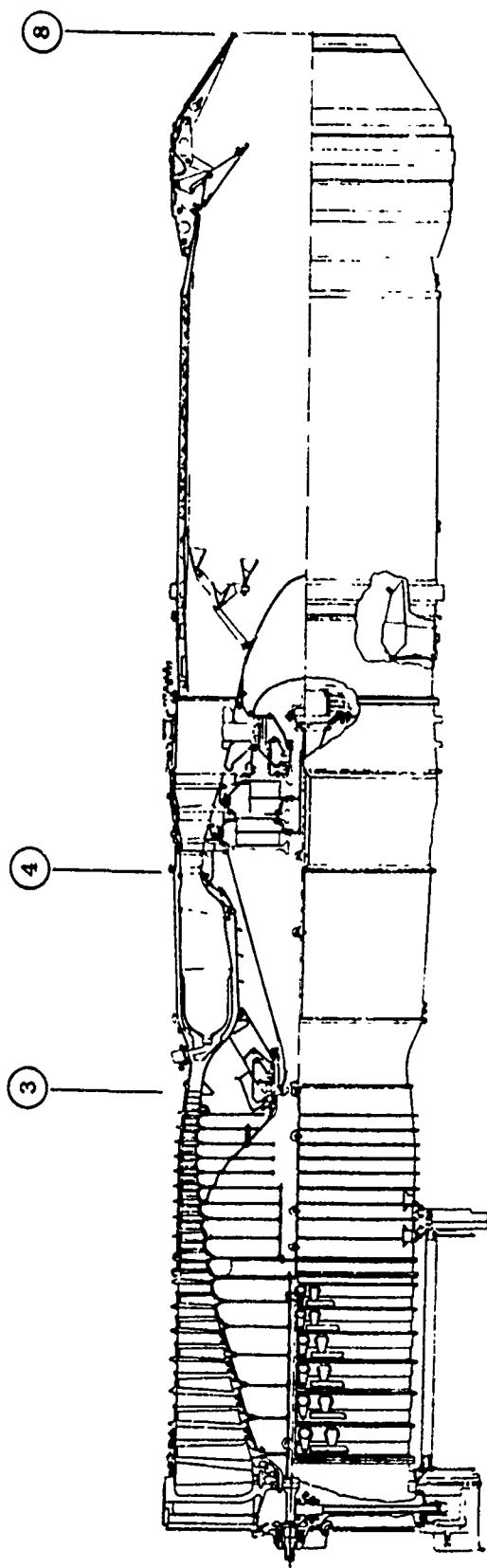
Figure 1. General Electric J79 Turbojet Engine.

OUTER COMBUSTION CASING

NOZZLE SUPPORT RING

COMBUSTION LINER

iNNER COMBUSTION CASING

COMPRESSOR REAR FRAME

TRANSITION DUCT

FIRST STAGE TURBINE NOZZLE

CROSS-IGNITION TUBE AND CLAMP

OUTER COMBUSTION CASING
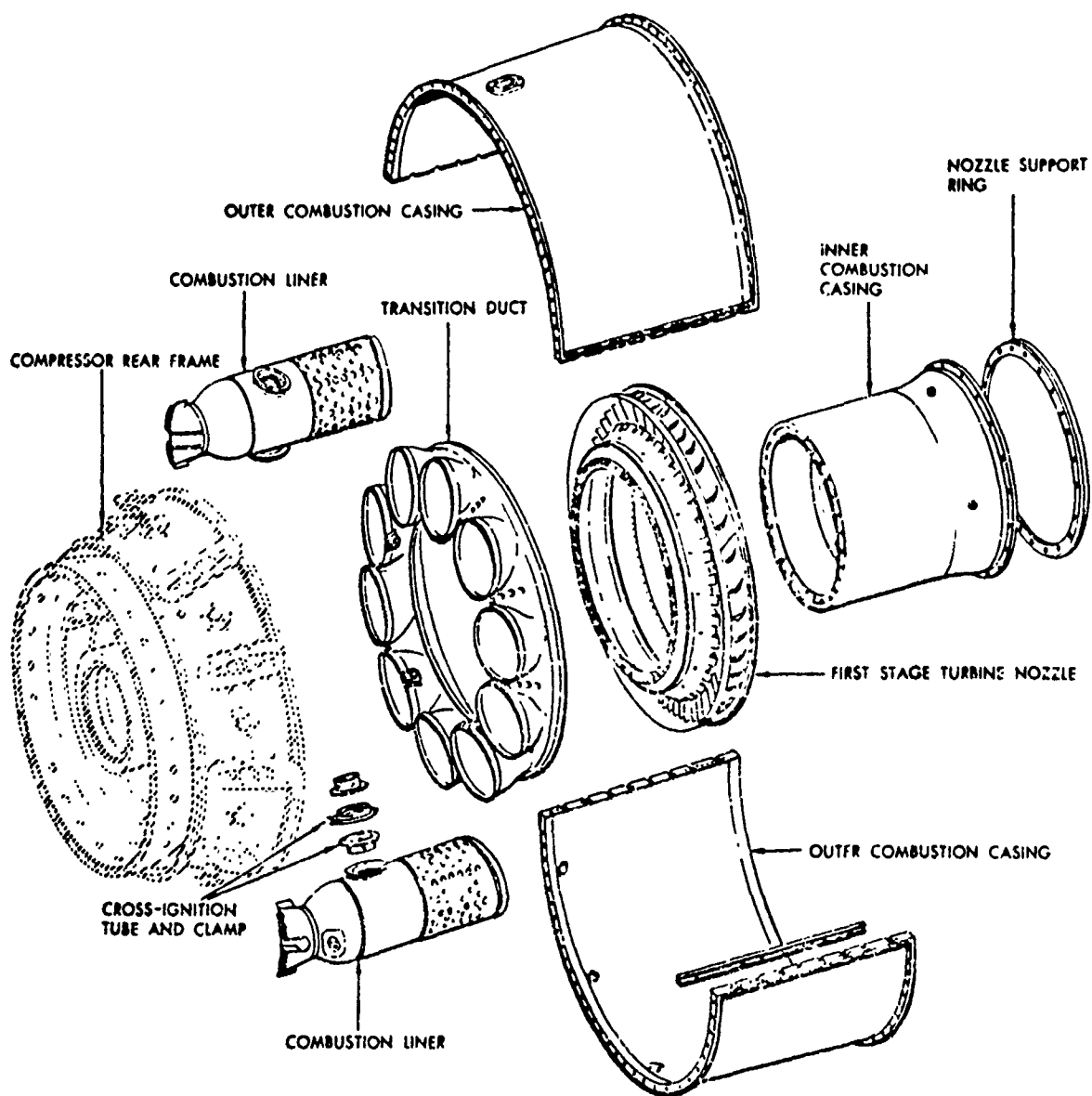
COMBUSTION LINER

Figure 2.   J79 Engine Combustion System, Exploded Pictorial View.
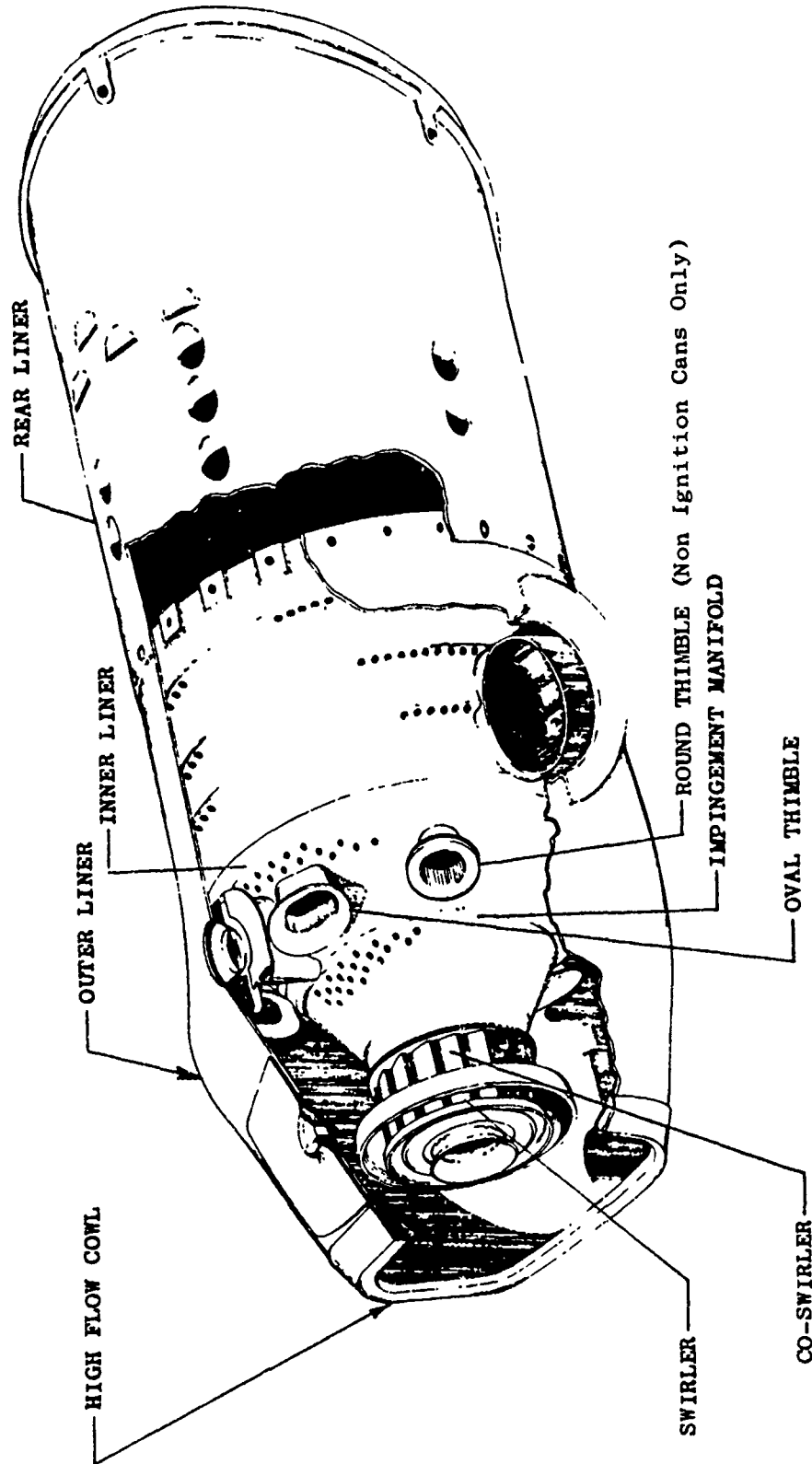
Figure 3. J79-17C Low Smoke, Long Life Combustor Assembly.

REAR LINER

INNER LINER

OUTER LINER

HIGH FLOW COWL

SWIRLER

CO-SWIRLER

ROUND THIMBLE (Non Ignition Cans Only)
IMPINGEMENT MANIFOLD

OVAL THIMBLE
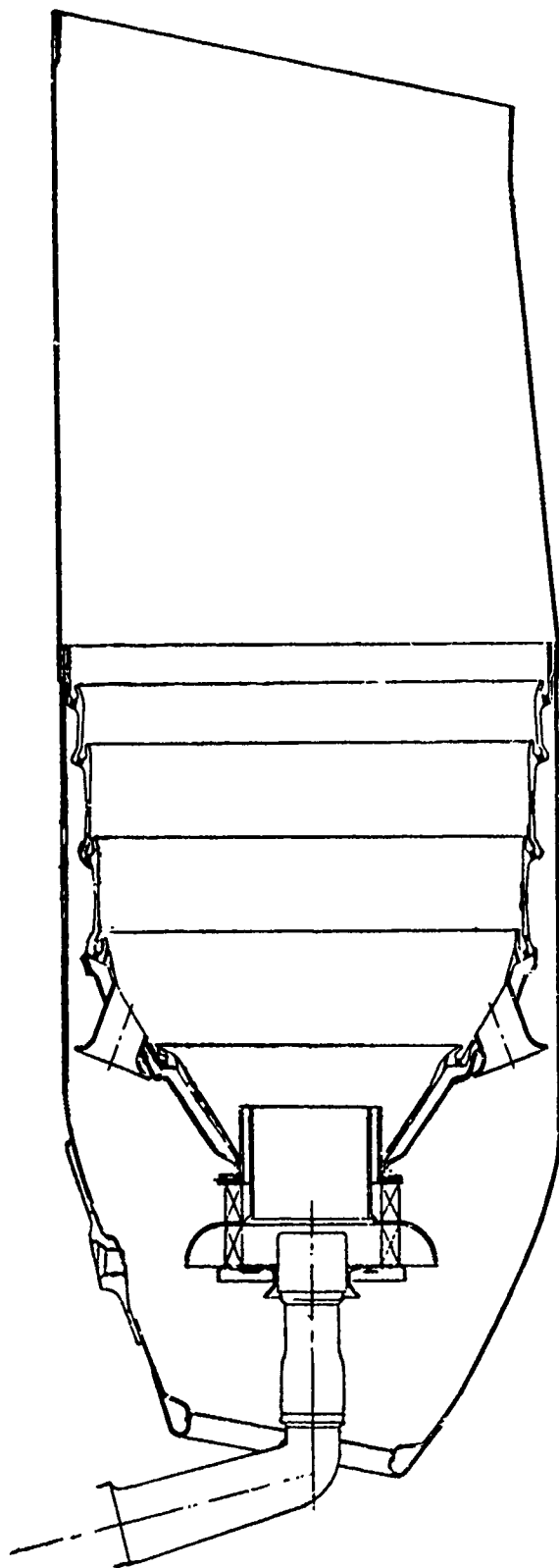
Figure 4. J79-17C Combustor Flowpath.
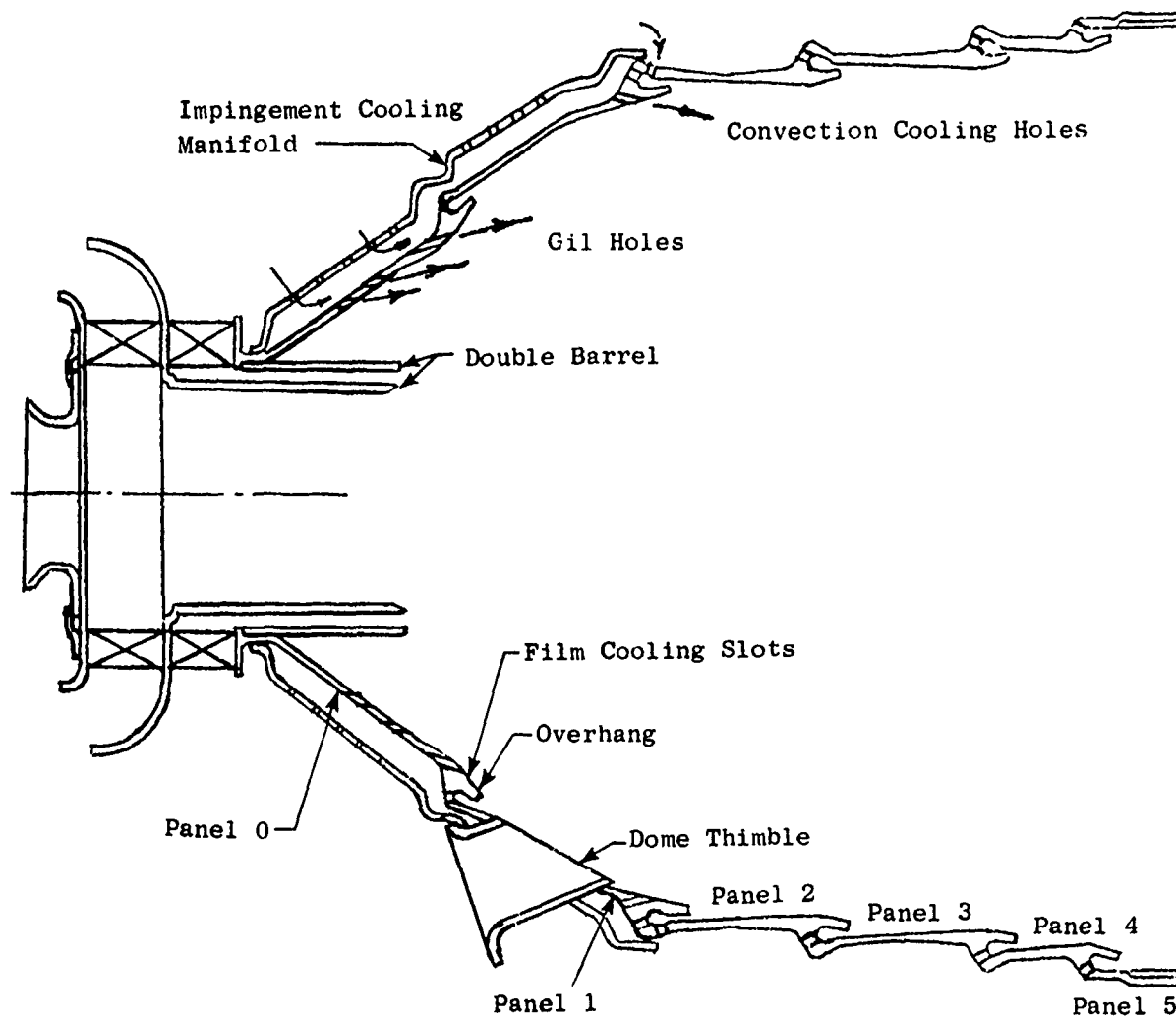
Figure 5. J79-17C Combustor Inner Liner Details.

place by mounting bolts at the forward ends. Axial stack-up and thermal growth
are accomplished by a sliding seal between the combustors and the transition
duct. The major liner material is Hastelloy X.

The transition duct provides a ring of ten oval inlet ports to accept the
ten combustion liners, and the exit of the transition duct is annular to match
up with the turbine flowpath. The transition section exit area is approxi-
mately one-half of the total exit area of the ten combustors providing an ac-
celerating flow stream into the turbine. The transition duct is mounted by
five radial support pins in the inner combustion casing. These pins have a
sliding fit with the transition duct, allowing for differential thermal growth,
but they maintain the axial location of the duct. Sliding seals are provided
with both the combustors and turbine.

All of the earlier J79 models featured the use of dual-orifice, pressure-
atomizing type fuel nozzles, with a single fuel inlet and a fuel-flow dividing
valve external to the mounting flange. For the J79-17C model, the fuel nozzle
is modified by replacement of the tip with one which has features to provide
air-blast atomization, and improved fuel/air mixing. It also is longer to mate
with the shortened inner liner. The J79-17C tip details are illustrated in
Figure 6. The new tip has a central primary pressure atomizing fuel orifice
and eight radial, low-pressure drop secondary fuel disributors on the fuel
nozzle outside diameter. The fuel flow schedule for a single fuel nozzle is
shown in Figure 7. The tip of each fuel nozzle is provided with an air shroud
which directs cooling-air across the face and around the fuel orifices to
reduce the tendency for carbon formation.

C.   Combustor Operating Conditions

The combustor must operate over a wide range of fuel flow, inlet airflow,
temperature and pressure. Table 2 presents the combustor operating parameters
at four important steady-state engine conditions which are typically encoun-
tered. At each of these conditions, fuel effects on combustor performance,
emissions and life are of particular interest.

In addition to steady-state operation, the combustion system must pro-
vide for starting over a wide range of conditions, ranging from cold day
ground start to relight at high altitude. Figure 8 presents the altitude
windmilling/relight conditions.

PRIMARY FUEL ORFICE

SECONDARY FUEL DISTRIBUTOR

P/N 3031M36P01
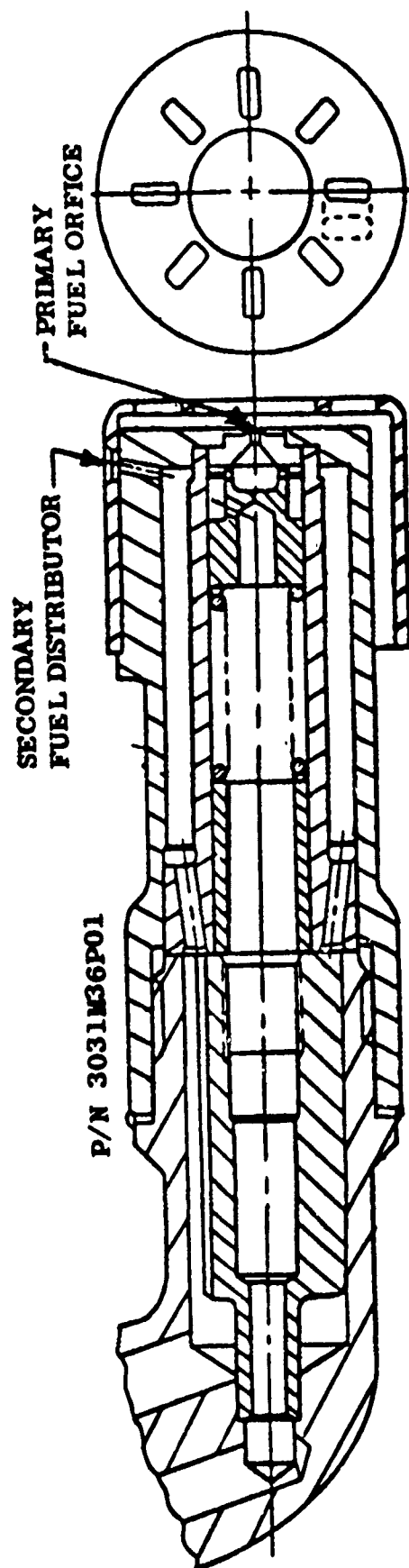
Figure 6. J79-17C Fuel Nozzle Tip Details.

14
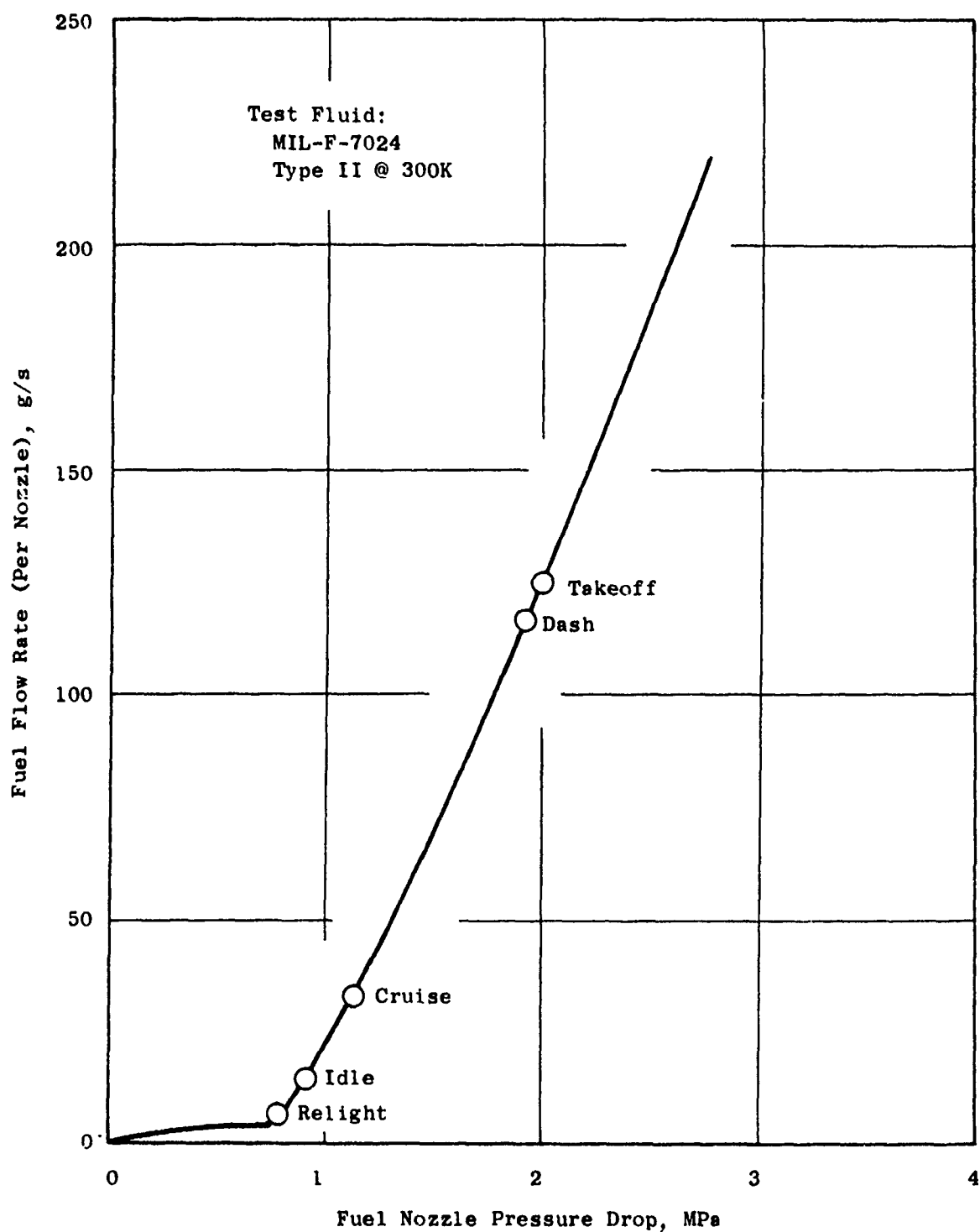
Figure 7. J79-17C Fuel Nozzle Flow Characteristics.

Table 2. J79-17C Engine Combustor Operating Conditions.

	Ground Idle	Takeoff	Subsonic Cruise	Supersonic Dash	Ground Start[3]
Flight Altitude, km	0	0	10.7	10.7	0
Flight Mach Number	0	0	0.9	2.0	0
W_3[1], Total Airflow, kg/s	18.3	75.2	29.5	87.5	~3.18
W_c[1], Combustor Airflow, kg/s	15.3	62.7	24.6	73.3	~3.18
W_f[1], Fuel Flow, kg/s	0.144	1.259	0.335	1.173	0.0649[4]
T_3, Inlet Total Temperature, K	421	664	559	781	$\geq$239
P_3, Inlet Total Pressure, MPa	0.254	1.359	0.471	1.589	0.101
f_4, Fuel/Air Ratio, g/kg	9.42	20.07	13.60	16.01	~20.4
T_4, Exit Total Temperature (Ideal), K	792	1064	1362	1335	---
V_r[2], Reference Velocity, m/s	24.2	28.6	27.2	33.5	~7.1

[1]Engine flows indicated (ten combustor cans).
[2]Based on W3 and Ar = 3684 cm^2.
[3]1000 rpm, typical starting speed.
[4]Minimum engine fuel flow schedule (normal).
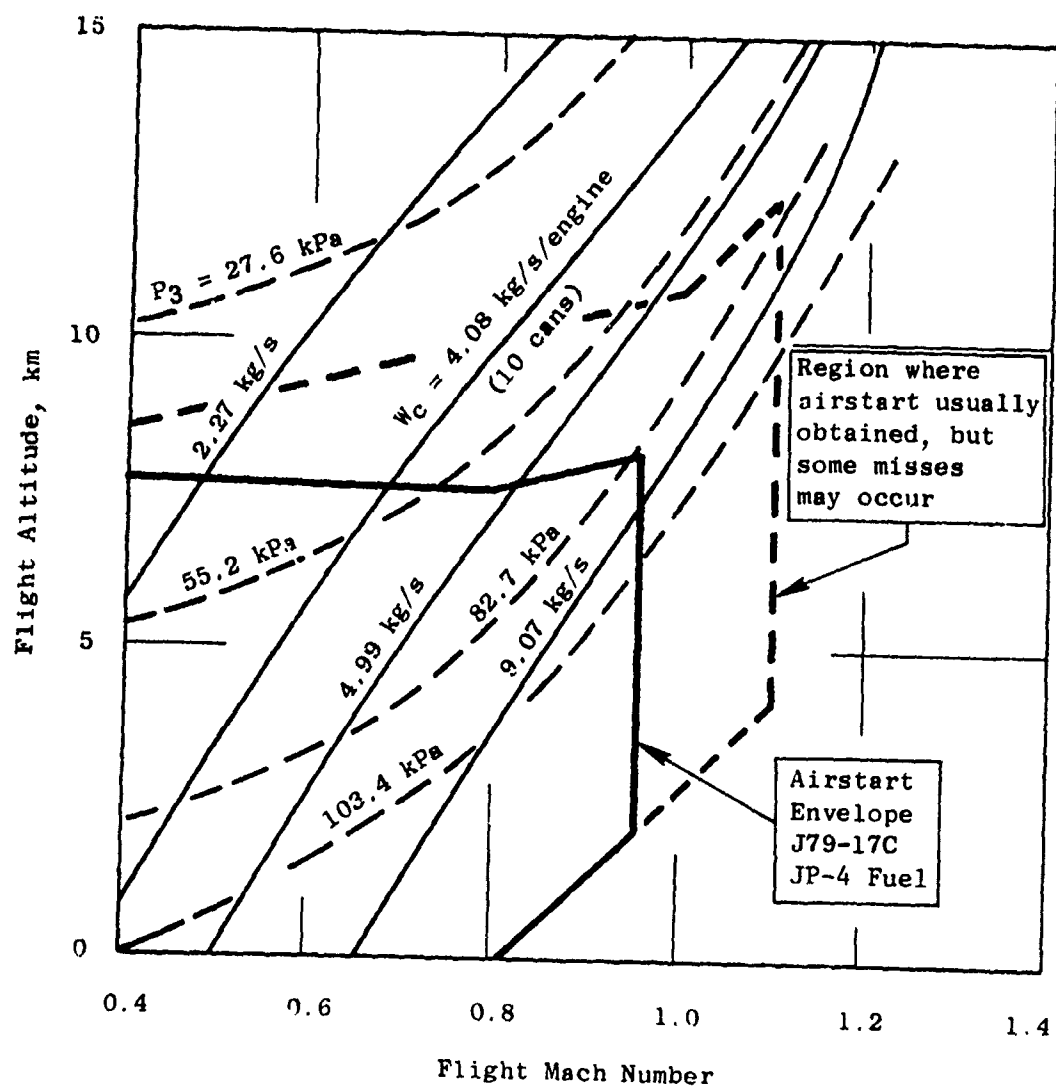
Figure 8. J79-17C Engine Altitude Windmilling/Relight Map.

SECTION V

APPARATUS AND PROCEDURES

All combustor and fuel nozzle testing in this program was conducted in specialized facilities at General Electric's Evendale, Ohio plant, using apparatus and procedures which are described in the following sections. Combustor performance/emissions/durability tests were conducted in a high pressure/temperature single-can combustor rig which is described in Section V-A. In parallel, combustor cold-day ground start/altitude relight tests were conducted in a low pressure/temperature single can rig which is described in Section V-B. Also in parallel, high temperature fuel nozzle fouling tests were conducted in a small specialized test rig described in Section V-C. Special fuel handling procedures used in all of these tests are described in Section V-D. Finally, procedures employed in analyses of these data are described in Section V-E.

New, engine-quality, current-model J79-17C engine combustion system components, listed in Table 3, were utilized in these tests. Pretest flow calibrations of the combustors and fuel nozzles are presented in Tables 4 and 5.

A. Performance/Emission/Durability Tests

High pressure/temperature single-can-combustor rig tests were conducted at simulated J79 engine idle, cruise, takeoff, and dash operating conditions with each of the fuels to determine the following characteristics:

1) Gaseous emissions (CO, HC, and NO_x).

2) Smoke emissions.

3) Carbon particle emissions.

4) Carbon deposition.

5) Liner temperatures.

6) Flame radiation.

7) Combustor exit temperature profile and pattern factor.

8) Idle stability (lean blowout and ignition) limits.

Thus, a large part of the total data was obtained in these tests using apparatus and procedures described in the following sections.

18

Table 3. J79-17C Engine Combustor Test Parts List.

Part Name	GE Part Number	National Stock Number
Ignition Combustor Liner Assembly	7012M89G05	2840-00-126-2856
Fuel Nozzle (Parker-Hannifin 1445-623386)	3031M36P02	2925-00-126-5730
Main Ignition Unit (Bendix 10-358765-1, 115 VAC, 400 cps)	106C5281P3	2925-00-992-7904L
Main Igniter Plug (Champion FHE 281-3	696D256P06	2925-00-126-2879
Main Ignition Lead (81482-59386)	106C5282P1	2925-00-065-0801

Table 4. Combustor Pretest Flow Calibrations.

Combustor	Combustor Effective Airflow Area, cm^2	
	Low Pressure Test S/N 03623	High Pressure Test S/N 03551
Front Liner Assembly	30.02	30.20
Aft Thimbles and Trim Holes	29.75	29.41
Aft Cooling Louvers and Seal	9.97	10.83
Total	69.75	70.45

Table 5. Fuel Nozzle Pretest Flow Calibrations.

Fuel Nozzle Serial Number	W_f, Flow Rate, g/s @ ΔP_f = MPa							Test Use
	0.552	0.862	2.068	2.758	2.068	0.862	0.552	
180271	3.11	12.28	134.6	216.2	134.6	12.23	3.10	Fouling, Run 4
180272	3.26	12.41	135.8	211.3	135.8	12.42	3.10	Fouling, Run 6
180273	3.16	11.86	134.6	217.6	134.6	11.96	3.14	Fouling, Run 3
180274	3.35	12.30	135.2	216.2	134.6	12.15	3.12	Fouling, Run 7
180275	3.14	11.61	133.2	221.3	134.4	11.36	3.04	Fouling, Run 2
180276	3.21	12.23	132.0	216.3	132.5	11.86	3.16	Spare
180277	3.15	12.51	133.3	218.7	133.3	12.23	3.09	Fouling, Run 5
180278	3.20	12.49	138.3	222.6	138.3	12.28	3.04	Fouling, Run 1
180279	3.09	12.60	140.9	216.2	141.5	12.22	3.09	High Pressure Rig
180280	3.14	12.05	135.8	221.3	138.3	12.55	2.91	Low Pressure Rig
Mean	3.181	12.234	135.37	217.77	135.79	12.126	3.079	
Std Dev., %	2.44	2.55	1.92	1.53	2.03	2.76	2.20	

1. **High Pressure Test Rig Description**

These tests were conducted in the Small Combustor Test Facility, Cell A5, located in Building 304 of the Evendale Plant. This test cell is equipped with all of the ducting, fuel and air supplies, controls, and instrumentation required for conducting small combustor high pressure/temperature tests. High pressure air is obtained from a central air supply system, and a gas-fired indirect air heater is located adjacent to the test cell. For the single-can-combustor rig, J79 engine idle, cruise, and takeoff operating conditions can be exactly duplicated. Dash operating conditions can be exactly duplicated with respect to temperature, velocity, and fuel/air ratio, but pressure and flow rates must be reduced about 25 percent in order to be within the facility airflow capability.

The High Pressure Combustor Test Rig, shown in Figures 9 and 10, exactly duplicates a one-tenth sector of the engine flowpath from the compressor out-let guide vane (OGV) to the first-stage turbine nozzle diaphragm (TND). As shown in Figure 9, the test rig inlet flange which bolts up to a plenum cham-ber in the test cell, incorporates a bellmouth transition to the simulated OGV plane. The combustor housing is a ribbed, thick-walled vessel which forms the inner flowpath contour and side walls, covered by a thick lid that forms the outer flowpath contour. Figure 10 shows a combustor installed in the pressure vessel with the lid removed. The combustor exit engages an actual segment of an engine transition duct. Immediately downstream of the transi-tion duct is an annular sector section which contains an array of water-cooled instrumentation rakes in the TND plane, indicated by an arrow in Figure 9. Additional details of the exit instrumentation rakes are shown in Figure 11. Downstream of the rakes the combustion gases are water-quenched and the sector flowpath transitions to circular, which is bolted up to a remote-operated back-pressure valve in the test cell ducting. Two other features of the test rig can be seen in Figure 9: a flame radiation pyrometer, mounted to view the combustor primary zone through a crossfire duct window; and bleed air pipes to withdraw, collect, and meter simulated turbine cooling airflow.

2. **High Pressure Test Rig Instrumentation**

A summary of the important combustor operating, performance, and emission parameters which were measured or calculated in these tests is shown in Table 6. Airflow rates were measured with standard ASME orifices. Fuel flow rates were measured with calibrated turbine flowmeters corrected for the density and vis-cosity of each test fuel at the measured supply temperature. Combustor inlet temperature and pressure were measured with plenum chamber probes.

Combustor outlet temperature, pressure, and gas samples were measured with a fixed array of seven water-cooled rakes, arranged and hooked up as shown in Figure 12. Each rake contained five capped chromel-alumel thermo-couple probes, located on radial centers of area, and four impact pressure/gas sample probes, located midway between thermocouple elements. As shown in Figure 12, eight of the impact probe elements were hooked up for total-pres-sure measurement, and the other 20 elements were manifolded to four heated gas sample transfer lines leading out of the test cell to the gas composition

21

Optical Pyrometer

Turbine Cooling Extraction

Exit Instrumentation Rakes
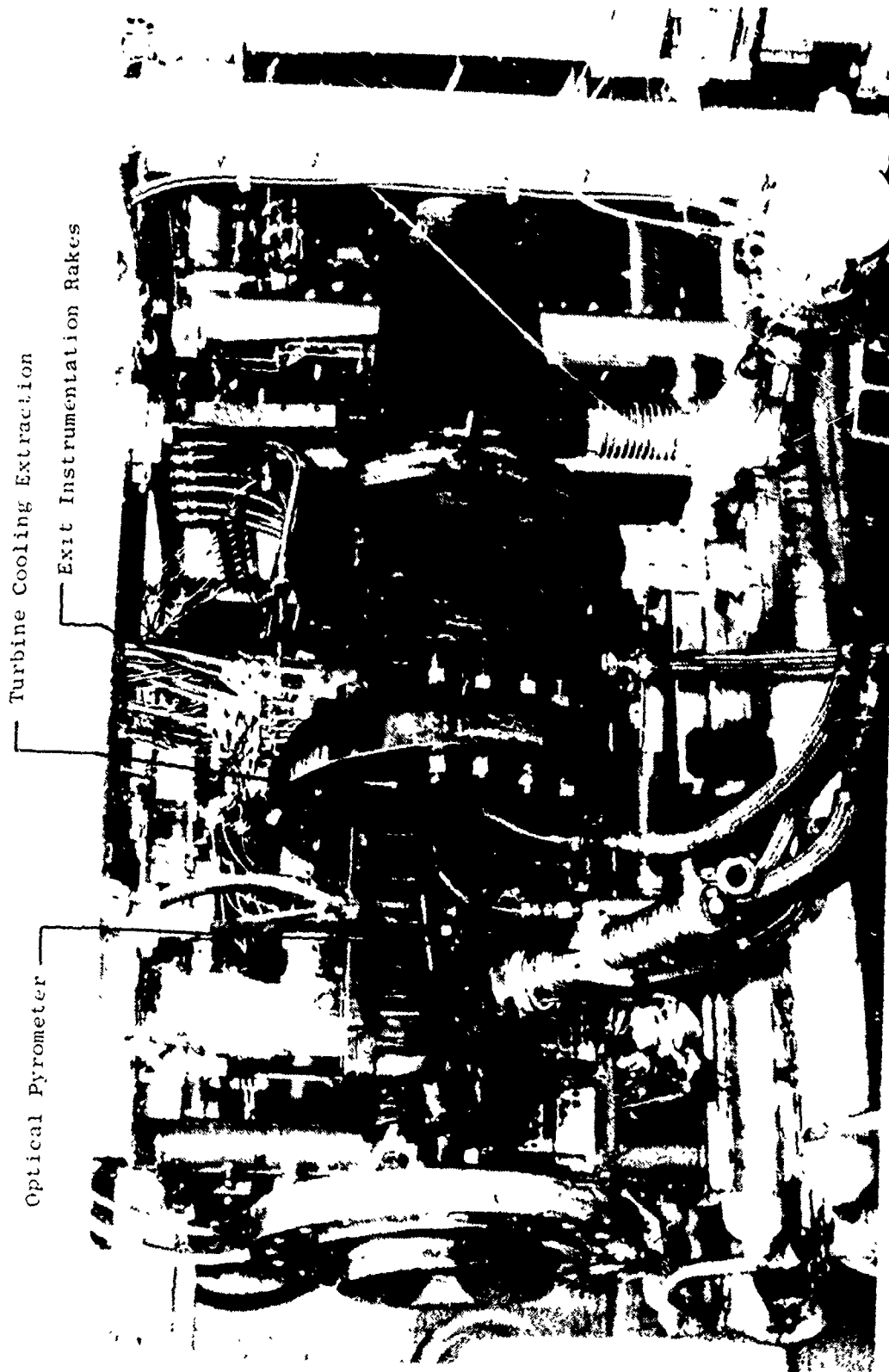
Figure 3. ... ... de View of High Pressure ... Turbine Combustor Case Plug.
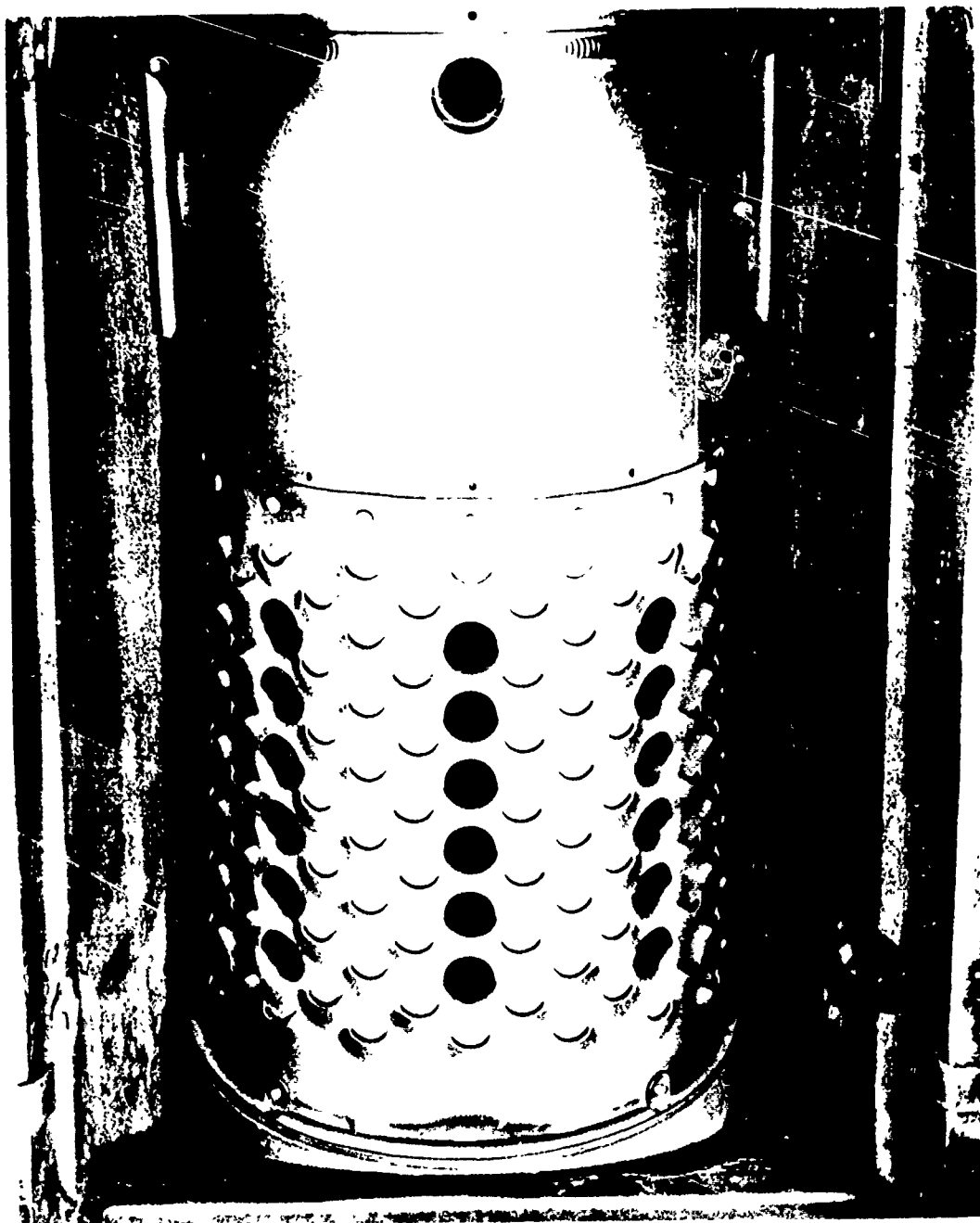
Figure 10. Combustor Installation in High Pressure J79 Test Rig.
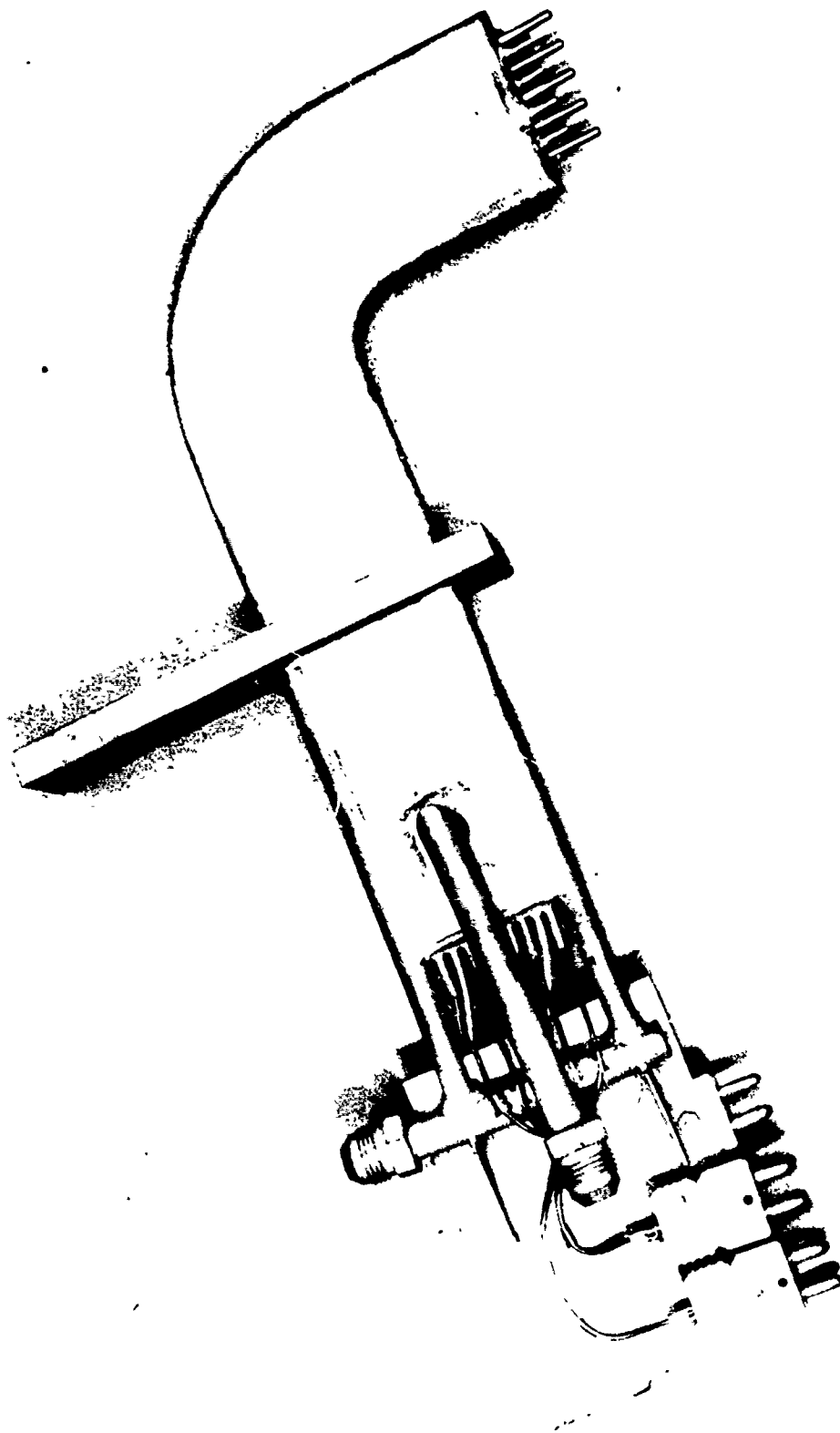
Figure 11. Combustor Exit Instrumentation Rake

Table 6. Summary of Measured and Calculated Combustor Parameters in High Pressure Combustor Tests.

Parameter	Symbol	Units	Measurement/Calculation Method
Inlet Total Pressure	P_3	MPa	Average of measurements from 3 impact probes
Exit Total Pressure	P_4	MPa	Average of measurements from 8 impact probes
Total Pressure Loss	$\Delta P_T/P_3$	%	$100(P_3-P_4)/P_3$
Total Inlet Airflow	W_3	kg/s	ASME Orifice
Turbine Cooling Airflow	W_{tc}	kg/s	ASME Orifice
Combustor Airflow	W_c	kg/s	W_3-W_{tc}
Fuel Flow	W_f	g/s	Turbine flowmeters corrected for density and viscosity
Metered Fuel/Air Ratio	f_m	g/kg	W_f/W_c
Inlet Air Humidity	h_3	g/kg	Dewpoint hygrometer
Inlet Total Temperature	T_3	K	Average of measurements from 3 probes
Exit Total Temperature	T_4	K	Average of measurements from 35 probes
Pattern Factor	PF	-	$(T_{4max}-T_{4avg})/(T_{4avg}-T_3)$
Profile Factor	PrF	-	$(T_{4lmm. max.}-T3)/(T_{4avg}-T_3)$
Reference Velocity	V_r	m/s	$V_r = W_3/\rho_3 A_r = 0.0093297\, W_c T_3/P_3$
Combustor Metal Temperature	T_L	K	35 Metal Thermocouples
Combustor Dome Static Pressure	P_{sd}	MPa	Average of measurements from 2 wall taps
Combustor Liner Static Pressure	P_{sL}	MPa	Average of measurements from 2 wall taps
Fuel Temperature	T_f	K	Thermocouple at fuel nozzle inlet
Fuel Nozzle Pressure Drop	ΔP_f	MPa	Pressure tap at fuel nozzle inlet (P_f-P_{sd})
Fuel Nozzle Effective Area	A_{fe}	mm^2	$A_{fe} = W_f/\sqrt{2g\rho_f \Delta P_f}$
Combustor Total Flame Radiation	$\dot{q}_R$	kW/m^2	Optical pyrometer at crossfire duct
Combustor Exit Smoke Number	SN_4	-	Manifolded 12-point gas sample and ARP1179 (Ref. 6)
Smoke Emission Index	EI_s	g/kg	GE correlation at SN_4 & f_s (Appendix F)
Engine Exit Smoke Number	SN_8	-	GE correlation at EI_s (Appendix F)
Gas Sample Fuel/Air Ratio	f_s	g/kg	Manifolded 12-point gas sample & equation in ARP1256 (Ref. 7)
CO Emission Index	EI_{CO}	g/kg	Manifolded 12-point gas sample & equation in ARP1256 (Ref. 7)
HC Emission Index (as CH_n)	EI_{HC}	g/kg	Manifolded 12-point gas sample & equation in ARP1256 (Ref. 7)
NO$_x$ Emission Index (as NO_2)	EI_{NO_x}	g/kg	Manifolded 12-point gas sample & equation in ARP1256 (Ref. 7)
Gas Sample Combustion Efficiency	η_{GS}	%	$\eta_{GS} = 100 - (EI_{HC}/10.0)+(EI_{CO}/42.8)$
Thermocouple Combustion Efficiency	η_{TC}	%	$\eta_{TC} = 100 \left[\text{Ideal Fuel/Air Ratio @ } (T_4-T_3)\right] /f_m$
Large Carbon Particle Emissions	$\overline{X}_C$	g/kg	2 Manifld 4-point smple for mass rate/particle size analysis

Rake

Imm

A B C D E F G

1
1
2
2
3
3
4
4
5

◁ Thermocouple 5 Elements/Rake, 35 Total

◯ Total Pressure, 8 Elements Read Individually

▢ Smoke/Gas Sample, 6 Elements Manifold to Line I

◇ Smoke/Gas Sample, 6 Elements Manifold to Line II

△ Particulate Sample, 4 Elements Manifold to Line III

◿ Particulate Sample, 4 Elements Manifold to Line IV

Rake-Element

A1
F1
D2   I
B3
D3
G4

G1
B2
E2   II
F3
A4
C4

Smoke
Console

Gas
Sample
Console
(CAROL)

Sample Each at
Points 2-9

Cascade
Impactor

B1
C2   III
E3
F4

Sample at Selected
Test Points for
Mass Emission Rate
and Particle Size
Analyses

Milipore
Sampler

E1
A2   IV
G3
D4

Figure 12. High Pressure Test Rig Exit Instrumentation.

26

measurement instruments. Transfer Lines I and II were connected through se-
lector valves to a smoke measurement console (Figure 13) and a gas analysis
console (Figure 14). Transfer lines III and IV were connected to heated, high-
pressure, soot/particulate samplers located near the test rig. The lines then
continued on to flow control/metering apparatus in the control room area. Line
III was connected to the filter holder (Millipore, 47 mm diameter glass fiber
filters) for total mass emission rate determination, and Line IV was connected
to an 8-stage particle fractionating sampler (Anderson Sampler Inc. Mark III
with glass fiber filters) for particle size determination. Details of the
fractionating sampler are shown in Figure 15.

The General Electric smoke measurement console (Figure 13) contains stan-
dard test equipment which fully conforms to SAE ARP 1179 (Reference 6). Smoke
spot samples are collected on standard filter paper at the prescribed gas flow
rate and at four soiling rates spanning the specified quoted soiling rate.
The spot samples are later delivered to the data processing area, where the
reflectances are measured and the SAE Smoke Number is calculated.

The gaseous emission measurement console, shown in Figure 14, is one of
several that were assembled to General Electric specifications for CAROL sys-
tems (Contaminants Analyzed and Recorded On-Line) and that conform, generally,
to SAE ARP 1256 (Reference 7). This system consists of four basic instruments:
a flame ionization detector (Beckman Model 402) to measure total hydrocarbon
(HC) concentrations, two nondispersive infrared analyzers (Beckman Models 865
and 864) for measuring carbon monoxide (CO) and carbon dioxide (CO_2) concen-
trations, and a heated chemiluminescent analyzer (Beckman Model 951) for mea-
suring oxides of nitrogen (NO or $NO_x = NO + NO_2$) concentrations. Each of
the instruments are fully calibrated with certified gases before and after
each test run; and periodically during testing, zero and span checks are made.
Readings from the instruments are continuously recorded on strip charts and
hand-logged on test and calibration points for later calculation of concentra-
tion, fuel/air ratio, and emission indices, using a computer program which in-
corporates the equations contained in ARP 1256. Gas sample validity was
checked by comparison of sample to metered fuel/air ratios.

Carbon deposition tendencies with JP-4 and Diesel No. 2 fuels were
assessed by conducting 24 hour tests with each fuel, starting with a clean
combustor and fuel nozzle. At the completion of these tests, the combustor
and fuel nozzle was removed, visually inspected, and photographed to document
the carbon deposition tendencies.

Combustor metal temperature was measured by an array of 35 thermocouples
located on the assembly as listed in Table 7 and shown in Figures 16 through
21. The inner liner instrumentation pattern was selected to provide detailed
data in the vicinity of the known hottest regions of the liner.

Flame radiation in the primary burning zone of the combustor was measured
by a total-radiation pyrometer (Brown Radiamatic, Type R-12), which can be seen
in Figure 9. A diagram of the optical view path is shown in Figure 22. The
pyrometer sensing element is a thermopile which provides a direct current
voltage output. The flame radiation is focused on the thermopile with a
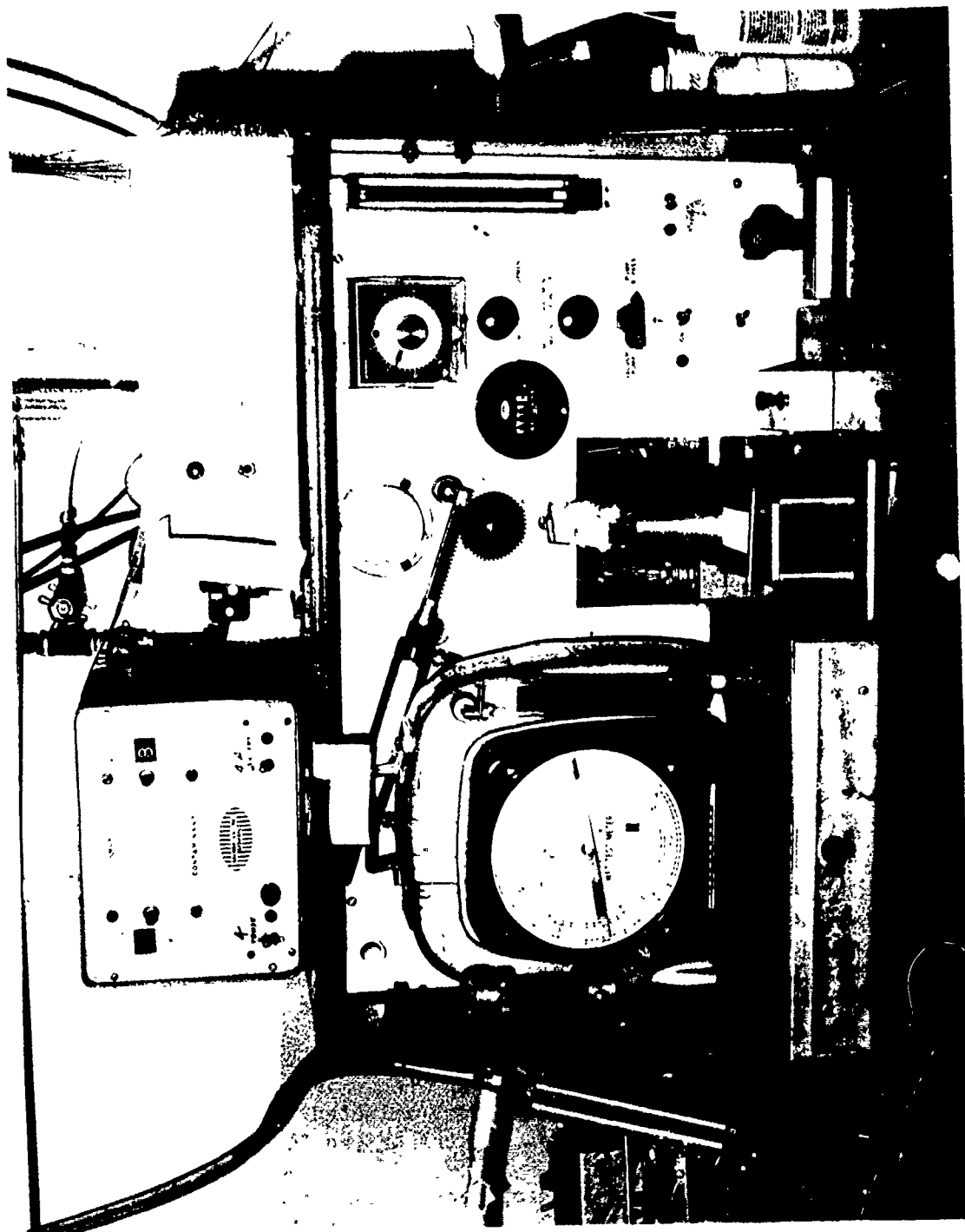
Figure 13. General Electric Smoke Measurement Console
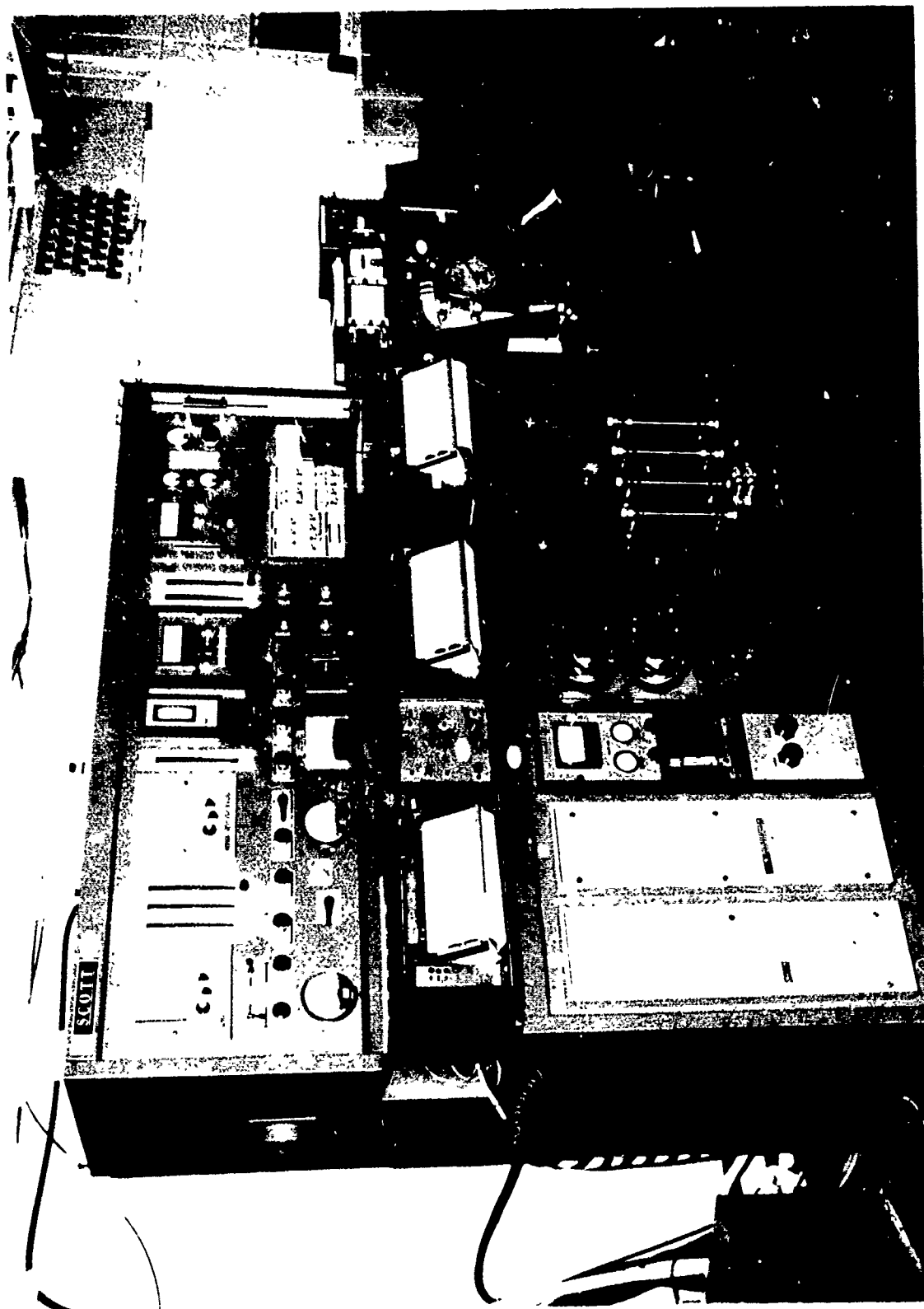
Figure 11. General Electric Laser Ranging/Break-out Console (CAROL IV)
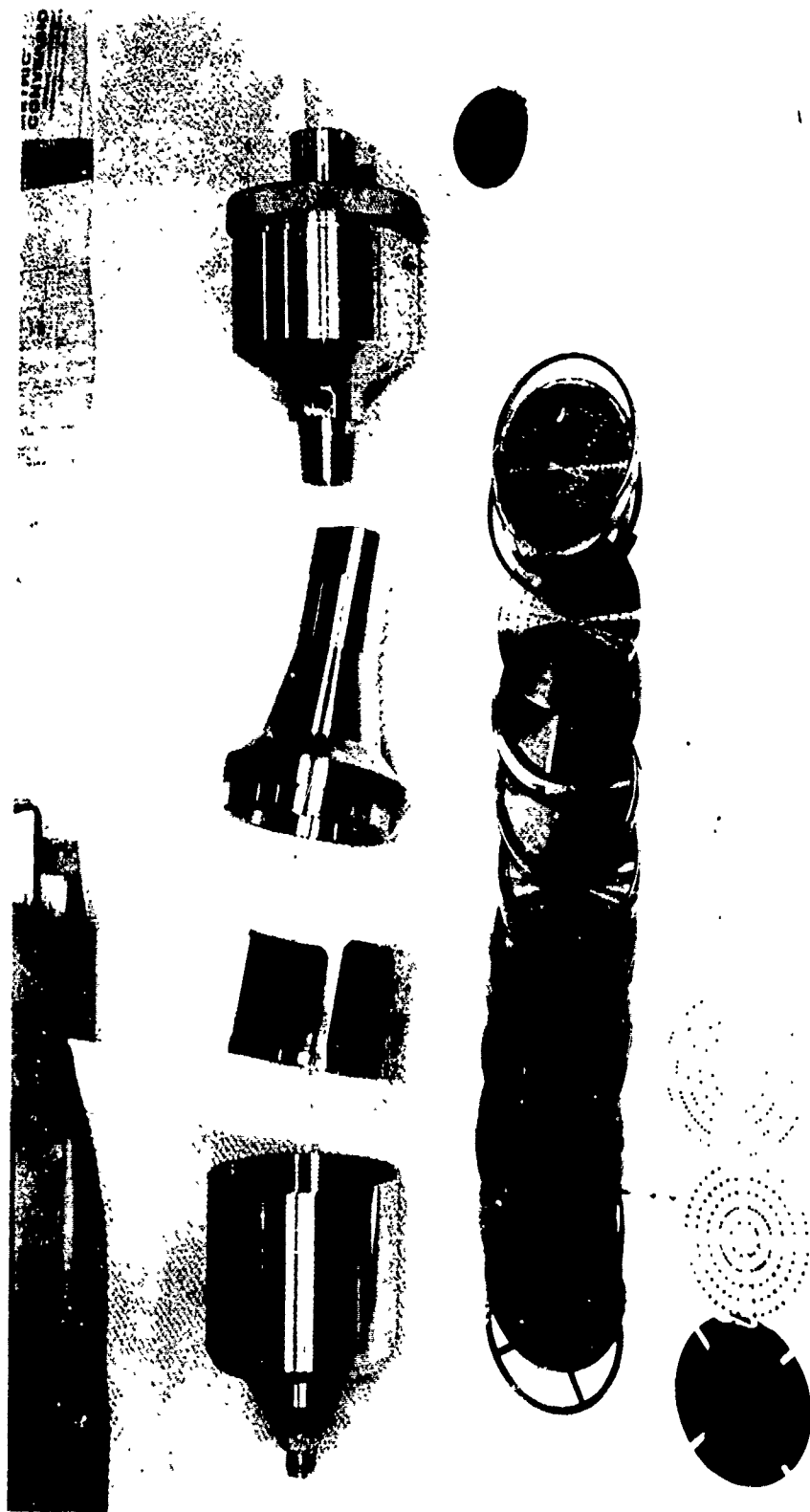
Figure 15   Particle Fractionating Sampler Details.

Table 7. Combustor Metal Temperature Instrumentation, High Pressure Rig Tests.

Thermocouple Number	Part	Circumferential Location, Degrees CWALF	Axial Location, millimeters	Type Thermocouple(1)
1	Inner Liner	180	Panel Zero, 15.2 from Trailing Edge (T.E.)	I
2	Inner Liner	180	1st Cooling Ring Overhang, 1.5 from T.E.	I
3	Inner Liner	0	Panel One, 9.5 from T.E.	I
4	Inner Liner	0	2nd Cooling Ring Overhang, 2.4 from T.E.	I
5	Inner Liner	0	Panel Two, 14.5 from G.E.	S
6	Inner Liner	0	3rd Cooling Ring Overhang, 2.2 from T.E.	I
7	Inner Liner	0	Panel Three, 12.7 from T.E.	S
8	Inner Liner	0	4th Cooling Ring Overhang, 2.0 from T.E.	I
9	Inner Liner	0	Panel Four, 11.4 from T.E.	S
10	Inner Liner	30	Panel Zero, 15.2 from T.E.	I
11	Inner Liner	30	1st Cooling Ring Overhang, 1.8 from T.E.	I
12	Inner Liner	45	Panel One, 8.6 from T.E.	I
13	Inner Liner	30	2nd Cooling Ring Overhang, 1.8 from T.E.	I
14	Inner Liner	30	Panel Two, 14.5 from T.E.	S
15	Inner Liner	30	3rd Cooling Ring Overhang, 2.2 from T.E.	I
16	Inner Liner	30	Panel Three, 12.7 from T.E.	S
17	Inner Liner	30	4th Cooling Ring Overhang, 2.0 from T.E.	I
18	Inner Liner	30	Panel Four, 11.4 from T.E.	S
19	Inner Liner	180	Panel One, 9.1 from T.E.	I
20	Inner Liner	180	Panel Two, 14.5 from T.E.	S
21	Inner Liner	180	Panel Three, 12.7 from T.E.	S
22	Inner Liner	180	Panel Four, 11.4 from T.E.	S
23	Inner Liner	108	Aft of Crossfire Port	S
24	Inner Liner	252	Aft of Crossfire Port	S
25	Rear Liner	0	25.4 Fwd of Dilution Holes	S
26	Rear Liner	0	10.7 Aft of Dilution Holes	S
27	Rear Liner	0	12.7 Aft of Trim Holes	S
28	Rear Liner	30	25.4 Fwd of Dilution Holes	S
29	Rear Liner	30	10.7 Aft of Dilution Holes	S
30	Rear Liner	30	12.7 Aft of Trim Holes	S
31	Transition Duct	90	38.1 from Combustor Axis	S
32	Transition Duct	180	38.1 from Combustor Axis	S
33	Fuel Nozzle	---	Stem Leading Edge, 34.3 from Flange	S
34	Fuel Nozzle	---	Stem Leading Edge, 40.6 from Flange	S
35	Fuel Nozzle	---	Stem Leading Edge, 47.0 from Flange	S

(1) I = Hot Side imbedded
    S = Cold Side surface
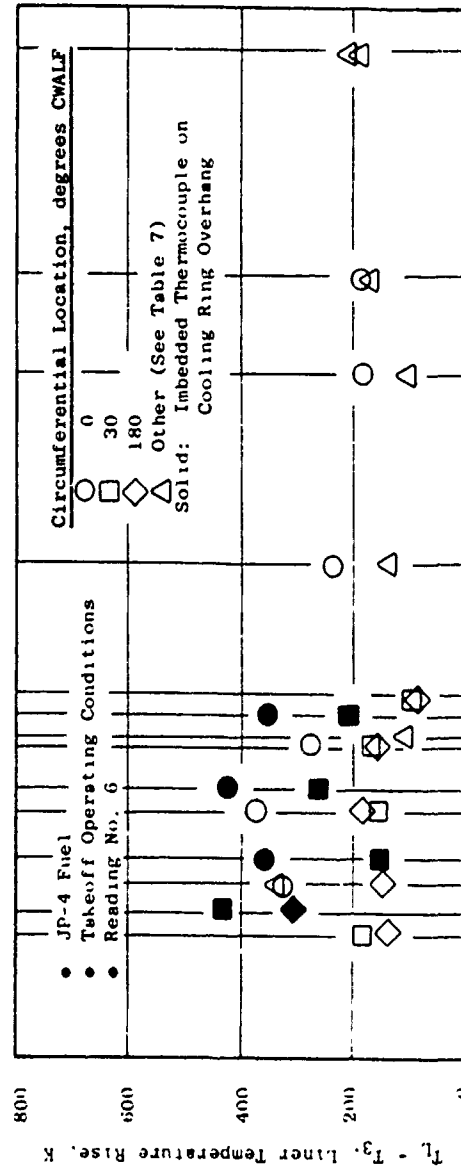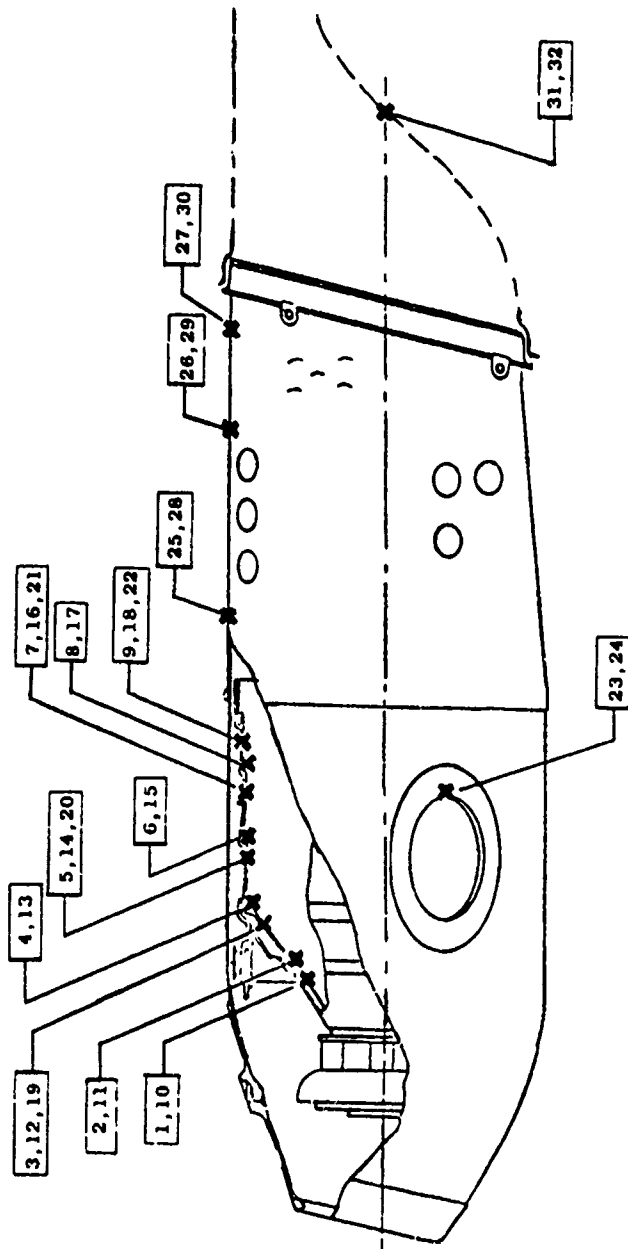
Figure 16. Combustor Liner Temperature Measurement Locations and Typical Measured Temperature Levels.
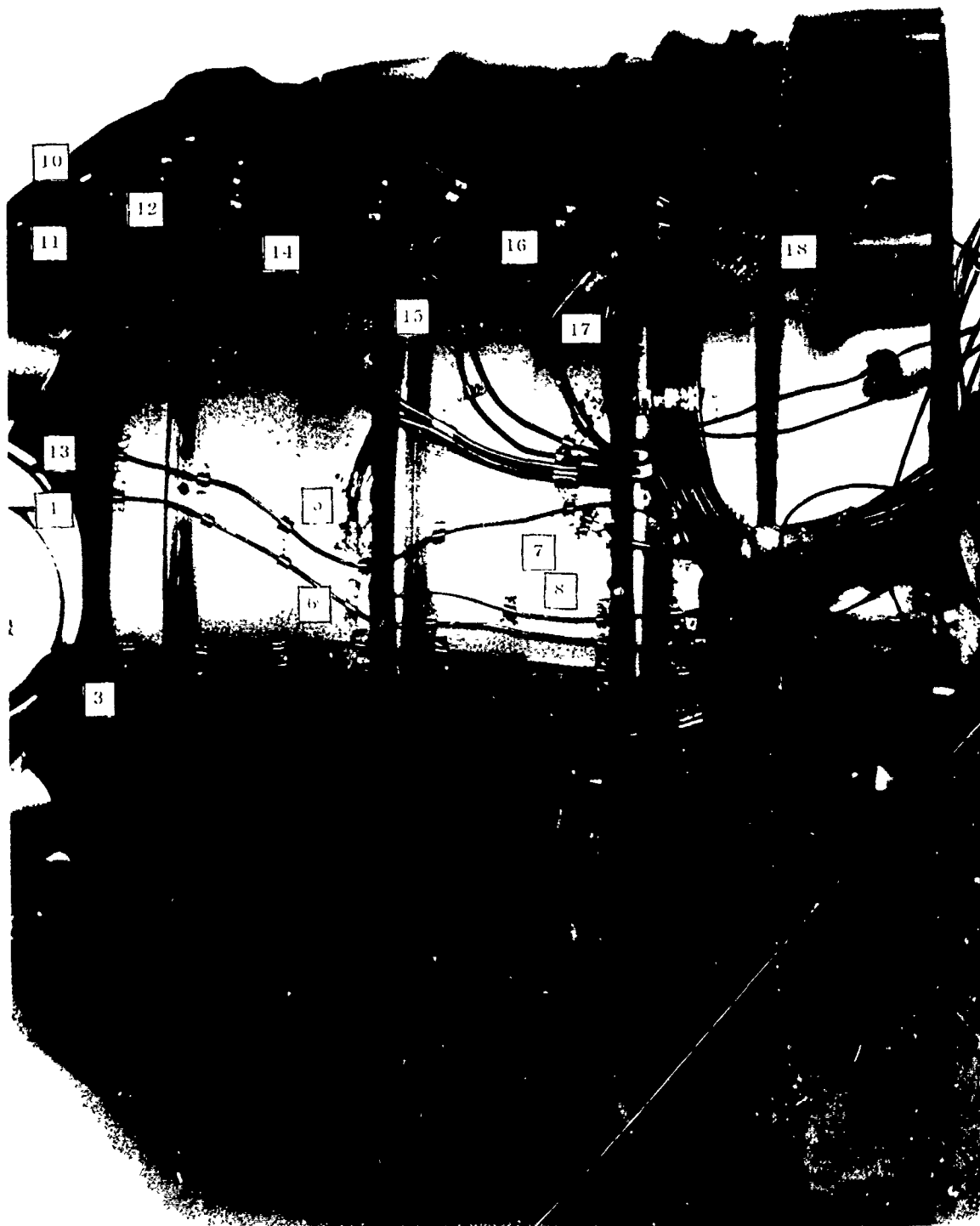
Figure 17.   Inner Liner Temperature Instrumentation at 0° CWALF.

Figure 18. Inner Liner Temperature Instrumentation at 180° CWALF.
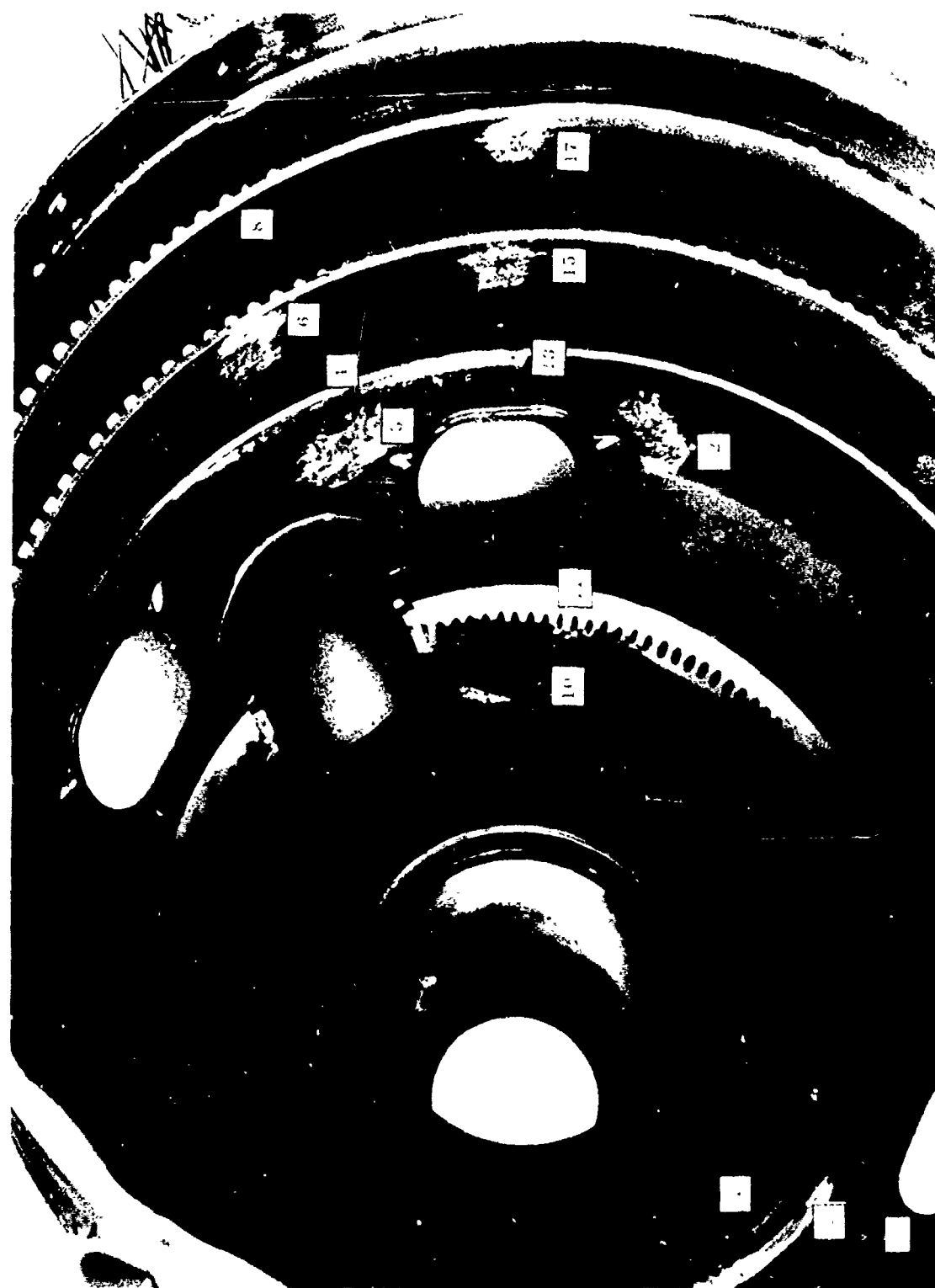
Figure 19. Dome Temperature Instrumentation.

Figure 20. Rear Liner Temperature Instrumentation.
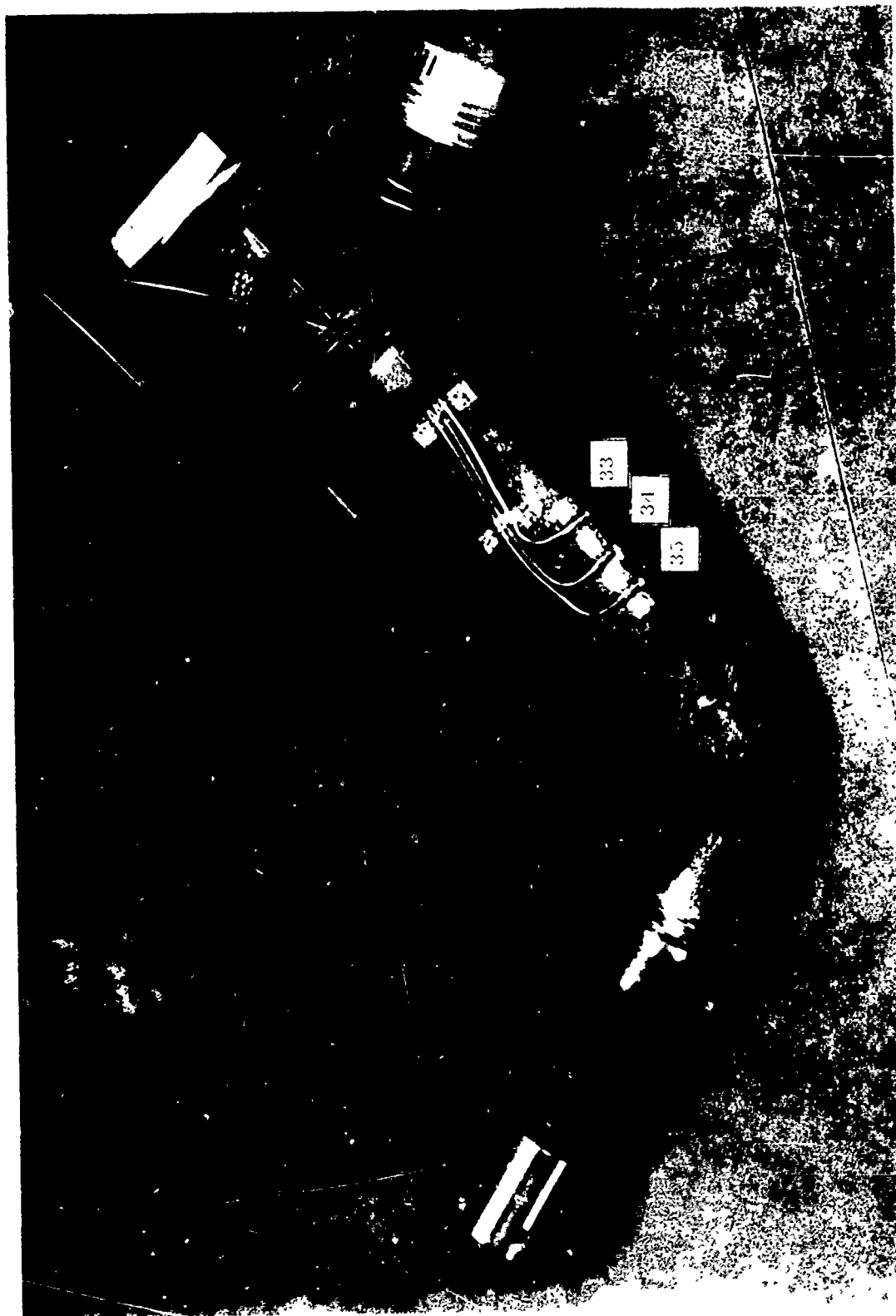
Figure 21. Fuel Nozzle Temperature Instrumentation.
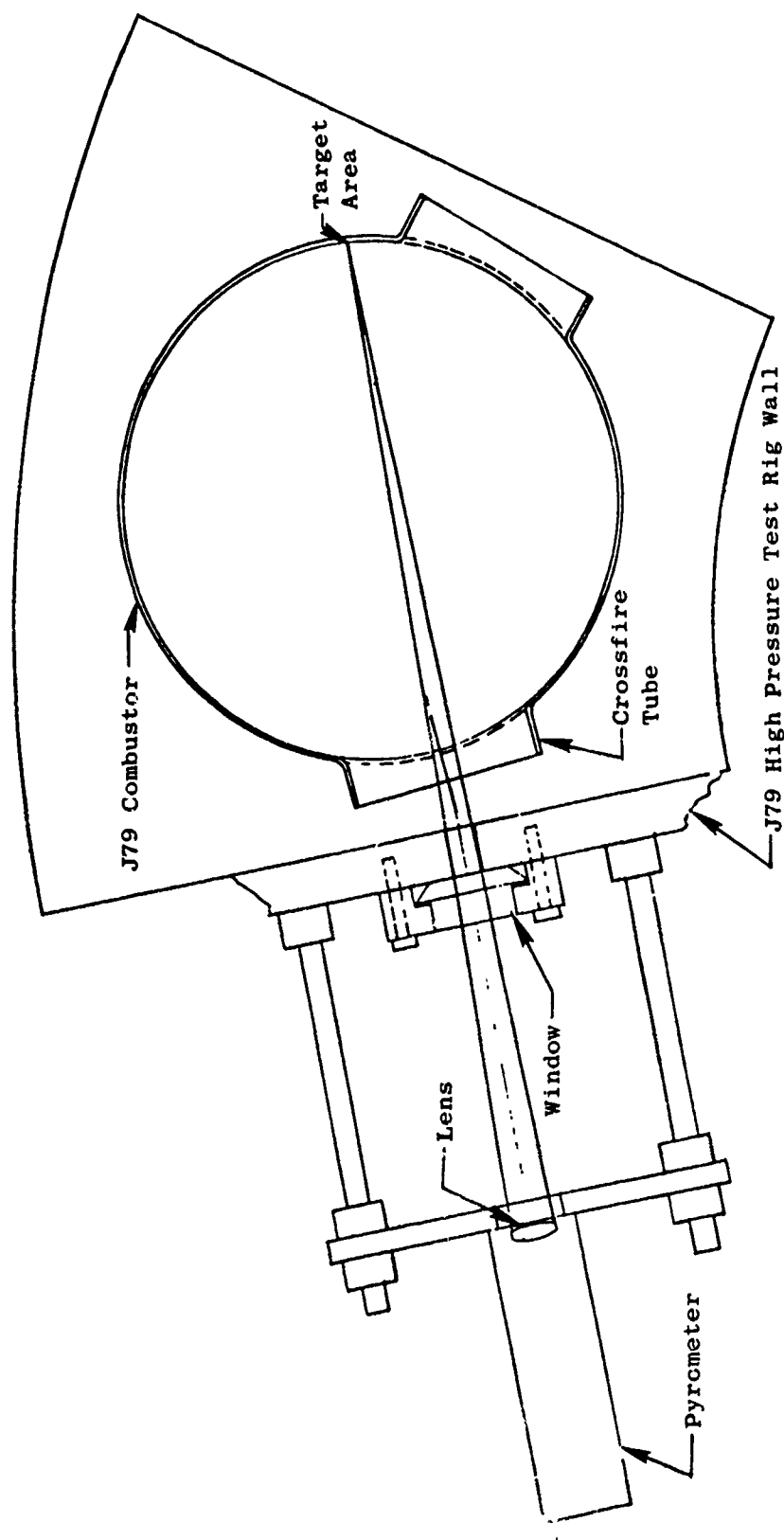
Figure 22. Optical Pyrometer Setup in High Pressure Test Rig.

calcium fluoride lens which is transparent to radiation of wavelengths less than three microns. The pressure seal at the test rig wall is formed by a sapphire window which is transparent to radiation of even longer wavelengths. The sapphire window was swept clean by a small flow of filtered air. The pyrometer was calibrated by viewing a resistance-heated-carbon backbody furnace through the same optical system used in the combustor test. The furnace temperature was measured with a disappearing-filament optical pyrometer.

3. High Pressure Test Procedures

A total of 14 high pressure rig tests were run: one for each test fuel plus a repeat test with fuel No. 1 to establish test variability. The same fuel nozzle and combustor were utilized in all tests.

Each test was conducted to the 9-point test schedule shown in Table 8. On Point No. 1, minimum lightoff and lean blowout limits at idle inlet conditions were determined. On Points No. 2 through 9, steady-state operating, performance, and emissions measurements were obtained at simulated engine idle, cruise, takeoff, and dash operating conditions. At each of these simulated engine operating conditions, data were recorded at two nominal fuel/air ratios: 80 and 100 percent of the engine cycle value corrected for the test fuel heating value. However, if the data indicated that the 100 percent fuel/air ratio point would locally exceed the gas temperature limits of the exit thermocouple rakes, a lower fuel/air ratio point was substituted. This limit was usually exceeded at simulated takeoff and dash conditions, so lower fuel/air ratio points were substituted and a higher fuel/air ratio was run at cruise conditions.

B. Cold-Day Ground Start/Altitude Relight Tests

Low-pressure/temperature single can combustor rig tests were conducted at simulated J79 engine ground cranking and altitude windmilling operating conditions to determine the cold-day ground start and altitude relight characteristics of each of the test fuels. The apparatus and procedures which were utilized are described in the following sections.

1. Low Pressure Test Rig Description

These tests were conducted in the Building 301 Combustion Laboratory at the Evendale Plant. This facility has capabilities for testing small combustor rigs over a wide range of simulated ground start and altitude relight conditions. Liquid nitrogen heat exchangers are used to obtain low fuel and air temperatures, and steam ejectors in the exhaust ducting are used to obtain low combustor inlet pressures.

The low-pressure, single-can J79 combustor rig used in these tests is shown in Figure 23. The combustor housing is made from actual engine parts and the rig exactly duplicates a one-tenth segment of the engine combustion system flowpath. Combustor inlet temperatures and pressures are measured with probes in the plenum chamber. The combustor assembly is installed from the rear of the combustor housing which bolts up to a segment of an engine combustor transition duct. An array of thermocouples is located in the transition

Table 8. High Pressure Test Point Schedule.

Test Point Number	W_3 Total Airflow kg/s	W_c Combustor Airflow, kg/s	P_3 Inlet Total Pressure, MPa	T_3 Inlet Total Temperature, K	V_r Reference Velocity, m/s	W_f(1) Fuel Flow Rate, g/s	f(1) Fuel/Air Ratio g/kg	Engine Simulation Operating Condition	Engine Simulation Inlet Pressure %	Engine Simulation Fuel/Air Ratio %
1	1.83	1.53	0.254	421	24.2	Determine ignition and Lean Blowout Fuel Flow		Idle	100.0	---
2	1.83	1.53	0.254	421	24.2	11.5	7.5	Idle	1υ0.0	80.0
3	1.83	1.53	0.254	421	24.2	14.4	9.4	Idle	100.0	100.0
4	2.94	2.46	0.47!	559	26.0	33.5	13.6	Cruise	100.0	100.0
5	2.94	2.46	0.471	559	26.0	46.8	19.0	Cruise	100.0	140.0
6	7.51	6.28	1.359	664	28.6	85.5	13.6	Takeoff	100.0	68.0
7	7.51	6.28	1.359	664	28.6	125.9(2)	20.0(2)	Takeoff	100.0	100.0
8	6.57	5.49	1.191	781	33.5	65.9	12.0	Dash	75.0	75.0
9	6.57	5.49	1.191	781	33.5	87.8(2)	16.0(2)	Dash	75.0	100.0

(1) Based on JP-4 fuel. For other fuels, adjust for heating value.

(2) Adjust (reduce) if necessary to exit rake peak temperture limit.

40
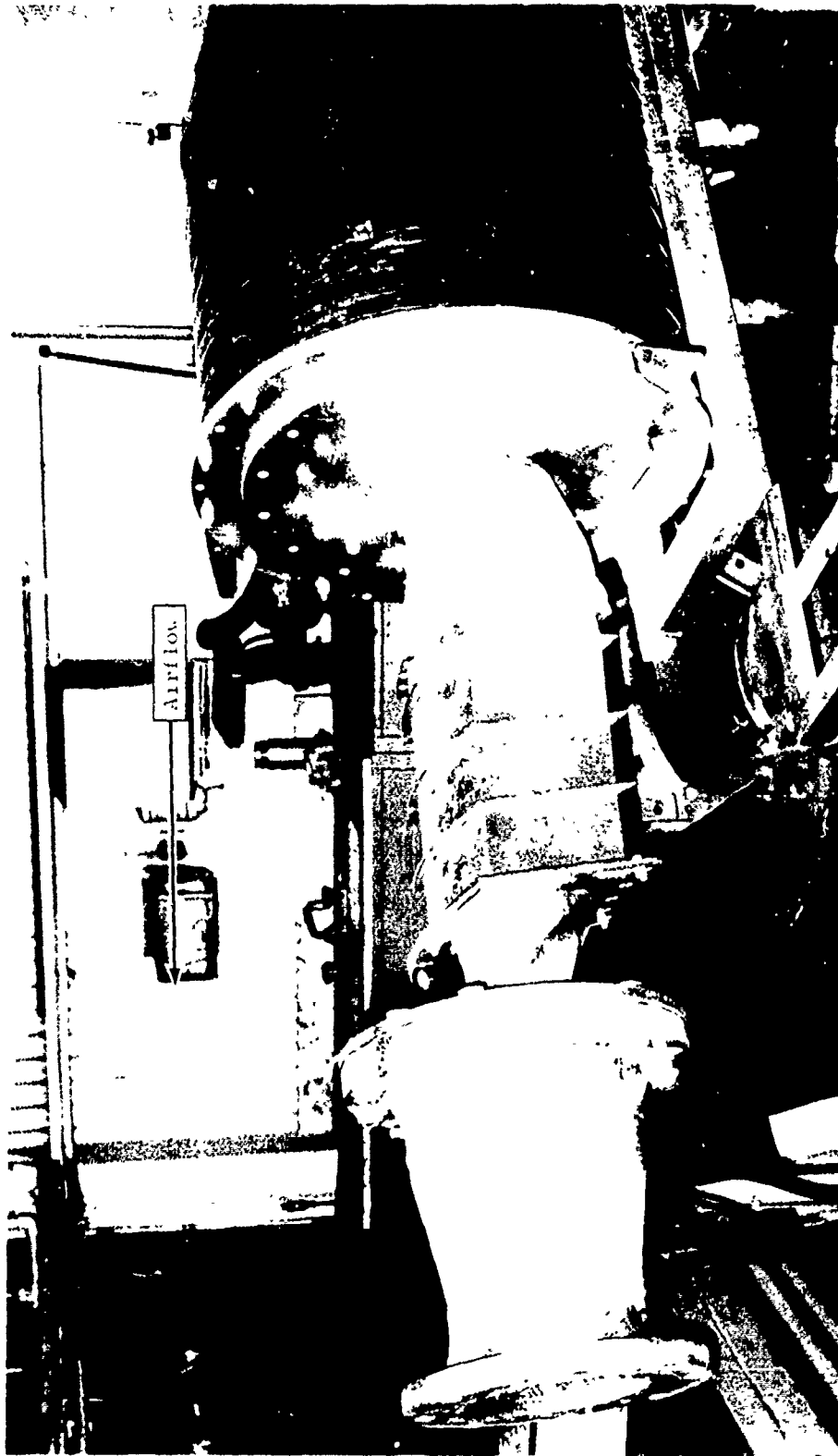
Figure 23. Low Pressure J79 Combustor Test Rig.

duct to sense ignition and blowout. This rig has no provisions for turbine cooling-air extraction.

Air obtained from the central supply system was dried at the facility to a dew point of about 240 K and metered with a standard ASME orifice. Fuel flow rates were measured with calibrated turbine meters corrected for the density and viscosity of each test fuel at the measured supply temperature. All temperature, pressure, and flow data were read on direct indicating instruments (manometers, potentiometers, etc.) and hand logged by the test operator.

2.   Cold-Day Ground Start Procedure

The first part of the test with each fuel was structured to evaluate cold-day ground starting characteristics. The test point schedule is shown in Table 9. The airflow rate (0.318 kg/s) and combustor inlet pressure (ambient) were set to simulate typical engine ground starting conditions (1000 rpm). Fuel and air temperature were lowered from ambient to 239 K minimum (JP-8 freeze point) in steps to simulate progressively colder days. At each temperature step, minimum ignition and lean blowout fuel flow rates were determined. Maximum fuel flow rate was taken as 12.6 g/s/can, which is well above the current engine minimum fuel flow rate (6.49 g/s/can). The test sequence was as follows:

1)   With inlet conditions set, energize the igniter and slowly open the fuel control valve until lightoff is obtained. Record lightoff fuel flow rate. Deenergize igniter.

2)   Slowly decrease fuel flow rate to blowout. Record lean blowout fuel flow rate.

3)   Decrease fuel and air inlet temperatures in 5 to 8 K increments and repeat Steps 1 and 2.

When the minimum temperature limit was established, the altitude relight portion of the test was initiated.

3.   Altitude Relight Test Procedure

The second portion of the test with each fuel was structured to evaluate altitude relight and stability characteristics. The test schedule is also shown in Table 9. Investigations were carried out at four airflow rates (0.23, 0.41, 0.50, and 0.91 kg/s) selected to span the J79 engine altitude relight requirement map (Figure 8). Air temperature was selected from the windmilling data and ranged from 244 K to ambient. Fuel temperature was matched to the air temperature. The test sequence was structured to determine:

1)   The maximum relight and blowout pressure altitudes with current engine minimum fuel flow rates (4.22 g/s/can).

2)   The minimum relight and lean blowout fuel flow rates at the relight altitudes determined in (1).

42

Table 9. Low Pressure Test Point Schedule.

Test Point Number	Simulated Flight Altitude, km	Simulated Flight Mach Number	W_c, Combustor Airflow, kg/s	P_3, Air Inlet Pressure, kPa	T_3, Air Inlet Temperature, K	T_f Fuel Inlet Temperature, K	W_f, Fuel Flow, g/s	Comments(1)
1.1.1	0	0	0.318	101	278	278	0-12.60	Determine W_f at LO
1.1.2	0	0	0.318	101	278	278	0-12.60	Determine W_f at LBO
1.2.1	0	0	0.318	101	272	272	0-12.60	Determine W_f at LO
1.2.2	0	0	0.318	101	272	272	0-12.60	Determine W_f at LBO
1.3.1	0	0	0.318	101	266	266	0-12.60	Determine W_f at LO
1.3.2	0	0	0.318	101	266	266	0-12.60	Determine W_f at LBO
Continue 1.X.X. Sequence Until Ground Start T_3 Limit is determined, or $T_3 = 239$ K								
2.1.0	15.2	0.89	0.227	24.1	244	244	6.49	Starting point for Series
2.1.1	--	--	0.227	--	244	244	6.49	Determine P_3 min. at LO
2.1.2	--	--	0.227	--	244	244	6.49	Determine P_3 min. at PBO
2.1.3	--	--	0.227	--	244	244	0-12.60	Determine W_f min. at LO
2.1.4	--	--	0.227	--	244	244	0-12.60	Determine W_f min. at LBO
2.2.0	15.2	1.08	0.408	41.4	278	278	6.49	Same sequence as 2.1 to determine altitude LO, LBO, and PBO limits.
2.3.0	15.2	1.14	0.499	62.0	Amb.	Amb.	6.49	
2.4.0	15.2	1.22	0.907	68.9	Amb.	Amb.	6.49	

(1) LO = Lightoff (Increasing W_f or P_3)

    LBO = Lean Blowout (Decreasing W_f)

    PBO = Pressure Blowout (Decreasing P_3)

The test sequence was as follows:

1) With 15.7 km altitude conditions set, energize the igniter, set fuel flow rate at 6.49 g/s, then increase combustor inlet pressure (reduce altitude and flight Mach number) until ignition occurs. Deenergize the igniter and record maximum relight altitude conditions.

2) With fuel flow rate at 6.49 g/s, slowly reduce combustor inlet pressure until blowout occurs. Record maximum pressure altitude blowout conditions.

3) Energize igniter and increase fuel flow until lightoff. Deenergize igniter and record minimum lightoff fuel flow rate at maximum relight altitude.

4) Slowly reduce fuel flow rate until blowout. Record lean blowout fuel flow rate at maximum relight altitude conditions.

5) Repeat Steps 1 through 4 at each airflow setting.

C. Fuel Nozzle Fouling Tests

Tests with the low and high thermal stability fuels (No. 2 Diesel and JP-8 respectively) were conducted to determine the relative tendency to cause fuel nozzle fouling, which might be in the form of valve sticking and/or orifice plugging. The J79 fuel nozzle is known to have a long troublefree service life and to be quite tolerant of fuel property variations. It was anticipated, therefore, that the test conditions would need to be far more severe than encountered in normal service to produce significant fouling in a reasonably short time.

The tests were conducted in the Building 304 1/2 Combustion Laboratory using a 7.62 by 12.7 cm flame tunnel setup shown in Figures 24 and 25. In this setup, hot fuel is pumped through the fuel nozzle which is immersed in a high velocity hot gas stream to simulate engine operations. Thermocouples welded to the upstream side of the nozzle stem (Figure 21) were used to monitor and control the nominal peak metal temperature at 672 K which usually required an inlet gas temperature of about 720 K. Two thermocouples immersed in the fuel line close to the nozzle were used to monitor and control fuel inlet temperatures. A cylindrical fitting was fabricated and attached to the nozzle tip to conduct spent fuel to a 3.785 m^3 fuel cart.

Fuel from the supply system was heated to approximately 422 K by high pressure steam, then heated to the desired temperature using Therminol 55 heat transfer fluid. The latter was supplied by a Chromalox electric fluid heat transfer system, Model PFOV-650-9. Heat transfer from the Therminol to the fuel as well as from the steam to the fuel, were accomplished by Graham Heliflow heat exchangers.

In each test, one-hour simulated mission cycles were run, as indicated in Figure 26. For fifty-seven minutes of each hour, tests were run at a simulated steady-state cruise condition, but to reduce fuel requirements to

44
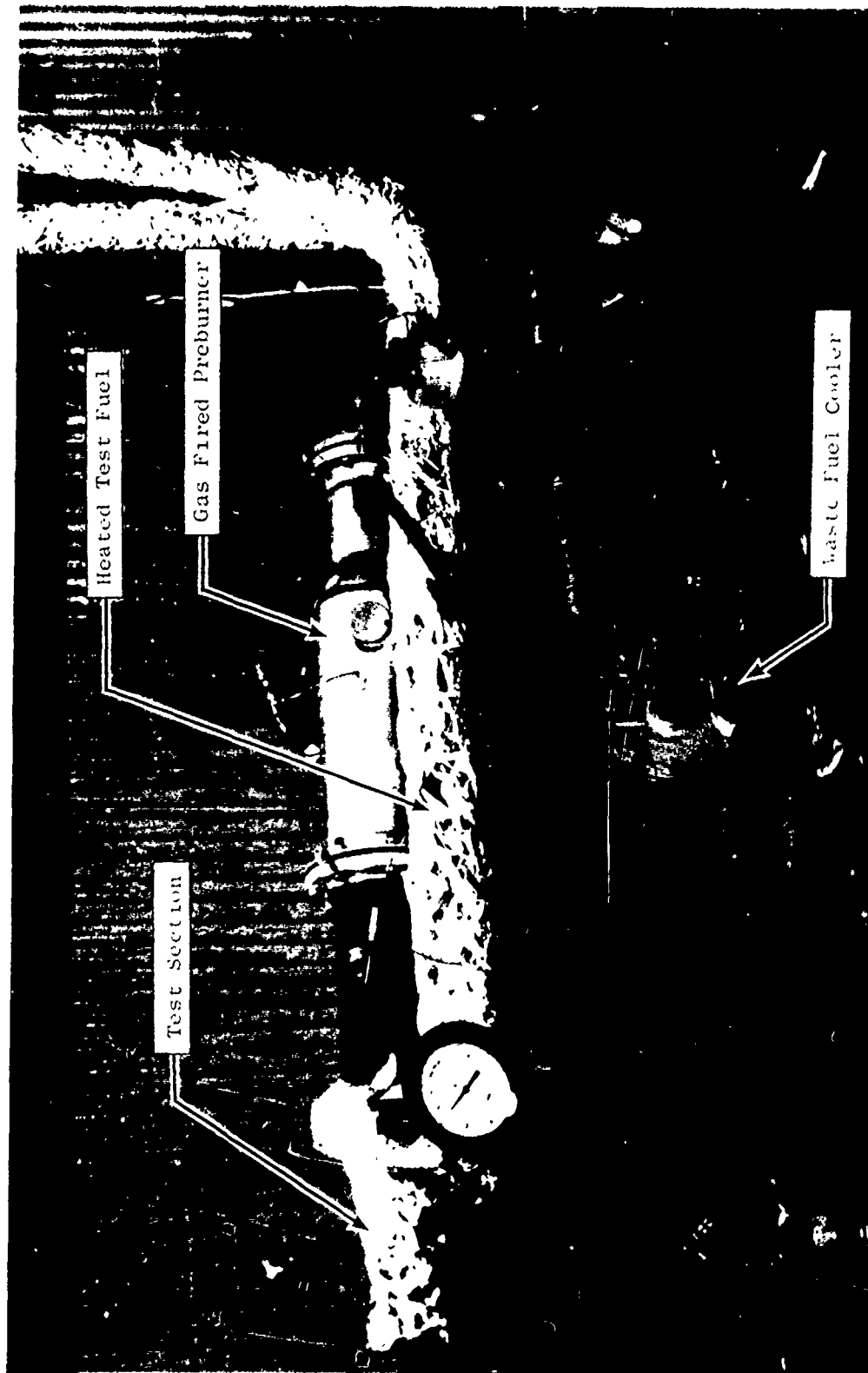
Figure 24. Fuel Nozzle Fouling Test Rig - Overall Installation.
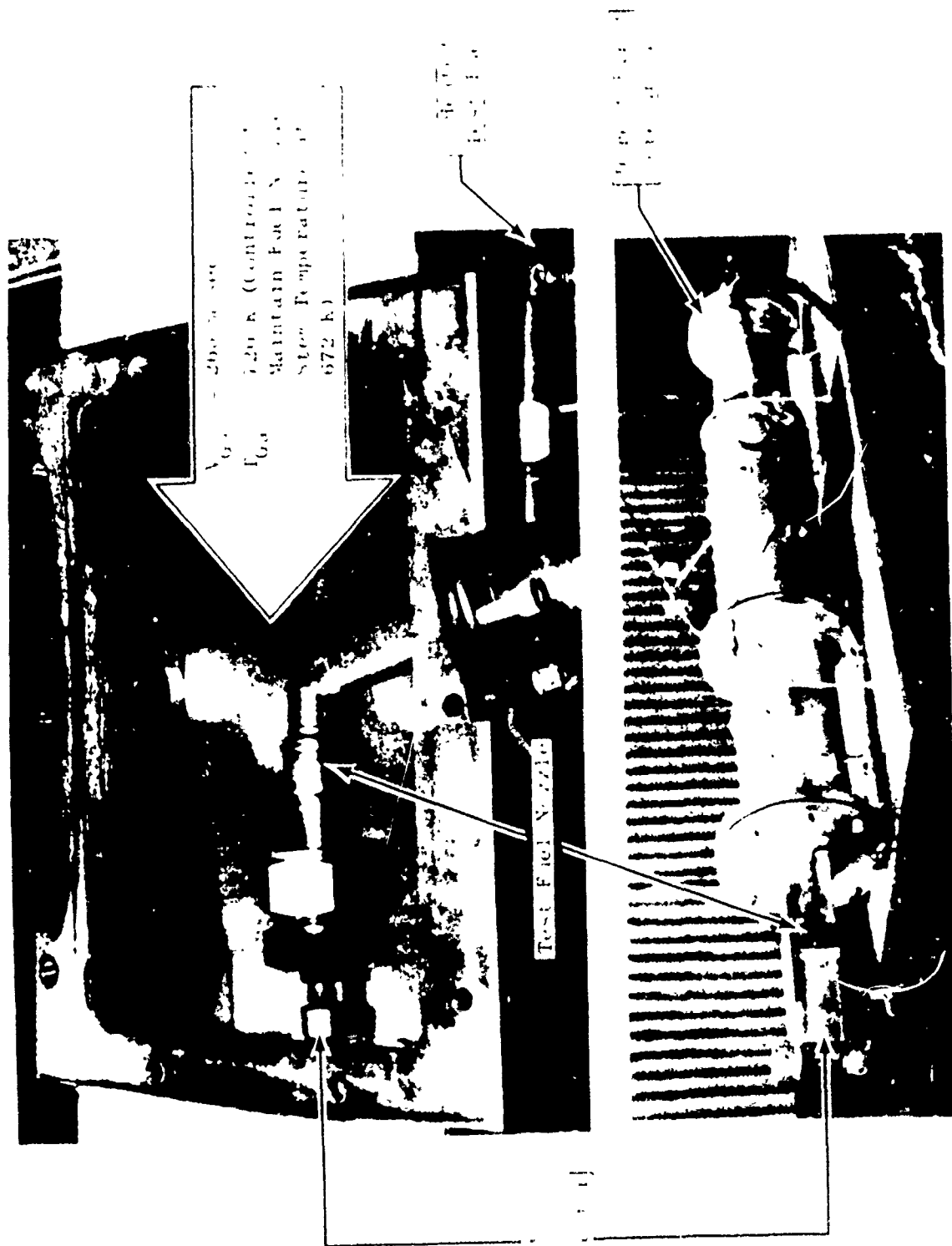
Figure 25. Fuel Nozzle Fouling Test Rig – Details.
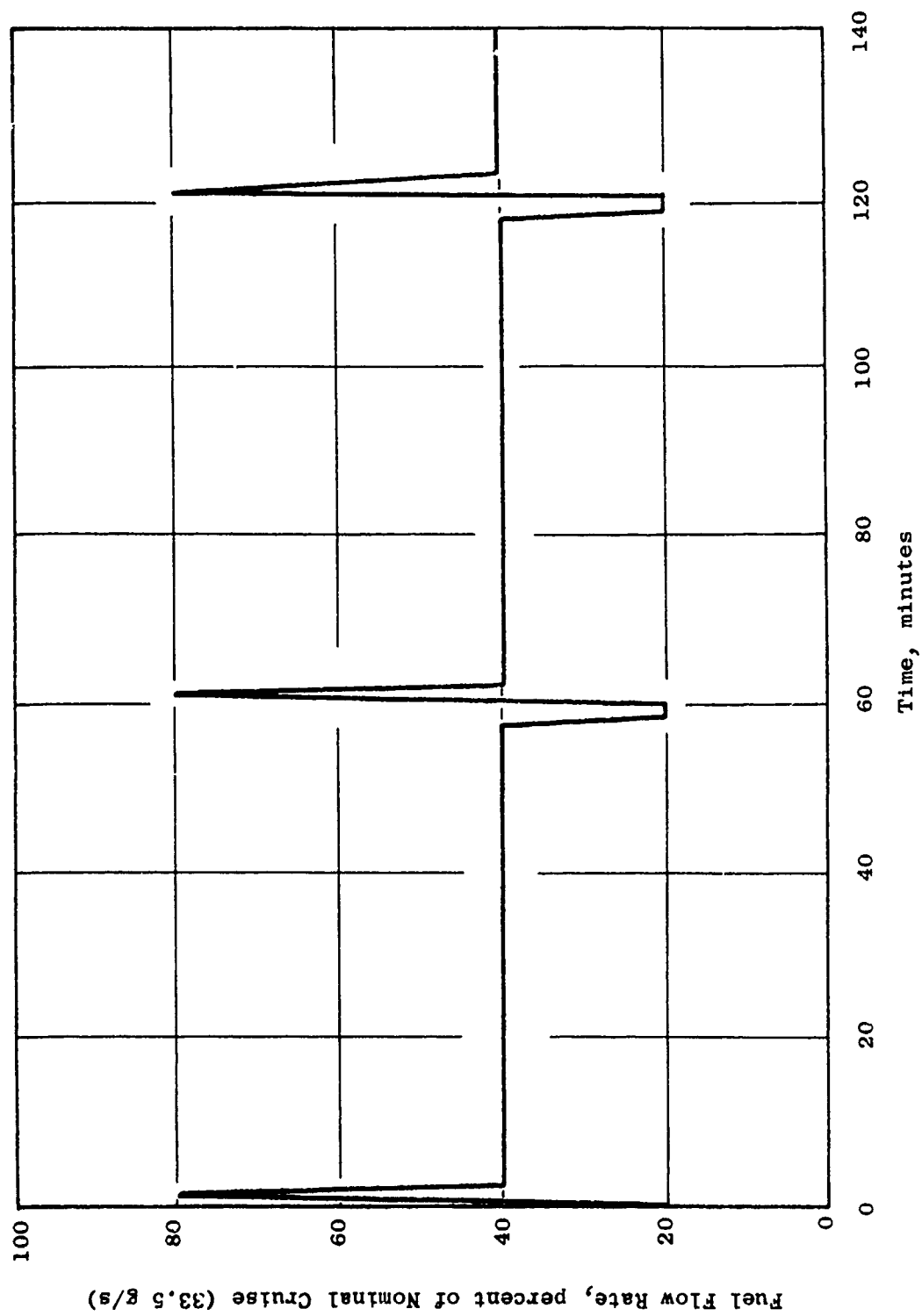
Figure 26. Fuel Nozzle Fouling Test Cycle.

47

a more manageable volume, the flow rate maintained was reduced to 13.4 g/s, which is only 40% of actual engine cruise flow rate. This is still high enough to assure flow through the secondary system. To add realism to the test, flow rates were increased and decreased (as shown in Figure 26) without changing heat inputs, to obtain flow divider valve action, short temperature excursions, and flushing action between the simulated cruise periods.

In order to avoid excessive temperatures in the fuel nozzle at startup and shutdown, the following procedures were followed:

For startup:

1) Establish desired fuel flow rate.

2) Set desired fuel temperature.

3) Establish airflow rate of 0.45 kg/s.

4) Start burner and set desired stem temperature

For shutdown:

1) Turn off preburner fuel supply.

2) Turn off steam supply and Chromalox power supply.

3) Open Therminol bypass around Graham heat exchanger.

4) Remove insulation from nozzle.

5) When nozzle temperatures drop to 394 K, shut off fuel and air supplies, remove nozzle and recalibrate.

Normally, calibration of the nozzle was accomplished at the start and after every six hours of operation on the test cycle. However, if it appeared that the calibration was, or might be, changing rapidly, recalibration was performed as frequently as every three hours. Under mild conditions which caused little or no change in calibration, the test was continued up to 75 hours. Under severe conditions, the test was terminated at around 20 hours, which was adequate to establish a trend.

D. Test Fuel Handling Procedures

The test fuels were delivered as needed by a USAF multicompartment tank trailer, and stored in General Electric multicompartment tank trailers and underground tanks, depending on the availability of storage and the volumes of fuel required. All of this tankage was used previously only in clean distillate service. Prior to loading with a test fuel, each tank was drained and visually examined to be sure it was empty. It was then rinsed with a small volume of test fuel and drained again before loading. In the case of of underground tanks, they could not be completely emptied by their installed pumps because their suction lines terminated several inches above the bottom.

48

In these cases, the manhole covers were removed and a portable pump was used to empty the tank. It was then rinsed with clean aviation kerosene and re-emptied. This process was repeated as often as necessary until the rinsings appeared as clean as the clean kerosene.

The fuels for the low-pressure tests were handled in drums filled from the storage tanks. Before loading, the drums were examined to be sure they were empty and clean. They too, were rinsed with a small volume of test fuel before loading.

All the storage tanks and drums of test fuels were carefully marked with the appropriate fuel identification.

Before taking data on any test point, the fuel system connecting the test fuel supply tank with the test vehicle was flushed with a quantity of test fuel equal to at least twice the volume of the connecting system.

Each test site had a provision for taking a representative fuel sample from the fuel supply line as close as practical to the test vehicle. Duplicate 0.95 dm^3 samples of each test fuel were taken during each run for all tests except the fuel nozzle fouling tests, in which case 3.8 dm^3 samples were taken in epoxy-lined containers. Before taking any sample, the sampling line was first flushed, then the sample container was rinsed twice with the test fuel. All sample containers were labeled for complete identification, logged, and delivered to the USAF for analysis.

It should be noted that the 13 test fuels used in this program were blended anew to duplicate the 13 fuels used in the two preceding programs (References 1 and 2). Since it is likely that fuels of the same number, blended on two different occasions, will differ slightly in composition and analysis, those used in this program have been distinguished by adding the suffix "A" to their numerical designations.

Fuel No. 13 was delivered on two consecutive days, for a total quantity of 15.14 m^3. This material was co-mingled and used in fouling tests Nos. 1, 2, and 3, and depleted after test No. 3. A third shipment of 7.57 m^3 of Fuel No. 13 was then received, and used in fouling tests Nos. 4 and 6.

Since gas chromotographic analyses performed by the Air Force on the co-mingled shipments and on the third shipment showed a slight difference in composition, it was believed that the two batches might have different thermal stability breakpoints. Therefore, they were treated as different fuels and tested separately on the JFTOT to determine their breakpoints.

E.   Data Analysis Procedures

Generally standard data reduction and presentation techniques were employed. Key parameters and calculation procedures are indicated in Table 6 and Appendix B. Some additional special procedures are described in the following sections.

49

1. Fuel Property Correlation Procedures

    Analyses of the experimental test results were conducted to: (1) cor-
relate the performance and emission parameters with combustor operating con-
ditions; (2) as appropriate, correct the measured rig data to true standard
day engine operating conditions; and (3) correlate the corrected data with
the appropriate fuel properties from Section III. Generally, these procedures
were identical to those utilized in the previous J79 combustor evaluations and
are described in Reference 1. In the few cases where new procedures have been
utilized they are described in the Results Section, Section VI.

2. Combustor Life Prediction Procedures

    The advanced low-smoke J79-17C combustor has a much improved life compared
with the older design, J79-17A, which was the subject of Reference 1. The im-
proved life is currently being demonstrated in U.S. Navy J79-10 service (Refer-
ence 8) and the time between replacements is being extended as experience with
this combustor increases. The failure mode of most significance to this study
is the development of low cycle fatigue cracks in the forward portion of the
combustor due to thermal gradients. The cracks form in the vicinity of the
cooling slots in the conical dome region and gradually propagate upstream.
The conical shape of this structure, however, permits limited cracks to exist
while still retaining the structural shape, thus resulting in a life signifi-
cantly longer than the time to crack initiation.

    A second life limitation feature occurs in the vicinity of crossfire
elements. However, this limitation is thought to be vibration induced and
not affected by fuel type.

    The remainder of the liner, in general, lasts satisfactorily until hot sec-
tion overhaul. However, since the cooling on these liners was not grossly over
designed, if fuel type greatly increased the metal temperatures, new life
limiting regions could become important.

    In its initial design and throughout its development, the J9-17C liner
temperatures, stresses, and life have been calculated by deta. ' computer
analyses, with adjustments to the heat transfer inputs as test   ta identified
the magnitude of specific contributors to the liner heating. referring to
Figure 27, the combustor is heated by convection and radiation from the hot
combustion gases. These gases are hottest in the r in end of the burner
and drop toward the exit temperature as the air c   through the dilution
holes mixes and cools the gas. The local gas velocities and temperatures
are calculated by computer program based on the air distribution, and these
values are then modified as indicated by subsequent combustor test data. The
combustor liner is protected by the film air introduced through the film cool-
ing slot. The rate at which the hot combustor gases mix through this protec-
tive film has been established from laboratory test data and combustor experi-
ence for the various specific film slots throughout the liner. Additional
inputs to the heat transfer calculation include the flame radiation heating,
metal radiation cooling, the convective cooling rates on the cold side of the

$$T_{Film} = T_{Gas} - \eta \left(T_{Gas} - T_{Coolant} \right)$$

η = Film Effectiveness

T_{Gas} = Flame Temperature

$T_{Coolant}$ = Coolant Temperature
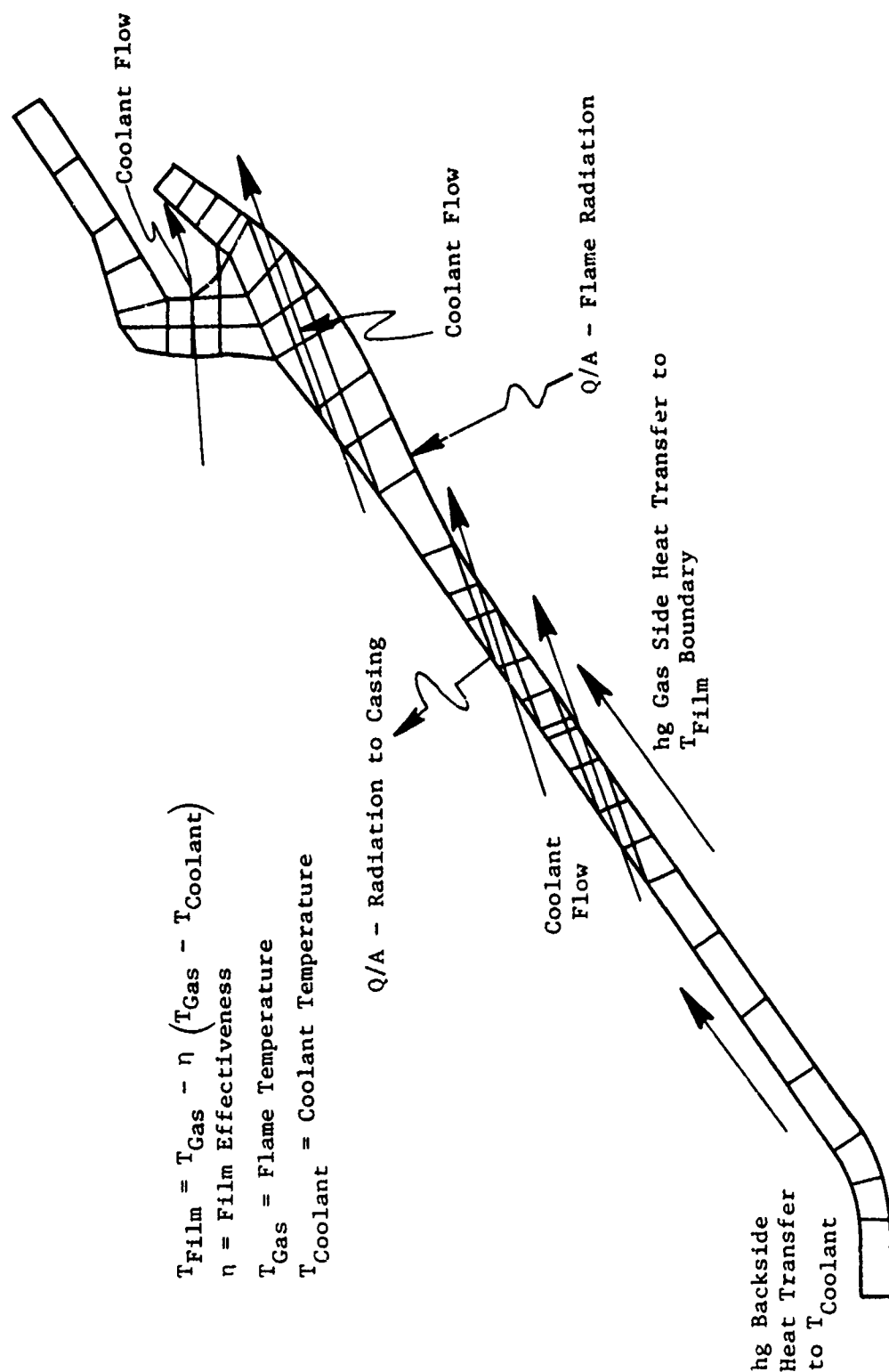
Figure 27. Node Model for J79 Combustor Showing Heat Transfer Quantities.

51

liner, and the impingement cooling rate on the cooling slot overhang. The flame radiation being the least well-defined from other data can be determined by back calculation from measured metal temperatures. With the aid of a computer program to calculate the thermal conduction through the metal structure, the above heat transfer inputs or correlations are used to calculate the detailed temperature distribution within the combustor liner. These temperatures are then used as input to a stress analysis program together with inputs for mechanical and aerodynamic loads, which then calculates the elastic stresses throughout the structure. These stresses are then used together with low cycle fatigue material properties (Figure 28) to predict life to first cracking, with an appropriate multiplier from experience to determine total life.

3. Turbine Life Prediction Procedures

If alternate fuels created substantial changes in temperature pattern factor or temperature profile in the combustor exit gases, changes in turbine component life would be predicted. However, as discussed in Section VI-A-6, no changes were found in these parameters.

The turbine vane heat load is made up of both convection and radiation and the relative levels vary around the perimeter of the vane. The leading edge of the vane has a view of the dome region and thus changes in flame luminosity due to fuel type would result in changes in the radiation load and corresponding changes in the vane leading edge temperature. The relative radiation load depends also on the view factor of the dome region. The rear liner and transition piece have small view factors of the dome and changes in these metal temperatures, due to changes in fuel type, provide an indication of the vane temperature changes. Figure 29 illustrates the very small view factor which the stator leading edge has of the luminous flame region and it also shows the similar view factor for the instrumented liner location. Temperatures were measured in the program on both the inner and rear liners as well as on the transition piece as discussed in Section V-A-2. As discussed in Section VI-A-6, the rear liner temperatures, which are well away from the high flame luminosity, were less affected by fuel changes than were the inner liner temperatures, and the effect decreased at locations farther downstream. A thermocouple was located on the transition piece such that the view factor of the dome region was very similar to that of the stator vanes. The temperature at this location was essentially unaffected by changes in fuel hydrogen content. Since the transition piece temperature was unaffected by fuel hydrogen content, negligible effects are predicted for the stator vane.
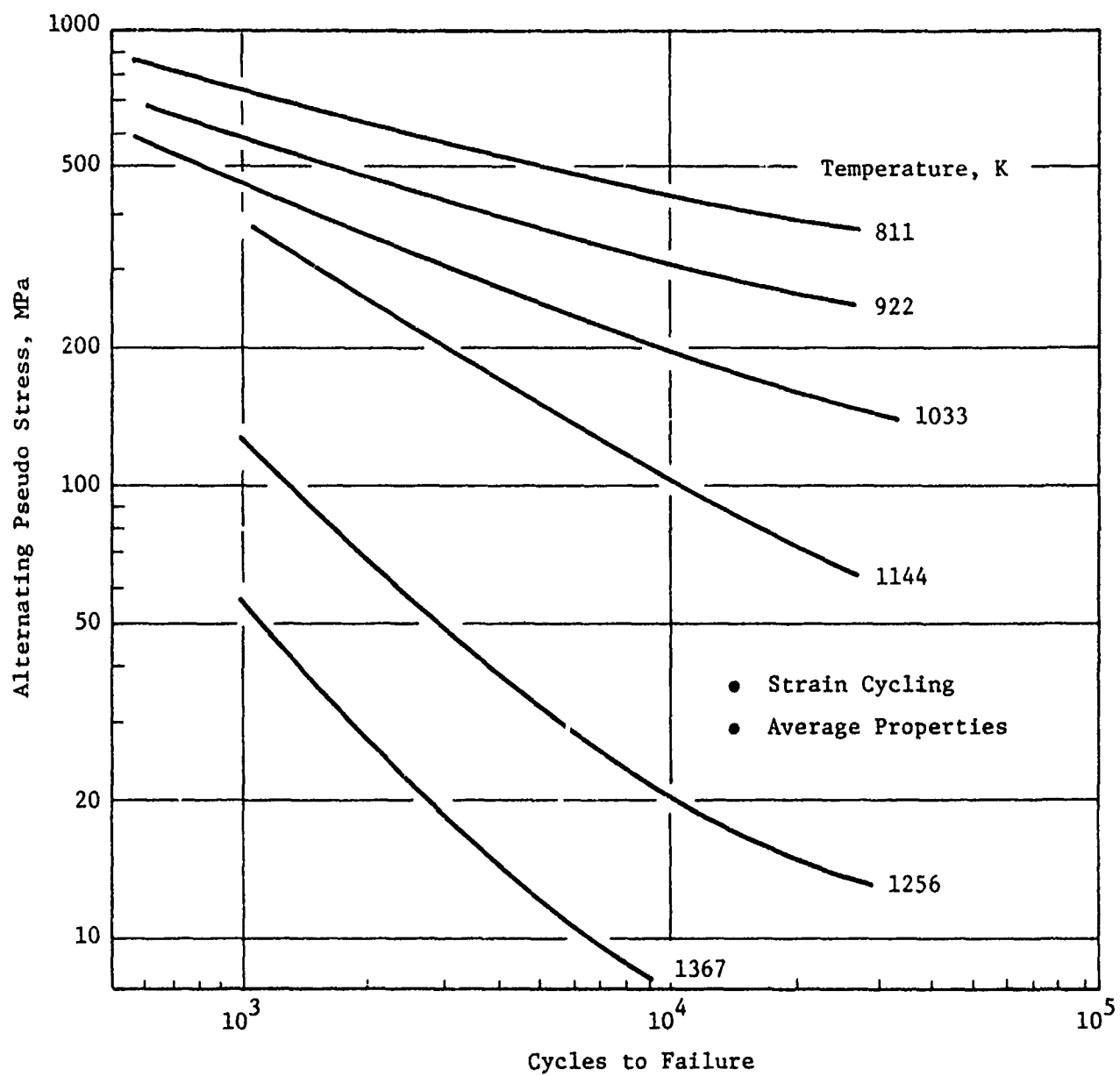
Figure 28. Fatigue Diagram for Hastelloy-X Sheet Stock.
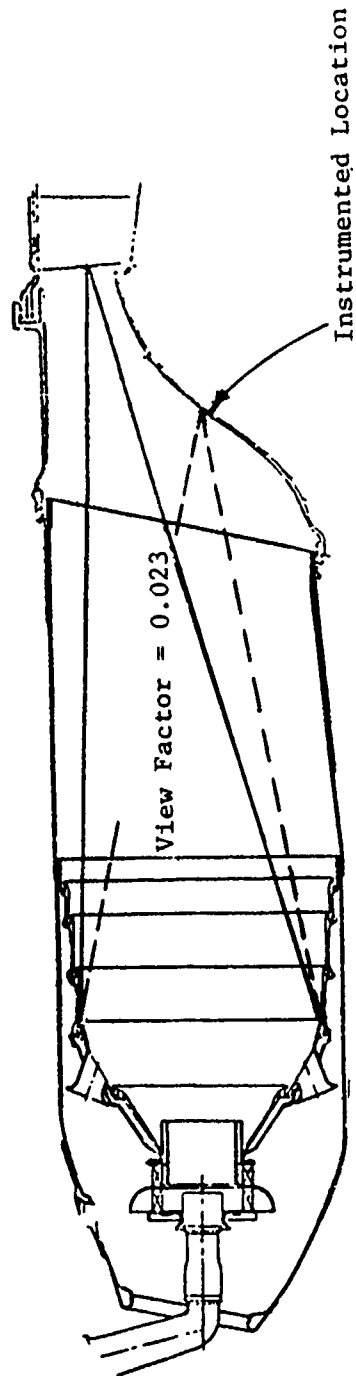
Figure 29. Turbine Nozzle Diaphragm and Instrumented Location View Factors.

SECTION VI

RESULTS AND DISCUSSION

All planned test series (35 total) were completed and no major problems were encountered. In general, results were well ordered and consistent with published data insofar as comparisons could be made. Detailed test results, which are listed in Appendices B through E, are summarized and discussed in the following section. Engine system life prediction analyses based on these results are then presented in Section VI-B. Comparisons of these and previously obtained data are presented in Section VI-C.

A. Experimental Test Results

Fourteen high-pressure rig tests were conducted to obtain the performance/emission/durability data. These data are listed in Appendices B and C and summarized in Sections VI-A-1 through VI-A-7. Fourteen low pressure rig tests were conducted in parallel to obtain the ground start and altitude relight data. These data are listed in Appendix D and summarized in Sections VI-A-7 and 8. Also in parallel, seven fuel nozzle fouling tests were conducted to obtain the data listed in Appendix E and summarized in Section VI-A-9.

1.   CO and HC Emissions

Carbon monoxide (CO) and unburned hydrocarbons (HC) are both products of incomplete combustion and are, therefore, generally highest at low power operating conditions (idle and cruise). Figure 30 shows the strong effect of combustor operating conditions on the CO emission levels with JP-4 fuel. At idle operating conditions, the CO emission index is about 66 g/kg which corresponds to a combustion inefficiency of about 1.5%, and is about the same level as that produced by the standard combustor (Reference 1).

At cruise, takeoff, and dash operating conditions, the CO emission levels are approximately 15, 2, and 1%, respectively, of the idle CO emission level, which indicates the strong effect of combustor inlet temperature and pressure on combustion reaction rates, and hence, on combustion efficiency and CO emission levels. In this correlation, the fuel/air ratio and temperature effects were determined by multiple regression curve-fit techniques of these data, and all are somewhat stronger than were found for the standard combustor (Reference 1).

Carbon monoxide emission trends like those shown in Figure 30 were obtained with each of the fuels, and a summary listing of the results is presented in Table 10. At takeoff and dash operating conditions, CO emission levels are low with all of the fuels, so no fuel property effect is evident. However, as shown in Figure 31, at both cruise and idle operating conditions, CO emission levels are clearly lowest with the baseline JP-4 fuel and up to 50% higher with those fuels having reduced hydrogen content, reduced vaporization properties (as indicated by both 10 and 90% recovery temperatures) and reduced atomization properties (as indicated by calculated relative spray droplet size, SMD/SMD_{JP-4}, from Table A-3).

55
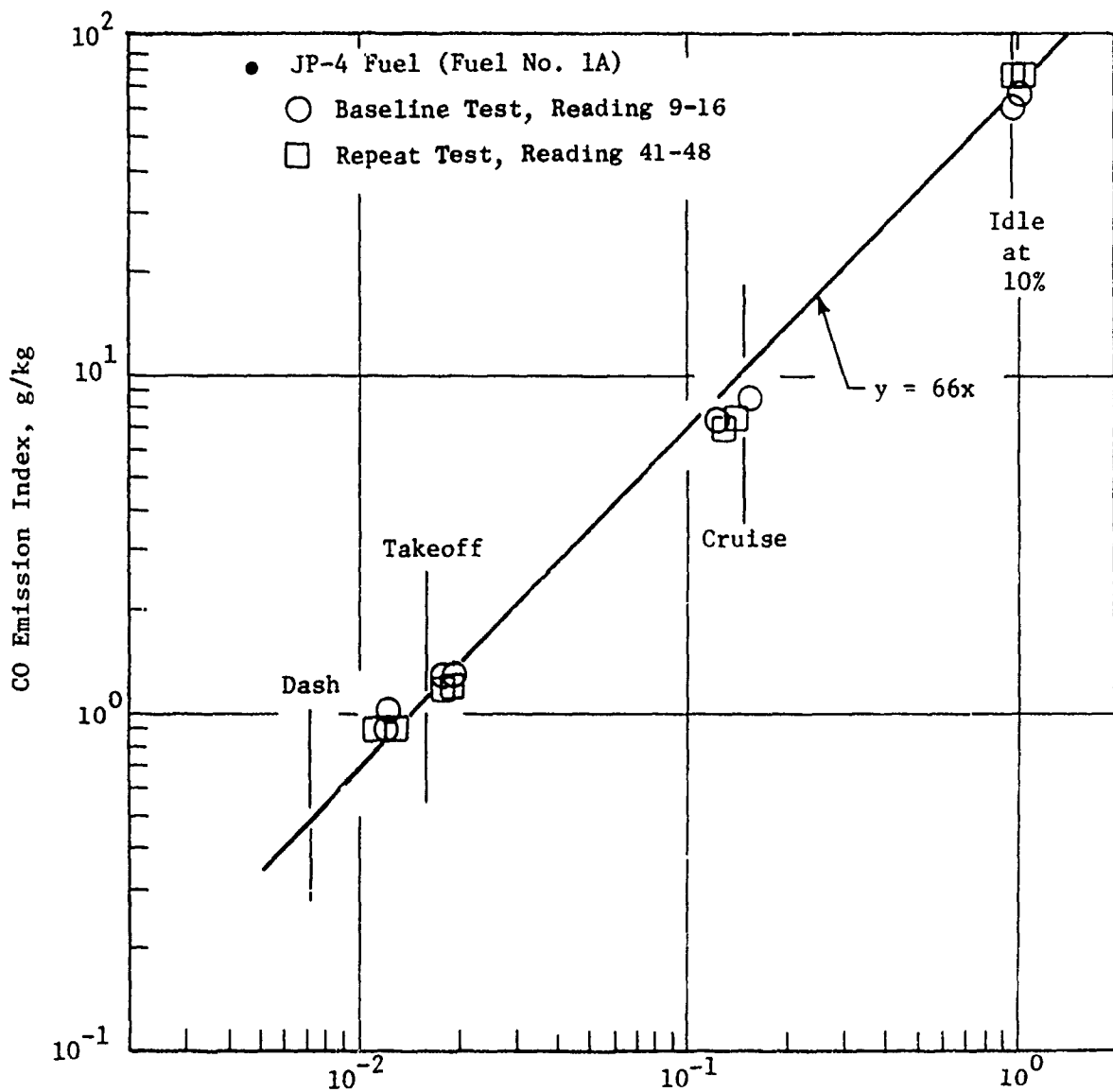
$$S_{co} = \left(\frac{V_r}{24.2}\right) \left(\frac{0.254}{P_3}\right)^{1.25} \left(\frac{9.42}{f}\right)^{0.5} \left[\exp\left(\frac{421-T_3}{133}\right)\right] \text{, m/s, MPa, g/kg, K}$$

Figure 30. Effect of Operating Conditions on CO Emission Levels.

Table 10. Summary of CO Emission Test
Results.

Fuel	CO Emission Index, g/kg			
Number	Idle	Cruise	Takeoff	Dash
1A	63.3	8.5	1.1	0.6
1AR	71.0	7.8	1.0	0.5
2A1	85.2	9.0	1.1	0.6
3A	100.4	10.1	0.9	0.4
4A	110.5	10.9	1.3	0.6
5A	92.1	10.1	1.2	0.6
6A	90.2	9.7	1.3	0.6
7A	104.2	11.6	1.2	0.6
8A	80.4	11.7	1.5	0.6
9A	87.6	11.3	1.6	0.6
10A	96.1	9.2	1.3	0.6
11A	96.1	9.2	1.2	0.6
12A	94.3	9.9	1.2	0.6
13A1	100.9	12.9	1.5	0.7
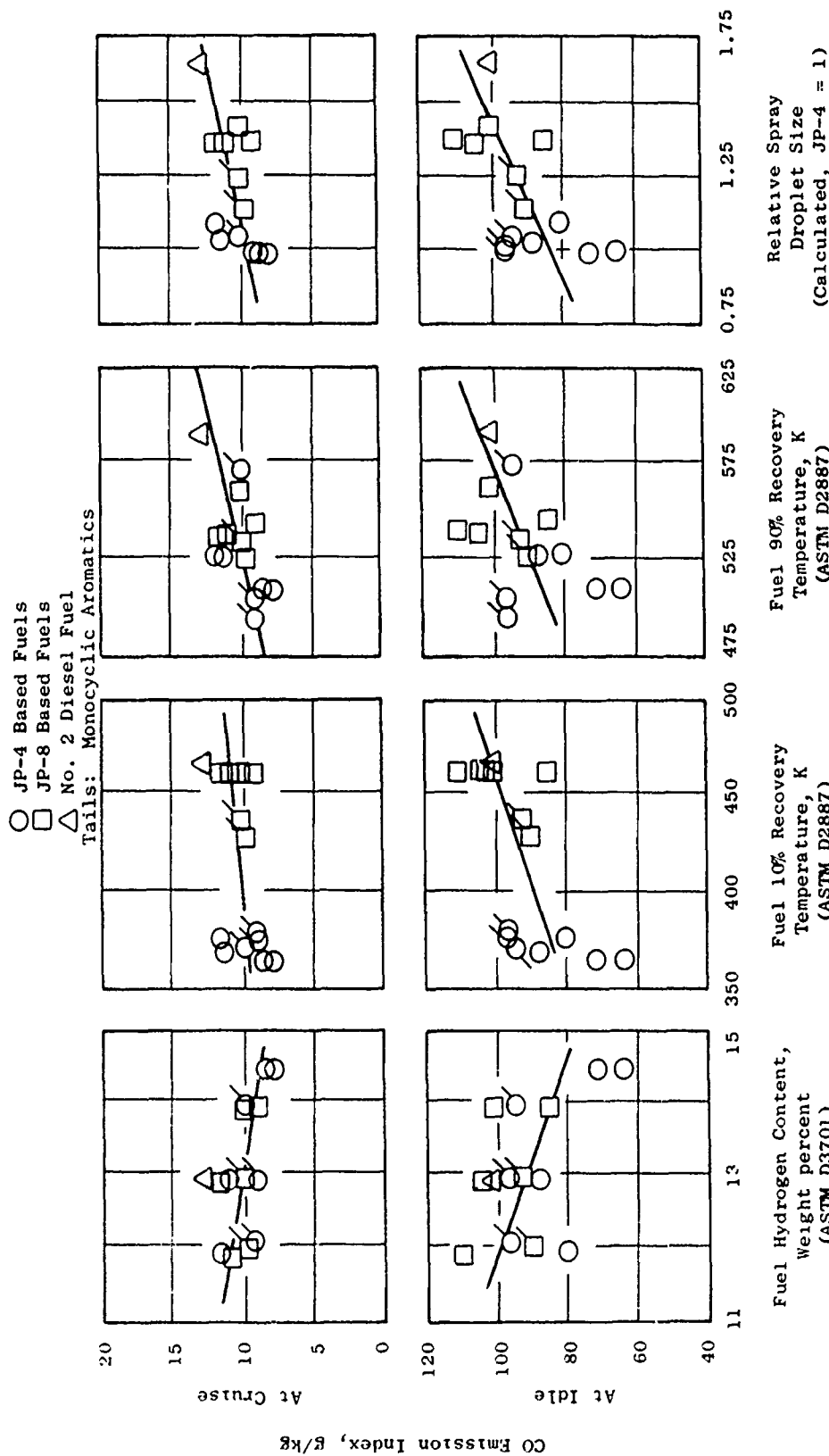
Figure 31. Effect of Selected Fuel Properties on CO Emission Levels at Idle and Cruise Operating Conditions.

58

The atomization properties (viscosity, density, and surface tension) and vaporization properties (recovery temperatures) of these fuels turn out to be highly interrelated, so it is not possible to separate their effects on CO emission levels in these tests. The data do correlate somewhat better with relative droplet size than either of the recovery temperatures. The relative effects of atomization and hydrogen content were therefore, determined by multiple regression analyses which are illlustrated in Figure 32. At both idle and cruise operating conditions, statistically significant correlations were obtained showing CO emission indices to be approximately inversely proportional to hydrogen content and directly proportional to the square root of droplet size. A similar joint dependency on fuel chemical composition and physical properties was shown in References 1 and 9, but not in Reference 2. It, therefore, appears that the relative importance of the fuel chemical and physical properties are quite configuration dependent.

Hydrocarbon emission levels generally have been found to follow the same trends as do CO emissions, but to be more sensitive to combustor operating conditions and to exhibit more variability. Both of these trends were observed in the present tests and are illustrated in Figure 33, where HC emission levels are plotted against CO emission levels for the idle and cruise test points and all fuels. At idle the HC index is about 27 g/kg (2.3% inefficiency). At cruise the levels are about two orders of magnitude lower, and at takeoff and dash conditions the levels were very low. There is considerable scatter in the cruise and idle data, but the regression curve fit exponent (2.14) is in good agreement with past experience (about 1.5 to 3.0). Table 11 summarizes the HC results for all fuels and operating conditions. At idle operating conditions, the HC emission levels are clearly lowest with the baseline JP-4 fuel and up to 100% higher with those fuels having reduced hydrogen and/or reduced atomization evaporation properties. As with the CO data, a multiple regression analysis was made (Figure 34) to show the relative effects of atomization and hydrogen content, and the results are similar; the HC emission index is approximately inversely proportional to hydrogen content and directly proportional to the square root of the droplet size.

2. NO_x Emissions

Oxides of nitrogen (NO_x) may form from oxidation of nitrogen which originated either in the air or in the fuel. Current jet engine fuels and all of the fuels used in this program contain negligible amounts of bound nitrogen, so the following discussion is applicable only to the "thermal" NO_x production characteristics of current and advanced fuels. Fuels containing significant quantities of bound nitrogen have been investigated in other programs, and typical results are contained in References 9, 10, and 11.

In contrast to CO and HC emission, which are products of incomplete combustion and are, therefore, generally significant only at low power conditions, "thermal" NO_x is an equilibrium product of high temperature combustion and is, therefore, highest at high power operating conditions. Figure 35 shows the strong effect of combustor operating conditions on NO_x emission levels with JP-4 fuel. In this correlation, the pressure, temperature, velocity, humidity effects were taken from previous studies (Reference 1) and the fuel/air ratio

59
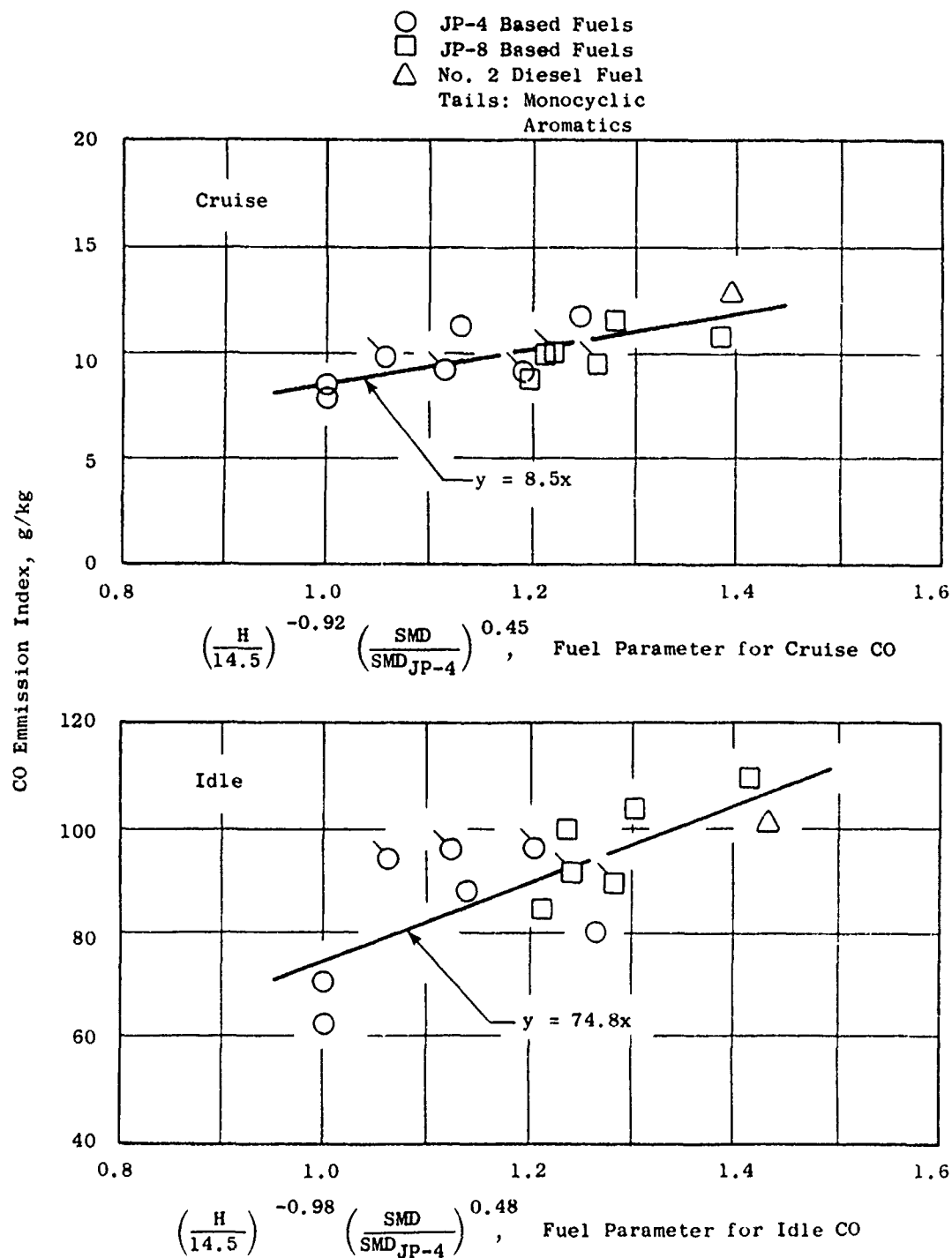
Figure 32. Effect of Fuel Hydrogen Content and Spray Droplet Size on CO Emission Levels.

60
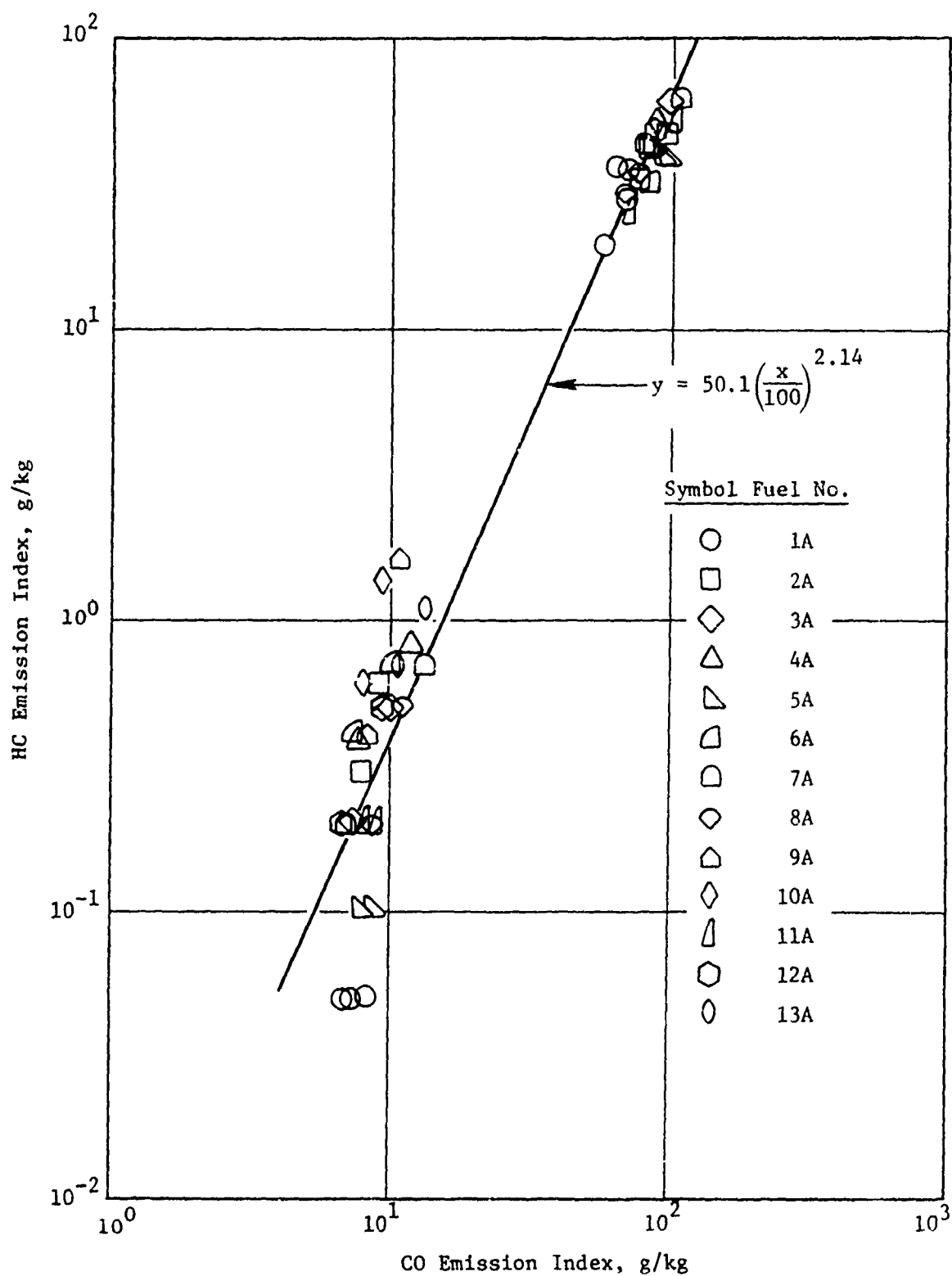
Figure 33. Variation of HC Emission Levels with CO Emission Levels, Idle and Cruise Operating Conditions.

Table 11. Summary of HC Emission Test
Results.

Fuel Number	HC Emission Index, g/kg			
	Idle	Cruise	Takeoff	Dash
1A	26.6	0	0	0
1A (Repeat)	27.2	0	0	0
2A1	35.5	0.5	0.1	0
3A	48.7	0.4	·0.1	0.2
4A	50.7	0.7	0.2	0.1
5A	37.1	0.2	0	0
6A	34.5	0.6	0.2	0.1
7A	47.5	0.6	0.1	0
8A	35.4	0.4	0.1	0.1
9A	47.5	1.2	0.1	0.1
10A	50.2	1.2	0.4	0.2
11A	38.8	0.2	0.1	0
12A	46.9	0.5	0.2	0.1
13A1	44.9	1.0	0.2	0
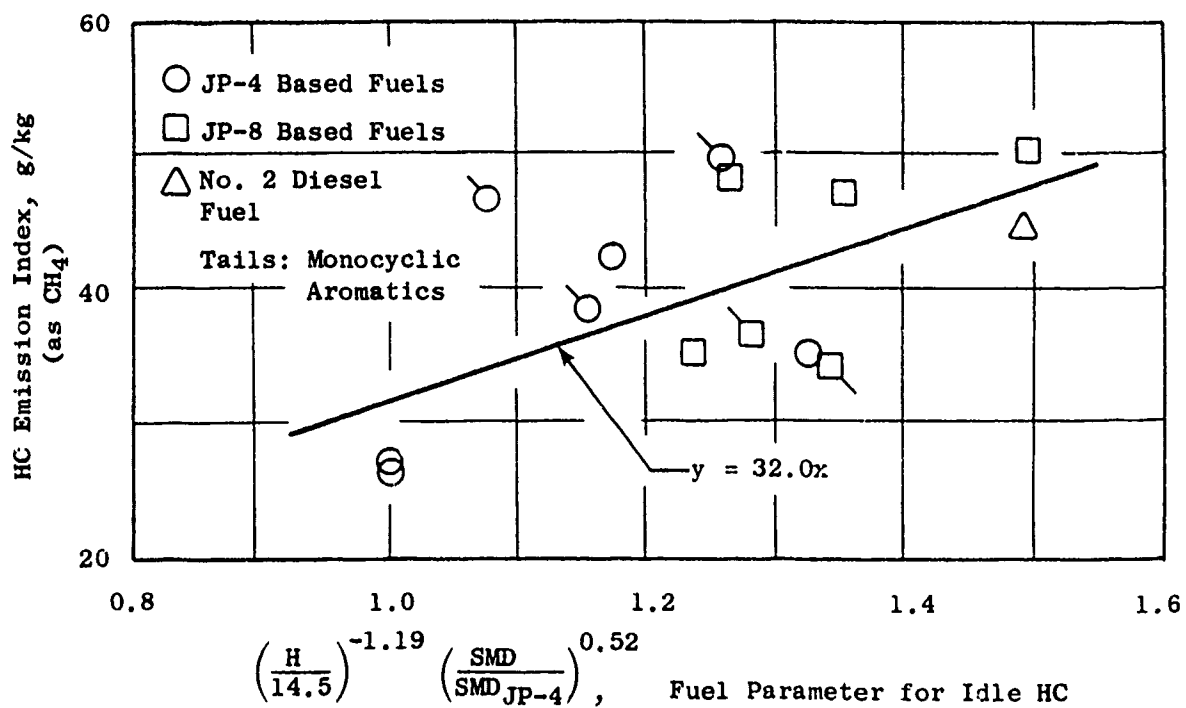
Figure 34. Effect of Fuel Hydrogen Content and Spray Droplet Size on Idle HC Emission Levels.
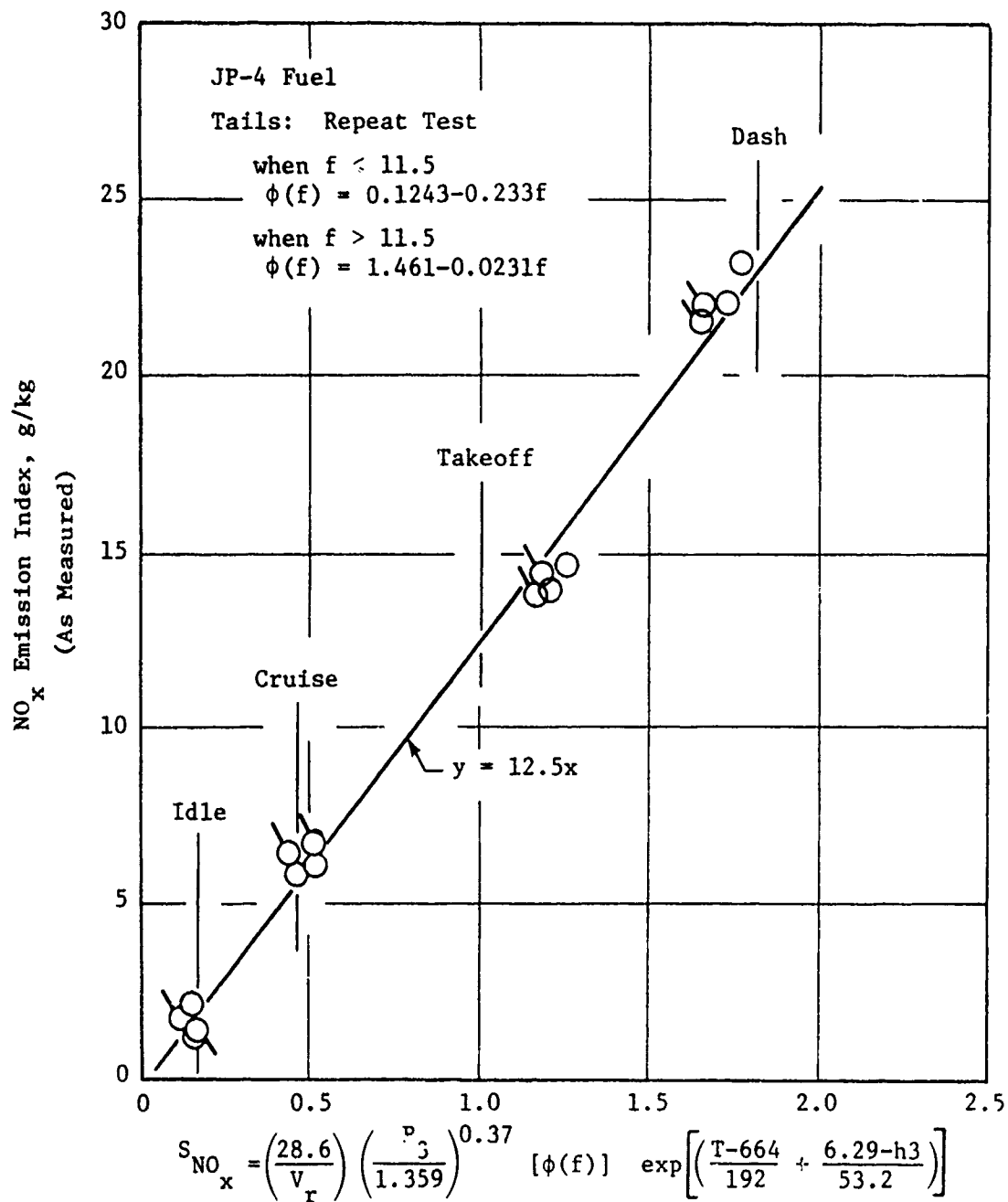
Figure 35. Effect of Operating Conditions on NO_x Emission Levels.

effect was determined by curve fitting the new data. At takeoff operating conditions, the NO_x emission index is about 12 g/kg. At dash, cruise and idle operating conditions, the NO_x levels are approximately 180, 50 and 20%, respectively of the takeoff levels. These NO_x emission levels are about 20% higher than those produced by the standard high smoke combustor (Reference 1), but are also in good agreement with data from J79 engines equipped with low smoke combustion systems (Reference 12).

NO_x results similar to those shown in Figure 35 were obtained in each of the tests. Emission indices for each fuel are listed in Table 12 and are plotted against fuel hydrogen content in Figure 36. At idle and cruise operating conditions, virtually no effect of fuel properties is evident, but at the high power operating conditions (takeoff and dash), NO_x levels decreased with fuel hydrogen content. This dependence on fuel hydrogen content is expected in diffusion flame processes such as these because of the stoichiometric flame temperature dependence on fuel hydrogen content and, in turn, the strong effect of flame temperature on NO_x formation rates. Figure 37 shows the effect of stoichiometric flame temperature (from Table A-3) on the NO_x emission levels at takeoff.

3. Smoke Emissions

Smoke, like CO and HC, is a product of incomplete combustion, but combustors with virtually 100% combustion efficiency can produce highly visible exhaust plumes, because the soot particle sizes are of the same order as the visible light wavelengths. The J79-17C combustion system produces nearly invisible exhaust plumes when fueled with current hydrogen content fuels (Reference 13).

The effect of combustor operating conditions on smoke levels with JP-4 fuel is shown in Figure 38. No simple operating parameter could be derived from the data, so smoke number is merely plotted against combustor fuel/air ratio and keyed as to inlet conditions. Within the test range, there is virtually no fuel/air ratio effect, and the repeatability and agreement with previous engine measurements is fair. At true idle, cruise and 75% density dash operating conditions, the smoke levels are approximately 18, 19, and 38%, respectively, of the smoke level at true takeoff operating conditions. At full density dash operating conditions, smoke levels might be expected to be somewhat higher at the combustor exit plane and then be partially consumed in the afterburning process. Because of the uncertainty of the extent of these two opposing processes, no corrections were made. However, in Figure 38 and Table 13, all of the data have been corrected to engine outlet fuel/air ratio according to the procedure outlined in Appendix F to account for turbine cooling air dilution of the main combustor products and allow comparisons to engine measurements. Also shown in Table 13 are corresponding smoke emission indices, calculated from the smoke number by the procedure described in Appendix F.

Table 12.   Summary of NO_x Emission Test
Results.

Fuel Number	NO_x Emission Index, g/kg[1]			
	Idle	Cruise	Takeoff	Dash
1A	1.8	5.8	11.6	23.3
1A (Repeat)	1.9	6.6	12.0	23.7
2A1	3.7	6.3	11.7	23.6
3A	1.9	6.2	11.9	23.1
4A	1.3	6.2	13.1	23.5
5A	2.3	6.4	12.3	23.3
6A	2.6	---	11.6	21.9
7A	1.8	6.4	12.0	23.3
8A	2.2	6.2	12.3	25.3
9A	2.0	5.6	12.9	27.2
10A	1.8	6.2	13.0	26.1
11A	2.9	6.2	---	---
12A	2.1	6.0	11.8	23.7
13A1	1.5	6.6	13.2	26.3

[1]Corrected to ambient humidity of 6.3 g/kg
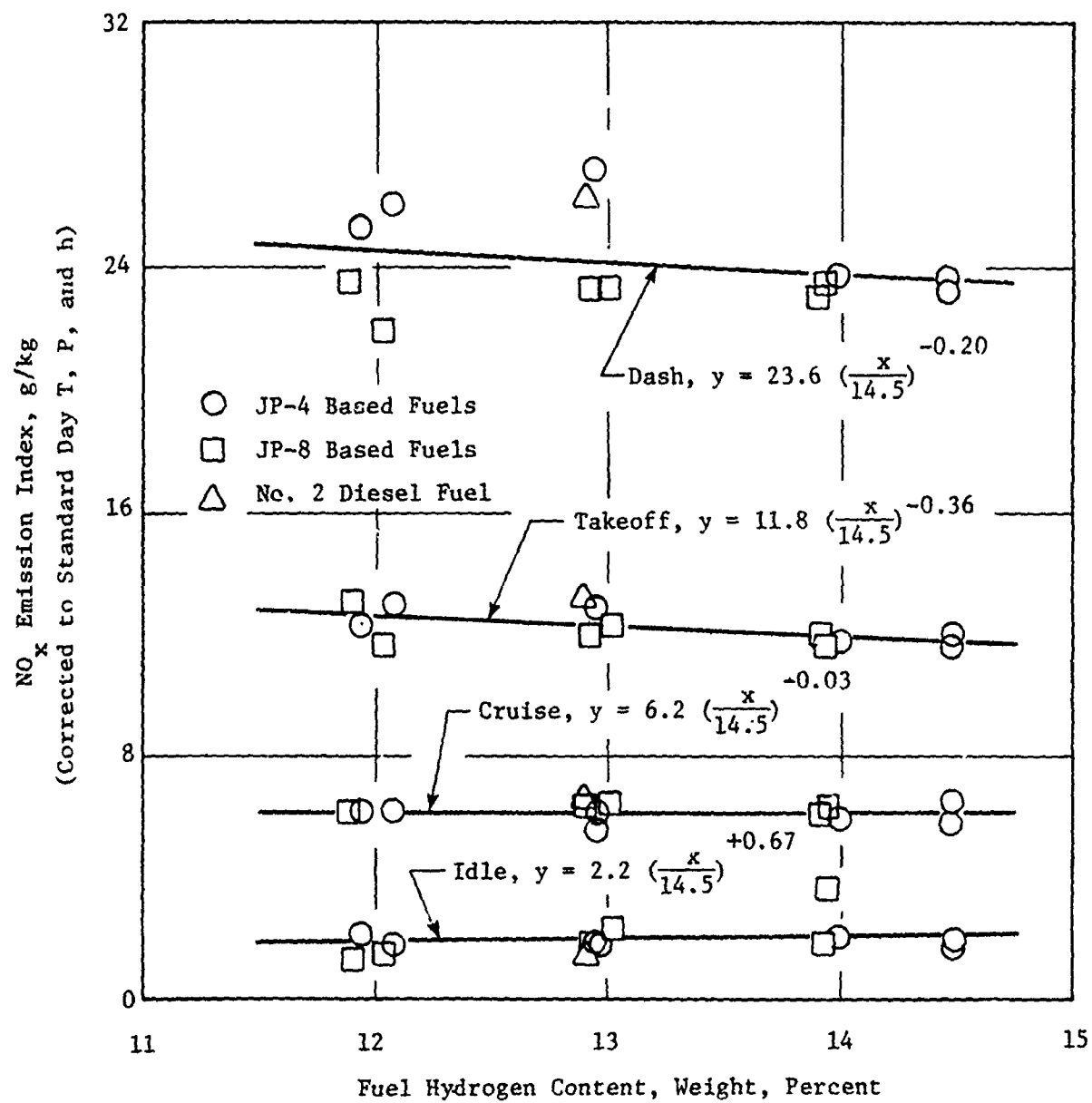
Figure 36. Effect of Fuel Hydrogen Content on NO_x Emission Levels.

The y-axis is labeled: NO_x Emission Index, g/kg (Corrected to Standard Day T, P, and h)

The x-axis is labeled: Fuel Hydrogen Content, Weight, Percent

Legend:
○ JP-4 Based Fuels
□ JP-8 Based Fuels
△ No. 2 Diesel Fuel

Dash, $y = 23.6 \left(\frac{x}{14.5}\right)^{-0.20}$

Takeoff, $y = 11.8 \left(\frac{x}{14.5}\right)^{-0.36}$

Cruise, $y = 6.2 \left(\frac{x}{14.5}\right)^{-0.03}$

Idle, $y = 2.2 \left(\frac{x}{14.5}\right)^{+0.67}$
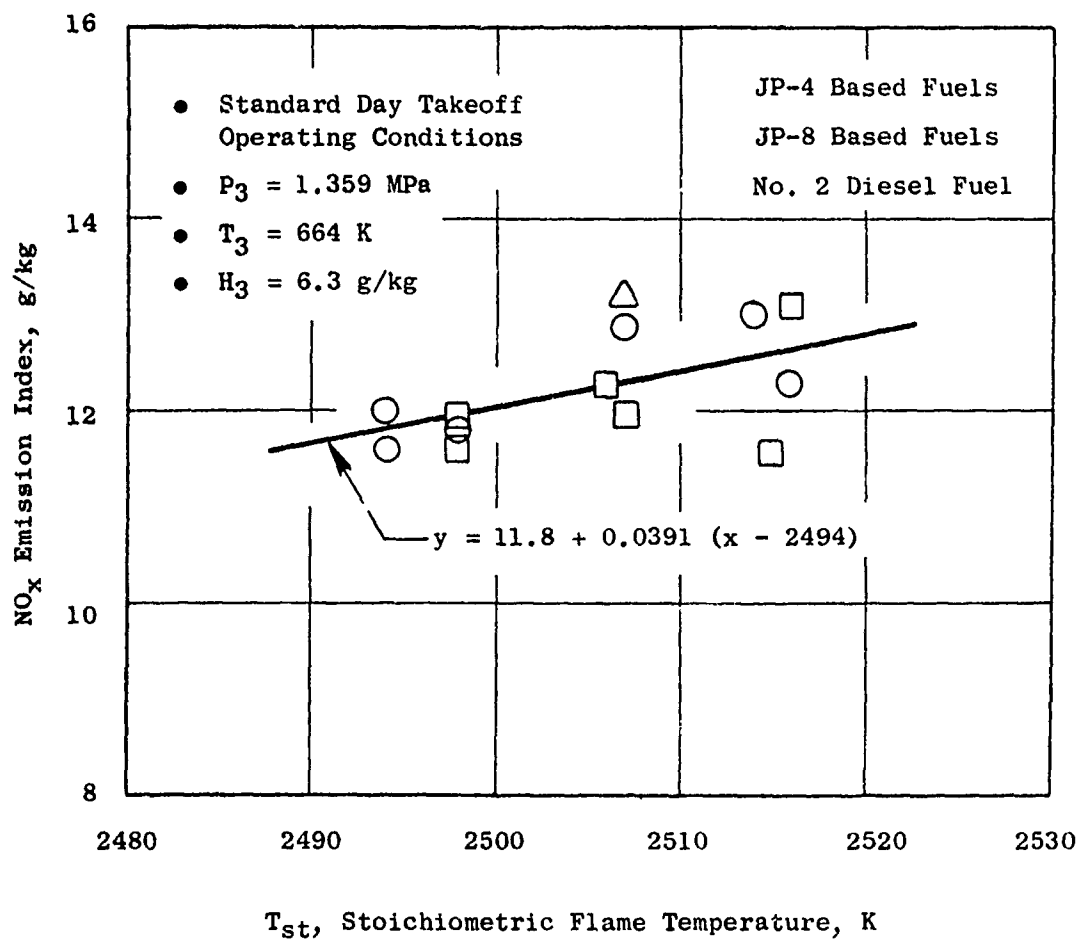
Figure 37. Effect of Flame Temperature on NO_x Emission Levels.
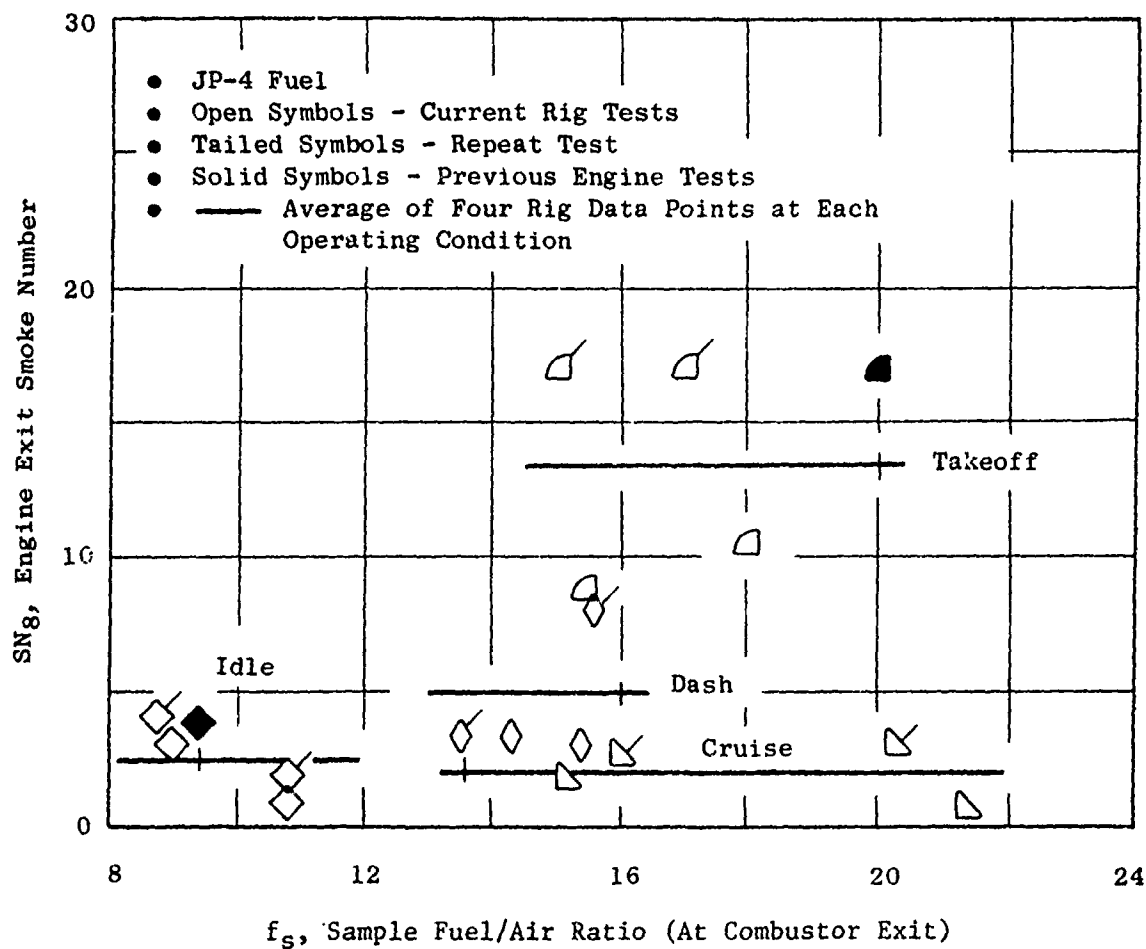
Figure 38. Effect of Operating Conditions on Smoke Emission Levels.

Table 13. Summary of Smoke Emission Test Results.

Fuel Number	SN_g, Smoke Number at Engine Exit				EI_s, Smoke Emission Index, g/kg			
	Idle	Cruise	Takeoff	Dash	Idle	Cruise	Takeoff	Dash
1A	1.9	2.3	9.7	3.2	0.015	0.011	0.045	0.017
1AR	2.9	2.8	17.1	7.0	0.026	0.017	0.083	0.035
2A1	3.1	8.6	13.2	3.7	0.027	0.055	0.063	0.019
3A	2.8	11.5	18.3	4.2	0.024	0.075	0.090	0.022
4A	12.2	25.9	23.7	14.0	0.118	0.213	0.130	0.080
5A	3.0	14.4	22.3	7.4	0.025	0.096	0.118	0.041
6A	10.7	12.7	13.7	5.7	0.124	0.086	0.063	0.031
7A	6.9	19.5	27.7	8.8	0.062	0.143	0.168	0.049
8A	6.0	19.9	40.0	8.2	0.054	0.148	0.288	0.045
9A	8.4	11.3	24.0	7.6	0.077	0.075	0.137	0.041
10A	14.4	15.9	31.0	7.9	0.141	0.111	0.208	0.042
11A	7.1	5.1	20.2	10.8	0.067	0.031	0.102	0.060
12A	2.0	3.5	15.1	4.4	0.019	0.021	0.072	0.023
13A1	3.8	18.2	26.7	5.5	0.031	0.130	0.155	0.029

In Figure 39, the effect of fuel hydrogen content on engine smoke number is shown. At each power level, smoke number increases exponentially with decreasing hydrogen content, but there is considerable scatter in the data, particularly at takeoff operating conditions where the smoke levels are highest. The scatter does appear to be associated with fuel volatility or atomization characteristics, but there is some trend with aromatic type, or fuel naphthalene content.

In order to quantify the effect of aromatic type on smoke levels, the smoke numbers at each power level were normalized for hydrogen content, by use of the regression equations shown in Figure 39, and plotted against fuel naphthalene content as shown in Figure 40. Generally, the hydrogen normalized smoke numbers are seen to be within the range 0.5 to 1.5, but there is no clear trend with fuel naphthalene content. The line and equation shown in Figure 40 are the result of a second regression analysis of all of the normalized smoke numbers with fuel naphthalene content as the independent variable. The slope of the line (0.00711) is a measure of the average effect of fuel naphthalene content on smoke number of constant hydrogen content. A 10% by volume increase in fuel naphthalene content can be expected to produce a 7.1% increase in smoke number. For comparison, a 1% by weight increase in fuel hydrogen content can be expected to produce an 89, 96, 31 and 36% increase in smoke number at idle, cruise, takeoff and dash operating conditions, respectively.

4. Carbon Deposition and Emission

As discussed in Section V-A-2, two 24-hour high pressure combustor tests were conducted with procedures established to provide information on the relative carbon deposition tendencies of Fuel 1A (Repeat JP-4) and Fuel 13A1 (diesel). Both tests began with clean combustors and fuel nozzles. Inlet conditions were varied over the idle, cruise, takeoff, and dash operating conditions on an approximately equal time basis. At the completion of each test, visual assessments of the relative carboning tendencies were made which are summarized in Table 14. Photographs, which are included in Appendix C, were also made to fully document the carbon deposition tendencies.

As shown in Table 14 and the posttest photographs, some carbon deposition was found in both tests, with the greater accumulation occurring using Fuel 13A (diesel). It should be noted that carbon deposition was not considered excessive for either fuel and no adverse effects due to carboning are anticipated using either fuel. For example, Figure 41 shows no long term changes in pattern factor using either fuel. These detailed pattern factor data are presented in Table C-1 in the Appendices.

Also as discussed in Section V-A-3, carbon emission data were obtained on selected fuels using a millipore filter for total carbon collection, and a cascade impactor for total carbon collection and particle size distribution. For both measurements, samples were withdrawn through the exit emission rakes at isokinetic conditions for 40 minutes. Table 15 summarizes the total carbon emissions measured by the millipore filter and cascade impactor.

71
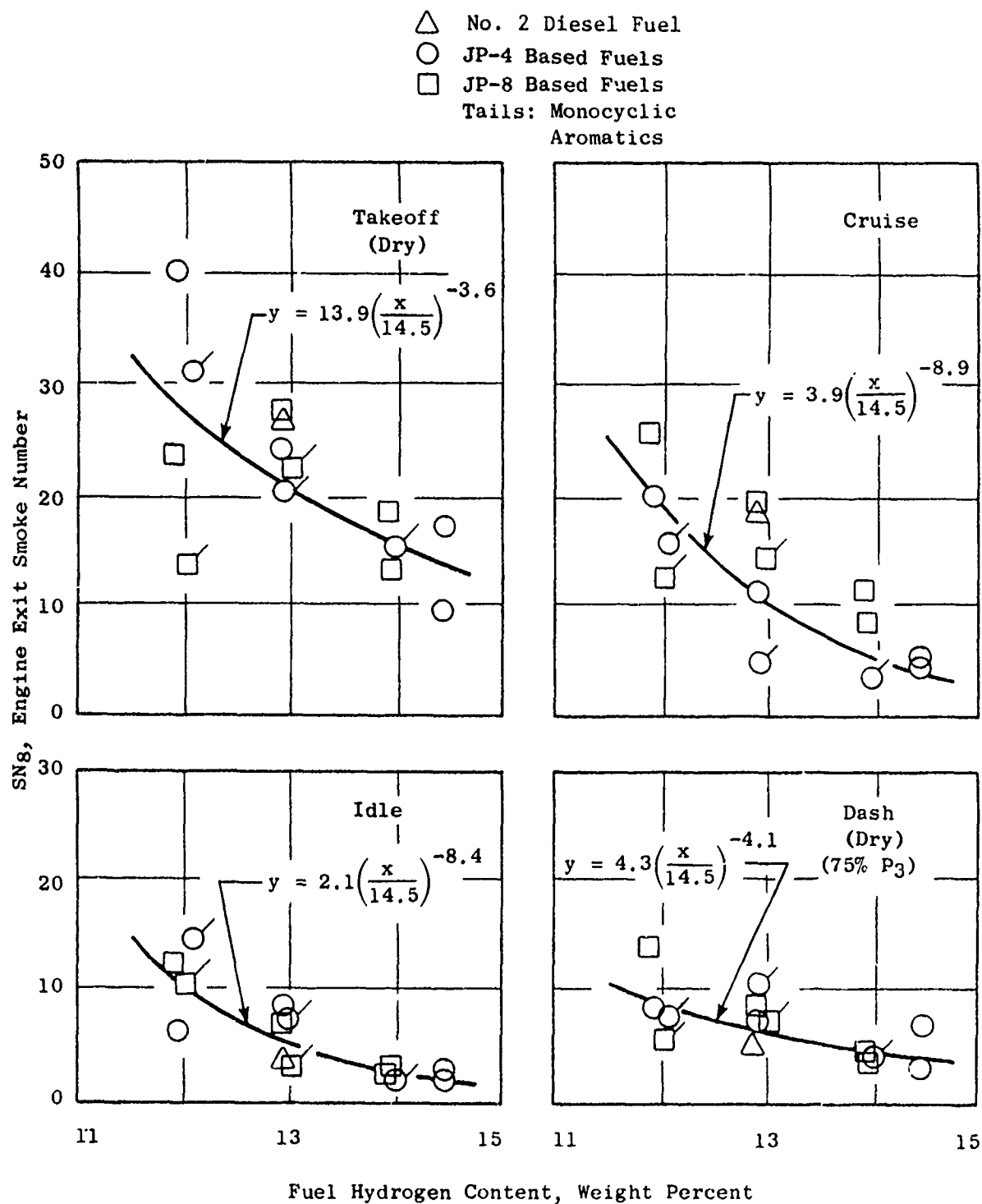
Figure 39. Effect of Fuel Hydrogen Content on Smoke Emission Levels.
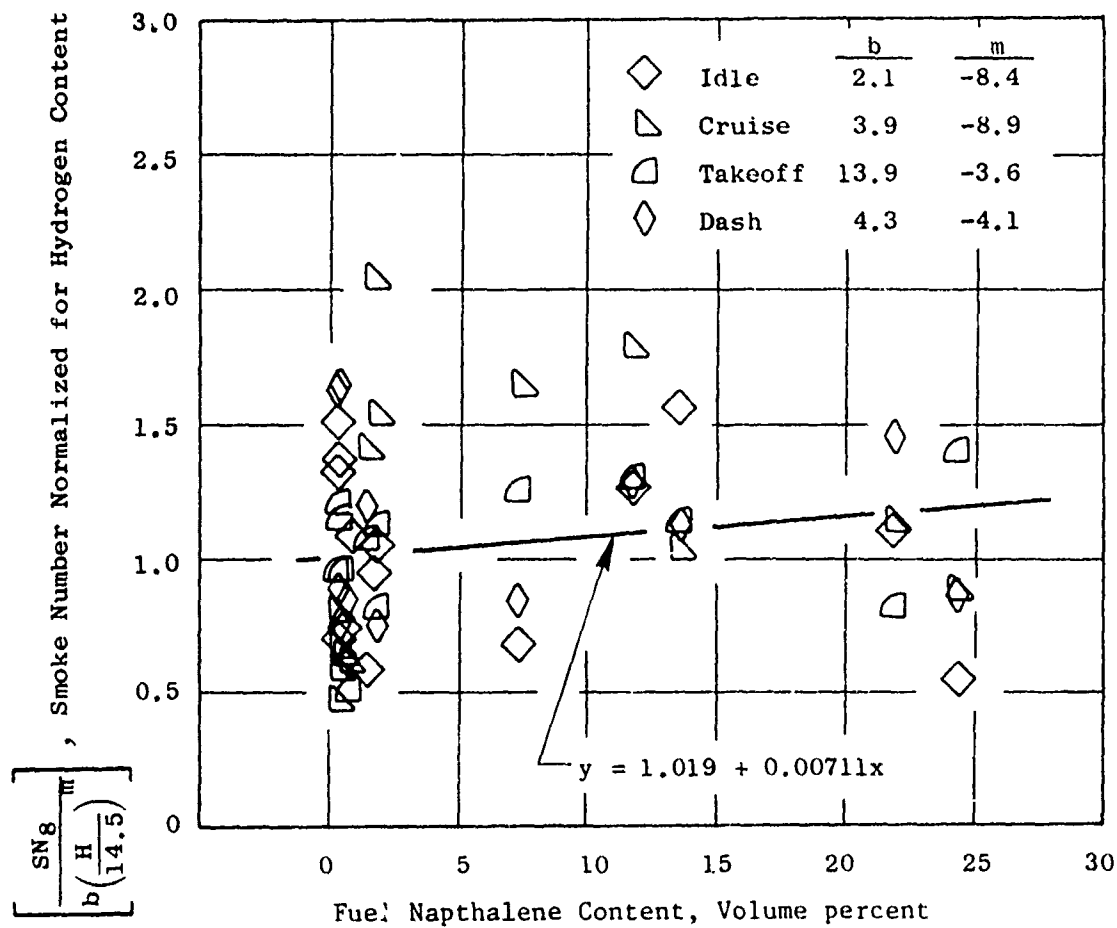
Figure 40. Effect of Fuel Naphthalene Content on Smoke Number Normalized for Hydrogen Content.

73

Table 14. Summary of Carbon Deposition After 24 Hour Tests.

	Fuel 1A (Repeat)	Fuel 13A
Fuel Nozzle	Irregular deposits to 0.1 mm high on face. Black stain around secondary fuel ports	Hard black, shiny, uniform deposit on face to 0.8 mm thick and to 0.3 mm around secondary ports
Venturi	Soft, easily removed deposit to 1 mm thick	Hard black deposits to 6 mm thick
Inner Liner	Very light discoloration easily wiped away	Dull to shiny black deposits up to 0.6 mm thick
Aft Liner	Same as inner liner	Light dull to shiny black deposit less than 0.1 mm
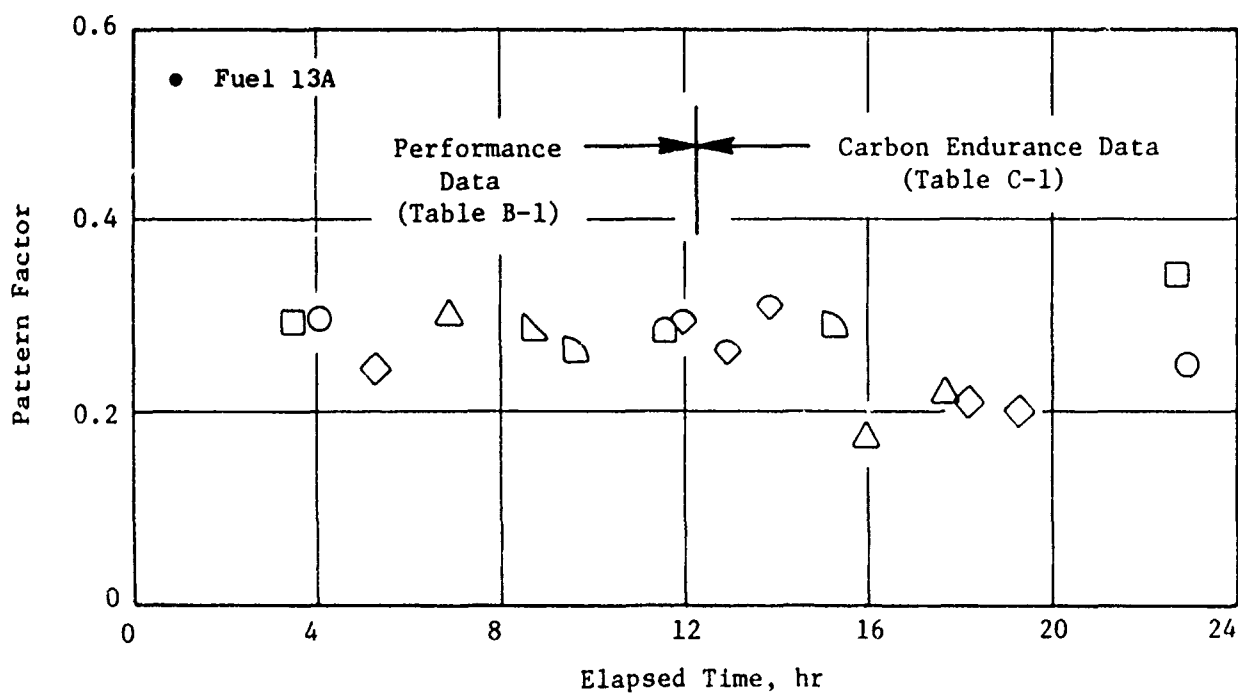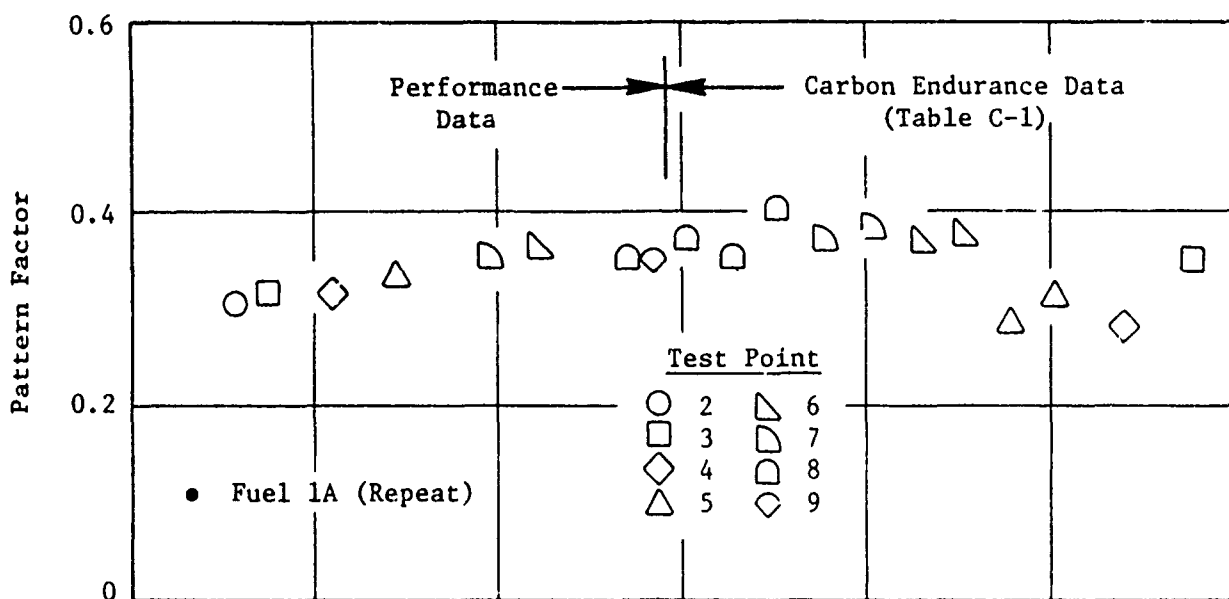
Figure 41. Pattern Factor Variation During Carbon Endurance Tests.

Table 15. Summary of Total Carbon Emission
Test Results.

Fuel Number	Test Point Number	Carbon Particle Emission, mg carbon/kg gas	
		Millipore Filter	Cascade Impactor
1A	4	11.3	---
	7	9.7	---
2A	4	6.4	---
4A	4	---	19.3
6A	4	10.5	---
10A	4	17.1	12.0
13A	4	5.4	---
	7	29.6	---

Figure 42 presents this data versus fuel hydrogen content for the cruise test point (Point 4). A moderate trend of increased carbon emission with decreased hydrogen content is noted. However, considerable data scatter is present.

Figure 43 presents the particle mass distributions for two fuels as measured by the cascade impactor. The detailed impactor data are presented in Table C-2. Little difference in particle distribution is evident between these two fuels. In general, about 50% of the carbon emissions by weight are less than 1 micron in diameter and about 30% are greater than 10 microns in diameter. This constitutes basically a two tailed distribution with either extremely small particles (less than 1 micron) or relatively large particles (greater than 10 micron) present.

5. Liner Temperature and Flame Radiation

Liner temperature measurements were obtained in the high pressure combustor tests at the locations described in Section V-A-2. Detailed data are listed in Appendix B and peak data are summarized in Table 16. The data are presented as metal temperature rise above the inlet air temperature (T2-T3). Typical levels and spatial variations at takeoff operating conditions are shown in Figure 16, and effects of variations in operating conditions on selected typical thermocouples are shown in Figure 44.

Generally, as shown in Figure 16, the rear liner and transition metal temperatures are quite moderate and uniform. The highest measured metal temperatures are in the forward or inner liner. The hottest thermocouple (No. 11) is an imbedded installation in the conical dome section first cooling slot overhang. The internal swirling and burning flows emerge from the swirl cup as a separated flow, and create intense heat transfer to the conical dome surface, as they approach the wall and either reattach or create secondary flows. The film protection provided by the gill holes can be disrupted depending on the exact location of the reattachment process and result in effects that extend further downstream. There are non-axisymmetric circumferential geometry features such as dilution holes, the igniter, and the crossfire tube that result in circumferential variations in the flow reattachment process. This in turn results in extreme circumferential variations in metal temperature as seen in Figure 16. To counteract this intense heating, the conical dome region is provided with intense cooling mechanisms including impingement on the cold side, internal convective cooling and conduction from the film cooling or gill holes, as well as the film protection. These intense mechanisms provide adequate cooling to treat the hottest regions but result in much cooler metal temperature levels at locations that are not suffering the reattachment and film disruption.

As shown in Figure 44, inner liner temperature rises (both mid-panel surface mounted and cooling ring overhang imbedded thermocouple installations) tended to be dependent upon operating pressure and temperature, but independent of operating fuel/air ratio. The absence of a fuel/air ratio effect in the dome may be associated with near stoichiometric hot gas flows scrubbing the conical dome walls. Variations in overall fuel/air ratio may be accompanied

77
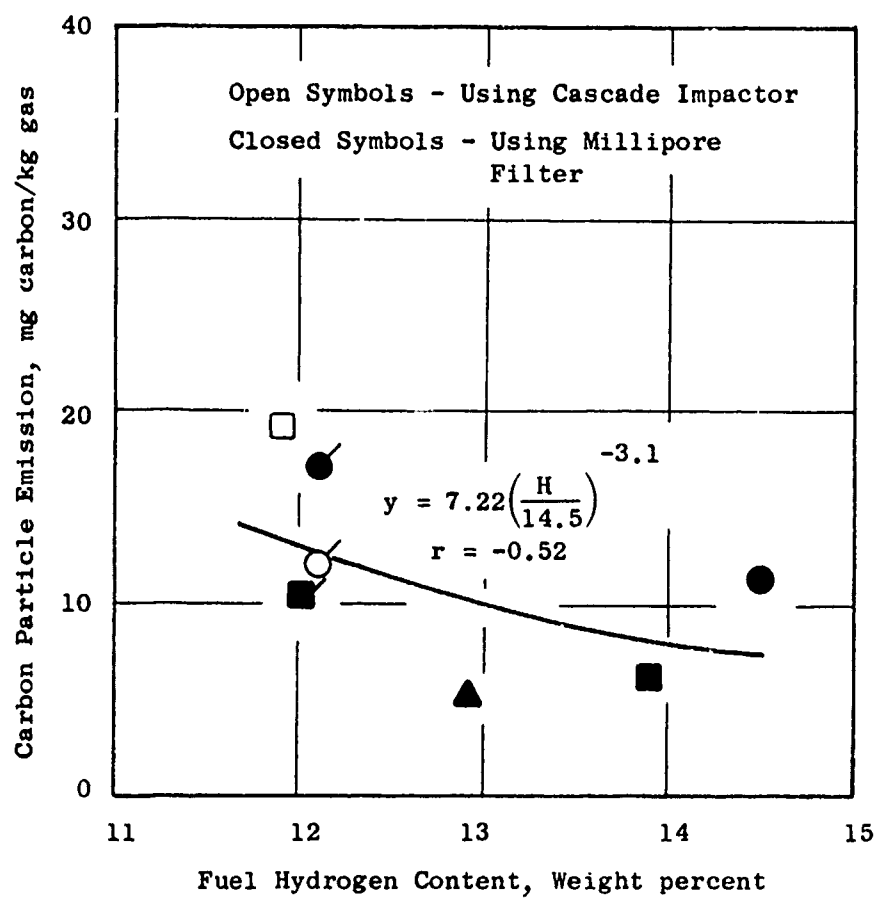
Figure 42. Effect of Fuel Hydrogen Content on Carbon
Emission Levels at Cruise (Test Point 4).
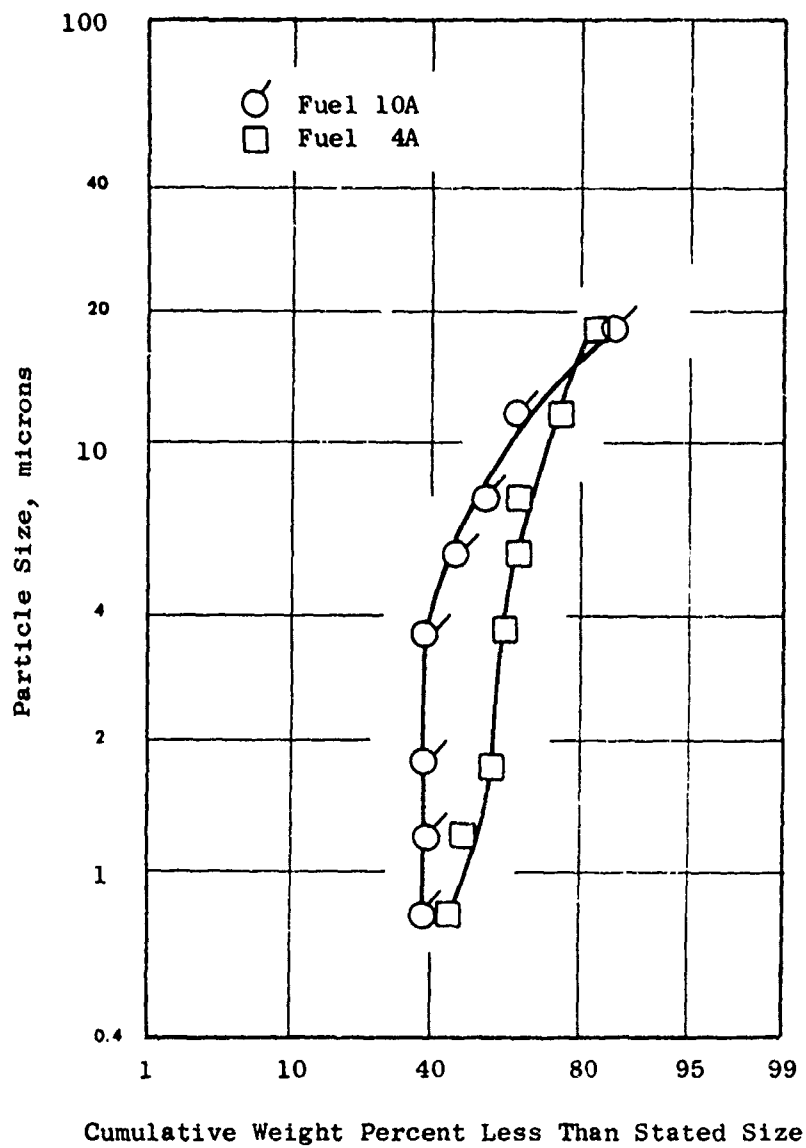
Figure 43. Carbon Particle Size Distribution at
Cruise Measured by Cascade Impactor.

Table 16. Summary of Peak Liner Temperature Results.

$T_L - T_3$, Liner Temperature Rise, K

Fuel Number	Idle 7[1]	Idle 11[2]	Idle Peak[3]	Cruise 7	Cruise 11	Cruise Peak	Takeoff 7	Takeoff 11	Takeoff Peak	Dash 7	Dash 11	Dash Peak
2A1	72	141+/42	141	142	300	340	346	501+	519	310	502+	505
1A	89	262+	262	152	398+	398	286	440+	443	299	509+	509
6A	74	147+/58	147	200	380+	390	346	481+	482	358	360	517
5A	88	91	179	258	237	392	332	294	463	330	311	487
11A	98	152+/68	244	197	230	359	322	274	494	349	311	498
1AR	79	42	173	108	224	397	295	259	411	300	261	454
13A1	72	46	109	210	164	364	323	263	499	347	283	423
10A	104	56	167	170	380+	420	304	499+	511	363	586+	595
12A	90	144+	163	164	392+	395	293	483+	487	323	561+	567
9A	112	78	152	179	398+	420	296	422+	463	361	303	500
8A	134	167+	226	279	213	374	340	258	468	363	302	535
4A	102	77	137	245	227	401	354	257	507	388	242	502
7A	102	43	135	240	157	383	350	187	511	364	209	478
3A	88	40	95	212	224	301	344	164	449	343	193	483

1.) Average of data points at two fuel/air ratios, thermocouple No. 7 (Surface mounted).

2.) Average of data points at two fuel/air ratios. Superscript + indicates separated film. Where two values are given one fuel/air ratio had attached and one fuel/air ratio had separated film, thermocouple No. 11 (imbedded, overhang).

3.) Maximum value for either fuel/air ratio at test condition.
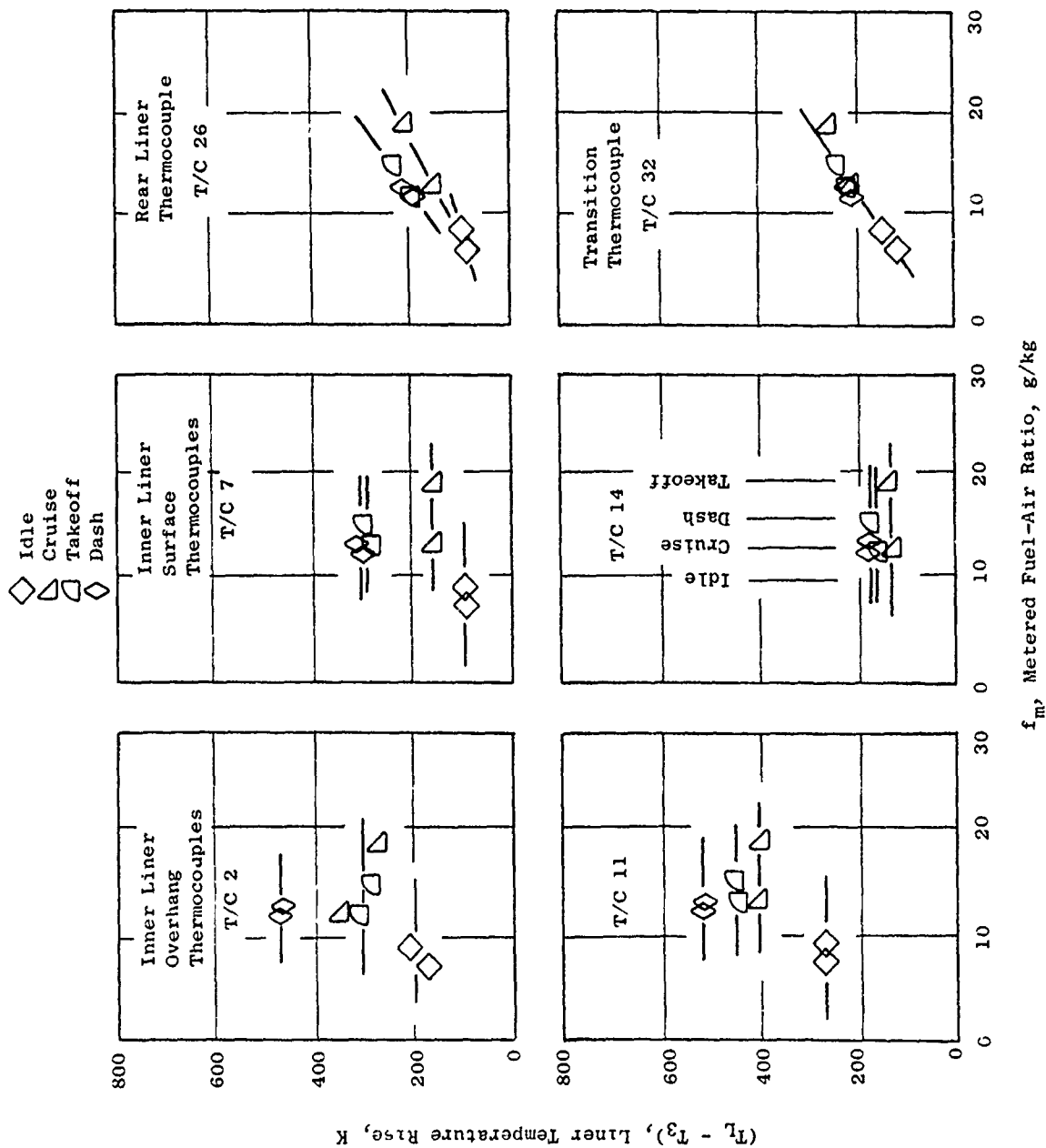
Figure 14. Effects of Installation and Film Flow Mode on Liner Temperature Response.

by burning rate differences and features in the separated and reattaching flow regions along the conical dome that permit these near stoichiometric flame temperatures to exist over a significant range of overall fuel/air ratios. This unusual flow phenomena is also thought to result in some randomness in the data in this dome reattachment region.

As further shown in Figure 44, rear liner and transition metal temperature rises, tended to be directly proportional to operating fuel/air ratio, but independent of operating pressure on temperature. This behavior is thought to indicate the absence of any significant radiant heat transfer to these regions, due to the small flame view factor.

Detailed analyses of the liner temperature data to identify fuel property effects was complicated by factors which are illustrated in Figures 45 and 46. Thermocouple attrition was such that, after reading number 56, the entire array was replaced for the final seven fuel test series (designated combustor installation No. 3). In spite of extreme care to attach the new thermocouples in the same spot, some thermocouples responded quite differently. As shown in Figure 45, thermcouple No. 12 consistantly responded lower and thermocouple No. 13 responded higher in the last installation. Other thermocouples, such as No. 11 also illustrated in Figure 45, exhibited two response levels associated with cooling film flow mode (attached or separated), but excellent reproducibility between installations. Also, as shown in Figure 46, the liner thermocouple leadout bundle created a blockage which disrupted the rear liner cooling flow thereby invalidating thermocouple No. 25 completely, and perhaps No. 26 and 27 partially. Because of these installation and metastable flow phenomena, fuel effect analyses were made for individual thermocouples, rather than for peak and average data as was done in References 1 and 2.

The effect of fuel hydrogen content on liner temperature rise was determined for each thermocouple and installation/film flow mode by regression analyses, as illustrated in Figure 45, for the takeoff operating conditions. These results are tabulated in Appendix B, Table B-9, and summarized in Figure 47, where the slope of the regression equation (Kelvin increase in liner temperature rise per percent decrease in fuel hydrogen content) is plotted against spatial location. Clearly, the forward panels of the inner liner are most sensitive (20 to 40 K/percent H) while the rear liner and transition are virtually independent of fuel hydrogen content.

The effect of engine operating conditions on sensitivity of liner temperature rise to fuel hydrogen content was also determined by regression analyses, for selected thermocouples. The trends are not easily generalized. One example is tabulated in Appendix B, Table B-10 and summarized in Figure 48. The thermocouple illustrated shows the largest sensitivity at cruise (35.2 K/ percent H) and a relatively low sensitivity at takeoff (13.0 K/percent H), but other thermocouples respond differently. This thermocouple was selected for illustration to examine other fuel property effects, and make comparisons to previous studies (in a following section).
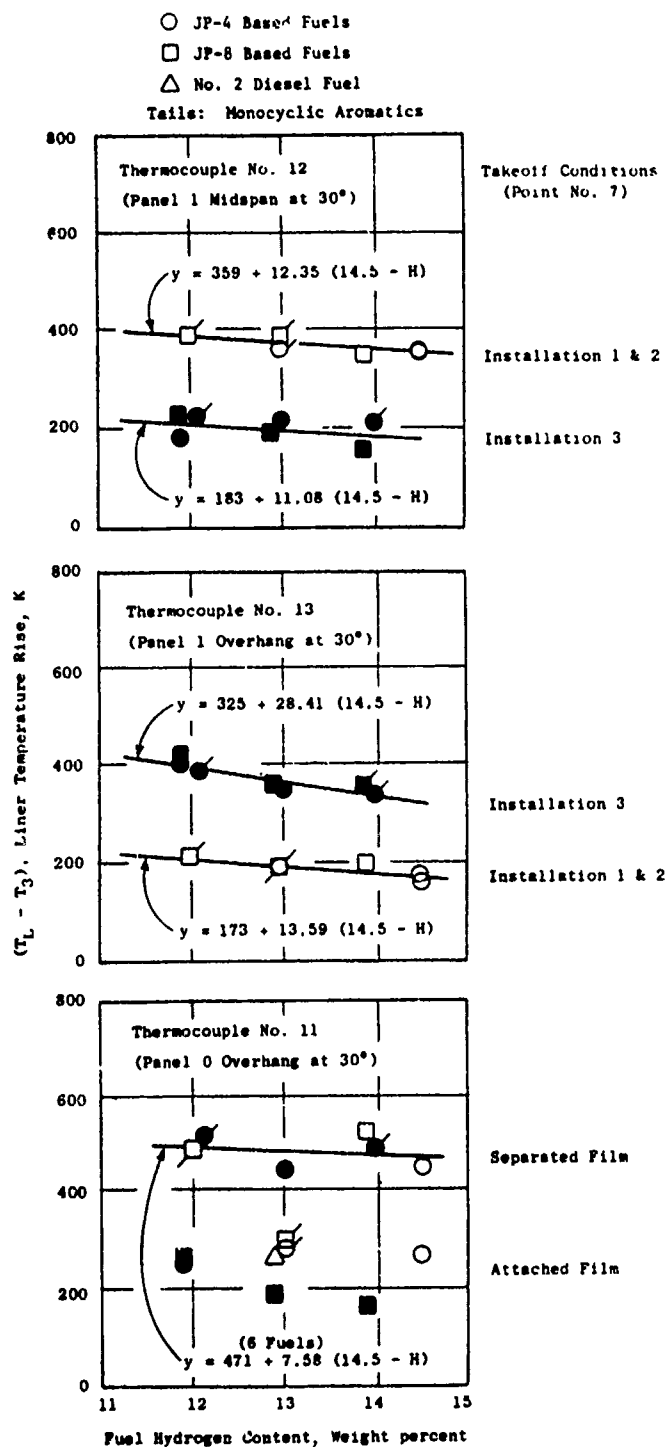
Figure 45. Effects of Installation and Film Flow Mode on Liner Temperature Response.

Figure 46. Rear Liner Hot Spot Caused by Thermocouple Leads.
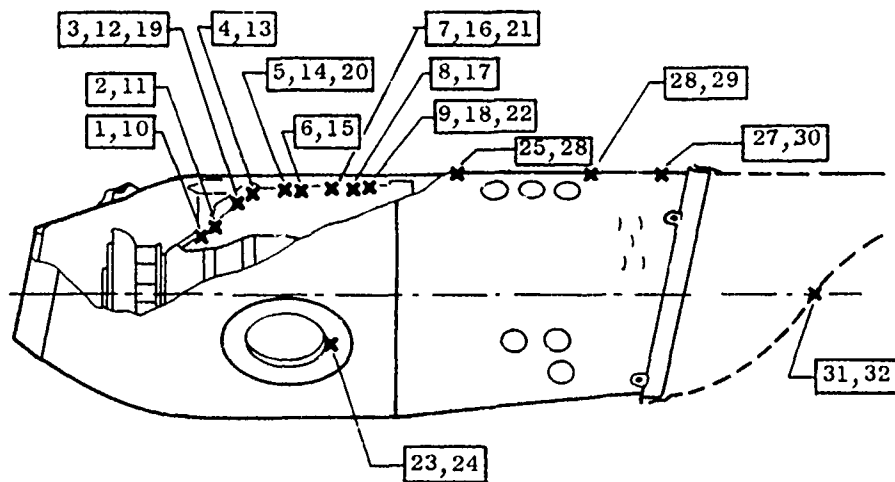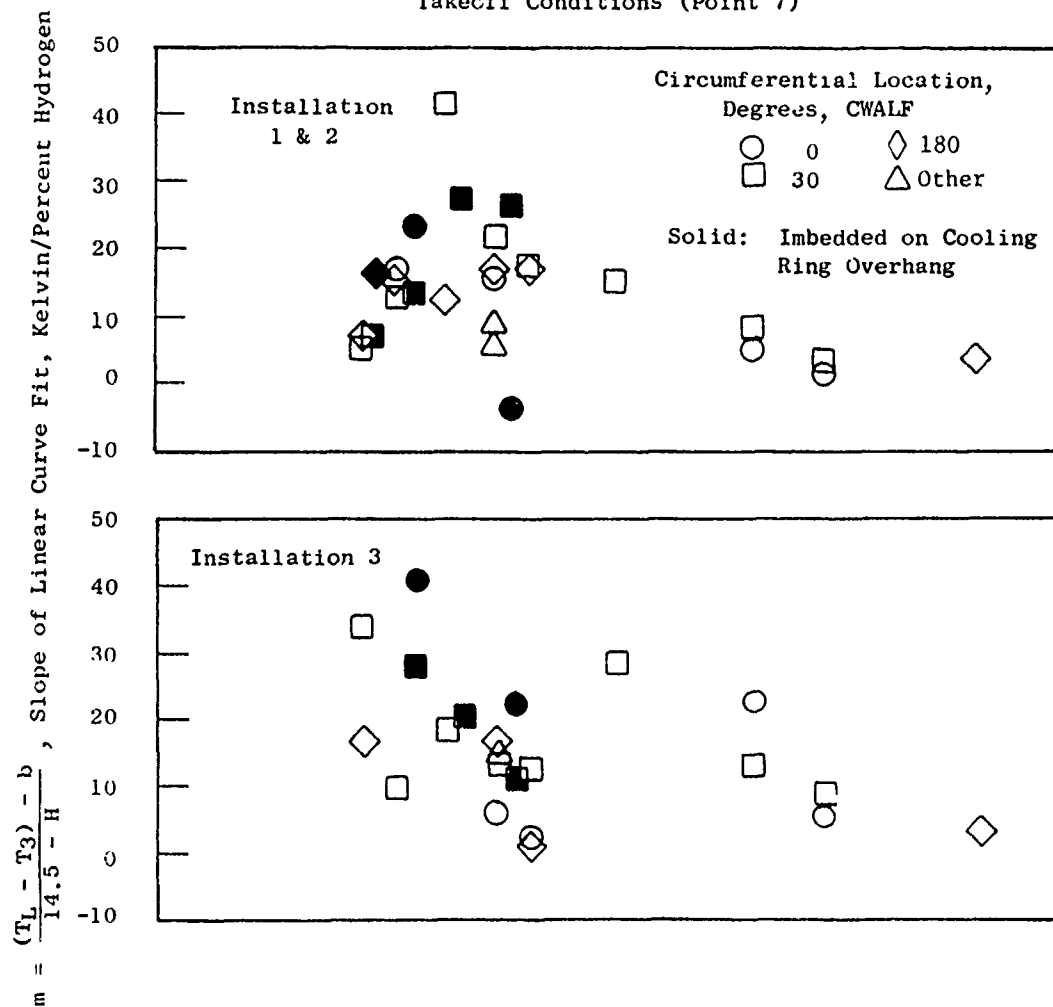
Figure 47. Spatial Variation in Rate of Change of Liner Temperature with Fuel Hydrogen Content.
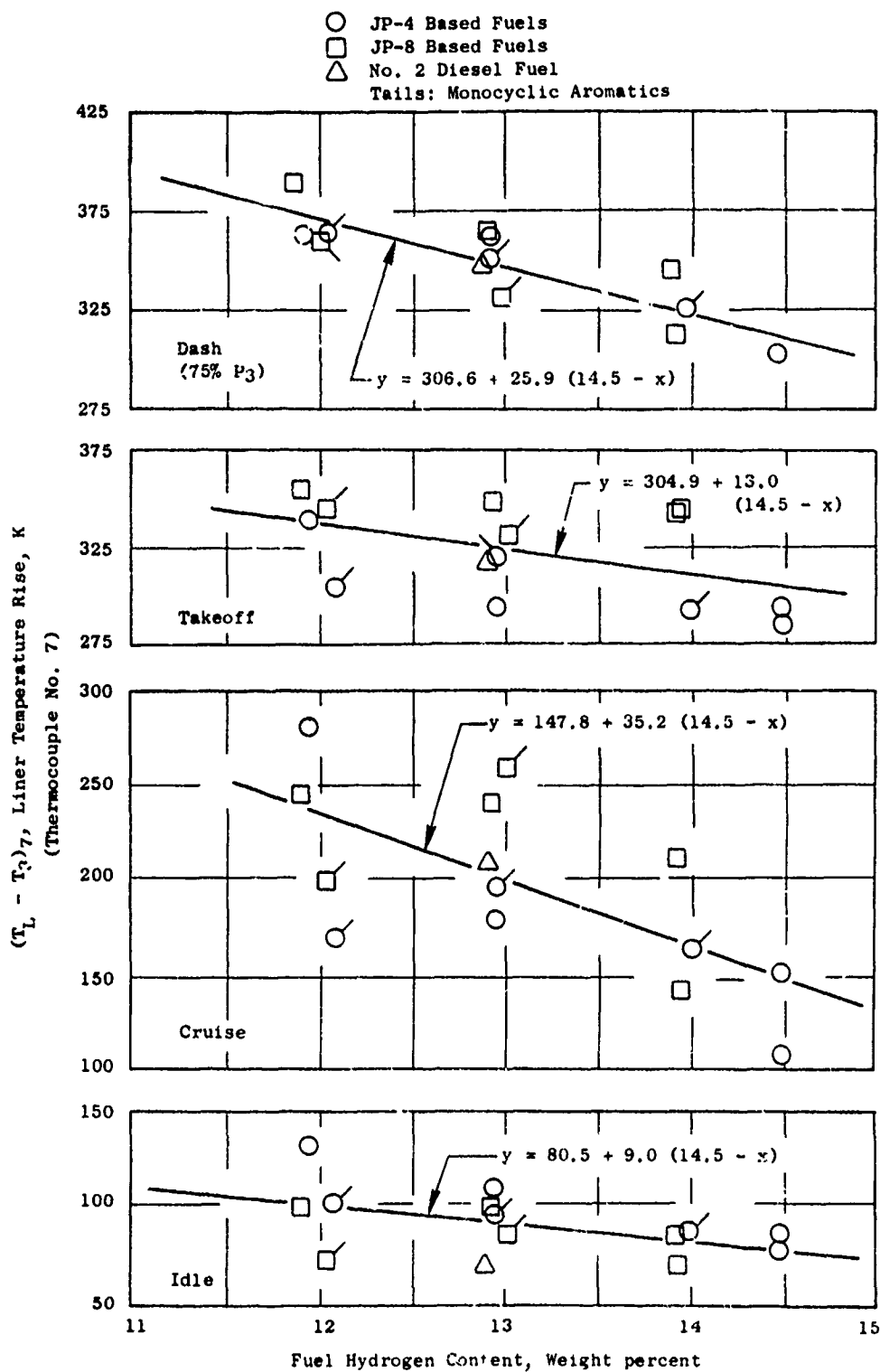
Figure 48. Effect of Operating Conditions on Rate of Change of Liner Temperature with Fuel Hydrogen Content.

As shown in both Figures 45 and 48, liner temperature rise does not appear to be dependent upon fuel atomization or vaporization properties, particularly at high temperature operating conditions. Also, the data do not appear to show sensitivity to aromatic structure, but this analysis is complicated because all of the 2040 solvent blends were tested in the third installation. However, to illustrate the effect of aromatic stuctures, the data for thermocouple No. 7 (Figure 48) were normalized for fuel hydrogen content and plotted against fuel naphthalene content in Figure 49 with the regression analysis line. As expected, this analysis shows a very low sensitivity of liner temperature rise to fuel naphthalene content at constant fuel hydrogen content.

Flame radiation measurements at the crossfire port plane were obtained with the apparatus and procedures described in Section VI-A-2; detailed results are listed in Appendix B. Due to an undetected noise source in the pyrometer signal, valid flame radiation measurements were not obtained for the first six fuels tested. For the last seven fuels, Figure 50 shows the effect of combustor operating conditions on flame radiation. The severity parameter shown was identified using regression analysis procedures. The parameter is similar to the one derived for the J79-17A (Reference 1) except no fuel/air ratio effect is evident in the current data. Figure 51, which summarizes the data of Table B-10, illustrates the effect of fuel hydrogen content on flame radiation. Unlike the J79-17A high smoke combustor, only a moderate fuel effect is observed. The absolute levels of flame radiation for the J79-17C combustor for all fuels are close to the level for J79-17A combustor with JP-4 fuel, except at dash where the J79-17C values are about 50% of the J79-17A levels. These relatively low and fuel insensitive levels may be due to the low smoke levels of the J79-17C combustor which would produce a nearly nonluminous flame for all fuels. In addition, the burning in the leaner dome J79-17C combustor may occur largely upstream of the crossfire port location and the pyrometer would, therefore, not view peak flame radiation but some lower radiation level from a cooler gas temperature. This latter possibility may also explain why some inner liner temperatures vary more with fuel hydrogen content than do the measured radiation.

Figure 52 presents radiant heat flux normalized for fuel hydrogen content plotted against fuel naphthalene content to examine the effect of fuel aromatic structure. The plot clearly shows that in this test series, dicyclic aromatics produce no greater radiant heat flux beyond that predicted by fuel hydrogen content.

6.   Combustor Exit Profile and Pattern Factor

Combustor exit temperature distributions were measured in the high pressure tests using the fixed thermocouple rake array described in Section V-A-2. Detailed data are listed in Appendix B, and trends are illustrated in Figures 53, 54, and 55.
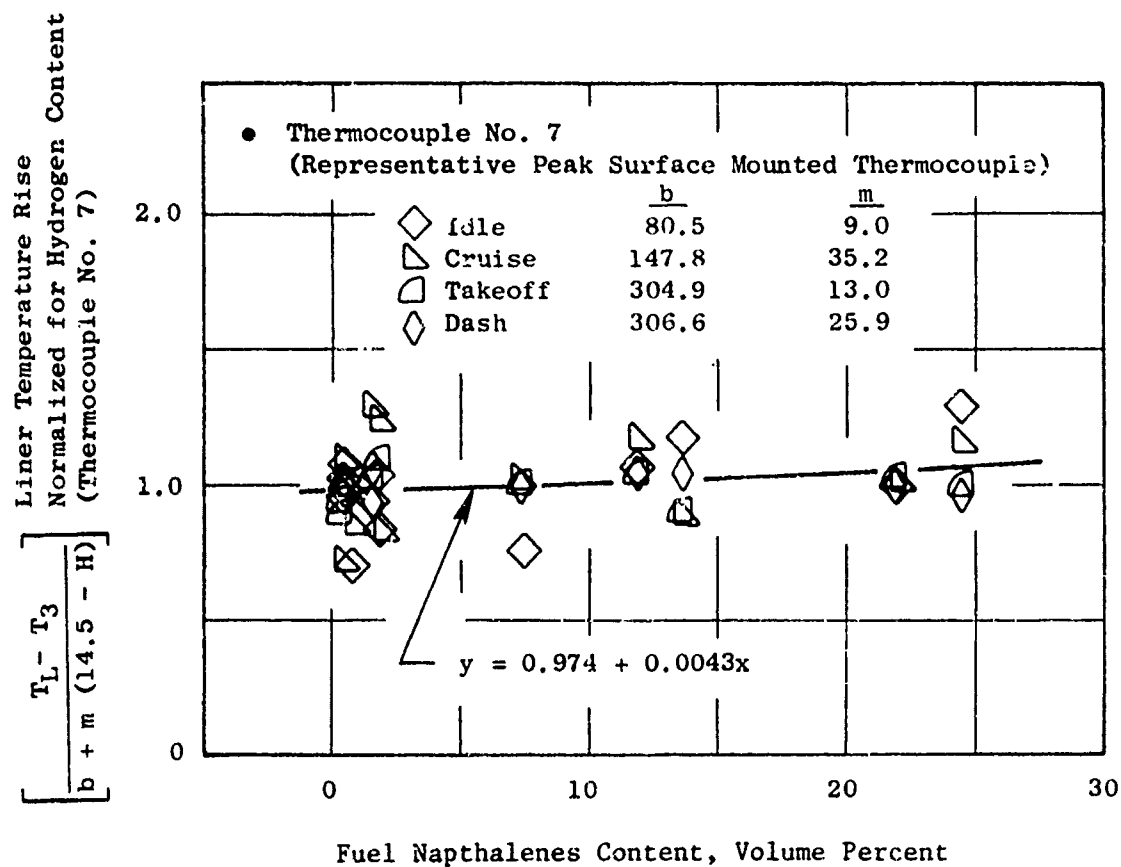
Figure 49. Effect of Fuel Napthalenes Content on Liner
Temperature Rise Normalized for Hydrogen Content.

Figure 50. Effect of Combustor Operating Conditions on Flame Radiation.
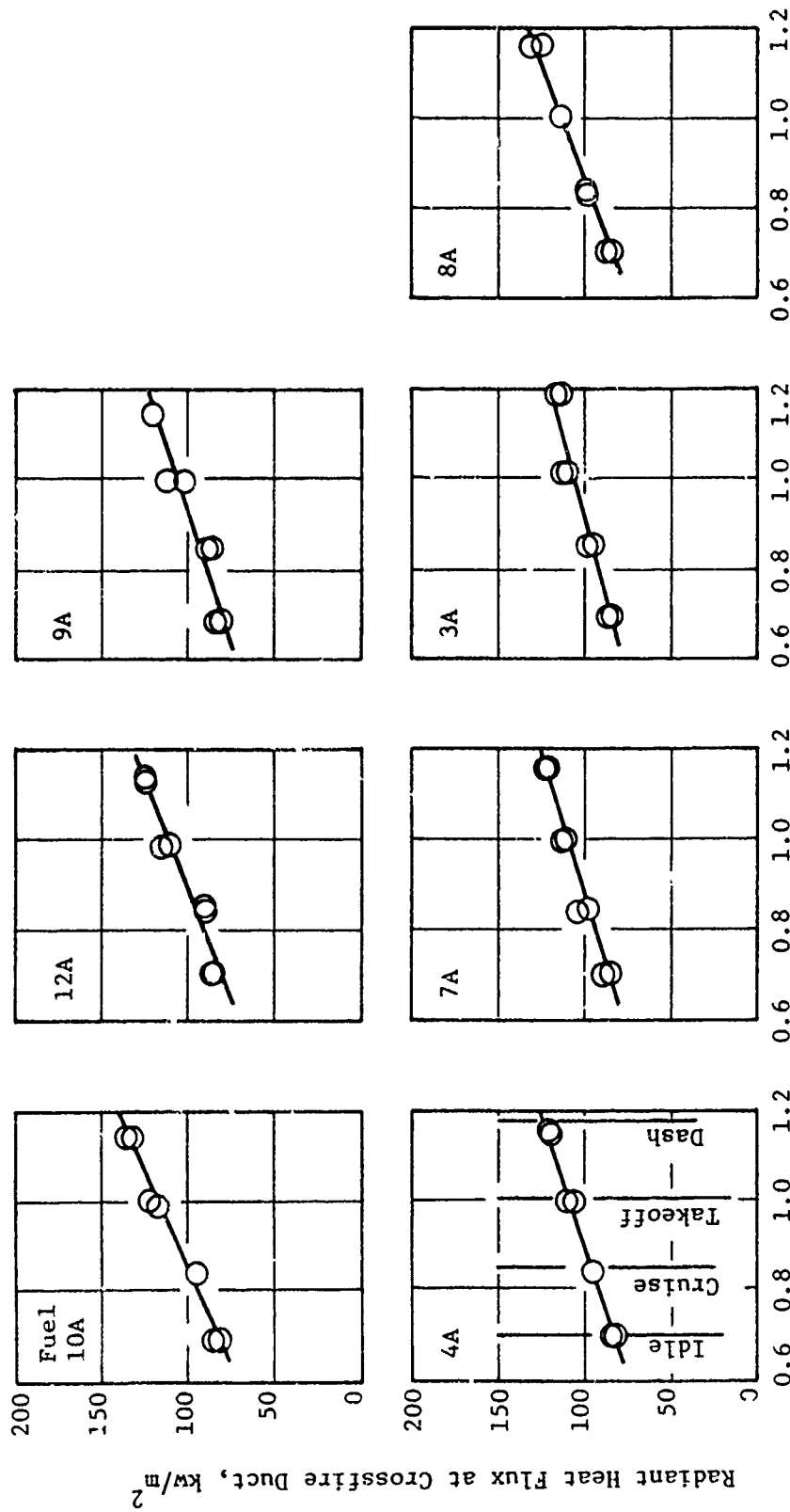
$$\text{Exp.}\left(\frac{P_3 - 1.359}{34.6} + \frac{T_3 - 664}{T_{35}}\right), M_{Pa}, K$$

89
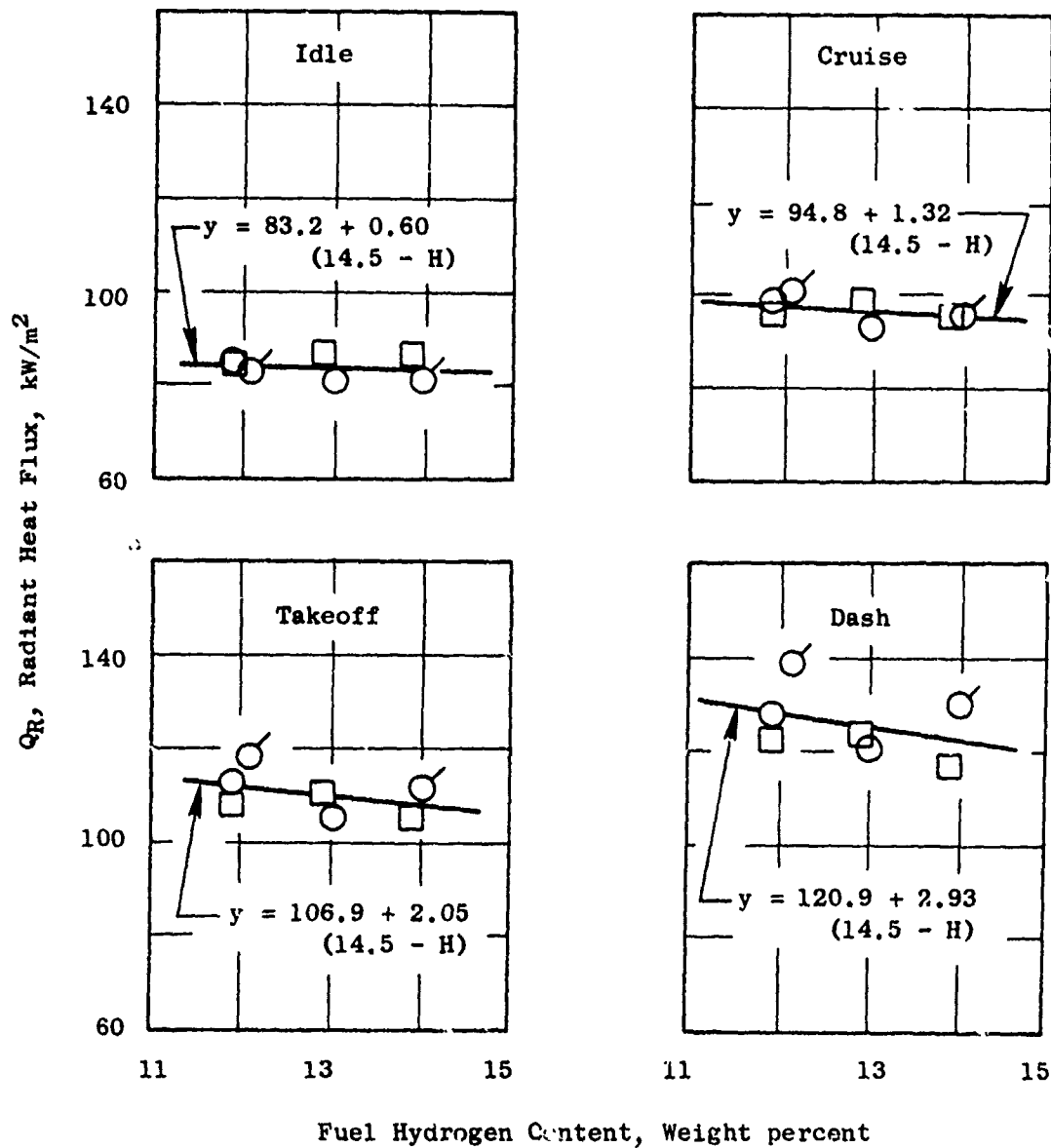
Figure 51. Effect of Fuel Hydrogen Content on Flame Radiation.
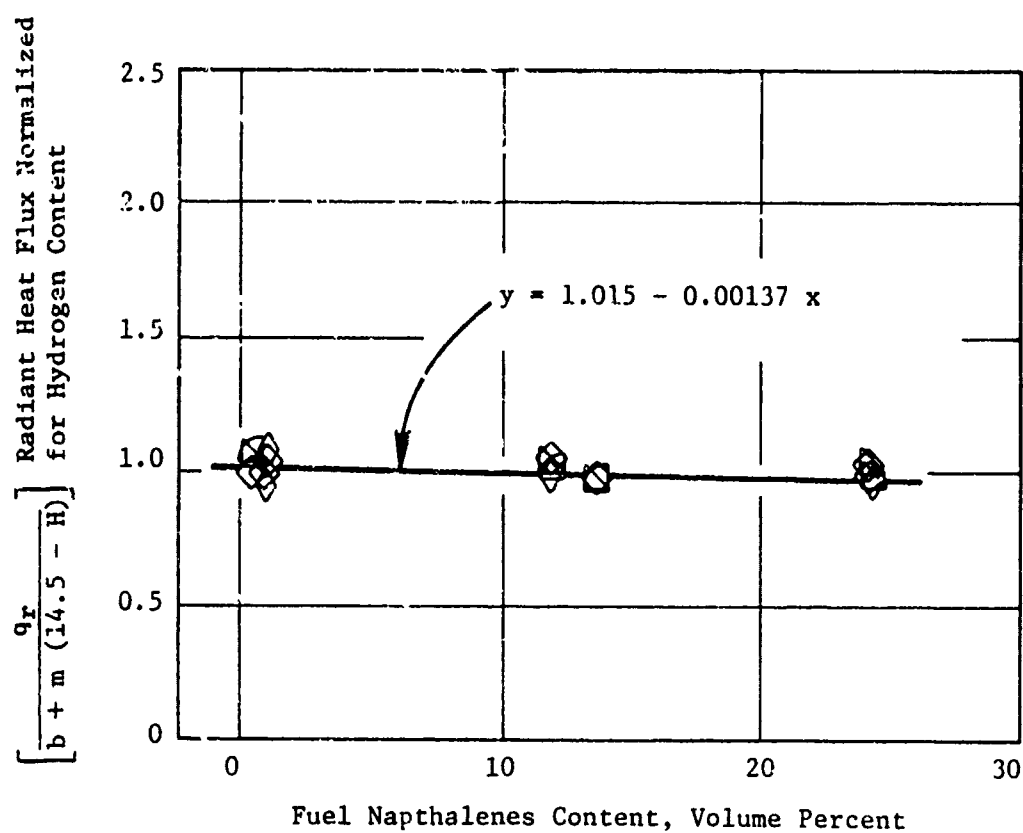
Figure 52.   Effect of Fuel Napthalenes Content on Radiant
Heat Flux Normalized for Hydrogen Content.
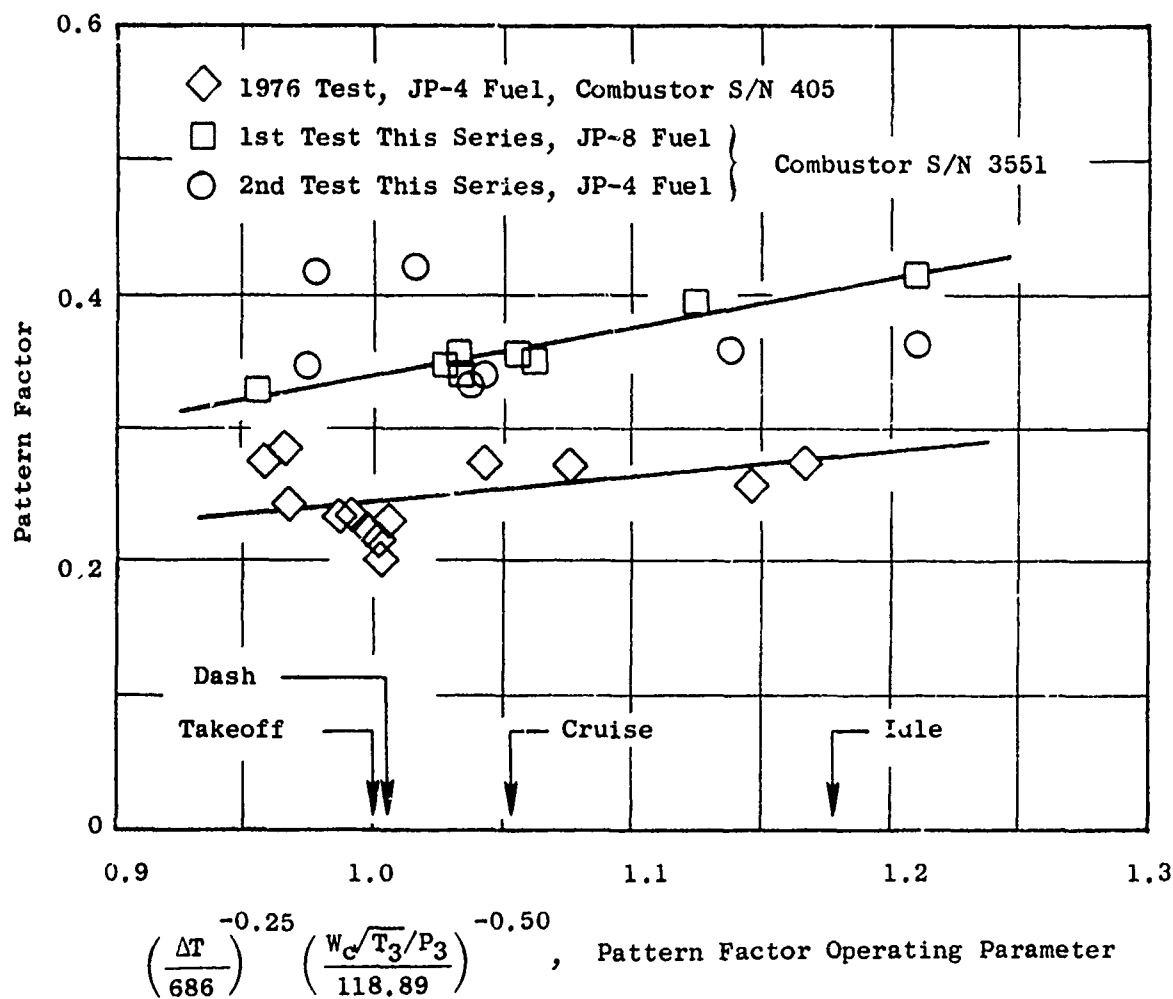
Figure 53. Effect of Operating Conditions on Pattern Factor.

The figure plots Pattern Factor (y-axis, 0 to 0.6) against the Pattern Factor Operating Parameter (x-axis, 0.9 to 1.3):

$$\left(\frac{\Delta T}{686}\right)^{-0.25} \left(\frac{W_c\sqrt{T_3}/P_3}{118.89}\right)^{-0.50}, \quad \text{Pattern Factor Operating Parameter}$$

Legend:
◇ 1976 Test, JP-4 Fuel, Combustor S/N 405
□ 1st Test This Series, JP-8 Fuel)
○ 2nd Test This Series, JP-4 Fuel) Combustor S/N 3551

Operating condition markers: Dash, Takeoff, Cruise, Idle
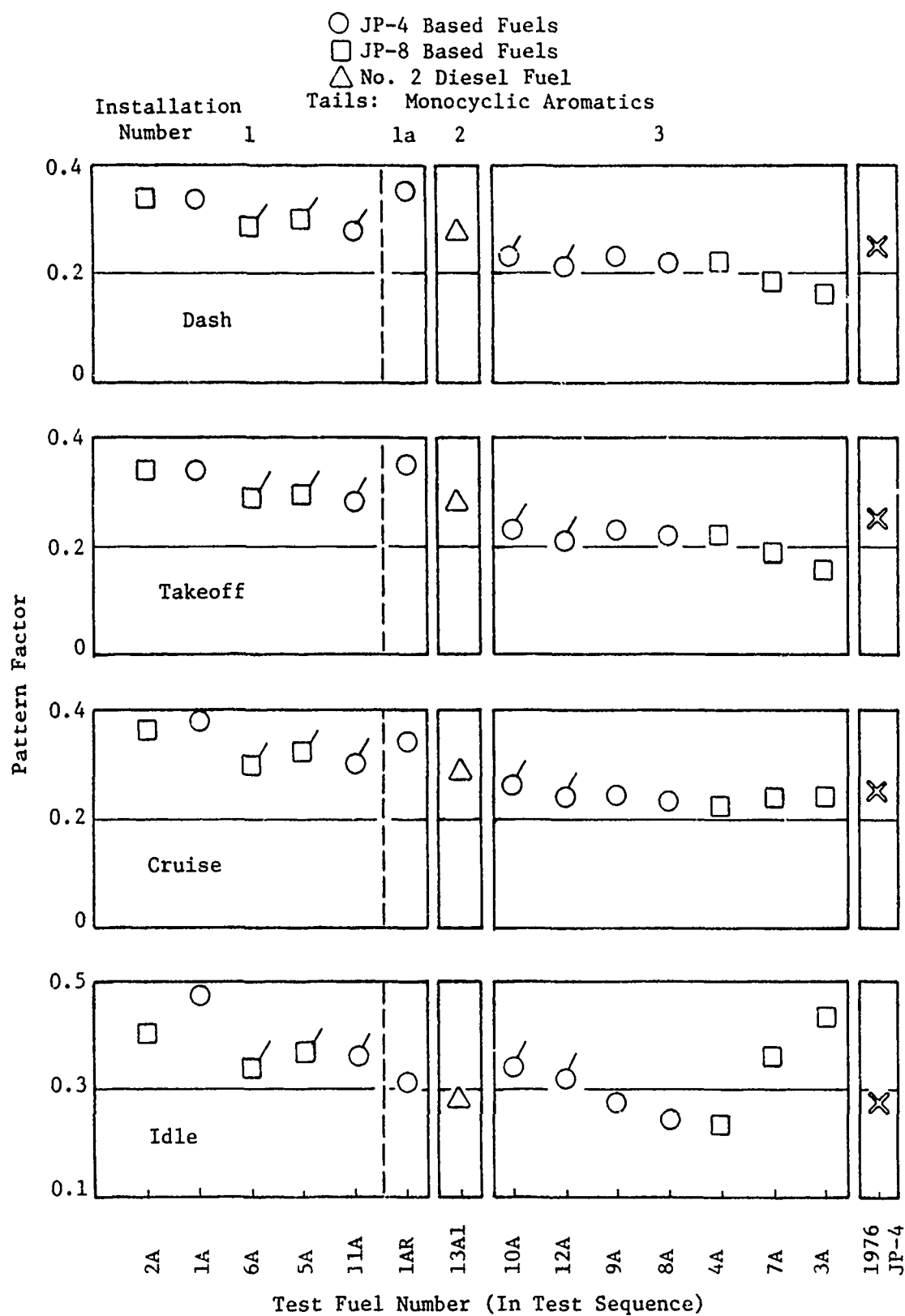
Figure 54. Variation in Pattern Factor with Test Sequence.
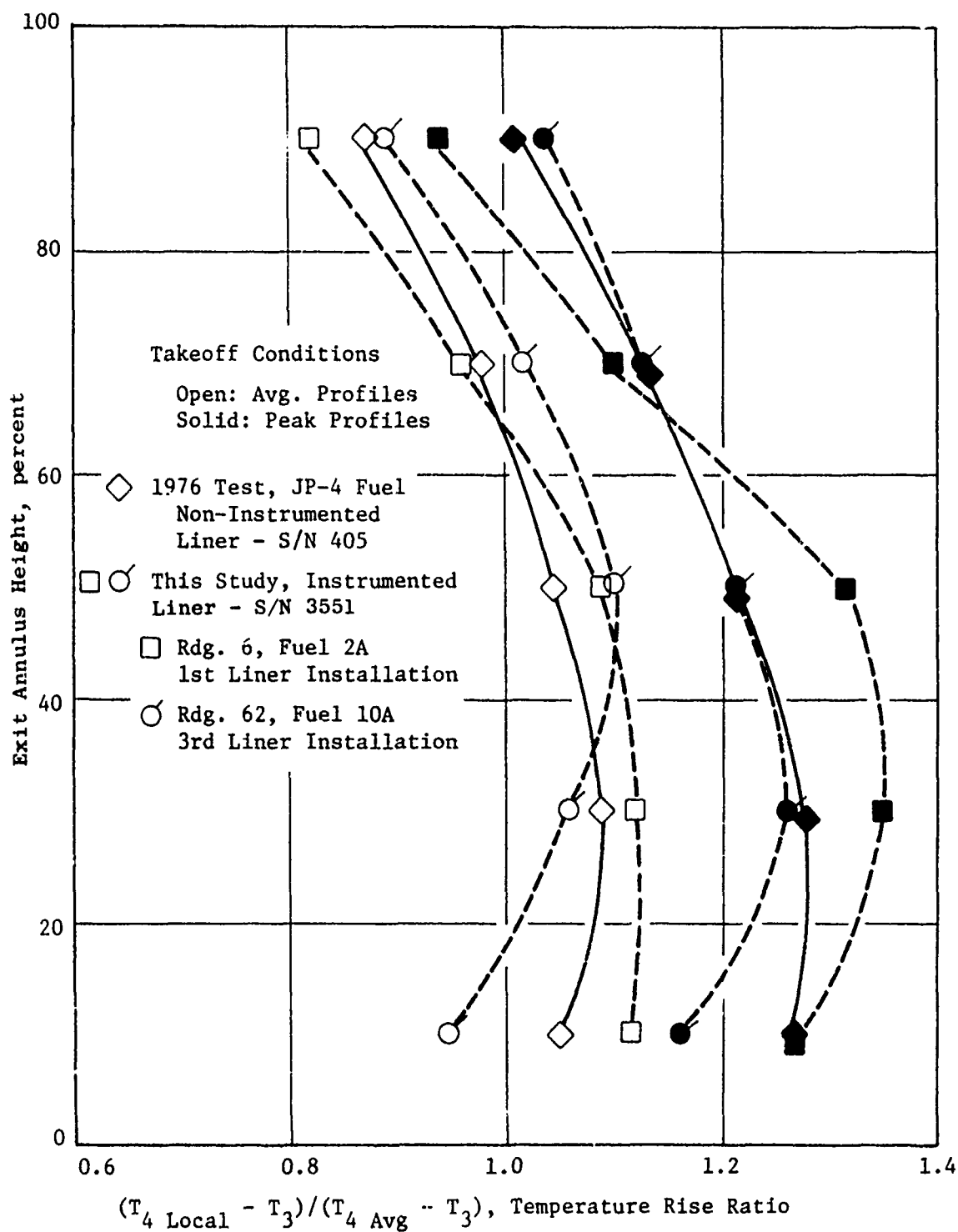
Figure 55. Comparison of Combustor Exit Temperature Profiles.

It was anticipated from previous experience with this combustor model that exit temperature distributions would be relatively insensitive to combustor operating conditions and fuel type. As shown in Figure 53, both of these expected data trends were verified in the first two fuel evaluations, but the pattern factor levels were significantly higher than had been measured in previous tests of the same combustor model, in the same test rig, as part of a vendor substantiation program. The differences in pattern factor levels were too large to be attributed to either normal variations between combustor assemblies or test repeatabilities. But, at the time, no other obvious explanations could be found, so the test series were therefore continued as planned.

In subsequent fuel evaluations, exit temperature distributions varied considerably, as shown in Figures 54, and 55, and a probable reason for the variation was identified. In Figure 54, pattern factor (from Table B-12) for each operating condition and fuel type is plotted in chronological test order, separated by "installation number" which is defined in Table 17. It is seen that pattern factor levels were relatively constant within an installation, but varied significantly between installations. The pattern factor levels in installation No. 3 are in fair agreement with those expected from previous tests. As shown in Figure 55, detailed profiles also tend to display similar peak levels, but noticeable difference in profile shape.

In Table 17, all hardware changes in the test series which might have affected either combustor exit temperature distributions or temperature measurements are listed. The major changes in pattern factor levels (Figure 54) are associated with the two liner removals. Exit rake replacement and fuel nozzle seem to have had little effect on pattern factor levels.

A mechanism by which liner removal might affect pattern factor was identified in a posttest inspection of the outboard side of the rear liner. As shown in Figure 46, the liner thermocouple leadout blockage disrupted the airflow to the rear liner in this region, causing a hot spot. Very probably the dilution hole airflows were also reduced, which could very easily have increased pattern factor. The effective blockage of the thermocouple leadout wires probably varied between installations, thus introducing an extraneous variation in the test series. The most valid pattern factor measurements, therefore, would be obtained with a noninstrumented liner, as was used in the previous vendor substantiation program.

As noted above and shown in Figure 54, seven fuels were tested in installation No.3, and pattern factor levels were relatively constant. JP-4 and JP-8 based fuels with hydrogen contents of 12, 13, and 14 weight percent were included in this installation series, so pattern factor must be virtually independent of fuel type.

7.   Cold-Day Ground Starting and Idle Stability

Fourteen cold-day ground start tests were conducted in the low pressure rig using procedures described in Section V-B-2. Detailed test results are listed in Appendix D and typical results are illustrated in Figure 56. In

Table 17. Chronology of Hardware Changes
During Test Series.

Installation No.	Run No.	Fuel No.	Hardware Change Made After Run			
			Exit Rakes	Fuel Nozzle Removed for Cleaning	Liner Removed for Photos	Liner Re-instrumented
1	1	2A,1A	2 rakes	No	No	No
	3	6A,5A,11A	No	No	No	No
1a	4	1AR	No	Yes	Yes	No
2	5	13A	4 rakes	Yes	Yes	Yes
3	6	10A,12A, 9A,8A	No	No	No	No
	7	4A,7A,3A	End of This Test Series			
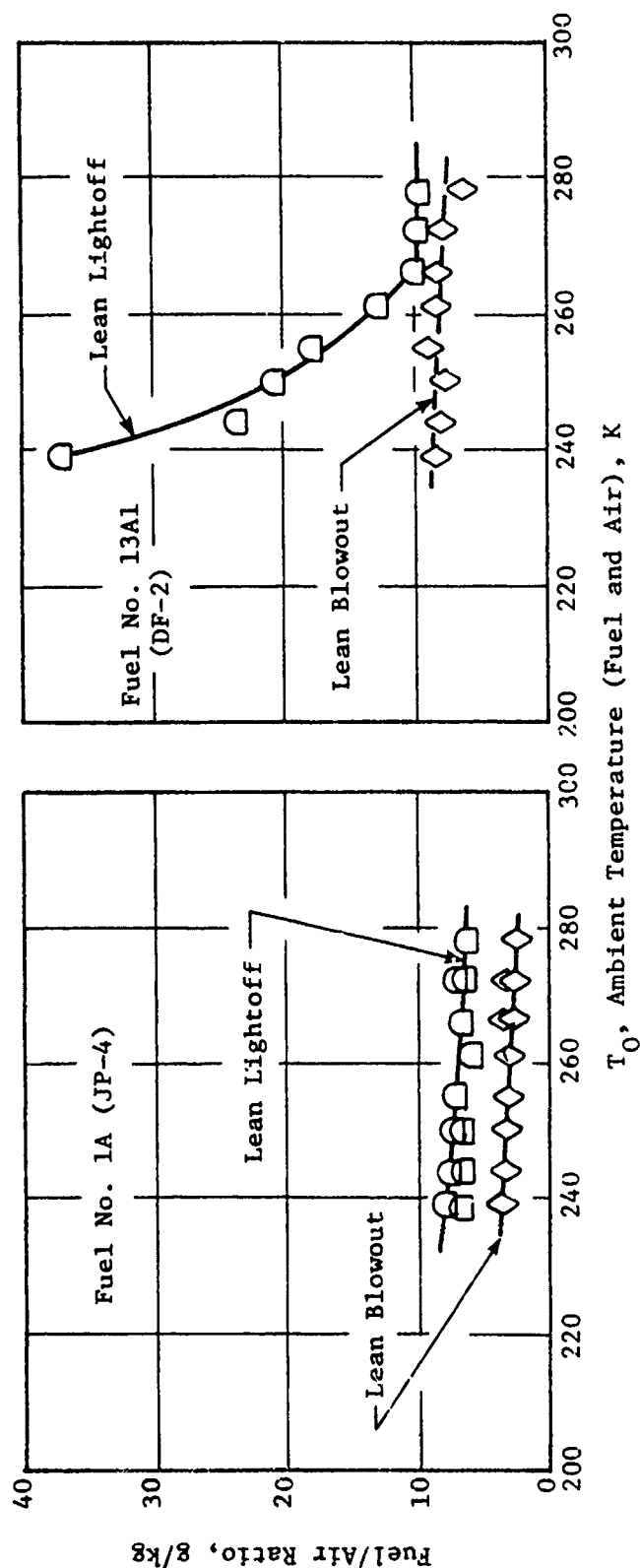
Figure 56. Typical Ground Start Characteristics.

each test, 1000 rpm engine motoring conditions were simulated, and lean light-off and lean blowout limits were determined as a function of ambient (fuel and air) temperature in steps from test cell ambient down to 239 K (-30° F). As shown in Figure 56, even with the most viscous fuel (No. 13A1, Diesel Fuel) lightoffs were obtained down to 239 K, but the fuel/air ratios required were fuel-type and temperature dependent. Lean blowout fuel/air ratios were usually about half of those required for lightoff, with only minor fuel-type and temperature dependence. Results for all fuels are summarized in Table 18. Effects of fuel properties on lean lightoff fuel/air ratio at both standard and cold day start conditions are illustrated in Figure 57. The standard day data exhibit virtually no fuel dependence, but the cold day data are fuel de-pendent and correlate very well with the relative spray droplet size parameter (calculated from fuel viscosity, density and surface tension) which is derived and listed in Appendix A.

Lean lightoff and blowout limits were also measured at idle operating con-ditions for all of the test fuels, as part of the high pressure test series. These data are summarized in Table 19. Lean blowout fuel/air ratios were less than 2.5 g/kg with all fuels. Lightoff fuel/air ratios ranged from 5.1 to 13.7 g/kg. The variation is attributed to data scatter rather than to any fuel property effect. At these inlet conditions, both lightoff and blowout are probably more dependent on fuel spray geometry and dome airflow than upon any of the fuel properties.

8. Altitude Relight

Fourteen altitude relight tests were conducted in the low pressure rig using procedures described in Section V-B-2. Detailed results are listed in Appendix D and summarized in Tables 20 and 21. In each test, altitude relight/blowout limits and lean relight/blowout limits were determined at four airflow/temperature levels selected to span the engine windmilling/air start map (Figure 8).

Altitude relight limits (Table 20) agreed well with previous rig test results wherever comparison could be made, but tended to be pessimistic rela-tive to engine results (Figure 8) with respect to both altitude and flight Mach number limits. Pressure blowout limits (Table 21) tended to be rela-tively close to relight limits in all cases.

Effects of fuel properties on altitude relight limits are illustrated in Figure 58. Like the ground start data, the altitude relight limits correlate well with the relative spray droplet size parameter when the air and fuel temperatures are low (low Mach number flight conditions). At higher Mach number conditions, where air and fuel temperatures are elevated, altitude relight limits become independent of fuel type. These fuel effect trends on both altitude relight and cold day ground start are very much like those found for the F101 combustor (Reference 2).

Table 18. Summary of Ground Start Test Results.[1]

Fuel Number	Fuel-Air Ratio, g/kg			
	Standard Day (288.2K)		Cold Day[2] (239.0K)	
	Lean Lightoff	Lean Blowout	Lean Lightoff	Lean Blowout
1A	6.7	2.4	7.0	3.6
1A (Repeat)	6.5	2.5	8.0	3.7
2A	6.0	4.2	10.4	8.3
3A	6.8	4.5	23.9	10.3
4A	8.2	4.7	14.5	7.3
5A	6.2	4.3	9.3	7.3
6A	6.0	3.5	8.6	6.9
7A	7.5	5.0	11.9	8.8
8A	7.0	2.3	7.0	5.4
9A	6.5	2.0	9.2	5.4
10A	6.7	2.7	7.2	4.0
11A	6.2	2.5	6.5	4.1
12A	6.0	2.8	7.2	4.4
13A1	8.7	7.2	37.0	8.5

[1] Simulated 1000 rpm Cranking Conditions

P_3 = 101 kPa

W_c = 3.18 kg/s per engine

[2] All fuels light-off to 239K (at least)
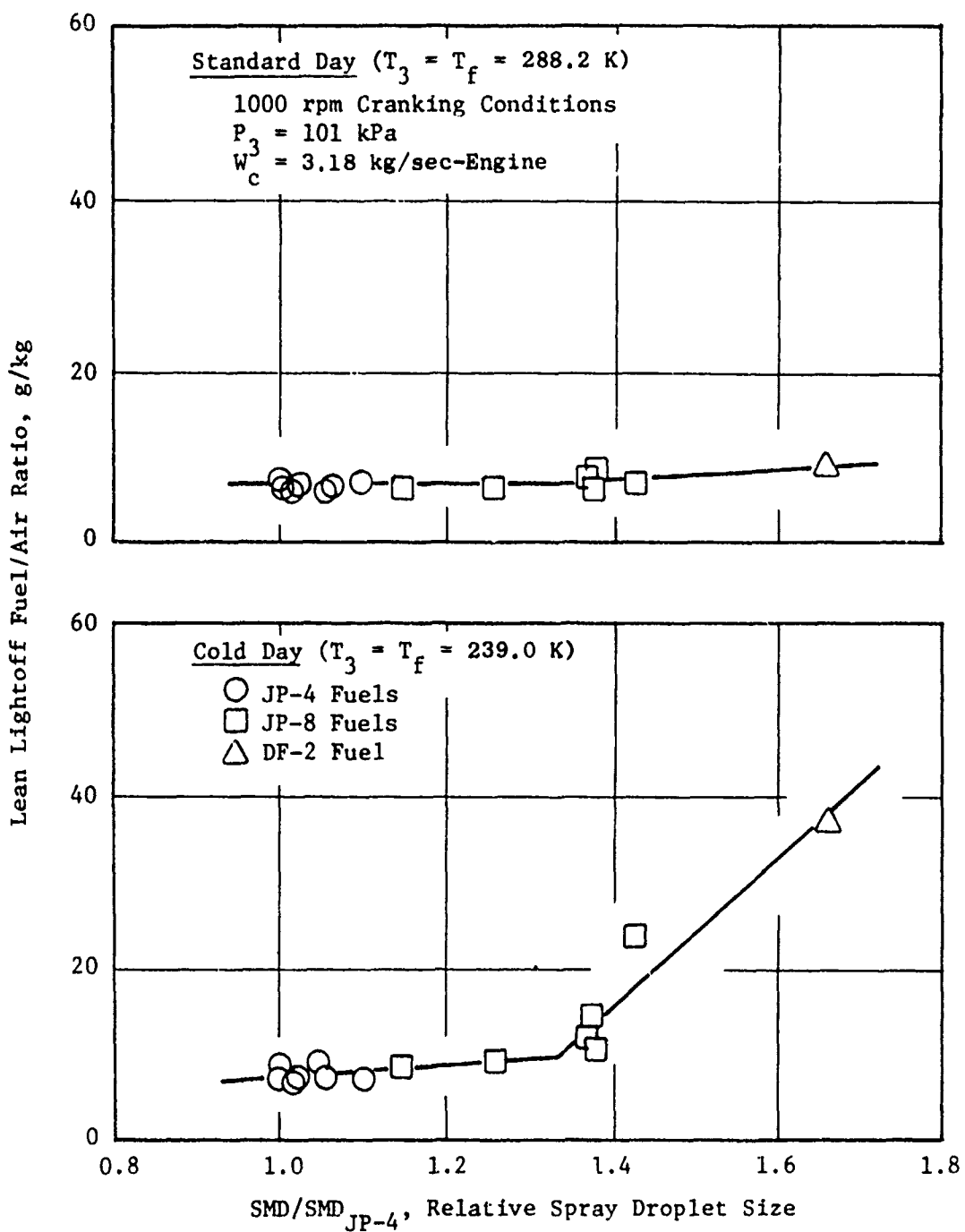
Figure 57. Effect of Fuel Atomization on Ground Start.

Table 19. Summary of Idle Stability Test Results.

$$P_3 = 0.254 \text{ MPa}$$

$$T_3 = 421 \text{K}$$

$$V_r = 24.2 \text{ m/s}$$

Fuel Number	Lightoff		Lean Blowout	
	W_f, Fuel Flow, g/s/can	f, Fuel-Air Ratio, g/kg	W_f, Fuel Flow, g/s/can	f, Fuel-Air Ratio, g/kg
1A	11.7	7.5	<2.3	<1.5
1A (Repeat)	11.6	7.4	<2.3	<1.5
2A	12.1	8.0	<2.5	<1.7
3A	10.0	6.0	2.3	1.4
4A	18.3	11.8	3.8	2.5
5A	8.1	5.1	<2.5	<1.7
6A	10.8	7.1	<2.5	<1.7
7A	13.1	8.4	2.8	1.8
8A	21.8	13.7	<1.3	<0.8
9A	16.8	10.2	11.6	7.7
10A	20.5	13.3	<1.3	<0.8
11A	11.7	7.6	<2.5	<1.7
12A	11.7	7.6	<1.3	<0.8
13A1	10.0	6.7	<2.5	<1.7

Table 20. Summary of Altitude Relight Limits.

	$W_c = 2.27$ kg/s		$W_c = 4.08$ kg/s		$W_c = 4.99$ kg/s		$W_c = 9.07$ kg/s	
$W_f = 64.9$ g/s								
Fuel Number	Alt km	M_O	Alt km	M_O	Alt km	M_O	Alt km	M_O
1A	6.7	0.43	4.6	0.55	5.2	0.65	No Light	
1A (Repeat)	7.3	0.46	6.1	0.62	6.1	0.69	No Light	
2A	4.3	0.36	5.9	0.61	4.6	0.62	No Light	
3A	5.2	0.39	5.8	0.61	6.3	0.70	3.1[1]	0.78[1]
4A	2.4	0.33	5.3	0.58	4.5	0.62	No Light	
5A	6.4	0.42	5.8	0.60	4.6	0.62	No Light	
6A	6.0	0.41	5.6	0.60	4.0	0.60	No Light	
7A	5.0	0.38	5.7	0.60	6.3	0.70	No Light	
8A	6.6	0.43	7.1	0.37	5.7	0.67	No Light	
9A	6.6	0.43	7.9	0.70	6.3	0.70	No Light	
10A	6.2	0.42	6.4	0.62	6.3	0.70	3.6[1]	0.76[1]
11A	6.7	0.44	6.9	0.66	6.8	0.73	4.9	0.84
12A	6.4	0.43	7.0	0.66	6.3	0.70	No Light	
13A1	4.6	0.37	3.9	0.53	6.5	0.71	No Light	

[1]$W_c = 7.9$ kg/s

Table 21. Summary of Altitude Pressure Blowout Limits.

$W_f = 64.9$ g/s								
	$W_c = 2.27$ kg/s		$W_c = 4.08$ kg/s		$W_c = 4.99$ kg/s		$W_c = 9.07$ kg/s	
Fuel Number	Alt km	M_o	Alt km	M_o	Alt km	M_o	Alt km	M_o
1A	7.8	0.48	8.7	0.74	6.7	0.72	Not Determined	
1A (Repeat)	8.4	0.51	8.4	0.73	8.0	0.78	Not Determined	
2A	6.9	0.44	7.5	0.69	7.3	0.75	Not Determined	
3A	7.7	0.48	7.5	0.68	7.8	0.77	9.3[1]	1.00[1]
4A	7.3	0.46	7.6	0.69	7.6	0.76	Not Determined	
5A	6.8	0.44	7.9	0.70	8.0	0.78	Not Determined	
6A	8.3	0.51	7.2	0.67	7.1	0.74	Not Determined	
7A	7.0	0.45	7.9	0.70	6.5	0.78	Not Determined	
8A	9.1	0.55	8.0	0.71	7.8	0.77	Not Determined	
9A	8.3	0.50	8.9	0.75	7.5	0.75	Not Determined	
10A	8.2	0.50	8.1	0.71	8.6	0.81	8.8[1]	0.97[1]
11A	7.7	0.48	7.9	0.70	8.2	0.79	13.7	1.19
12A	7.8	0.48	8.4	0.73	7.5	0.76	Not Determined	
13A1	5.8	0.40	6.4	0.63	7.8	0.77	Not Determined	

[1]$W_c = 7.9$ kg/s
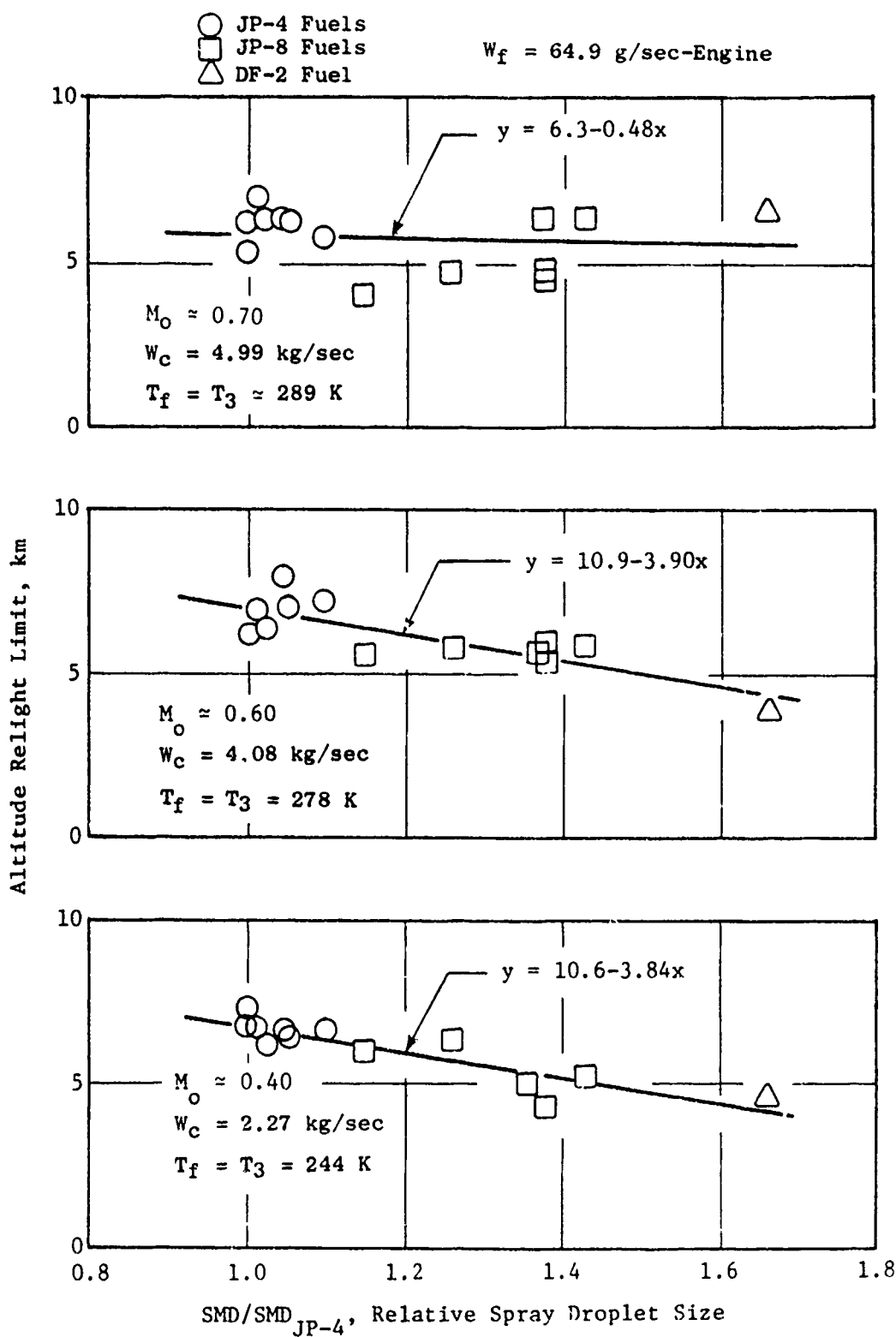
Figure 58. Effect of Fuel Atomization on Altitude Relight Limits.

9. Fuel Nozzle Fouling

Seven fuel nozzle fouling tests were conducted, for a total of 346 hours. The first four and the sixth used Fuel No. 13, the low thermal stability No. 2 diesel fuel. The fifth and seventh (Test No. 15) used Fuel No. 2, the high thermal stability JP-8.

The first test was run at 464 K, a temperature estimated to cause a moderate nozzle failure time, based on previous experience and knowledge of the fuel quality. However, the nozzle failed in only 14 hours and the test was terminated.

The second test was, therefore, run at a lower temperature of 450 K. At this condition, the nozzle showed only a small performance loss in 71 hours.

The third test was run at a higher temperature, 469 K, resulting in a moderate loss in performance in 54 hours.

The fourth test was run at a much higher temperature, 491 K, and a large loss in performance was observed in 30 hours, though not as large as the loss in the first test at a much lower temperature.

A review of the first four tests at this time indicated that the first test was inconsistent with the other three. The tip of the first nozzle was, therefore, opened for inspection. The interior was found to contain heavy "carbon" deposits which would explain its performance, but which would not be expected with the fuel temperature maintained. It was then observed that the nozzle stem was discolored, quite different from the other three, indicating it had reached temperatures much higher than the desired 672 K gas stream temperature. It was concluded that the first test was not run according to the prescribed conditions, and the results were invalid and would not be considered further.

Figure 59 shows photographs of the primary slot piece from the tip of the nozzle used in the first test, alongside comparable photographs of the primary slot piece used in the fourth test. In the latter case, the test was twice as long and the fuel temperature was 27 K higher, thus, reinforcing the suggestion that the rapid failure in the first test was caused by excessive nozzle stem temperature.

The fifth test was run with Fuel No. 2 at 491 K for 75 hours, and showed very little performance degradation, much less than with Fuel No. 13 at the same temperature.

A sixth test was then run for 40 hours at 478 K, a temperature between two previously run tests, and the results appeared quite consistent with the others.

A seventh and final test (No. 15) was then run for 62.5 hours at 505 K to validate the data previously obtained on Fuel No. 2. All of the periodic flow

Test No. 1   Test No. 4

Fuel
Inlet

3.1 mm
Diameter

Annulus
Feed
Port

1.3 mm
Diameter

Spin
Chamber
Inlet
Port

0.6 mm
Diameter
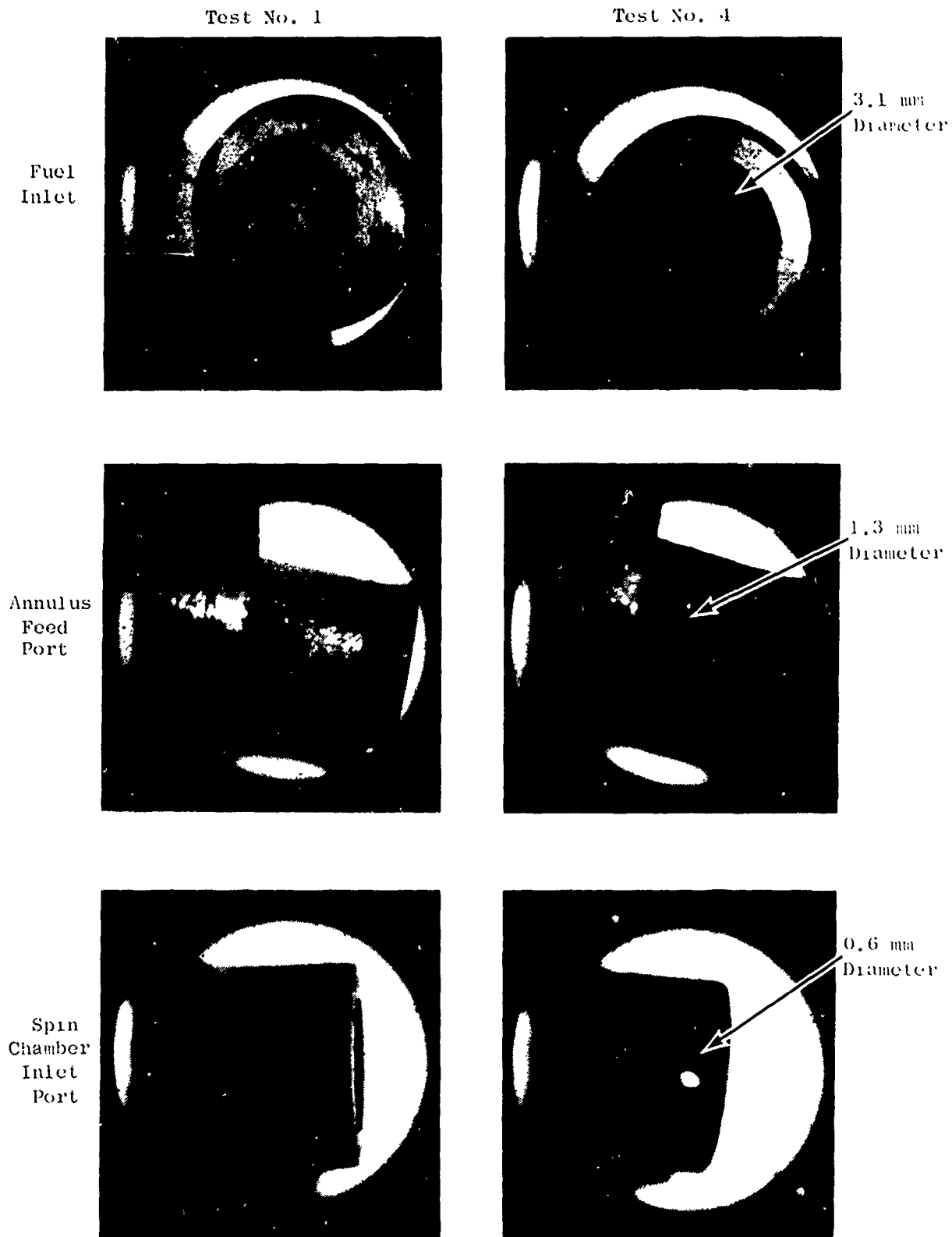
Figure 59.   Posttest Appearance of Fuel Nozzle Primary Slot
Pieces, Fuel Nozzle Fouling Tests.

calibration data acquired in these tests are listed in Appendix E. Because of the specific design characteristics of the J79-17C nozzle, it was decided to analyze three distinct aspects of its performance:

1. Primary orifice metering performance (with flow divider valve closed).

2. Secondary orifice metering performance (with flow divider valve full open).

3. Flow hyteresis, caused by abnormal drag forces on the valve due to "gum" deposits.

It was also established, somewhat arbitrarily, that "failure" would be either a 10% reduction in primary flow, a 5% reduction in secondary flow, or a 10% increase in hysteresis. These values are considered to be high enough to cause significant degradation in nozzle performance, without requiring excessive test time or excessively severe test conditions.

The orifice performance data were reasonably well-ordered. However, the valve hysteresis data were quite erratic, which should not be surprising when considering the factors involved in gum formation and deposition. Curve-fitting techniques were applied, examples of which are shown in Figure 60. However, it was concluded that these refinements were not warranted, particularly in the case of hysteresis data. It is believed that a single incident of high hysteresis can be just as damaging to an engine as a value obtained from a curve. In the top curve, Figure 60, for example, a failure point of 8 hours was considered just as valid as the value of 24 hours from the curve. Therefore, the failure times of the nozzles by the three performance criteria were established by visual inspection of the tabulated data, applying judgement and interpolation. In a few cases, the hysteresis data were considered invalid because the first value obtained was excessive. A summary of the data obtained is shown in Table 22.

"All of the data were analyzed by a stepwise multiple linear regression program. The correlation curves and equations are shown on Figure 61.

These fouling test data correlation equations can be utilized to estimate the fuel-limiting life expectancy of fuel nozzles. For example, consider a fuel with a breakpoint temperature, T_{BP}, of 533K (by JFTOT visual rating), operating at a temperature, T_F, of 408K. Using these data, the J79-17C fuel nozzle would be expected to last about 7500 hours before 'failure' by hysteresis. However, applying the same conditions to an F101 fuel nozzle (Reference 2), 'failure' by hysteresis would be expected in only 260 hours. The difference is attributed to the smaller clearances in the F101 flow divider valve as compared to the clearances in the J79-17C valve.

However, the J79-17C nozzle would probably 'fail' first by primary or secondary orifice plugging, at about 140 hours, under these same conditions. The F101 nozzle has very large discharge orifices, which would not be expected to plug for a very long time.
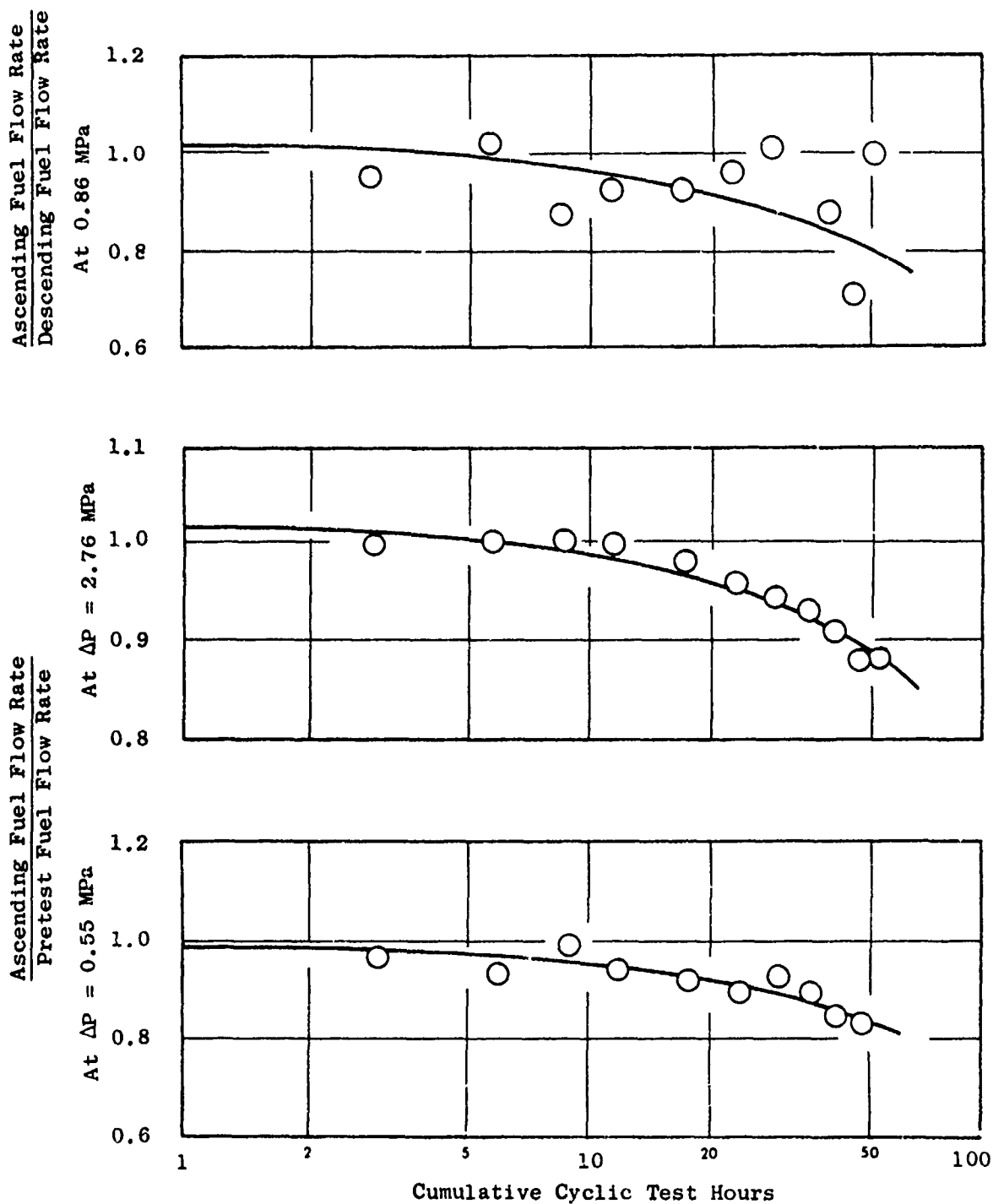
Figure 60. Typical Effect of Time on Performance of J79-17C Fuel Nozzle with Heated Fuel (Run 3, Diesel Fuel at 469 K).

Table 22. Summary of J79-17C Fuel Nozzle Fouling Test Results.

Test Number	Fuel Number	T_{BP}, Fuel Breakpoint, K	T_F, Fuel Temperature, K	$(T_{BP}-T_F)$, Temperature Difference, K	Cyclic Test Time (hours) to Produce Indicated Levels of Performance Degradation		
					Primary Orifice, 10% Flow Reduction @ 0.55 MPa	Secondary Orifice, 5% Flow Reduction @ 2.76 MPa	Divider Valve, 10% Flow Hysteresis @ 0.86 MPa
5	2A1	573	491	82	53	>75	20
15	2A2	593 ± 10	505	88 ± 10	>63	>63	17
2	13A1	523	450	73	55	66	---
3	13A1	523	469	54	36	28	---
6	13A2	503	478	25	26	31	6
4	13A2	503	491	12	19	18	1.5 ± 1.5
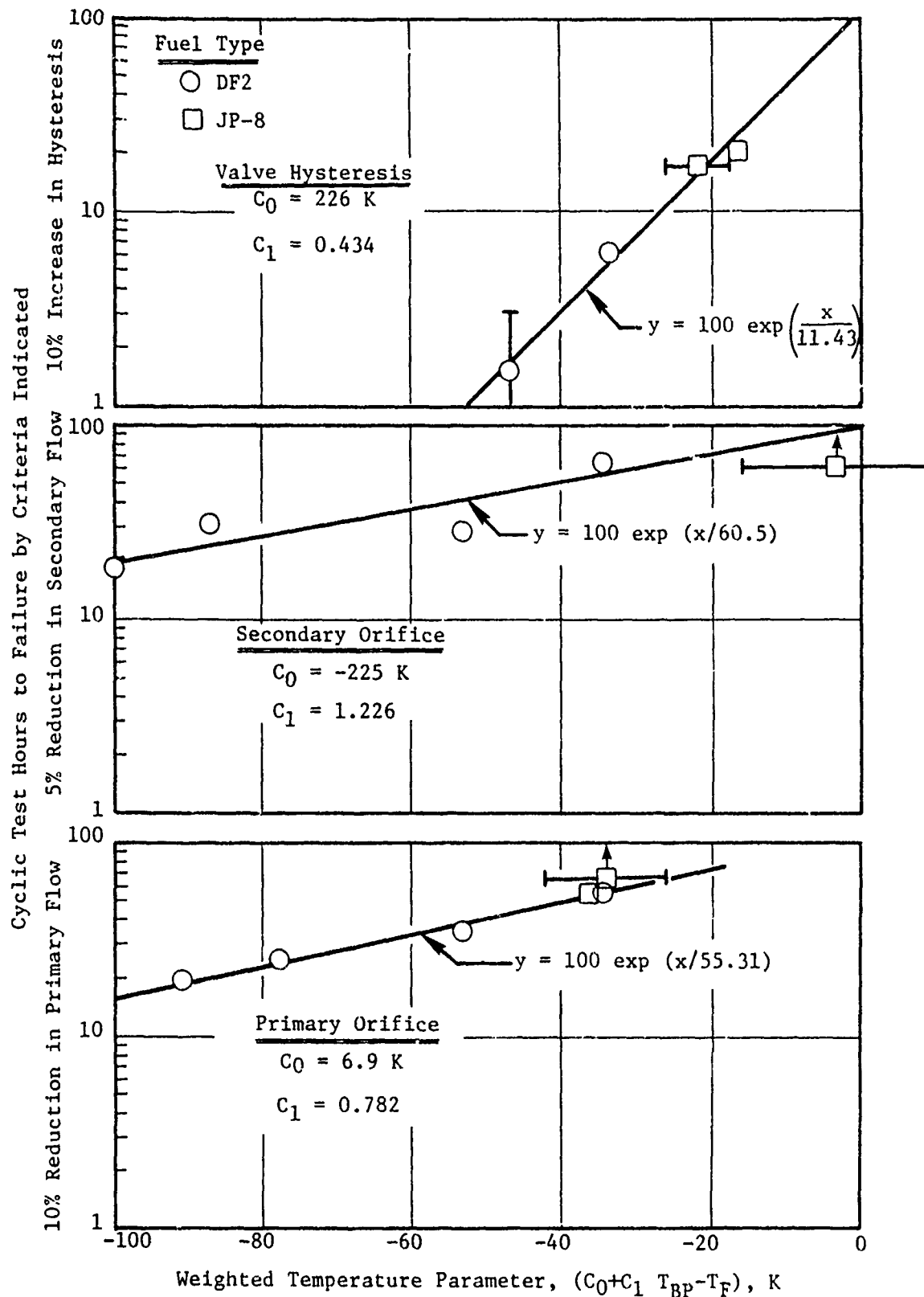
Figure 61.   Correlation of J79-17C Fuel Nozzle Fouling Test Results.

The equations can also be used to estimate the effects of fuel quality and fuel temperature on nozzle 'life'. For example, a 10K increase in fuel temperature would reduce the life expectancy of the J79-17C fuel nozzle by about 16%, as a result of reduced primary flow, and a 10K reduction in fuel thermal stability breakpoint would reduce its life expectancy about 18% as a result of reduced secondary flow."

B. Engine Systems Life Predictions

1. Combustion System Life Predictions

The life analyses described in Section V-E-2 were conducted assuming a flame radiation level for Fuel 1 (current JP-4) and adjusting the hot gas temperature and film effectiveness level to achieve a match between the measured and calculated temperatures on the panels. Similar data match curves were prepared for other fuels by maintaining a constant film effectiveness level and by adjusting the flame radiation to achieve the data match. This detailed approach permits the metal temperature to be calculated with high accuracy providing the desired accurate input for the stress calculations. Although supersonic dash conditions involved the most severe temperature conditions, only a small portion of actual flights encounter this condition; the actual combustor life is controlled by the sea level static condition which is therefore the basis for the following life discussion. The maximum temperatures were measured on the overhang at the downstream end of panel zero (see Figure 16) and data match curves based on best fit data (liner temperature rise versus fuel hydrogen content) were prepared for this panel for fuels containing 14.5, 14.0, 13.0, and 12.0 weight percent hydrogen. A typical data match curve is shown in Figure 62 for simulated takeoff conditions.

The actual takeoff condition involves a higher fuel/air ratio than could be tested in the test rig. Fuel/air ratio trends are available in the data, including the data at cruise inlet conditions where both cruise fuel/air ratios as well as the higher takeoff fuel/air ratios were tested. However, for consistency between the fuels, the fuel/air extrapolation for life calculations was done using the methods in established design extrapolations. The resulting life effects between fuels that result, are very close to the same as for the initial lower fuel/air ratio data before extrapolation.

Temperature profiles were prepared for the four fuels mentioned above for true engine takeoff conditions. The temperature profiles were used as inputs to the SNAPTS II Computer Program and effective stress levels were calculated for the various fuels. The stress and temperature distributions were combined with available material property data (Figure 28) to predict cycles to crack initiation. The predicted cyclic life for the inner-liner for fuels containing 12.0 weight percent hydrogen is about 75 percent of the life predicted for the fuel containing 14.5 weight percent hydrogen. This decrease in life is due to two effects. The first and smaller effect is due to increases in effective stress levels because of increases in temperature gradients between the panel and the cooling slot. The second and more significant effect is due to the rapid decay in material properties due to increase in temperature. The specific predicted effects of fuel hydrogen content on combustor life are:

111
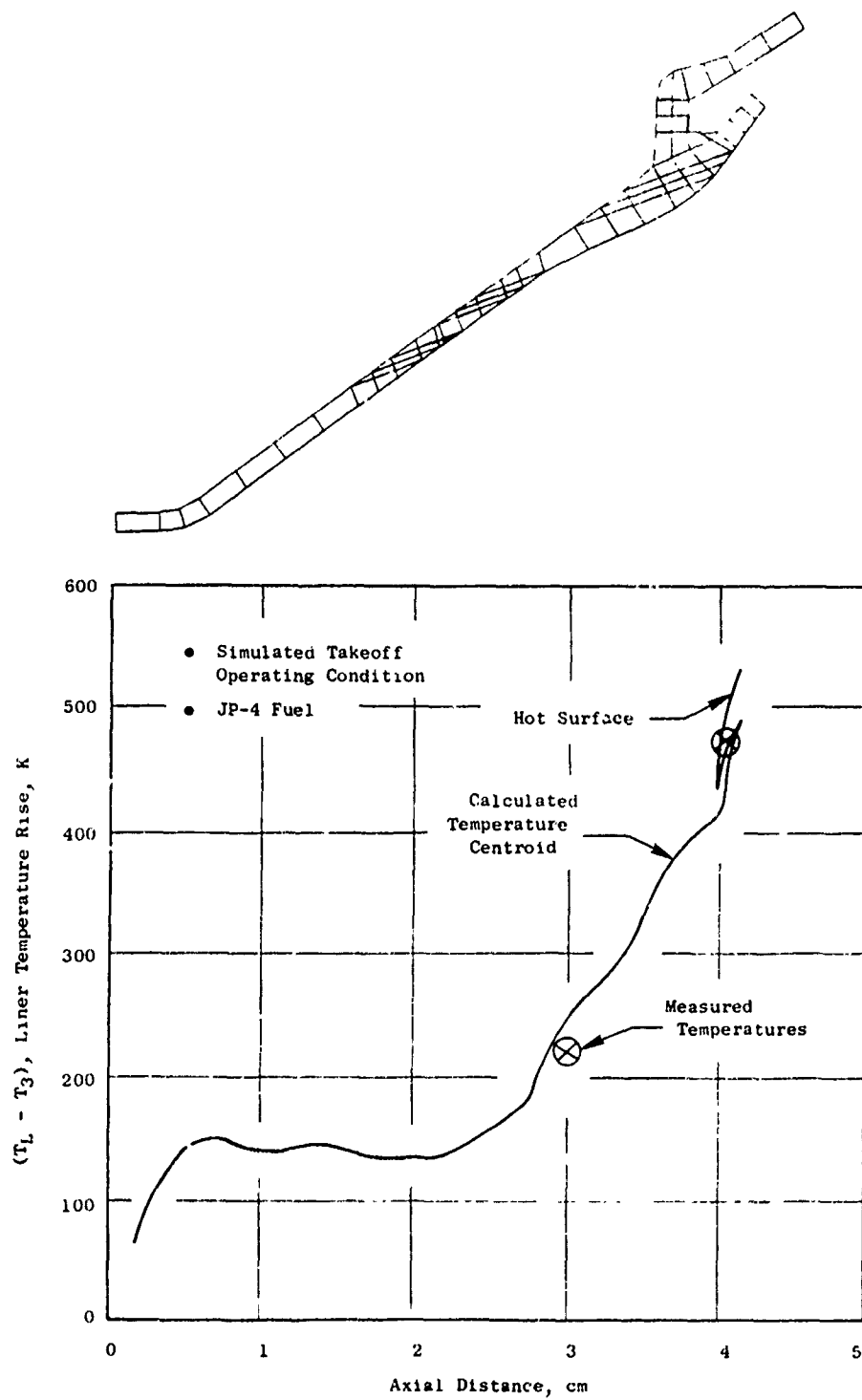
Figure 62. Typical Panel Zero Temperature Distribution.

Fuel Hydrogen Content, Weight Percent	Relative Inner Liner Life
14.5	1.0
14.0	0.93
13.0	0.83
12.0	0.74

The life limiting region analyzed above at the panel zero overhang does not show as much response to fuel effects as some other locations which, however, are not life limiting regions. For example as indicated in Section VI-A-5, the change in metal temperature with respect to hydrogen content was only about 8 K/% on the panel zero overhang, as compared to 20 to 30 K per percent hydrogen for instrumented locations further downstream, accounting for the small predicted change in life. A slope of 25 K per percent hydrogen content applied to the same absolute temperature level measured on the panel one overhang would have resulted in a predicted life for fuels containing 12.0 weight percent hydrogen of less than half of the predicted life for fuels containing 14.5 weight percent hydrogen. This would have agreed with the life decrement predicted for the F101 liner in Reference 2. The reduced effect for this J79-17C combustor liner is partly due to the more intense cooling mechanisms that exist in the hottest regions.

2. Turbine Life Predictions

As discussed in Section V-E-3, flame radiation changes are not predicted to affect turbine nozzle diaphragm temperatures because of the small viewing angle. Profile or pattern factor changes would be expected to directly affect turbine temperatures, but as was anticipated, no fuel effects on combustor outlet temperature distribution were observed. The J79-17C turbine life is therefore not expected to be affected by the fuel property changes investigated in this program.

C. Comparison of Results

Comparisons of the data acquired in this J79-17C engine combustor study to that previously acquired in the J79-17A and F101 engine combustor studies (References 1 and 2), have been made to identify common trends and/or key differences in fuel effects on the three combustion systems. Key design features of the three engine combustion systems are listed in Table 23, which shows:

1. The J79-17A and J79-17C engine combustors have several major differences in design features (such as cooling technique, primary zone airflow, fuel/air mixing technique, etc.) so comparisons of these data should provide an indication of the effects of combustor design features on the sensitivity to fuel property variations within the same envelope and operating conditions.

2. The J79-17C and F101 engine combustors have many of the same low-smoke long-life design features, so comparisons of these data should provide

Table 23. Comparison of Engine Combustor Design Features.

Design Characteristic	J79-17A (Reference 1)	Engine System J79-17C (This Study)	F101 (Reference 2)
Engine Type	Augmented Turbojet	Augmented Turbojet	Augmented Turbofan
Compression Ratio	13.4	13.4	26.8
Combustor Type	Can-Annular	Can-Annular	Full Annular
Fuel Injector Type	Dual Orifice Pressure Atomizer (Primary and Secondary)	Dual Orifice Hybrid Atomizer (Pressure Atomizing Primary and Low ΔP_f Airblast Secondary)	Simplex Atomizer Low ΔP_f Airblast
Primary Zone Type	Rich, Liner Thimble Air Feed	Lean, Liner Thimble Plus Corotating Swirler Air Feed	Lean, Liner Thimble Plus Counterrotating Swirler Air Feed
Combustor Cooling Type	Punched Louvers Throughout	Dome Impingement + Film Inner Liner – Machined Ring Aft Liner – Punched Louvers	Dome Impingement + Film Liners – Machined Ring
Smoke Emission Level (Current Fuel)	High	Low	Very Low
Liner Life (Current Fuel)	Short	Long	Very Long

114

an indication of the effects of engine design features (such as pressure ratio and turbine inlet temperature) on the sensitivity to fuel property variations.

Comparisons which have been made are shown in Tables 24 through 27. Key findings from these comparisons are discussed below.

Table 24 is a verbal summa.y of the major effects of operating conditions and fuel property variations on each of the combustor parameters which were measured in the current and previous evaluations. The table shows that while each of the combustor parameter levels with the baseline JP-4 fuel are highly engine system and operating condition dependent, fuel property variation effects are very similar in each engine system. In particular, the following fuel property trends are indicated:

1. Fuel hydrogen content is the key fuel property at high pressure/ temperature operating conditions, with respect to smoke, NO_x, liner temperature and flame radiation levels and hence, combustor durability. Each of these parameters increased with decreasing fuel hydrogen content at takeoff and dash operating conditions.

2. Fuel aromatic structure, as indicated by fuel naphthalene content is a relatively less important fuel property. However, at high engine pressure/ temperature conditions, some effects of fuel naphthalene content on flame radiation (J79-17A only) and smoke emission (J79-17C only) were observed, when the concentrations were high (12 - 25 volume percent). Peak liner temperature levels were virtually independent of naphthalene content in all cases.

3. Relative spray droplet size (calculated from fuel viscosity, density and surface tension) is a key fuel parameter at low pressure/temperature operating conditions. Low temperature relight capability (both cold day ground start and low Mach number altitude relight) decreased with this parameter. Idle and cruise CO and HC emission levels also increased with this parameter, alone in some cases, and jointly with decreasing fuel hydrogen content in others. In the one case where high temperature atmospheric pressure tests were conducted (F101), pattern factor increased with relative spray droplet size. However, in full density tests of the J79 combustors no fuel effects were found, and none are expected for the F101 at full density.

4. Fuel vaporization characteristics (as indicated by boiling range) of the fuels tested are highly confounded with the atomization characteristics, so some of the combustor parameters correlated by relative spray droplet size could be alternately attributed, at least partially, to vaporization properties.

5. Fuel breakpoint temperature (by JFTOT) is a key parameter with respect to fuel nozzle fouling, and hence, durability.

Table 25 presents a quantitative comparison of the effects of fuel property variations on exhaust emission characteristics. Coefficients (k_0, k_1, and k_2) determined by regression analyses are listed for each engine, operating

115

Table 24. Comparison of Operating Condition and Fuel Property Effects(1).

Combustor Parameter	J79-17A Observed Results (Reference 1)	J79-17C Observed Results (This Study)	F101 Observed Results (Reference 2)
1 CO&HC Emissions (Table 25)	• Levels Decreased With Engine Power (T_3, P_3). o Idle Levels Correlated With SMD Which Is Confounded With Volatility. No Fuel H or H Effect Evident. o Cruise Levels Correlated With Fuel H, Independent of Other Fuel Properties.	a. Levels Decreased With Engine Power (P_3, T_3, t_4) and Were Negligible at Takeoff and Dash. b. Idle and Cruise Levels Correlated Jointly With Fuel H and SMD. c. Compared to J79-17A, Emissions Higher at Idle, but Lower at Higher Power Conditions.	a. Levels Decreased With Engine Power (T_3, P_3, t_4) and Were Negligible Except at Idle. b. Idle Levels Correlated With SMD Which is Confounded With Volatility. No Fuel A or H Effect Evident. c. Compared to J79, Emissions Much Lower.
2 NOx Emissions (Table 25)	a. Levels Increased With Engine Power (T_3, P_3). b. Levels Decreased Slightly With Fuel H Only (No Nitrogen in These Fuels) at Higher Power Conditions.	a. Levels Increased With Engine Power (T_3, P_3). b. Levels Decreased Slightly With Fuel H Only (No Nitrogen in These Fuels) at Higher Power Conditions.	a. Levels Increased With Engine Power (T_3, P_3). b. Levels Decreased Slightly With Fuel H Only (No Nitrogen in These Fuels) at Higher Power Conditions.
3 Smoke Emissions (Table 25)	a. Levels Were High With all Fuels at all Power Conditions (Highly Visible at Cruise and Takeoff). b. Levels Decreased With Fuel H, Nearly Independent of H.	a. Compared to J79-17A, Levels Much Reduced at all Power Conditions (Invisible With Current Fuels). b. Levels Decreased With Fuel H, Nearly Independent of H.	a. Levels Were Low With all Fuels at all Power Conditions (Invisible). b. Levels Decreased With Fuel H, Nearly Independent of H.
4 Carbon Deposition	• Degree of Carbon Buildup Generally Decreased With Fuel H, but Light in 6.5 Hour Tests.	• Degree of Carbon Buildup Significantly Heavier With Diesel Fuel Than With JP-4, but Still no Problem Indicated in 24 Hour Test.	• Degree of Carbon Buildup Generally Decreased With Fuel H, but Light in 6.5 Hour Test.
5 Liner Temperature Rise (T_L - T_3) (Table 26)	a. Rise Increased With Engine Power (T_3, P_3). b. Peak Levels Decreased With Fuel H, Independent of H.	a. Rise Increased With Engine Power (P_3, T_3) b. Peak Levels Decreased With H, Nearly Independent of H. c. Compared to J79-17A and F101, Life Limiting Regions Less Sensitive to H.	a. Rise Increased With Fuel/Air Ratio, Nearly Independent of Engine Power (T_3, P_3). b. Peak Levels Decreased With Fuel H, Nearly Independent of H.
6 Flame Radiation (Table 26)	a. Levels Increased Significantly With Engine Power (P_3, T_3). b. Levels Correlated With Fuel H, With Secondary Effect of H.	a. Levels Increased Moderately With Engine Power (P_3, T_3). b. Levels Correlated With Fuel H, With no Discernable Effect of H.	• Not Measured
7 Pattern Factor	a. Levels Decreased With Engine Power. b. No Fuel Effect Observed (Full Density Tests).	a. Levels Decreased Slightly With Engine Power b. No Fuel Effect Observed (Full Density) (Tests).	a. Levels Decreased With Engine Power. b. Effect of SMD Observed in Atmospheric Pressure Tests, but no Effect Expected at Full Density.
8 Stability at Idle	a. No Fuel Effect Evident.	a. No Fuel Effect Evident.	a. No Fuel Effect Evident.
9 Ground Start	a. Starting Capability was Excellent (≤ 239 K Ambient Temperature) With all Fuels b. At 239 K Starting Fuel/Air Ratio Correlated With Fuel SMD.	a. Starting Capability was Excellent (≤ 239 K Ambient Temperature) With all Fuels b. At 239 K Starting Fuel/Air Ratio Correlated With Fuel SMD.	a. Minimal Ambient Temperature for Normal Start Increased Significantly With Less Volatile/More Viscous Fuels
10 Altitude Relight	• Altitude Capability was Generally Excellent (215.7 km) With JP-4 and JP-6 Fuels, but was Reduced With Diesel Fuel	• Altitude Capability Reduction Correlated With Fuel SMD, Particularly at Low Flight Mach Numbers	• Altitude Capability Reduction Correlated With Fuel SMD, Particularly at Low Flight Mach Numbers.
11 Fuel Nozzle Fouling	• No Significant Problem Indicated by Short (5 Hour) but Severe Tests	a. In Longer Term (≥25 Hour) Cyclic Tests, Significant Effects of Fuel Inlet Temperature (T_f) and Thermal Stability Rating (JFTOT Breakpoint, T_{BP}) on Relative Life Observed	a. No Clear Effects Indicated in Short (5 Hour) but Severe Tests. b. In Longer Term (≥100 Hour) Cyclic Tests, Strong Effects of Fuel Inlet Temperature (T_f) and Fuel Thermal Stability Rating (JFTOT Breakpoint, T_{BP}) on Relative Life Observed.

(1) H, H and SMD indicate fuel hydrogen content, naphthalene (dicyclic aromatic) content and relative spray droplet size.

116

Table 25. Comparison of Fuel Effects on Exhaust Emission Characteristics.

Engine Combustion System	Engine Operating Condition	CO Effects $EI_{CO} = k_o \left(\frac{14.5}{H}\right)^{k_1} \left(\frac{SMD}{SMD_{JP-4}}\right)^{k_2}$			HC Effects $EI_{HC} = k_o \left(\frac{EI_{CO}}{EI_{CO,\,JP-4}}\right)^{k_1}$		NO$_x$ Effects $EI_{NO_x} = k_o \left(\frac{14.5}{H}\right)^{k_1}$		Smoke Effects $SM_8 = k_0 \left(\frac{14.5}{H}\right)^{k_1} (1 + k_2 N)$		
		k_0	k_1	k_2	k_0	k_1	k_0	k_1	k_0	k_1	k_2
J79-17A	Idle	65.9	0	0.41	23.1	---	2.6	-0.41	18.4	6.3	-0.0002
	Cruise	14.8	1.38	---	0.5	---	4.6	0.07	42.2	3.3	0.0088
	Takeoff	4.5	0.20	---	0.1	---	10.8	0.39	55.2	1.8	0.0062
	Dash	2.2	-0.07	---	0.1	---	17.9	0.48	35.1	3.0	0.0058
	Overall	---	---	---	---	1.8	---	---	---	---	0.00316
J79-17C (This Study)	Idle	74.8	0.98	0.48	26.9	---	2.2	-0.67	2.1	8.4	-0.0045
	Cruise	8.5	0.92	0.45	<0.1	---	6.2	-0.03	3.9	8.9	0.0103
	Takeoff	1.0	---	---	0	---	11.8	0.36	13.9	3.6	0.0144
	Dash	0.5	---	---	0	---	23.6	0.20	4.3	4.1	0.0070
	Overall	---	---	---	---	2.1	---	---	---	---	0.00711
F101 (Reference 2)	Idle	28.7	0	0.94	1.0	---	3.1	1.38	0.2	9.7	0.0038
	Cruise	2.0	---	---	0.1	---	8.9	0.86	1.5	2.7	0.0035
	Takeoff	0.5	---	---	0	---	25.2	0.67	3.0	1.7	0.0029
	Dash	0.3	---	---	0	---	29.6	0.65	2.2	1.6	0.0038
	Overall	---	---	---	---	3.4	---	---	---	---	0.00350

Table 26. Comparison of Fuel Effects on Liner Durability Characteristics.

Engine Combustion System	Engine Operating Condition	Flame Radiation Effects $q_r = k_o \left[1 + k_1(14.5-H) \right] (1 + k_2 N)$			Peak Liner Temperature Effects $(T_{LM} - T_3) = k_o \left[1 + k_1(14.5-H) \right] (1 + k_2 N)$		
		k_o	k_1	k_2	k_o	k_1	k_2
J79-17A (Reference 1)	Idle	100.8	+0.250	+0.0127	196.5	+0.267	+0.0003
	Cruise	104.1	+0.262	+0.0092	326.8	+0.129	+0.0004
	Takeoff	135.2	+0.418	+0.0149	433.5	+0.050	+0.0001
	Dash	241.8	+0.392	+0.0145	463.7	+0.051	+0.0004
	Overall	---	---	0.0138	---	---	+0.000097
J79-17C(1)(2) (This Study)	Idle	83.2	+0.0072	+0.00011	80.5	+0.112	+0.0085
	Cruise	94.8	+0.0139	+0.00103	147.8	+0.350	+0.0065
	Takeoff	106.9	+0.0192	+0.00106	304.9	+0.043	+0.0008
	Dash	120.9	+0.0240	+0.00266	306.6	+0.084	+0.0013
	Overall	---	---	+0.00137	---	---	+0.0043
F101(3)(4) (Reference 2)	Idle	---	---	---	163.1	-0.0281	-0.0017
	Cruise	---	---	---	263.7	+0.0618	+0.0001
	Takeoff	---	---	---	313.2	+0.1006	+0.0003
	Dash	---	---	---	300.9	+0.0914	+0.0006
	Overall	---	---	---	---	---	-0.00019

(1) Radiation Heat Flux correlation based on data from Fuels 3, 4, 7, 8, 9, 10 and 12.

(2) Peak Temperature correlation based on representative peak surface mounted thermocouple (No. 7).

(3) Radiant Heat Flux not measured in this series.

(4) Peak Temperature correlation based on data from Fuels 4 through 13 only.

condition and type of emission. In each case, the first constant (k_0) represents the emission level with current JP-4 fuel; the second constant (k_1) represents the sensitivity to the primary fuel property (generally hydrogen content); and the third constant (k_2) represents the sensitivity to any other property (relative spray droplet size or naphthalene content).

Comparison of the coefficients in Table 25 shows that, as noted previously, the emission levels (k_0) are highly engine system and operating condition dependent. However, the fuel effects (k_1 and k_2) are relatively consistent both in their presence or absence in each case. The magnitudes of the fuel effects (k_1 and k_2) are also fairly consistent, and the differences are probably related to basic engine combustor design features, such as pressure ratio, stoichiometry and residence time.

Table 26 presents a quantitative comparison of the effects of fuel property variations on parameters which influence combustor liner durability. Again the listed coefficients were determined by regression analyses and have the same representation as those in the emission comparisons. In this table, however, the fuel coefficients (k_1 and k_2) always represent the linear slope of the normalized durability parameter [q_r/k_0 or $(T_{LM} - T_3)/k_0$] to a decrease in hydrogen content (k_1), or an increase in naphthalene content (k_2). In every case, k_2 is at least an order of magnitude less than k_1, and generally they differ by two orders of magnitude. These comparisons quantitatively illustrate the general insensitivity of these combustion systems to fuel naphthalene content, at least within the ranges tested.

Table 27 presents a comparison of the effects of fuel hydrogen content on predicted relative combustor life. The relative lives of the J79-17A and F101 combustors are expected to be quite similar and sensitive to fuel hydrogen content, even though they incorporate vastly different cooling design technologies and hence, much different absolute lives. The relative life of the J79-17C combustor is predicted to be significantly less sensitive to fuel hydrogen content which, as described in Section VI-B-1, is attributed to the high front end cooling.

119

Table 27. Comparison of Hydrogen Content Effects on Predicted Combustor Liner Life.

Fuel Hydrogen Content Weight Percent	Relative Combustor Life		
	J79-17A (Reference 1)	J79-17C (This Study)	F101 (Reference 2)
14.5 (Current JP-4)	1.00	1.00	1.00
14.0 (Current JP-8)	0.78	0.93	0.72
13.0 (ERBS Fuel, (DF2) Reference 5)	0.52	0.83	0.52
12.0 (Minimum, percent these Programs)	0.35	0.74	0.47

SECTION VII

CONCLUSION AND RECOMMENDATIONS

Based on the J79-17C combustion system experiments and analyses conducted in this program together with comparisons to previously conducted J79-17A and F101 experiments and analyses, the following conclusions and recommendations are made:

A. Conclusions

1. Fuel hydrogen content strongly affects smoke emissions, liner temperature, flame radiation and NO_x emissions. Hydrogen content is, therefore, probably the most significant fuel property, particularly with respect to high pressure/temperature performance, emission characteristics, and combustor liner durability (life).

2. Fuel Vaporization and atomization properties become more significant at lower temperature/pressure conditions. Cold day starting and altitude relight capability are highly dependent upon these properties. At least for the fuels tested, these properties do not correlate with combustion results as well as the relative spray droplet size calculated from fuel viscosity, density, and surface tension.

3. Within the range tested, fuel aromatic type (predominantly monocyclic xylenes or dicyclic naphthalenes) had relatively little effect on combustion characteristics.

4. Fuel breakpoint temperature (by JFTOT) is probably the most significant fuel property with respect to fuel nozzle fouling. In accelerated cyclic tests, fuel nozzle fouling rates were satisfactorily correlated by this fuel property.

5. Fuel property effects on combustion system performance and durability generally tend to be similar for the J79-17A, J79-17C and F101 engines, even though the design features, operating conditions and absolute performance and durability levels differ significantly. The most apparent exception is in respect to the decreased sensitivity of the J79-17C combustor life to fuel hydrogen content.

B. Recommendations

1. Selected engine tests are recommended to verify the trend established in these rig tests and analyses, particularly with respect to liner temperature, flame radiation, and hence, durability.

2. The fuel nozzle fouling testing in this program appears to have been successful in establishing accelerated test techniques and

121

data analysis methods. Additional tests with greater variations in fuel and air temperatures, fuel types and longer cyclic tests are recommended to validate the procedures and results.

APPENDIX A

FUEL PROPERTY DATA

A. Detailed Physical and Chemical Properties

Thirteen test fuels were supplied by AFWAL/POSF for evaluation in this program. Detailed physical and chemical properties of these fuels were determined from AFWAL/POSF retained samples and are listed in Tables A-1 and A-2. Selected data from this table together with a general description and rationale for selection of the fuels utilized in these evaluations are presented in Section III of this report.

It should be noted that as before (References 1 and 2) total aromatics determined by fluorescent indicator adsorption (ASTM Method D1319) were always significantly higher than the values obtained by spectrometry (ASTM Method D2789). ASTM Method D1319 is not recommended for fuels having end distillation temperatures over 587 K, but only the diesel fuel exceeded this value. ASTM Method D2789 is not recommended for fuels having 95% distillation temperatures over 484 K and all of the fuels exceeded this value. Recognizing this fact, Monsanto applied an alternative method (their No. 21-PQ-38-63) to five of the fuels shown in Table A-2. With the exception of a few of the components of Fuels 8A and 9A, the results by the two methods were not substantially different.

Samples returned to POSF were checked for any contamination that may have occurred through shipment, storage or handling, by glass capillary gas chromatography with each returned sample's retained counterpart. Some returned samples showed variation from their retained samples, but in all cases these differences were not significant, inasmuch as they did not adversely affect any test or related data analyses. Major differences were noted in returned samples of fuel 2A1, dated 15 Jan 80 and 8 Feb 80, from the Fuel Nozzle Fouling Test Rig. These samples, which differed in high boiling components, C15 and above, also had lower JFTOT breakpoint temperatures. The apparent cause and effect of these differences are explained below.

B. Computed Combustion Parameters

Table A-3 shows several fuel parameters which were computed from the physical and chemical properties for use in conducting the combustion tests and analyses of the results.

Fuel hydrogen-carbon atom ratio (n) was used in the exhaust gas sample calculation. It was calculated directly from the hydrogen weight percent (H) by the relationship:

$$n = \frac{11.915H}{100 - H} \tag{2}$$

Table A-1. Detailed Test Fuel Property Data.

Fuel Property	ASTM Test Method	Test Lab(1)	1A	2A1(2)	3A	4A	5A	6A	7A	8A	9A	10A	11A	12A	13A1(2)
Hydrocarbon Type Analyses, Volume Percent															
By Mass Spectrometry	D2789	MRC													
Paraffins			61.4	43.2	44.0	30.6	34.4	25.4	36.8	36.1	44.9	31.7	44.0	57.2	45.7
Monocycloparaffins			23.6	39.9	39.7	27.9	31.0	20.8	34.0	22.2	27.4	12.4	17.2	22.2	30.4
Dicycloparaffins			5.0	3.7	3.5	2.6	3.3	1.6	3.2			2.4	3.5	5.2	2.3
Alkylbenzenes			8.5	7.4	7.2	11.1	28.0	51.4	9.3	12.9	11.3	52.7	14.3	11.8	8.1
Indans and Tetralins			1.0	3.9	3.8	5.8	1.7	---	4.8	4.4	2.7	0.4	0.6	1.1	6.0
Indenes and Dihydronaphthalenes			---	---	---	---	---	---	---	---	---	---	---	---	---
Naphthalenes			0.5	1.9	1.8	22.0	1.6	0.8	11.9	24.5	13.7	0.4	0.4	0.5	7.5
By Fluorescent Indicator Absorption	D1319	SFQLA													
Total Aromatics			12.3	16.8	16.9	42.5	42.2	57.1	29.0	43.1	29.6	58.3	40.7	18.5	32.1
Olefins			1.5	2.1	2.7	1.2	3.5	2.0	1.4	0.7	0.5	1.2	1.0	1.5	2.9
Total Paraffins			86.2	81.1	80.4	56.3	54.3	40.9	69.6	56.2	69.9	40.5	58.3	80.0	65.0
Hydrogen Content, Weight Percent															
By Nuclear Magnetic Resonance	D3701	POSF	14.48	13.94	13.92	11.90	13.02	12.04	12.93	11.94	12.93	12.08	12.96	13.99	12.91
By Calculation	D3343	SFQLA	14.46	13.78	13.78	12.33	12.72	11.90	13.02	12.26	13.10	11.71	12.69	14.01	13.08
Sulfur Content, Weight Percent															
Mercaptan	D1219	SFQLA	0.0004	0.0004	0.0002	0.0000	0.0006	0.0001	0.0000	0.0000	0.0000	0.0001	0.0001	0.0000	---
Total	D2622	SFQLA	0.03	0.11	0.06	0.04	0.10	0.04	0.05	0.03	0.02	0.03	0.04	0.04	0.20
Net Heat Combustion, MJ/kg															
By Bomb Calorimeter	D240	MRC	43.65	43.21	43.14	42.19	42.65	42.07	42.70	42.31	42.78	42.35	42.93	43.46	42.58
By Calculation	D3338	SFQLA	43.61	43.24	43.23	42.41	42.69	42.23	42.80	42.39	42.86	42.11	42.63	43.38	42.55
Luminometer Number	D1740	SFQLA	77	48	49	14	31	24	28	10	31	24	43	62	25
Smoke Point, mm	D1322	SFQLA	25.0	26.0	25.0	12.0	15.0	15.0	17.0	11.0	16.0	12.0	15.0	26.0	15.0
Reid Vapor Pressure, kPa	D2551	MRC	17.24	---	---	---	---	299(3)	---	11.72	14.48	6.90	13.10	14.48	---
Freezing Point, K	D93	SFQLA	---	---	320(3)	---	---	223	---	---	---	---	---	---	339
			209	327	240	335	323		333	228	218	200	204	239	250
						227	224		225						
Actual Distillation, K	D86	SFQLA													
Initial Boiling Point			333	456	444	461	444	404	458	339	336	344	336	337	466
10% Recovered			370	475	475	477	452	431	476	380	374	396	381	376	489
20% Recovered			383	481	482	482	458	439	481	401	392	410	397	391	499
50% Recovered			419	494	497	497	480	452	494	467	446	430	427	433	527
90% Recovered			497	521	540	523	519	514	521	516	519	474	487	561	577
Final Boiling Point			521	540	569	545	539	536	540	548	549	520	522	574	60.
Kinematic Viscosity, m²/s	D445														
#238 7K		SFQLA	2.46	9.10	13.50	11.58	6.94	4.00	11.49	3.79	3.30	2.32	2.53	3.46	---
#244 3K		MRC	2.21	3.53	10.70	9.05	5.66	3.42	9.02	3.30	2.67	2.08	2.08	2.75	---
#273 3K		MRC	1.29	2.23	3.94	3.39	2.52	1.84	3.43	1.69	1.46	1.20	1.22	1.52	5.77
#294 3K		MRC	0.955	1.665	2.45	2.13	1.69	1.24	2.17	1.21	1.07	0.900	0.910	1.11	3.27
#310 9K		MRC	0.788		1.807	1.591	1.304	0.988	1.620	0.963	0.871	0.744	0.752	0.903	2.306
Surface Tension, mN/m	Capillary Rise														
#244 3K		MRC	---	28.7u	28.47	29.98	29.47	32.80	29.03	26.55	25.30	26.70	28.60	25.90	30.07
#273 2K		MRC	25.05	27.08	26.36	27.77	27.80	29.85	27.00	24.59	23.62	24.81	26.35	24.20	28.60
#294 3K		MRC	23.28	25.69	25.05	26.05	26.46	27.82	25.30	23.03	22.10	23.30	24.73	22.86	26.68
#310 9K		MRC	21.73					26.20					23.43		
Density, kg/m³	Dilatometer														
#244 3K		MRC	795.7	846.0	846.6	896.7	859.8	870.2	870.6	870.9	839.3	851.9	828.2	810.0	---
#273 2K		MRC	772.3	825.2	825.5	874.6	838.0	868.0	848.8	847.5	815.6	828.1	804.9	787.6	858.9
#294 3K		MRC	755.7	809.6	810.4	858.9	821.9	831.4	833.3	830.9	799.0	811.0	787.8	771.2	843.4
#310 9K		MRC	742.3	797.7	798.6	846.9	809.7	818.8	821.3	818.2	785.8	798.0	---	758.7	831.9
True Vapor Pressure, kPa	D2551														
#273 2K		MRC	5.33	1.40	2.27	1.66	1.07	1.07	1.93	4.07	4.53	3.40	3.67	3.67	1.53
#294 3K		MRC	11.00	2.07	3.27	2.27	1.87	2.27	2.67	8.53	9.73	7.20	8.13	8.53	2.20
#310 9K		MRC	19.46	2.73	4.13		2.73	1.93	3.33	14.66	16.93	12.00	14.00	15.46	2.80

(1) MRC = Monsanto Research Corporation
    SFQLA = WPAFB Quality Control Lab
    POSF = WPAFB Fuels and Lubrication Division Aero Propulsion Lab

(2) Fuels 2A2 and 13A2 used only in fuel nozzle fouling tests, detailed property data not obtained

(3) By test method 056

124

Table A-2. Hydrocarbon Type Analysis Comparison.

Component	4A		7A		8A		9A		13A-1	
	Method 1	Method 2	Method 1	Method 2	Method 1	Method 2	Method 1	Method 2	Method 1	Method 2
Paraffins	30.6	29.6	36.8	36.0	36.1	32.5	44.9	42.5	45.7	44.8
Monocycloparaffins	27.9	30.1	34.0	37.1	22.2	17.9	27.4	22.7	30.4	31.2
Dicycloparaffins	2.6		3.2		-		-		2.3	
Alkylbenzenes	11.1	13.7	9.3	11.2	12.9	17.8	11.3	15.9	8.1	9.5
Indans/Tetralins	5.8	4.6	4.8	3.9	4.3	3.8	2.7	2.6	6.0	4.7
Indenes/Dihydro-naphthalenes		0.4		0.1		0.4		0.2		0.6
Napthalenes	22.0	21.6	11.9	11.7	24.5	27.6	13.7	16.1	7.5	9.2

Method 1. Modified ASTM D2789-71.
Method 2   Monsanto 21-PQ-38-63.
           This method combines mono- and dicycloparaffins into a single value.

-Dash indicates none found.

125

Table A-3. Test Fuel Combustion Parameters.

Fuel Number	n, Hydrogen-to-Carbon Atom. Ratio	f_{st}, Stoichiometric Fuel/Air Ratio, g/kg	T_{st}, Stoichiometric Flame Temperature at Takeoff, K	$(W_f)/(W_f)JP-4$ Relative Required Fuel Flow Rate	$(SMD)/(SMD)JP-4$ Relative Fuel Spray Droplet Size
1A	2.017	67.52	2494	1.0000	1.000
2A1	1.930	68.08	2498	1.0103	1.381
3A	1.927	68.10	2498	1.0118	1.431
4A	1.609	70.31	2516	1.0347	1.383
5A	1.784	69.07	2506	1.0236	1.260
6A	1.631	70.15	2515	1.0375	1.153
7A	1.769	69.17	2507	1.0223	1.375
8A	1.616	70.26	2516	1.0318	1.104
9A	1.773	69.14	2507	1.0205	1.046
10A	1.637	70.10	2514	1.0306	1.022
11A	1.774	69.13	2506	1.0169	1.017
12A	1.938	68.03	2498	1.0044	1.056
13A1	1.766	69.19	2507	1.0251	1.662

and ranged from 1.616 to 2.017 as hydrogen content increases.

Stoichiometric fuel/air ratio (f_{st}) was used to calculate comparative adiabatic flame temperature. It was calculated from the fuel hydrogen-to-carbon ratio (n) by the relationship:

$$f_{st} = \frac{0.0072324\ (1.008\ n + 12.01)}{(1 + 0.25\ n)} \qquad (3)$$

which assumes that the fuel is CH_n, that the air is 20.9495 volume-percent oxygen, and that the air has a molecular weight of 28.9666. For the test fuels the stoichiometric fuel/air ratio ranged from 67.52 to 70.31 g-fuel/kg-air as hydrogen content decreased.

Stoichiometric flame temperature was used in analyses of NO_x emissions. It was calculated at takeoff operating conditions (T3 = 664 K, P3 = 1.359 MPa) using a standard equilibrium-thermodynamics computer program (Reference 14) and ranged from 2494 to 2516 K as hydrogen content decreased.

Relative required fuel flow rate was used in all combination tests to adjust the JP-4 fueled engine cycle operating fuel flow rates for the reduced heating values of the other fuels. The factor is merely the ratio (Q_{JP-4}/Q) and ranged from 1.00 to 1.0375.

Relative fuel spray droplet size was used in analyses of the low-power emissions and relight performance. The J79-17C combustion system employs hybrid pressure-airblast atomizing fuel nozzles, but even at relight fuel flow rates, the bulk of the fuel is injected through the secondary airblast atomizers. Therefore, El-Shanawany and Lefebvre's correlation parameter for pure air atomizing nozzles (Reference 15) was used to estimate the relative fuel spray droplet Sauter Mean Diameter (SMD) from the test density (ρ), surface tension (σ), and viscosity (ν) by the relationship:

$$\frac{SMD}{SMD_{JP-4}} = \left(\frac{\sigma}{\sigma_{JP-4}}\right)^{0.6}\left(\frac{\rho}{\rho_{JP-4}}\right)^{0.1}\left[\frac{1 + C_2\left(\dfrac{\nu\rho}{\sigma^{1.1}}\right)^{0.4}}{1 + C_2\left(\dfrac{\nu_{JP-4}\ \rho_{JP-4}}{\sigma_{JP-4}^{1.1}}\right)^{0.4}}\right]$$

where:

$$C2 = \left(\frac{0.015}{0.073}\right)\left(D_P^{0.1} U_A^{1.2} \rho_A^{0.7}\right)$$

127

and D_p, U_A ρ_A are atomizer diameter, air velocity and air density and all parameters are expressed in basic kg-m-s units. For these relative spray droplet diameter comparisons, J79 idle operating conditions were assumed for which $C_2 = 381.8$.

As shown in Table A-2, none of the blending agents appreciably changed the predicted relative droplet size of the base fuel. However, the JP-8 based fuels are predicted to produce mean droplet sizes about 38% larger than those of the JP-4 fuel. Further, the diesel fuel is expected to produce mean droplet sizes about 66% larger than those of the JP-4 fuel.

C.   Thermal Stability Characteristics

When performing hot fuel tests in nozzles (or other fuel system components) it is essential to know the actual thermal stability of the test fuels. This is not done in routine fuel analyses, since the fuel specifications require only that the fuels pass the thermal stability requirement at 533 K when using ASTM procedure D3241 (JFTOT). In order to determine the actual thermal stability, it is necessary to run additional tests at higher temperatures until a temperature is reached at which the fuel forms heater tube deposits of Code 3 or darker, and/or a filter pressure drop of 25 mm Hg or more in less than 150 minutes. The highest temperature that can be run without reaching these values is known as the thermal stability "breakpoint" temperature. It is not uncommon for aviation fuels to have breakpoints that exceed the specification value by 50 to 75 K.

When selecting fuels for studying the effect of fuel thermal stability on component performance, it is desirable to select two or more fuels that differ significantly in breakpoint temperatures. The precision of the JFTOT procedure has not been established, but experience indicates that repeatability of the breakpoint determination is probably no better than 5 to 10 K. Therefore, fuels differing in breakpoint by at least 20 K are desired.

It is also desirable to show thermal stability effects in a reasonable period of time, without applying unrealistically high temperatures. This requires using at least one fuel with a marginally acceptable, or even a failing thermal stability. Such fuels are extremely difficult to find.

It was originally proposed to use a JP-4 from a refinery which has occasionally produced low thermal stability fuel by a copper-sweetening process. However, when a sample was checked in June, 1979, it was found to have a breakpoint of 573 K (40 K above the specification requirement).

Another candidate, low thermal stability fuel was located at a west coast refinery newly engaged in jet fuel production. This one has a breakpoint of about 511 K, and was of sufficient interest that the Air Force planned to secure and store a quantity for future testing. However, before this could be accomplished, the refiner changed his processing and improved the fuel quality substantially.

It was ultimately agreed that a satisfactory low-quality fuel would be a No. 2 diesel available locally. This was estimated to have a breakpoint of approximately 513 K. The higher quality fuel proposed for comparison was a JP-8 with an estimated breakpoint of approximately 598 K.

Emphasis was placed on determining the breakpoints of the two fuels used in the nozzle fouling tests. When it was determined that the breakpoint temperatures of the returned samples of fuel 2A1 were about 25 degrees less than their retained counterpart, samples of fuel 2A1 were sent to two outside laboratories, Alcor and Exxon. Their results, as well as POSF data, are shown in Table A-4. Acknowledging the differences in the returned fuel's breakpoint, it was decided to use the returned samples' breakpoint temperatures in any of the required data analyses. It was later ascertained that another JP-8 fuel, 2B, was used instead of the supplied fuel 2A which was, at that time, nearly exhausted. The reported breakpoint temperature of fuel 2B is 573 Kelvin which matches the returned samples of fuel 2A1. Later, a second quantity of JP-8 was requested from POSF for delivery in early April 1980. This fuel, drawn from the 2A1 source tank, was designated as fuel 2A2. Returned samples of this fuel have the same break-point, within the accepted limits of repeatability, as its retained sample. Fuel 13A1 breakpoint temperatures also match their retained counterparts, within repeatability limits. Fuel 13A2 represents a second quantity of fuel 13A which came from a different source than 13A1 and was not expected to have the same breakpoint temperature.

It should be noted that, in every case, breakpoints were based on pre-heater tube deposits since filter pressure drop did not reach the failure level until after the tube deposit reached a visual rating of 3.

Table A-4. Thermal Stability Rating of Test Fuels.
(ASTM Method D3241)

Fuel Number	JFTOT Breakpoint[1], K			
	Retained Samples			Returned Samples USAF
	USAF	ALCOR	EXXON	
1A	538			
2A1	593	653[2],553	603	573,573
2A2	-	-	-	603,603 583,583
3A	593	-	-	-
4A	578,563	-	-	-
5A	583	-	-	-
6A	573	-	-	-
7A	560	-	-	-
8A	538	-	-	-
9A	541,533	-	-	-
10A	543	-	-	-
11A	576	-	...	-
12A	553	-	-	-
13A1	533	523,523	523	523,523
13A2	-			503,503

[1]Defined as the highest temperature at which a maximum visual
rating of the heater tube deposits is less than a code 3.

[2]Sample contaminated by red gasket material.
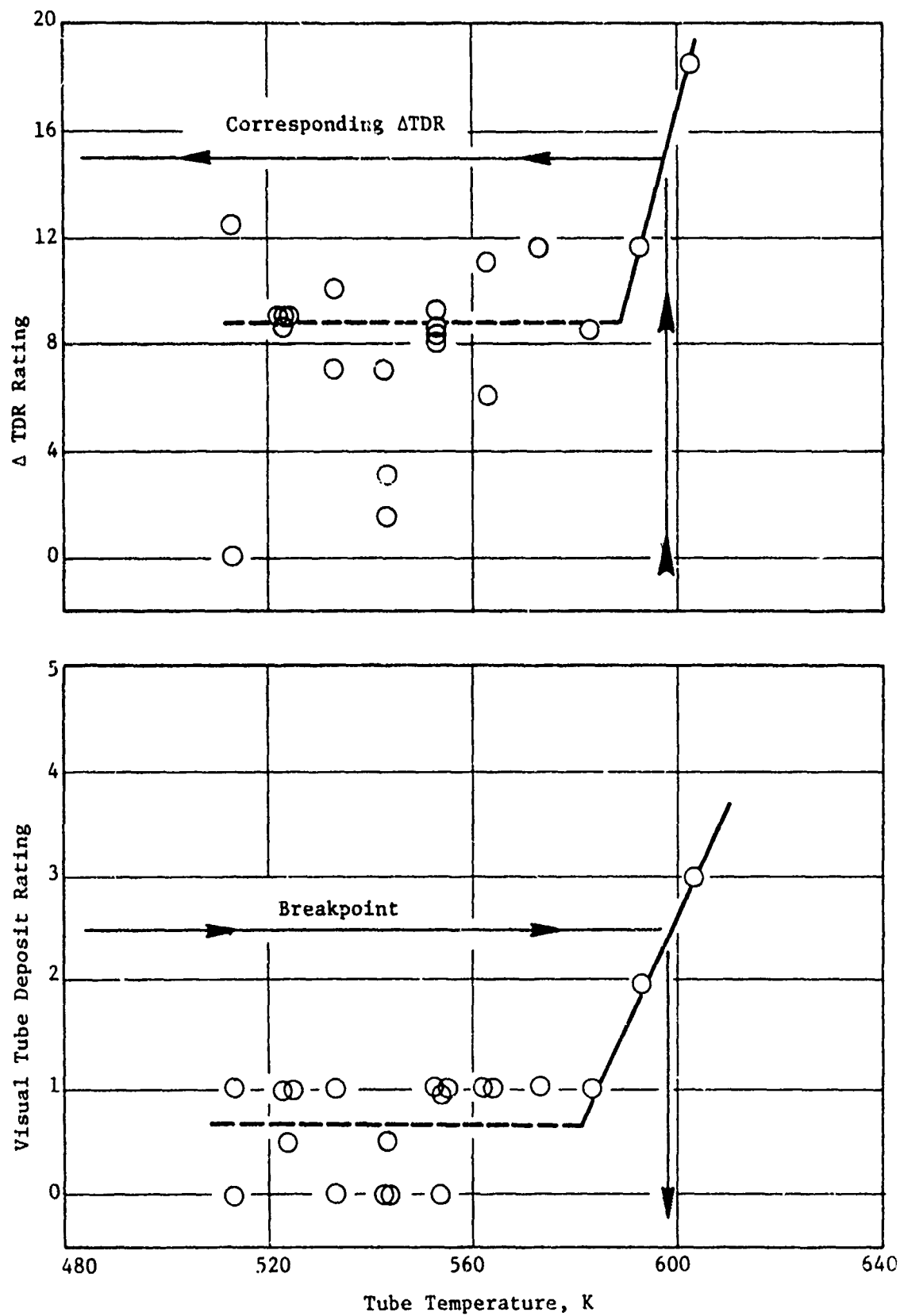
Figure A-1. JFTOT Results on Retained Sample of Fuel No. 2A1, by USAF.

131

APPENDIX B

HIGH PRESSURE TEST DATA

Table B-1 presents a summary of the key reduced data from the high pressure performance and emission tests. Table B-2 presents additional measured and calculated parameters for these tests.

Table B-3 presents the measured and corrected CO emission test data at the four engine operating conditions. The procedure for correcting the measured data to engine conditions by the ratio of the severity parameters is also shown. As can be seen, the corrections are all relatively small except at dash operating conditions were the test pressure was reduced. Measured and corrected hydrocarbon emission data are similarly presented in Table B-4. NO_x data are similarly presented in Table B-5. Small differences in measured and corrected NO_x emission indices are primarily due to the humidity correction.

Table B-6 presents the smoke data analysis. As described in Section VI-A3, no operating condition severity parameter could be readily found, so the data are presented as they have been corrected to engine Station 8 fuel/air ratio conditions, described in Appendix F, and averaged at each simulated engine power level.

Detailed liner temperature measurements are listed in Table B-7 (inner liner) and Table B-8 (rear liner) for the high pressure performance tests. The data are presented as liner temperature rise ($T_{liner} - T_3$). The indicated thermocouple locations correspond to those shown in Figure 16 and Table 7. Correlations of the liner temperature rise data with operating conditions and fuel hydrogen content are summarized in Tables B-9 and B-10.

Table B-11 presents a summary of the flame radiation data analysis. Linear regression curve fits of the data (see Figure 50) were made and from these the quoted engine flame radiation levels were calculated.

Detailed combustor exit temperature profile and pattern factor data are listed in Table B-12. Linear regression curve fits of these data (see Figure 53) were made and are summarized in Table B-1, and are the quoted engine pattern factor levels in Figure 54.

Table B-1. Basic High Pressure Test Data.

Fuel Number	Reading Number	Test Point Number	W_3, Total Airflow, kg/s	W_c, Combustor Airflow, kg/s	P_3, Inlet Total Pressure, MPa	T_3, Inlet Total Temperature, K	f_a, Metered Fuel/Air Ratio, g/kg	h_3, Inlet Air Humidity, g/kg	$\Delta P_3/P_3$, Total Pressure Loss, %	q_R, Flame Radiant Heat Flux, kW/m²	ΔT_{avg}, Average Temperature Rise, K	η_{TC}, Thermal Combustion Efficiency, %	PrF, Profile Factor	Pf, Pattern Factor	$(T_{L,max} - T_3)$, Peak Liner Temperature Rise, K	EI_{CO}, CO Emission Index, g/kg	EI_{HC}, HC Emission Index, g/kg	EI_{NOx}, NOx Emission Index, g/kg	f_s, Sample Fuel Air Ratio, g/kg	η_{GS}, Gas Sample Combustion Efficiency, %	SN, Combustor Exit Smoke Number
2A1	1	3	1.794	1.538	0.253	422	9.0	1.3	3.31	-	349	102.0	1.158	0.395	141	80.9	11.9	3.5	17.5	95.36	3.6
	2	2	1.785	1.519	0.254	423	7.9	1.2	3.27	-	299	95.3	1.178	0.415	111	91.8	41.4	3.7	10.0	94.26	5.1
	3	4	2.950	2.527	0.468	560	13.8	1.0	3.63	-	521	101.4	1.158	0.340	140	9.5	0.6	6.8	16.9	99.22	12.2
	4	5	2.981	2.559	0.466	557	19.2	0.9	3.73	-	695	99.6	1.109	0.330	337	6.1	0.3	5.0	23.3	99.79	16.2
	5	6	7.596	6.475	1.366	656	13.3	1.3	3.14	-	529	108.7	1.137	0.156	480	1.3	0.2	13.8	16.6	99.95	11.1
	6	7	7.539	6.364	1.372	658	17.1	1.3	3.11	-	615	100.0	1.220	0.349	519	1.3	0.1	13.5	19.1	99.96	17.4
	7	8	6.487	5.548	1.198	770	13.0	1.4	3.91	-	458	99.0	1.150	0.351	505	0.8	0	22.6	15.2	99.98	3.6
	8	9	6.580	5.657	1.197	770	14.0	1.4	3.93	-	496	99.9	1.156	0.357	497	1.0	0	22.6	16.1	99.98	5.1
1A	9	8	6.572	5.634	1.191	769	12.6	1.3	4.00	-	466	99.9	1.160	0.365	509	1.0	0	23.2	14.3	99.98	3.6
	10	9	6.605	5.682	1.188	771	13.6	1.4	4.01	-	480	98.5	1.154	0.362	508	0.9	0	22.0	15.4	99.98	3.6
	11	6	7.503	6.398	1.349	664	13.5	1.3	3.27	-	505	101.9	1.150	0.341	435	1.3	0	14.6	15.5	99.97	8.1
	12	7	7.452	6.325	1.365	663	15.6	1.3	3.31	-	576	100.9	1.144	0.349	443	1.3	0	13.9	18.0	99.97	12.2
	13	4	2.870	2.454	0.464	560	11.7	1.7	3.54	-	471	91.2	1.226	0.418	394	8.5	0	4.1	15.2	99.80	2.8
	14	5	2.866	2.442	0.469	561	19.2	1.4	3.52	-	656	93.1	1.154	0.339	398	7.3	0	5.8	21.4	99.83	2.8
	15	3	1.837	1.601	0.249	427	7.3	1.2	4.26	-	368	94.2	1.174	0.534	261	0.9	19.2	1.2	10.8	96.91	1.2
	16	2	1.819	1.560	0.269	432	7.7	1.1	3.25	-	262	92.2	1.180	0.422	261	68.4	35.9	2.1	9.0	95.27	3.2
6A	17	2	1.821	1.570	0.256	417	7.8	0.4	3.80	-	287	92.5	1.118	0.337	107	100.1	45.5	2.6	9.2	93.74	19.0
	18	3	1.819	1.555	0.253	418	9.9	0.3	3.66	-	365	93.4	1.107	0.324	147	89.5	32.1	2.5	11.6	93.13	6.2
	19	4	2.909	2.486	0.467	560	14.0	0.5	3.67	-	516	98.9	1.097	0.282	368	10.2	0.8	-	16.5	99.69	14.5
	20	5	2.938	2.512	0.474	557	19.0	0.7	3.62	-	690	99.9	1.082	0.262	39?	7.5	0.4	-	23.4	99.78	25.7
	21	6	7.436	6.304	1.384	667	16.0	0.7	3.13	-	522	102.5	1.105	0.318	480	1.5	0.2	16.0	17.1	99.95	14.5
	22	7	7.459	6.339	1.375	672	15.5	0.7	3.32	-	586	105.1	1.099	0.311	482	1.4	0.3	13.8	19.4	99.94	15.2
	23	8	6.556	5.639	1.198	775	12.9	0.7	3.79	-	471	102.8	1.108	0.311	517	1.0	0.4	-	16.0	99.95	3.4
	24	9	6.568	5.635	1.200	774	14.9	0.7	3.86	-	534	101.7	1.106	0.316	460	0.9	0.2	21.5	18.1	99.96	11.1
5A	25	9	6.531	5.601	1.201	768	15.9	0.6	3.99	-	554	100.2	1.109	0.329	451	0.9	0	-	17.3	99.98	15.3
	26	8	6.557	5.631	1.198	772	12.7	0.6	3.91	-	448	100.3	1.121	0.345	450	0.9	0	21.6	13.8	99.98	2.4
	27	6	7.304	6.368	1.373	663	13.6	0.8	3.22	-	512	104.6	1.130	0.301	463	1.3	0	15.2	15.1	99.97	22.6
	28	7	7.447	6.307	1.365	663	15.8	0.8	3.39	-	577	102.5	1.135	0.301	408	1.5	0	15.2	17.1	99.97	20.4
	29	4	2.846	2.420	0.468	569	10.4	0.9	3.61	-	655	94.2	1.145	0.284	321	8.1	0.1	6.7	20.4	99.80	23.2
	30	5	2.865	2.435	0.472	574	14.1	0.8	3.57	-	488	94.6	1.164	0.321	392	8.9	0.1	7.2	14.8	99.78	16.8
	31	2	1.826	1.575	0.252	425	8.0	0.8	6.04	-	277	88.2	1.208	0.334	179	92.5	42.0	2.4	8.8	94.20	3.6
	32	3	1.807	1.560	0.251	423	9.8	0.7	3.97	-	344	90.4	1.212	0.442	152	98.5	38.6	2.2	10.8	94.36	3.6
11A	33	8	6.568	5.636	1.202	783	12.7	0.7	3.96	-	454	101.2	1.103	0.331	498	0.9	0	-	14.0	99.98	8.6
	34	9	6.277	5.340	1.196	780	15.6	0.7	3.64	-	552	111.6	1.098	0.312	453	1.0	0.1	-	17.0	99.97	16.7
	35	6	7.486	6.365	1.364	656	13.7	0.1	3.36	-	517	104.2	1.117	0.267	494	1.5	0.1	-	15.0	99.96	19.0
	36	7	7.497	6.362	1.369	654	14.9	0.1	3.11	-	564	105.2	1.107	0.282	487	1.6	0.1	-	16.6	99.95	19.4
	37	4	2.959	2.536	0.467	550	13.4	0.1	3.86	-	481	96.9	1.173	0.355	359	9.4	0.2	6.5	14.9	99.76	3.6
	38	5	2.913	2.482	0.474	550	20.6	0.1	3.69	-	720	97.3	1.127	0.241	293	8.4	0.2	5.8	22.8	99.79	13.6
	39	2	1.750	1.513	0.255	429	8.2	0.1	3.68	-	281	86.9	1.225	0.380	176	110.7	50.6	3.2	4.1	93.04	13.6
	40	3	1.786	1.525	0.252	429	9.9	0.1	3.53	-	354	91.6	1.172	0.341	243	76.8	24.2	3.1	11.0	96.10	3.5
1AR	41	2	1.828	1.579	0.255	425	7.3	4.6	3.78	-	298	100.7	1.118	0.393	163	75.5	34.5	1.7	8.8	95.23	4.4
	42	3	1.808	1.573	0.252	425	9.1	4.8	3.55	-	375	103.6	1.101	0.320	173	75.2	27.8	1.4	10.8	95.82	2.8
	43	4	.781	2.443	0.478	562	13.4	4.8	3.20	-	536	105.6	1.095	0.319	397	7.4	0	6.6	14.0	99.83	3.6
	44	5	2.416	2.505	0.476	555	17.4	4.8	3.51	-	678	105.3	1.079	0.336	353	0	0	6.4	20.3	99.84	5.1
	45	7	7.?80	6.258	1.378	662	15.0	4.9	2.99	-	591	107.8	1.093	0.353	400	1.2	0	13.7	17.0	99.97	17.3
	46	6	7.?.7	6.286	1.368	663	13.4	5.1	3.11	-	524	105.8	1.110	0.366	410	1.2	0	14.4	15.0	99.97	15.7
	47	8	6.589	5.664	1.178	777	12.3	5.6	4.04	-	452	101.8	1.111	0.353	447	0.9	0	22.0	13.5	99.98	5.9
	48	9	6.540	5.628	1.200	776	14.2	5.5	3.94	-	523	102.9	1.099	0.351	453	0.9	0	21.5	15.6	99.98	8.1
13A1	49	3	1.790	1.543	0.258	419	10.0	4.9	3.46	-	358	92.4	1.115	0.291	101	99.4	49.5	1.4	11.9	97.65	5.4
	50	2	1.814	1.564	0.255	419	8.0	4.9	3.55	-	274	87.5	1.105	0.297	108	103.0	38.2	1.5	8.7	94.28	4.0
	51	4	2.923	2.493	0.475	556	13.5	4.9	3.62	-	513	103.0	1.090	0.242	364	14.0	1.1	-	15.1	99.57	20.3
	52	5	2.935	2.504	0.472	558	17.2	4.8	3.67	-	636	102.5	1.137	0.300	348	10.?	0.7	6.2	19.6	99.69	28.0
	53	6	7.657	6.499	1.377	658	13.1	4.9	3.27	-	510	108.2	1.094	0.288	499	1.8	0.4	15.9	14.3	99.92	25.8
	54	7	7.543	6.411	1.371	660	14.8	5.1	3.30	-	566	107.0	1.104	0.265	428	1.9	0.2	14.0	15.8	99.94	23.0
	55	8	6.464	5.344	1.186	775	12.3	5.1	4.01	-	436	100.7	1.113	0.284	378	1.2	0.1	21.8	13.1	99.96	4.7
	56	9	6.450	5.536	1.188	776	12.6	5.1	4.01	-	444	100.7	1.109	0.294	40?	1.1	0.1	25.4	13.5	99.96	6.1

Table B-1. Basic High Pressure Test Data (Concluded).

Fuel Number	Reading Number	Test Point Number	W_3, Total Airflow, kg/s	W_c, Combustor Airflow, kg/s	P_3, Inlet Total Pressure, MPa	T_3, Inlet Total Temperature, K	f_m, Metered Fuel/Air Ratio, g/kg	H_3, Inlet Air Humidity, g/kg	$\Delta P_4/P_3$, Total Pressure Loss, %	$\dot{q}$, Flame Radiant Heat Flux, kW/m²	ΔT_{avg}, Average Temperature Rise, K	η_{TC}, Thermal Combustion Efficiency, %	Prf, Profile Factor	PF, Pattern Factor	$(T_{L,max}-T_3)$, Peak Liner Temperature Rise, K	EI_{CO}, CO Emission Index, g/kg	EI_{HC}, HC Emission Index, g/kg	EI_{NO_X}, NO_X Emission Index, g/kg	f_s, Sample Fuel/Air Ratio, g/kg	η_{GS}, Gas Sample Combustion Efficiency, %	SN, Combustor Exit Smoke Number
10A	57	2	1.810	1.560	0.261	418	7.8	1.1	3.80	85.7	275	90.8	1.133	0.447	167	98.3	51.0	1.9	8.9	93.30	17.9
	58	3	1.792	1.533	0.261	418	9.9	1.1	3.57	85.7	338	88.9	1.110	0.319	136	88.2	43.0	1.7	11.1	94.23	16.4
	59	4	2.858	2.472	0.478	557	13.9	1.1	3.64	94.5	530	104.2	1.101	0.243	340	9.8	1.4	6.5	16.4	99.65	22.1
	60	5	2.849	2.454	0.478	550	19.4	1.3	4.00	96.1	489	100.9	1.112	0.300	420	8.4	0.6	6.2	22.2	99.75	24.5
	61	6	7.457	6.427	1.306	659	13.6	1.2	3.31	122.9	532	109.0	1.065	0.263	487	1.6	0.6	16.2	16.4	99.91	27.1
	62	7	7.189	6.205	1.376	655	16.6	1.7	2.78	117.8	620	105.5	1.098	0.259	511	1.5	0.5	15.0	19.3	99.92	37.0
	63	8	6.355	5.484	1.221	766	13.5	1.9	3.59	132.3	448	103.5	1.076	0.223	576	0.8	0.6	26.8	14.3	99.93	6.5
	64	9	6.430	5.566	1.219	765	13.7	1.8	3.65	135.5	490	102.5	1.078	0.248	595	1.0	0.4	25.3	16.0	99.94	11.1
12A	65	8	6.359	5.470	1.219	764	12.3	1.5	3.43	126.0	442	99.8	1.083	0.231	556	0.9	0.4	24.5	13.9	99.94	3.2
	66	9	6.468	5.661	1.227	756	13.3	1.6	3.10	126.0	487	102.2	1.085	0.246	567	1.0	0.6	22.3	15.4	99.94	6.5
	67	6	7.298	6.296	1.376	653	13.8	1.6	2.87	115.0	523	103.5	1.089	0.225	478	1.5	0.3	14.2	15.4	99.94	13.2
	68	7	7.476	6.264	1.381	656	16.4	1.4	3.38	110.3	614	103.5	1.090	0.227	487	1.3	0.3	13.8	18.4	99.95	17.5
	69	4	2.858	2.431	0.478	564	13.9	1.7	.47	92.0	506	97.2	1.089	0.258	388	9.6	0.5	6.5	16.2	99.74	3.6
	70	5	2.771	2.386	0.479	566	20.0	1.3	4.05	90.7	691	95.0	1.097	0.228	395	6.9	0.2	6.6	21.6	99.82	8.3
	71	3	1.778	1.547	0.256	432	9.4	1.3	5.08	85.7	340	91.2	1.118	0.362	163	82.6	34.2	2.4	10.2	95.10	2.4
	72	2	1.733	1.488	0.258	431	8.1	1.2	4.91	83.8	270	83.6	1.122	0.363	149	93.7	47.2	2.1	8.6	93.71	2.4
9A	73	3	1.737	1.506	0.256	415	9.8	1.2	4.52	83.8	324	84.5	1.097	0.311	150	86.2	44.1	2.0	10.1	94.17	5.7
	74	2	1.796	1.551	0.256	413	7.9	1.2	3.39	83.8	268	80.0	1.088	0.276	152	94.5	45.8	1.9	8.7	98.83	13.1
	75	4	2.735	2.486	0.477	564	13.4	1.7	3.50	85.7	476	96.3	1.095	0.264	375	11.1	1.6	6.2	14.2	99.61	14.1
	76	5	2.903	2.504	0.486	564	18.8	1.6	3.59	88.2	660	97.7	1.109	0.276	420	8.7	0.4	5.8	20.3	99.76	18.0
	77	6	8.092	7.122	1.335	659	11.9	3.4	4.43	102.6	454	105.0	1.094	0.222	463	2.5	0.4	13.8	14.3	99.91	16.7
	78	7	7.454	6.468	1.389	660	15.8	5.2	3.28	112.8	612	106.5	1.097	0.213	439	1.7	0.1	14.0	18.9	99.95	31.0
	79	8	6.414	5.593	1.206	771	12.0	8.7	3.85	120.3	438	102.5	1.078	0.213	500	1.1	0.2	24.7	14.2	99.96	6.1
	80	9	6.323	5.493	1.223	774	13.8	7.2	3.65	-	498	102.6	1.076	0.215	479	0.9	0.1	24.6	16.5	99.97	11.4
8A	81	8	6.391	5.375	1.205	775	12.1	3.8	3.89	129.5	434	102.4	1.072	0.263	535	1.0	0.2	25.6	14.8	99.96	7.6
	82	9	6.369	5.579	1.209	778	13.8	1.6	3.65	122.9	495	103.6	1.069	0.274	510	0.9	0.1	25.1	17.6	99.97	12.4
	83	6	7.376	6.382	1.390	659	13.9	1.3	2.97	112.8	524	105.8	1.082	0.197	468	1.6	0.2	15.2	16.6	99.95	36.0
	84	7	7.346	6.323	1.395	661	16.3	1.3	3.41	12.8	603	104.9	1.085	0.220	462	1.8	0.1	14.9	19.8	99.95	40.7
	85	5	2.858	2.481	0.477	560	19.3	1.9	3.35	98.3	692	100.8	1.086	0.194	338	8.5	0.2	6.3	23.0	99.78	28.9
	86	4	2.830	2.386	0.476	557	14.4	1.6	3.73	98.3	515	98.4	1.085	0.221	374	12.3	0.5	6.7	16.3	99.67	27.2
	87	3	1.760	1.547	0.259	433	9.7	1.1	3.49	88.2	349	93.7	1.084	0.237	226	73.8	28.4	2.4	11.2	95.82	9.3
	88	2	1.823	1.569	0.255	434	7.9	1.1	3.26	85.7	276	89.8	1.093	0.246	199	78.8	35.1	2.1	9.0	95.14	5.8
4A	89	2	1.805	1.494	0.257	421	8.5	1.0	4.00	83.8	296	90.3	1.073	0.214	134	102.3	49.2	1.6	9.8	93.36	15.2
	90	3	1.797	1.474	0.256	418	10.5	1.0	3.92	83.8	373	88.6	1.074	0.234	143	102.7	38.1	1.5	11.9	94.30	17.2
	91	4	2.873	2.496	0.477	555	13.9	2.1	3.65	96.1	536	105.7	1.068	0.186	389	12.2	0.8	6.3	16.1	99.64	28.7
	92	5	2.891	2.493	0.486	555	19.6	2.6	4.06	96.1	723	104.3	1.068	0.187	567	7.8	0.4	6.2	23.0	99.78	39.1
	93	6	7.331	6.301	1.385	662	13.8	2.3	3.12	105.2	538	109.4	1.066	0.219	475	1.7	0.3	16.2	17.4	99.94	23.8
	94	7	7.450	6.427	1.410	654	15.9	1.8	3.17	110.3	636	113.6	1.064	0.196	507	1.4	0.1	15.4	20.9	99.96	27.6
	95	8	6.382	5.496	1.219	771	12.9	1.7	3.94	120.3	459	106.9	1.062	0.280	502	1.0	0.2	24.5	15.9	99.96	15.3
	96	9	6.291	5.448	1.210	773	14.2	1.5	3.48	120.3	515	105.1	1.065	0.279	475	1.0	0.1	23.8	18.2	99.96	18.5
7A	97	8	6.357	5.577	1.220	777	12.0	1.3	3.52	122.9	465	105.3	1.068	0.252	478	1.0	0.1	25.0	15.2	99.97	7.2
	98	9	6.394	5.561	1.215	778	13.7	1.2	3.48	120.3	507	105.8	1.070	0.241	476	1.0	0.1	23.9	17.0	99.97	14.1
	99	6	7.203	6.164	1.395	671	14.0	1.1	3.17	112.8	536	106.7	1.069	0.243	522	1.3	0.1	15.8	17.6	99.96	31.3
	100	7	7.257	6.219	1.381	664	16.5	1.1	3.15	110.3	676	106.8	1.065	0.240	433	1.7	0.1	15.0	20.2	99.96	27.7
	101	4	2.871	2.495	0.476	552	13.7	1.1	3.77	102.4	504	99.2	1.105	0.195	383	13.9	0.7	6.6	15.9	99.61	23.0
	102	5	2.808	2.381	0.477	563	20.2	1.0	3.34	98.3	707	98.2	1.077	0.205	413	7.3	0.2	6.7	23.4	99.81	32.1
	103	3	1.846	1.601	0.256	426	9.4	1.0	5.49	85.7	334	90.9	1.104	0.226	140	101.4	42.0	7.0	10.7	93.99	7.9
	104	2	1.828	1.503	0.257	423	7.8	1.0	3.95	85.7	258	86.3	1.101	0.489	118	113.1	59.9	1.5	8.5	92.18	7.9
3A	105	8	6.241	5.488	1.216	793	12.0	1.0	3.56	112.8	452	105.4	1.062	0.246	483	0.6	0.3	26.4	15.0	99.94	4.3
	106	9	6.368	5.502	1.214	795	13.6	1.1	3.79	115.0	504	105.2	1.062	0.270	457	0.6	0.3	26.0	17.1	99.96	5.7
	107	6	7.357	6.344	1.379	668	13.4	1.2	3.04	112.8	540	110.4	1.072	0.223	423	1.1	0.2	14.7	14.8	99.96	18.6
	108	7	7.371	6.368	1.391	670	15.6	1.3	3.03	110.3	616	109.6	1.066	0.224	449	1.0	0.1	15.4	19.0	99.97	20.0
	109	4	2.908	2.468	0.473	564	13.2	1.4	3.72	98.3	495	100.8	1.092	0.179	289	11.0	0.5	6.5	15.2	99.70	14.7
	110	5	2.862	2.468	0.478	563	19.1	1.4	3.67	94.5	697	100.9	1.077	0.157	301	7.2	0.2	6.6	22.2	99.81	19.6
	111	3	1.928	1.669	0.262	618	9.1	1.1	4.26	85.7	337	94.1	1.115	0.330	115	102.2	46.5	1.9	10.4	93.57	3.5
	112	2	1.896	1.637	0.265	421	7.5	1.1	3.72	83.8	282	94.0	1.136	0.536	100	106.6	59.7	1.6	8.6	92.32	3.2

134

Table B-2. Supplementary High Pressure Test Data.

Fuel Number	Reading Number	v_r, Reference Velocity, m/s	fs/fm, Ratio of Sample to Metered Fuel-Air Ratio	T_f, Fuel Temperature, K	w_f, Fuel Flow Rate, g/s	ΔP_f, Fuel Nozzle Pressure Drop, MPa	A_{fe}, Fuel Nozzle Effective Area, mm²	X_{C8}, Engine Exit Gas Carbon Concentration, mg/kg	SN_8, Engine Exit Smoke Number	EI_S, Smoke Emission Index, g/kg	S_{CO}, CO Emissions Severity Parameter	S_{NO_x}, NOx Emissions Severity Parameter	S_{PF}, Pattern Factor Severity Parameter	S_R, Flame Radiation Severity Parameter
2A	1	23.9	1.30	288	14.8	0.920	0.383	0.144	2.0	0.018	0.976	0.192	1.125	-
	2	23.6	1.27	289	12.0	0.862	0.319	0.277	4.1	0.035	1.049	0.153	1.210	
	3	28.2	1.22	288	34.8	1.118	0.815	0.610	8.4	0.054	0.158	0.502	1.034	
	4	28.5	1.21	289	49.1	1.229	1.098	0.624	8.7	0.055	0.139	0.436	0.955	
	5	29.0	1.23	287	86.1	1.526	1.725	0.838	10.3	0.051	0.0210	1.201	1.056	
	6	28.5	1.11	286	100.8	1.649	1.944	1.236	16.0	0.075	0.0179	1.143	1.028	
	7	33.2	1 17	288	71.9	1.359	1.529	0.212	3.1	0.016	0.0122	1.817	1.064	
	8	33.9	1.16	288	79.1	1.428	1.640	0.293	4.3	0.022	0.0120	1.744	1.033	
1A	9	33.9	1.14	288	70.9	1.389	1.544	0.225	3.3	0.017	0.0128	1.784	1.060	-
	10	34.4	1.14	288	77.0	1.450	1.639	0.210	3.0	0.016	0.0124	1.736	1.035	
	11	28.9	1.15	287	86.1	1.551	1.772	0.629	8.8	0.038	0.0195	1.252	1.073	
	12	28.6	1.15	287	98.9	1.663	1.967	0.848	10.5	0.051	0.0182	1.205	1.043	
	13	27.6	1.11	288	33.6	1.081	0.830	0.136	1.8	0.012	0.157	0.505	1.071	
	14	27.2	1.12	287	46.9	1.235	1.082	0.097	0.8	0.009	0.128	0.463	0.993	
	15	25.6	1.16	289	14.9	0.858	0.412	0.081	0.7	0.010	1.043	0.176	1.121	
	16	25.6	1.26	290	11.3	0.796	0.326	0.160	2.2	0.020	1.003	0.136	1.186	
6A	17	23.9	1.18	288	12.2	0.828	0.328	1.340	17.0	0.171	1.108	0.147	1.212	-
	18	24.0	1.17	286	15.5	0.871	0.407	0.300	4.4	0.038	0.994	0.198	1.139	
	19	27.8	1.18	285	34.9	1.123	0.807	0.750	10.2	0.067	0.155	0.511	1.043	
	20	27.5	1.23	285	47.8	1.228	1.056	1.183	15.2	0.105	0.132	0.458	0.974	
	21	28.3	1.22	284	88.5	1.576	1.726	1.063	13.9	0.064	0.0181	1.306	1.077	
	22	28.9	1.25	284	98.3	1.660	1.869	1.008	13.5	0.061	0.0171	1.270	1.038	
	23	34.0	1.24	285	72.6	1.394	1.506	0.193	3.0	0.015	0.0121	1.849	1.047	
	24	33.9	1.22	285	84.0	1.502	1.680	0.603	8.3	0.046	0.0112	1.782	1.016	
5A	25	33.4	1.08	285	89.3	1.540	1.773	0.919	12.5	0.069	0.0112	1.711	1.012	-
	26	33.8	1.09	285	71.4	1.376	1.500	0.165	2.3	0.012	0.0124	1.842	1.062	
	27	28.6	1.11	285	86.6	1.537	1.720	2.202	24.2	0.133	0.0193	1.270	1.074	
	28	28.5	1.08	284	100.3	1.660	1.917	1.702	20.3	0.103	0.0180	1.215	1.044	
	29	27.4	1.05	285	47.1	1.206	1.057	1.139	14.9	0.101	0.121	0.481	0.993	
	30	27.6	1.05	286	34.3	1.069	0.816	1.020	13.6	0.091	0.136	0.552	1.068	
	31	24.8	1.10	286	12.6	0.826	0.342	0.215	3.2	0.028	1.090	0.150	1.205	
	32	24.5	1.10	286	15.2	0.856	0.406	0.176	2.7	0.022	0.992	0.195	1.146	
11A	33	34.2	1.10	285	71.6	1.403	1.520	0.585	8.0	0.044	0.0115	1.926	1.056	-
	34	32.6	1.09	285	83.5	1.529	1.699	1.006	13.5	0.076	0.0102	1.872	1.029	
	35	28.5	1.10	285	87.1	1.577	1.746	1.746	20.7	0.106	0.0204	1.239	1.071	
	36	28.3	1.12	285	94.5	1.640	1.857	1.621	19.6	0.098	0.0196	1.207	1.051	
	37	28.0	1.12	286	33.9	1.086	0.818	0.184	2.9	0.016	0.167	0.502	1.054	
	38	26.9	1.10	285	51.2	1.282	1.137	0.516	7.2	0.046	0.131	0.440	0.972	
	39	24.4	1.11	288	12.3	0.822	0.342	0.885	11.9	0.113	1.013	0.164	1.230	
	40	24.2	1.11	287	15.1	0.859	0.410	0.165	2.3	0.021	0.928	0.209	1.149	
1AR	41	24.5	1.20	293	11.6	0.825	0.327	0.269	4.0	0.034	1.110	0.126	1.189	-
	42	24.7	1.19	292	14.2	0.865	0.392	0.132	1.8	0.017	1.018	0.165	1.118	
	43	26.8	1.19	290	32.8	1 078	0.809	0.172	2.6	0.015	0.146	0.505	1.054	
	44	27.2	1.17	290	43.6	1.208	1.017	0.198	3.0	0.018	0.138	0.440	0.982	
	45	28.0	1.13	289	93.9	1.658	1.868	1.361	17.1	0.083	0.0181	1.162	1.047	
	46	28.4	1.12	290	84.4	1.580	1.721	1.354	17.0	0.082	0.0194	1.182	1.072	
	47	34.8	1.10	289	69.7	1.410	1.505	0.408	5.9	0.031	0.0127	1.674	1.046	
	48	33.9	1.10	289	80.0	1.511	1.669	0.500	7.0	0.038	0.0114	1.660	1.021	
13A	49	23.3	1.19	288	15.4	0.883	0.397	0.246	3.8	0.031	0.930	0.192	1.160	-
	50	24.0	1.09	288	12.6	0.849	0.332	0.245	3.8	0.031	1.087	0.140	1.222	
	51	27.2	1.12	287	33.6	1.100	0.779	1.311	16.6	0.116	0.156	0.479	1.054	
	52	27.6	1.15	287	43.0	1.193	0.955	1.626	19.8	0.144	0.139	0.441	0.993'	
	53	28.9	1.09	288	84.8	1.543	1.658	2.839	28.5	0.172	0.0206	1.146	1.067	
	54	28.8	1.07	288	95.0	1.621	1.812	2.265	24.8	0.137	0.0191	1.117	1.044	
	55	33.8	1.06	288	68.2	1.352	1.423	0.328	4.8	0.025	0.0124	1.726	1.071	
	56	33.7	1.08	289	69.4	1.371	1.440	0.427	6.2	0.032	0.0121	1.731	1.067	

Table B-2. Supplementary High Pressure Test Data (Concluded).

Fuel Number	Reading Number	V_r, Reference Velocity, m/s	fs/fm, Ratio of Sample to Metered Fuel-Air Ratio	T_f, Fuel Temperature, K	W_f, Fuel Flow Rate, g/s	ΔP_f, Fuel Nozzle Pressure Drop, MPa	A_{fe}, Fuel Nozzle Effective Area, mm²	X_{C8}, Engine Exit Gas Carbon Concentration, mg/kg	SN_g, Engine Exit Smoke Number	EI_s, Smoke Emission Index, g/kg	S_{CO}, CO Emissions Severity Parameter	S_{NO_x}, NOx Emissions Severity Parameter	S_{PF}, Pattern Factor Severity Parameter	S_R, Flame Radiation Severity Parameter
10A	57	22.8	1.146	289	12.1	-	-	1.29	16.5	0.164	1.024	0.154	1.240	0.693
	58	23.0	1.122	294	15.2	0.878	0.402	0.91	12.3	0.117	0.917	0.206	1.187	0.693
	59	27.0	1.178	294	34.3	1.136	0.800	1.33	16.8	0.118	0.150	0.518	1.053	0.843
	60	26.5	1.140	291	47.7	1.281	1.045	1.17	15.0	0.104	0.131	0.450	0.989	0.835
	61	28.7	1.203	293	87.7	1.663	1.687	2.71	27.6	0.164	0.0198	1.234	1.065	0.994
	62	27.7	1.162	289	103.3	1.780	1.917	4.14	34.4	0.251	0.0180	1.163	1.041	0.988
	63	32.2	1.160	288	67.7	1.430	1.401	0.43	6.2	0.033	0.0122	1.856	1.088	1.144
	64	32.7	1.167	293	76.3	1.513	1.539	0.68	9.5	0.051	0.0119	1.770	1.055	1.143
12A	65	32.2	1.134	292	67.2	1.442	1.424	0.20	3.0	0.015	0.0124	1.850	1.093	1.141
	66	32.7	1.157	289	75.2	1.511	1.554	0.40	5.7	0.030	0.0128	1.720	1.055	1.129
	67	28.0	1.121	292	86.5	1.656	1.711	1.07	14.0	0.065	0.0202	1.213	1.079	0.986
	68	27.9	1.123	293	102.5	1.793	1.949	1.28	16.2	0.078	0.0180	1.173	1.040	0.990
	69	26.8	1.171	290	33.8	1.153	0.799	0.16	2.3	0.014	0.141	0.535	1.071	0.851
	70	26.5	1.076	290	47.8	1.291	1.069	0.31	4.7	0.028	0.114	0.483	1.000	0.853
	71	24.4	1.085	294	14.6	1.082	0.357	0.13	1.7	0.017	0.920	0.194	1.160	0.706
	72	23.4	1.057	292	12.0	0.912	0.321	0.16	2.2	0.020	0.948	0.167	1.258	0.706
9A	73	22.9	1.030	293	14.8	0.900	0.389	0.31	4.7	0.040	0.961	0.200	1.201	0.690
	74	23.3	1.105	288	12.3	0.853	0.331	0.89	12.0	0.114	1.106	0.148	1.243	0.688
	75	27.4	1.061	287	33.2	1.100	0.790	0.85	11.5	0.076	0.147	0.528	1.074	0.851
	76	27.2	1.077	287	47.1	1.253	1.049	0.83	11.0	0.073	0.121	0.479	0.995	0.851
	77	32.9	1.202	288	84.5	1.604	1.664	1.52	18.6	0.092	0.0254	1.054	1.033	0.993
	78	28.8	1.199	293	102.2	1.771	1.920	2.98	29.3	0.181	0.0182	1.097	1.026	0.995
	79	33.6	1.176	289	67.4	1.429	1.406	0.41	5.8	0.031	0.0126	1.609	1.075	1.152
	80	32.6	1.192	294	75.9	1.521	1.539	0.68	9.3	0.051	0.0110	1.680	1.057	1.157
8A	81	33.7	1.227	289	67.5	1.422	1.385	0.48	6.3	0.036	0.0123	1.792	1.077	1.158
	82	33.7	1.260	292	76.9	1.520	1.529	0.71	9.6	0.054	0.0112	1.836	1.043	1.163
	83	28.3	1.197	295	88.6	1.638	1.699	4.54	36.0	0.276	0.0192	1.243	1.074	0.994
	84	28.1	1.212	292	103.2	1.766	1.904	4.92	37.6	0.299	0.0173	1.205	1.043	0.997
	85	27.3	1.191	293	47.9	1.264	1.045	1.48	18.2	0.131	0.126	0.456	0.981	0.846
	86	26.2	1.134	292	34.3	1.116	0.795	1.86	21.6	0.165	0.144	0.523	1.077	0.843
	87	24.3	1.155	292	15.0	0.894	0.788	0.47	6.6	0.061	0.882	0.205	1.158	0.707
	88	25.1	1.133	294	12.4	0.854	0.329	0.37	5.3	0.047	1.022	0.153	1.209	0.708
4A	89	22.8	1.159	287	12.6	0.856	0.328	0.93	12.4	0.120	0.977	0.174	1.232	0.696
	90	22.3	1.132	289	15.5	0.896	0.395	0.91	12.0	0.116	0.884	0.227	1.170	0.693
	91	27.1	1.160	288	34.7	1.125	0.788	2.10	24.2	0.186	0.153	0.501	1.045	0.840
	92	26.7	1.178	288	48.8	1.269	1.043	2.71	27.5	0.240	0.124	0.448	0.979	0.841
	93	28.2	1.261	289	87.1	1.610	1.653	2.10	23.5	0.128	0.0189	1.244	1.071	0.998
	94	28.0	1.316	288	102.0	1.722	1.871	2.17	23.8	0.132	0.0181	1.170	1.029	0.988
	95	32.6	1.291	289	67.5	1.392	1.378	1.00	13.4	0.075	0.0119	1.888	1.077	1.152
	96	32.6	1.288	288	77.2	1.492	1.521	1.11	14.5	0.084	0.0110	1.838	1.047	1.155
7A	97	33.3	1.274	289	66.7	1.385	1.384	0.46	6.5	0.035	0.0118	1.933	1.076	1.162
	98	33.4	1.287	288	76.1	1.471	1.535	0.82	11.0	0.062	0.0110	1.874	1.041	1.163
	99	27.8	1.261	288	86.2	1.585	1.672	3.24	30.5	0.197	0.0171	1.351	1.084	1.011
	100	28.0	1.224	288	102.7	1.734	1.905	2.29	24.8	0.139	0.0169	1.223	1.036	1.001
	101	27.1	1.155	287	34.3	1.127	0.788	1.48	18.3	0.131	0.158	0.504	1.061	0.837
	102	26.2	1.161	288	48.1	1.261	1.045	1.75	20.7	0.155	0.116	0.481	1.149	0.850
	103	25.0	1.129	280	15.1	0.900	0.390	0.43	6.2	0.055	0.986	0.185	1.149	0.701
	104	24.3	1.090	289	12.3	0.852	0.326	0.54	7.5	0.069	1.071	0.147	1.237	0.698
3A	105	33.6	1.248	289	66.1	1.382	1.394	0.26	3.8	0.020	0.0106	2.091	1.074	1.187
	106	33.8	1.262	289	74.8	1.467	1.530	0.31	4.5	0.023	0.0099	2.030	1.042	1.190
	107	28.9	1.247	288	85.3	1.574	1.679	1.50	18.5	0.091	0.0187	1.294	1.061	1.007
	108	28.7	1.219	285	99.5	1.711	1.881	1.47	18.0	0.089	0.0169	1.254	1.029	1.009
	109	27.6	1.159	292	32.5	1.117	0.762	0.84	11.5	0.075	0.151	0.524	1.063	0.851
	110	27.2	1.163	289	47.1	1.260	1.040	0.84	11.5	0.075	0.123	0.472	0.981	0.850
	111	24.8	1.152	294	15.1	0.903	0.396	0.17	2.5	0.022	1.026	0.172	1.141	0.693
	112	24.0	1.135	294	12.3	0.858	0.331	0.20	3.0	0.026	1.054	0.142	1.210	0.697

Table B-3. CO Emission Test Data Correlation.

(a) Data Correction to Engine Conditions:

$$EI_{CO}, \text{engine} = \left(EI_{CO}, \text{test}\right)\left(\frac{S_{CO}.\text{engine}}{S_{CO}, \text{test}}\right)$$

where:

$$S_{CO} = \left(\frac{V_r}{24.2}\right)\left(\frac{0.254}{P_3}\right)^{1.25}\left(\frac{9.42}{f}\right)^{0.5}\left[\exp\left(\frac{421-T_3}{133}\right)\right]$$

| Fuel Number | EI_{CO}, test g/kg as measured, Table B-1 at test points indicated | | | | | | | | EI_{CO}, engine, g/kg corrected to S_{CO} = 1.000, 0.153, 0.0160 and 0.0072 | | | |
| | Idle | | Cruise | | Takeoff | | Dash | | Idle | Cruise | Takeoff | Dash |
	(2)	(3)	(4)	(5)	(6)	(7)	(8)	(9)	(1.000)	(0.153)	(0.0160)	(0.0072)
1A	68.4	60.9	8.5	7.3	1.3	1.3	1.0	0.9	63.3	8.5	1.1	0.6
1AR	75.5	75.2	7.4	7.0	1.2	1.2	0.9	0.9	71.0	7.8	1.0	0.5
2A1	91.8	80.9	9.5	8.1	1.3	1.3	0.8	1.0	85.2	9.0	1.1	0.6
3A	106.6	102.2	11.0	7.2	1.1	1.0	0.6	0.6	100.4	10.1	0.9	0.4
4A	102.3	102.7	12.2	7.8	1.7	1.4	1.0	1.0	110.5	10.9	1.3	0.6
5A	92.5	98.5	8.9	8.1	1.3	1.5	0.9	0.9	92.1	10.1	1.2	0.6
6A	100.1	89.5	10.2	7.9	1.5	1.4	1.0	0.9	90.2	9.7	1.3	0.6
7A	113.1	101.4	13.9	7.3	1.3	1.2	1.0	1.0	104.2	11.6	1.2	0.6
8A	78.8	73.8	12.3	8.5	1.6	1.8	1.0	0.9	80.4	11.7	1.5	0.6
9A	94.5	86.2	11.1	8.7	2.5	1.7	1.1	0.9	87.6	11.3	1.6	0.6
10A	98.3	88.2	9.8	8.4	1.6	1.5	1.1	1.0	96.1	9.2	1.3	0.6
11A	110.7	76.8	9.4	8.4	1.5	1.6	0.9	1.0	96.1	9.2	1.2	0.6
12A	93.7	82.6	9.6	6.9	1.5	1.3	0.9	1.0	94.3	9.9	1.2	0.6
13A1	103.0	99.4	14.0	10.9	1.8	1.9	1.2	1.1	100.9	12.9	1.5	0.7

(b) Data Correlation with Fuel Hydrogen Content and Spray Droplet Size.

$$EI_{CO} = b\left(\frac{H}{14.5}\right)^m\left(\frac{SMD}{SMD_{JP-4}}\right)^n$$

Engine Power Level	Idle	Cruise
b, Intercept	74.79	8.45
m, Hydrogen Slope	-0.977	-0.922
n, Droplet Size Slope	+0.482	+0.446
r, Correlation Coefficient	0.740	0.756

Table B-4. HC Emission Test Data Correlation.

(a) Data Correction to Engine Conditions:

$$EI_{HC}, \text{ engine} = (EI_{HC} \text{ test}) \left(\frac{S_{CO}, \text{engine}}{S_{CO}, \text{ test}}\right)^{2.14}$$

where:

$$S_{CO} = \left(\frac{V_r}{24.2}\right) \left(\frac{0.254}{P_3}\right)^{1.25} \left(\frac{9.42}{f}\right)^{0.5} \left[\exp\left(\frac{421-T_3}{133}\right)\right]$$

Fuel Number	EI_{HC}, test g/kg (as measured, Table B-1 at test points indicated)								EI_{HC}, engine, g/kg (corrected to S_{CO} = 1.000, 0.153, 0.0160 and 0.0072)			
	Idle		Cruise		Takeoff		Dash		Idle	Cruise	Takeoff	Dash
	(2)	(3)	(4)	(5)	(6)	(7)	(8)	(9)	(1.000)	(0.153)	(0.0160)	(0.0072)
1A	35.9	19.2	0	0	0	0	0	0	26.6	0	0	0
1AR	34.5	27.8	0	0	0	0	0	0	27.2	0	0	0
2A1	41.4	31.9	0.6	0.3	0.2	0.1	0	0	35.5	0.5	0.1	0
3A	59.7	46.5	0.5	0.2	0.2	0.1	0.5	0.3	48.7	0.4	0.1	0.2
4A	49.2	38.1	0.8	0.4	0.3	0.1	0.2	0.1	50.7	0.7	0.2	0.1
5A	42.0	38.6	0.1	0.1	0	0	0	0	37.1	0.2	0	0
6A	45.5	32.1	0.8	0.4	0.2	0.3	0.4	0.2	34.5	0.6	0.2	0.1
7A	59.9	42.0	0.7	0.2	0.1	0.1	0.1	0.1	47.5	0.6	0.1	0
8A	35.1	28.4	0.5	0.2	0.2	0.1	0.2	0.1	35.4	0.4	0.1	0.1
9A	45.8	44.1	1.6	0.4	0.4	0.1	0.2	0.1	42.5	1.2	0.1	0.1
10A	51.0	43.0	1.4	0.6	0.6	0.5	0.6	0.4	50.2	1.2	0.4	0.2
11A	50.6	24.2	0.2	0.2	0.1	0.1	0	0.1	38.8	0.2	0.1	0
12A	47.2	34.2	0.5	0.2	0.3	0.3	0.4	0.4	46.9	0.5	0.2	0.1
13A1	38.2	49.5	1.1	0.7	0.4	0.2	0.1	0.1	44.9	1.0	0.2	0

(b) Data Correlation with Fuel Hydrogen Content and Spray Droplet Size.

$$EI_{HC} = b \left(\frac{H}{14.5}\right)^m \left(\frac{SMD}{SMD_{JP-4}}\right)^n$$

Engine Power Level	Idle	Cruise
b, Intercept	32.05	0.0426
m, Hydrogen Slope	-1.19	-13.2
n, Droplet Size Slope	+0.517	+3.44
r, Correlation Coefficient	0.597	0.744

Table B-5. NO$_X$ Emission Test Data Correlation.

(a) Data correction to Engine Conditions:

$$EI_{NO_x}, \text{engine} = \left(EI_{NO_x}, \text{test}\right)\left(\frac{S_{NO_x}, \text{engine}}{S_{NO_x}, \text{test}}\right)$$

where:

$$S_{NO_x} = \left(\frac{28.6}{V_r}\right)\left(\frac{P_3}{1.359}\right)^{0.37} [\phi(f)]^* \left\{\exp\left[\left(\frac{T_3 - 664}{192}\right) + \left(\frac{6.29 - h_3}{53.2}\right)\right]\right\}$$

and:

$\phi[f] = 0.1243\ f - 0.233$, when $f \leq 11.5$

$= 1.461 - 0.0231\ f$, when $f \geq 11.5$

| Fuel Number | EI$_{NO_x}$, test, g/kg (as measured, Table B-1 at test points indicated) | | | | | | | | EI$_{NO_x}$, engine, g/kg (corrected to S$_{NO_x}$ 0.168, 0.472, 1.000 and 1.816) | | | |
| | Idle | | Cruise | | Takeoff | | | Dash | Idle (0.168) | Cruise (0.472) | Takeoff (1.000) | Dash (1.816) |
	(2)	(3)	(4)	(5)	(6)	(7)	(8)	(9)				
1A	2.1	1.2	6.1	5.8	14.6	13.9	23.2	22.0	1.8	5.8	11.6	23.3
1AR	1.7	1.4	6.6	6.4	14.4	13.7	22.0	21.5	1.9	6.6	12.0	23.7
2A1	3.7	3.6	6.6	5.9	13.8	13.5	22.6	22.6	3.7	6.3	11.7	23.6
3A	1.6	1.9	6.5	6.4	14.7	15.4	26.4	26.0	1.9	6.2	11.9	23.1
4A	1.6	1.5	6.3	6.2	16.2	15.4	24.5	23.8	1.3	6.2	13.1	23.5
5A	2.4	2.2	6.7	7.2	15.2	15.2	23.6	---	2.3	6.4	12.3	23.3
6A	2.6	2.5	---	---	16.0	13.8	---	21.5	2.6	---	11.6	21.9
7A	1.6	2.0	6.6	6.7	15.8	15.0	25.0	23.9	1.8	6.4	12.0	23.3
8A	2.1	2.4	6.7	6.3	15.2	14.9	25.6	25.1	2.2	6.2	12.3	25.3
9A	1.9	2.0	6.2	5.8	13.8	14.0	24.7	24.6	2.0	5.6	12.9	27.2
10A	1.9	1.7	6.5	6.2	16.2	15.0	26.8	25.3	1.8	6.2	13.0	26.1
11A	3.2	3.1	6.5	5.8	---	---	---	---	2.9	6.2	---	---
12A	2.1	2.4	6.5	6.6	14.2	13.8	24.5	27.3	2.1	6.0	11.8	23.7
13A1	1.5	1.4	---	6.2	15.9	14.0	21.8	25.4	1.5	6.6	13.2	26.3

(b) Data Correlation with Fuel Hydrogen Content:

$$EI_{NO_x} = b\left(\frac{H}{14.5}\right)^m$$

Engine Power Level	Idle	Cruise	Takeoff	Dash
b, Intercept	2.220	6.18	11.80	23.65
m, Slope	+0.670	-0.034	-0.361	-0.195
r, Correlation Coefficient	+0.178	-0.051	-0.551	-0.228

Table B-6. Smoke Emission Test Data Correlation.

(a) Data Correction to Engine Conditions:

| Fuel Number | SN$_8$, test (From Table B-2 at test points indicated) | | | | | | | | SN$_8$, engine (Average of two SN$_8$ test at each engine condition) | | | |
| | Idle | | Cruise | | Takeoff | | Dash | | | | | Dash 75% P3 |
	(2)	(3)	(4)	(5)	(6)	(7)	(8)	(9)	Idle	Cruise	Takeoff (dry)	dry
1A	3.0	0.7	1.8	0.8	8.8	10.5	3.3	3.0	1.9	2.3	9.7	3.2
1AR	4.0	1.8	2.6	3.0	17.0	17.1	5.9	8.0	2.9	2.8	17.1	7.0
2A1	4.1	2.0	8.4	8.7	10.3	16.0	3.1	4.3	3.1	8.6	13.2	3.7
3A	3.0	2.5	11.5	I1.5	18.5	18.0	3.8	4.5	2.8	11.5	18.3	4.2
4A	12.4	12.0	24.2	27.5	23.5	23.8	13.4	14.5	12.2	25.9	23.7	14.0
5A	3.2	2.7	14.9	13.6	24.2	20.3	2.3	12.5	3.0	14.4	22.3	7.4
6A	17.0	4.4	10.2	15.2	13.9	13.5	3.0	8.3	10.7	12.7	13.7	5.7
7A	7.5	6.2	18.3	20.7	30.5	24.8	6.5	11.0	6.9	19.5	27.7	8.8
8A	5.3	6.6	18.2	21.6	36.0	44.0	6.8	9.6	6.0	19.9	40.0	8.2
9A	12.0	4.7	11.5	11.0	18.6	29.3	5.8	9.3	8.4	11.3	24.0	7.6
10A	16.5	12.3	16.8	15.0	27.6	34.4	6.2	9.5	14.4	15.9	31.0	7.9
11A	11.9	2.3	2.9	7.2	20.7	19.6	8.0	13.5	7.1	5.1	20.2	10.8
12A	1.7	2.2	2.3	4.7	14.0	16.2	3.0	5.7	2.0	3.5	15.1	4.4
13A1	3.8	3.8	16.6	19.8	28.5	24.8	4.8	6.2	3.8	18.2	26.7	5.5

(b) Data Correlation with Fuel Hydrogen Content:

$$SN_8 = b \left(\frac{H}{14.5}\right)^m$$

Engine Power Level	Idle	Cruise	Takeoff	Dash
b, Intercept	2.08	3.88	13.92	4.27
m, Slope	-8.37	-8.93	-3.64	-4.06
r, Correlation Coefficient	-0.865	-0.800	-0.671	-0.680

140

Table B-7. Detailed Inner Liner Temperature Data.

$T_L - T_3$, Inner Liner Temperature Rise, K at Thermocouple Number

Fuel Number	Reading Number	Avg.	1	2	3	4	5	6	7	8	9	10	11	12	13	14	15	16	17	18	19	20	21	22	23	24
2A	1	69	47	101	132	132	39	42	66	62		74	141	127	67	64	68	62	62	27	49	50	66	24		34
	2	60	47	81	111	94	47	59	78	80		33	42	70	48	54	71	61	58	27	70	78	68	23		34
	3	149	98	248	260	340	39	45	154	198		162	294	225	146	100	137	115	111	60	157	152	117	55		67
	4	138	91	217	258	337	23	13	130	125		154	306	220	118	87	127	118	111	63	146	121	142	64		71
	5	246	148	299	362	361	361	339	317	464		221	481	333	204	146	242	157	186	76	171	221	180	73		78
	6	249	156	299	368	343	330	283	374	441		234	520	356	199	149	246	168	198	83	157	221	200	88		83
	7	263	172	340	381	347	385	392	302	464		245	505	406	189	182	261	192	208	106	183	208	163	79		92
	8	264	173	345	374	366	362	355	317	392		239	498	423	186	181	276	201	232	117	177	216	182	94		100
1A	9	264	179	472	366	359	390	423	295	368		213	510	386	166	172	284	177	215	95	221	201	152	73		87
	10	264	171	451	362	347	386	420	303	386		228	508	389	175	170	255	181	208	101	219	208	164	82		91
	11	240	141	310	328	363	380	430	278	352		183	436	339	155	159	269	170	214	94	151	186	176	86		111
	12	247	140	286	335	387	363	410	294	386		196	444	359	163	168	274	184	229	107	142	189		99		117
	13	169	155	344	255	326	230	264	155	243		184	394	247	108	122	127	93	100	47	121	94	105	48	58	76
	14	150	135	278	254	267	98	132	148	218			399	265	114	127	139	105	114	57	100	28	102	57	75	95
	15	99	64	216	188	247	96	117	88				262	167	72		76	51	56	21	82	46	50	19	36	39
	16	100	58	176	188	240	109	133	90				261	164	78		79	51	56	21	95	61	51	18	33	38
6A	17	68	62	78	107	87	38	60	84				58	80	54	87	94	73	79	41	82	82	71	33	38	45
	18	70	49	61	117	99	25	30	63				147	144	55	95	103	74	85	43	47	47	71	37	46	49
	19	194	117	262	314	368	66	77	205			220	369	286	181	205	218	186	190	112	199	215	189	104	83	109
	20	199	124	241	317	383	47	29	195			200	390	283	176	202	228	211	218	138	159	147	217	143		137
	21	276	167	354	379	453	338	351	344			212	480	376	208	289	325	221	267	130	217	249	217	121		110
	22	272	168	344	379	440	285	294	348			214	482	390	209	292	325	229	276	138	196	243	224	137		116
	23	290	186	424	359	517	409	377	359			248	371	418	227	315	327	234	263	136	240	260	197	102		119
	24	287	186	391	339	461	386	361	357			243	348	416	228	319	341	250	288	154	222	256	224	126		127
5A	25	266	159	352	360	452	297	241	325	393		221	311	481	204	207	319	232	278	143	193	229	213	126		120
	26	285	170	422	401	450	424	487	335	451		222	311	423	199	288	305	212	237	117	216	220	177	90		109
	27	270	145	261	387	464	406	456	336	452		200	291	375	186	283	332	215	265	124	149	196	194	114		126
	28	257	149	264	376	457	310	308	328	359		200	296	388	188	276	319	223	280	134	145	194	204	128		133
	29	175	121	239	292	322	60	115	239	144			226	283	180	209	230	199	207	126	133	17	155	118	102	136
	30	212	126	254	329	393	301	352	276	184			248	285	188		241	193	200	113	155	143	168	97	87	123
	31	81	45	83	150	180	103	127	78				101	141	73		88	60	61	27	50	40	62		33	39
	32	72	38	56	135	152	86	109	98				81	136	60		87	63	63	30	24	20	54		39	47
11A	33	283	182	458	411	468	427	498	339	401		203	310	444	198	293	321	212	242	117	247	243	188	97	89	123
	34	290	171	380	299	435	411	451	358	456		220	312	454	214	321	364	253	301	157	221	258	229	137	115	144
	35	259	148	295	377	449	410	494	317	385		181	272	360	184	274	328	212	261	122	157	206	192	111	94	136
	36	263	147	286	372	442	413	487	327	402		189	275	364	189	277	330	222	275	133	151	207	202	121	102	143
	37	175	162	349	286	360	265	311	191	134		126	230	266	130	163	168	125	132	68	135	93	130	69	66	88
	38	172	138	286	273	252	119	153	203	222		136	234	294	147	179	196	159	168	98	120		120	92	92	122
	39	77	37	57	166	177	109	142	91				68	112	64	83	88	57	57	23	50		58	24	31	51
	40	102	64	176	198	244	112	140	105				152	169	77	90	97	66	69	32	77		64	30	41	49

Table B-7. Detailed Inner Liner Temperature Data (Continued).

$T_L - T_3$, Inner Liner Temperature Rise, K at Thermocouple Number

Fuel Number	Reading Number	Avg.	1	2	3	4	5	6	7	8	9	10	11	12	13	14	15	16	17	18	19	20	21	22	23	24
1AR	41	72	42	97	152	164	44	82	88	66			42	114	63		80	60	60	28	88	67	57		29	35
	42	66	36	79	153	173	19	36	70	35			42	128	61		80	59	62	29	73	54	64		35	39
	43	153	155	397	280	274	28	43	123	160			232	264	130		149	112	116	59	167	146	110		65	65
	44	135	134	353	260	218	5	4	92	153			216	266	122		146	114	116	61	130	130	116		74	68
	45	238	149	363	367	401	289	316	290	398		180	264	362	174	129	277	188	227	110	185	213	184	59	93	110
	46	239	155	389	370	410	323	342	299	411		183	254	355	168	233	275	177	218	101	193	202	164	104	82	115
	47	242	174	447	365	391	373	410	296	367		183	253	393	167	233	272	168	200	92	198	192	142	87	72	111
	48	252	180	454	353	364	357	369	303	444		212	269	352	190	270	257	202	212	113	210	216	171	88	89	127
13A	49	71		83	74	101	54	58	75			71	45			95	101	77	85	51	43	63	97	50		55
	50	65		74	70	109	66	61	69			65	46			89	91	67	71	41	36	76	81	35		40
	51	197		249	300	365	73	71	227			159	172			209	228	206	207	129	239	253	215	117		132
	52	190		235	295	349	57	40	192			149	155			199	226	213	216	139	215	234	236	137		147
	53	266		499	426	385	280	214	324	323		195	263			266	309	217	262	134	262	251	203	109		146
	54	281		469	426	368	379	348	321	415		209	262			269	311	215	258	131	248	237	220	124		135
	55	248		236	296	231	291	263	340	378		221	290			330	376	244	295	140	209	209	155	81		128
	56	259		209	393	223	261	300	354	404		227	275			343	423	256	321	144	194	213	159	82		131
10A	57	90	167		93	113	128	148	109	109	30	49	64	83	144	73	90	75	73	50	137		79	36		49
	58	71	99		82	99	67	93	98	102	25	43	48	49	136	58	78	54	63	39	108		77	29		48
	59	189	340		317	316	171	162	185	260	86	189	340	128	288	138	167	143	128	106	194		137	71		110
	60	180	328		292	291	27	26	155	193	84	217	420	140	297	150	175	149	141	107	170		178	102		141
	61	276	400		376	398	375	351	309	439	105	191	487	209	374	242	309	210	228	140	223		191	96		152
	62	265	335		303	364	280	264	299	433	101	213	511	223	387	255	306	217	230	142	198		221	118		170
	63	309	332		381	406	482	481	363	427	147	225	576	313	393	279	348	232	255	161	274		184	93		141
	64	294	318		259	265	427	318	362	412	146	326	595	338	397	279	332	249	263	178	241		201	112		155
12A	65	287	261		372	382	491	479	339	397	112	230	554	312	372	242	314	198	221	127			141	80		123
	66	279	252		325	348	423	418	307	497	110	228	567	305	365	238	278	201	211	134			152	87		134
	67	252	210		328	337	357	396	303	385	92	191	478	228	327	218	294	196	215	125			159	84		121
	68	246	213		269	289	211	261	283	407	152	212	487	212	341	240	240	203	221	132			180			138
	69	181	239		303	290	274	312	172	177	54	164	388	168	270	135	149	105	106	64			120	58		83
	70	150	216		146	136	70	126	155	217	66	169	395	147	241	137	170	118	123	75			122	71		109
	71	88	64		163	152	110	128	95	89	25	70	162	118	152	80	89	59	55	31			51	29		40
	72	79	56		149	144	110	84	84	80	21	60	125	104	143	75	80	51	51	26			56	21		31
9A	73	83	110		96	101	81	105	110	110	42	47	72	81	150	90	102	76	76	52			72	46		56
	74	87	112		97	109	97	117	114	108	43	54	83	99	152	98	108	79	79	53	87		64	38		54
	75	199	295		323	317	195	225	196	233	97	224	375	144	291	159	177	148	145	107	225		145	78		98
	76	186	256		288	288	15	34	161	223	92	252	420	134	298	153	159	159	166	115	190		205	119		134
	77	267	341		410	419	399	463	289	361	149	252	404	246	355	236	185	185	213	120	224		143	72		106
	78	267	384		303	284	303	303	303	437	156	317	439	218	350	245	236	205	227	148			219	118		148
	79	293	263		450	449	462	500	350	425	197	238	311	288	391	277	259	226	248	149	284		158	88		159
	80	295	213		407	479	411	393	372	422	213	247	294	309	417	298	278	250	284	174			175	108		161

142

Table B-7. Detailed Inner Liner Temperature Data (Concluded).

$T_L - T_3$, Inner Liner Temperature Rise, K at Thermocouple Number

Fuel Number	Reading Number	Avg.	1	2	3	4	5	6	7	8	9	10	11	12	13	14	15	16	17	18	19	20	21	22	23	24
8A	81	287	197		313	255	488	535	371	481	201	303	283	303	432	283	254	225	245	150			163	99		154
	82	299	189		295	350	459	510	354	455	218	301	320	301	430	315	276	267	287	185			184	119		171
	83	286	196		430	438	468	454	333	405	191	295	266	173	400	265	262	242	262	173			205	116		148
	84	284	211		421	433	409	393	346	462	192	283	250	180	403	263	263	230	260	166			217	128		173
	85	212	217		307	301	147	157	269	338	165	209	189	141	312	212	213	207	213	157			209	128		161
	86	245	251		363	348	349	374	289	308	161	222	237	176	326	232	214	205	210	157			213	130		139
	87	134	97		226	222	156	159	146	142	78	189	169	123	217	140	123	113	108	73			93	48		73
	88	116	88		199	198	146	145	121	112	58	179	164	117	198	125	107	92	87	53			62	33		51
4A	89	86	87		82	85	57	62	106	125	71	86	94	60	111	134	111	105	105	70	66		86	46		57
	90	76	70		49	54	40	50	98	137	68	59	59	33	95	118	105	104	105	73	49		114	60		63
	91	237	248		389	370	200	117	270	318	176	281	225	172	342	229	227	228	229	176	199		223	152		166
	92	233	233		401	387	172	91	220	182	167	285	229	196	355	243	232	233	243	185	190		270	186		205
	93	270	239		475	444	263	206	352	426	207	249	249	220	402	282	271	233	282	169	187		230	139		163
	94	295	279		447	418	405	374	356	507	191	317	264	228	414	280	256	219	261	162	214		284	163		167
	95	297	251		451	418		502	386	486	231	232	260	313	480	308	283	246	284	159	156		199	117		174
	96	270	253		358	363		374	390	440	218	227	223	277	393	285	270	238	285	167	137		215	123		166
7A	97	275	253		395	478		466	350	401	209	233	200	283	416	268	262	205	253	129			172	93		153
	98	277	267		397	413		363	377	423	212	236	217	286	403	276	260	223	271	155			203	114		166
	99	270	278		428	403		324	348	511	192	244	187	188	374	249	254	206	264	149			234	137		154
	100	264	285		415	396		241	351	433	195	229	186	195	361	257	260	215	279	159			251	163		148
	101	216	224		350	321		195	283	383	154	195	162	166	317	205	196	176	194	134			204	124		128
	102	206	227		324	300		46	197	264	159	201	151	168	319	212	207	197	212	154			226	161		197
	103	72	86		82	87		66	106	111	48	43	41	67	135	77	73	67	68	42			72	38		66
	104	67	92		74	79		60	98	99	44	44	45	74	118	79	73	64	63	40			65	29		50
3A	105	267	297		467	385		483	344	429	186	254	190	265	377	243	237	191	225	119			161	85		140
	106	269	298		457	385		427	342	381	191	253	195	268	387	253	244	210	249	135			182	100		158
	107	240	222		423	346	394	365	316	383	160	185	160	161	370	216	223	188	240	129			216	114		124
	108	250	237		424	341		365	371	449	171	194	167	157	356	221	223	189	237	134			237	137		147
	109	172	177		289	266		253	232	279	110	135	129	129	242	148	144	128	138	92			157	97		124
	110	169	184		301	277		56	192	263	117	145	118	145	264	159	155	145	159	108			175	117		141
	111	55	70		69	71		71	86	99	31	26	36	56	95	55	55	50	47	26			55	27		46
	112	60	81		74	74		71	89	89	35	35	44	70	94	64	61	56	51	31			59	24		40

143

Table B-8. Detailed Rear Liner, Transition Duct and Fuel Nozzle Stem Temperature Data.

Fuel Number	Reading Number	$(T-T_3)$, Temperature Rise, K, at Thermocouple Number										
		Rear Liner						Transition		Fuel Nozzle Stem		
		Avg.	26	27	28	29	30	31	32	33	34	35
2A	1	105	121	103	56	66	99	154	136	-44	-41	-39
	2	86	85	91	50	61	92	122	105	-43	-39	-37
	3	186	229	182	171	132	163	227	200	-74	-67	-65
	4	242	329	234	189	186	207	301	254	-80	-72	-70
	5	187	215	208	173	131	173	215	200	-69	-56	-58
	6	219	268	237	218	154	189	241	227	-70	-58	-60
	7	170	192	192	135	125	157	187	204	-101	-83	-87
	8	189	221	207	162	139	174	200	221	-102	-84	-89
1A	9	162	193	182	114	111	157	177	204	-111	-93	-100
	10	177	212	191	139	124	165	194	216	-114	-95	-102
	11	169	187	186	139	110	168	189	208	-79	-66	-70
	12	198	235	213	176	134	181	221	230	-78	-65	-69
	13	146	147	151	91	102	145	182	206	-82	-73	-74
	14	195	210	196	129	152	175	254	252	-87	-78	-80
	15	98	95	103	47	68	100	132	142	-52	-47	-47
	16	77	86	91	37	57			116	-52	-46	-45
6A	17	83	83	95	58	55	77	110	103	-44	-39	-38
	18	102	106	109	68	67	87	144	133	-48	-42	-42
	19	194	222	187	223	152	155	219	205	-84	-73	-74
	20	287	382	269	311	259	212	300	277	-86	-75	-77
	21	196	232	224	199	135	164	212	208	-73	-60	-64
	22	220	267	238	229	162	191	230	229	-76	-63	-67
	23	181	217	204	172	127	165	179	206	-109	-90	-95
	24	211	262	236	215	148	188	201	232	-110	-92	-97
5A	25	214	258	227	219	154	189	211	244	-104	-86	-90
	26	170	198	194	135	121	155	187	201	-102	-84	-87
	27	180	207	194	171	121	167	200	202	-71	-58	-60
	28	210	243	230	202	143	197	226	232	-72	-59	-62
	29	241	275	234	260	199	186	262	273	-89	-79	-80
	30	173	130	169	184	133	151	189	209	-87	-76	-77
	31	77	74	86	43	66			118	-47	-42	-41
	32	88	82	95	52	77			137	-49	-43	-43
11A	33	170	200	188	135	123	152	181	211	-114	-94	-99
	34	219	257	238	221	158	190	215	255	-118	-99	-104
	35	174	192	181	168	121	162	187	209	-75	-62	-65
	36	195	225	203	197	139	178	207	222	-76	-63	-66
	37	148	147	147	119	116	135	171	206	-85	-75	-75
	38	235	255	222	223	204	192	272	283	-85	-77	-79
	39	75	70	81	37	62	76	85	119	-52	-47	-46
	40	96	90	102	37	83	90	117	138	-54	-48	-48

Table B-8. Detailed Rear Liner, Transition Duct and Fuel Nozzle Stem Temperature Data (Continued).

Fuel Number	Reading Number	(T-T$_3$), Temperature Rise, K, at Thermocouple Number										
		Rear Liner						Transition		Fuel Nozzle Stem		
		Avg.	26	27	28	29	30	31	32	33	34	35
1AR	41	69	75	94	45	65				-48	-43	-42
	42	82	91	106	52	80				-50	-45	-44
	43	160	169	175	112	133	131	223	181	-87	-77	-77
	44	201	225	209	134	179	161	283	220	-88	-79	-79
	45	205	241	241	182	150	178	239	210	-75	-64	-65
	46	181	201	214	161	125	158	217	194	-74	-62	-63
	47	164	187	196	119	119	147	187	193	-112	-95	-96
	48	195	231	220	167	146	172	216	218	-111	-95	-96
13A	49	107	108	115		102	104				-38	-40
	50	83	81	96		68	87				-36	-37
	51	167		191		159	152				-63	-64
	52	213		239		215	187				-66	-67
	53	159		217		147	164				-53	-53
	54	170		239		187	179				-54	-54
	55	158		197		127	152				-75	-77
	56	164		198		133	161				-75	-77
10A	57	34	88	99	88	60	70	103				-34
	58	88	94	104	88	60	69	113				-45
	59	185	249	208	232	124	120	181				-69
	60	251	371	286	253	188	178	231				-72
	61	203	304	237	270	119	114	117				-55
	62	247	383	284	288	170	151	207				-52
	63	171	241	207	217	99	107	160				-81
	64	199	265	225	270	127	130	182				-79
12A	65	162	227	208	170	99	108	160				-74
	66	177	243	214	204	109	115	180				-77
	67	179	243	211	223	115	116	169				-58
	68	218	322	260	236	151	151	193				-56
	69	138	154	157	120	97	120	181				-69
	70	196	241	222	155	156	180	226				-75
	71	82	90	100	56	54	80	114				-46
	72	67	75	84	45	42	65	95				-44
9A	73	94	100	109	86	55	81	134				-33
	74	86	93	102	79	54	74	117				-27
	75	169	206	187	196	122	135	169				-62
	76	236	309	261	227	190	205	227				-68
	77	151	196	185	175	96	128	130				-46
	78	241	332	264	274	189	194	194				-55
	79	159	201	192	182	96	134	149				-87
	80	201	265	223	260	122	160	179				-89

Table B-8. Detailed Rear Liner, Transition Duct and Fuel Nozzle Stem
Temperature Data (Concluded).

Fuel Number	Reading Number	(T-T_3), Temperature Rise, K, at Thermocouple Number										
		Rear Liner						Transition		Fuel Nozzle Stem		
		Avg.	26	27	28	29	30	31	32	33	34	35
8A	81	164	231	202	163	103	139	149			-82	-85
	82	192	266	222	219	114	157	179			-84	-89
	83	209	256	214	304	139	167	177			-56	-59
	84	246	335	254	307	180	193	212			-57	-58
	85	264	321	261	317	232	213	241			-70	-70
	86	198	222	196	294	142	148	191			-65	-63
	87	101	111	116	118	62	82	117			-42	-41
	88	77	88	98	77	43	63	93			-43	-42
4A	89	100	119	134	94	57	87	111				-35
	90	115	127	143	118	69	99	137				-73
	91	242	321	280	303	162	186	204				-60
	92	354	567	412	345	255	265	285			-70	-68
	93	222	287	252	262	144	188	201			-53	-53
	94	260	360	299	293	186	204	218			-56	-55
	95	165	250	231	179	113	159	178			-71	-74
	96	205	270	251	224	133	167	189			-78	-84
7A	97	167	215	215	149	111	144	172			-78	-82
	98	199	265	255	202	126	160	189			-79	-80
	99	216	292	262	245	131	164	202			-56	-58
	100	245	328	281	271	163	194	238			-55	-55
	101	197	224	219	242	133	153	214			-59	-63
	102	294	413	332	295	227	221	281			-71	-72
	103	94	103	126	72	52	76	140			-36	-37
	104	79	88	108	58	40	70	113			-36	-36
3A	105	167	225	231	139	106	136	168			-77	-81
	106	190	244	244	186	121	157	192			-82	-86
	107	190	221	223	222	122	160	193			-53	-56
	108	227	303	275	241	153	180	213			-56	-55
	109	166	190	195	172	109	129	201			-68	-67
	110	233	292	273	216	192	188	241			-71	-70
	111	80	85	110	55	46	71	115			-39	-40
	112	71	79	100	51	40	64	95			-35	-38

Table B-9. Liner Temperature Data Correlation at Takeoff (Point 7).

Thermo-couple Number	Data Correlation with Fuel Hydrogen Content. $\Delta T = b + m (14.5-H)$						Comments
	Installation 1 & 2			Installation 3			
	m	b	r	m	b	r	
1	6.81	144	0.706	16.98	249	0.236	
2	16.36	276	0.527	---	---	---	Fuel 1AR and 13A excluded
3	16.65	357	0.577	---	---	---	Unstable film in Installation 3
4	23.15	400	0.841	41.09	321	0.976	Unattached only (1A,1AR,5A, 11A,6A,3A,4A,7A,8A)
5	---	---	---	---	---	---	Unstable film
6	---	---	---	---	---	---	Unstable film
7	15.44	309	0.491	6.38	319	0.168	
8	-3.70	404	0.102	22.73	410	0.633	
9	---	---	---	2.23	162	0.060	No Inst. 1&2 data
10	5.6	197	0.293	33.32	196	0.570	
11	7.58	471	0.238	7.58	471	0.238	Unattached both Installations (1A,2A,6A,9A,10A,12A)
12	12.35	359	0.810	11.08	183	0.383	
13	13.59	173	0.811	28.41	325	0.903	
14	40.17	205	0.868	18.00	221	0.863	Fuel 2A excluded
15	27.12	268	0.793	20.86	220	0.697	
16	21.71	180	0.851	13.13	189	0.884	
17	26.31	221	0.779	11.48	226	0.474	
18	16.40	101	0.756	12.10	129	0.792	
19	15.12	158	0.368	---	---	---	Insufficient Inst. 3 data
20	12.77	201	0.584	---	---	---	No Inst. 3 data
21	17.31	182	0.927	17.26	201	0.478	
22	16.56	96	0.872	0.72	137	0.028	
23	6.00	93	---	---	---	---	Fuels 1AR and 11A only
24	9.44	109	0.438	14.33	131	0.931	
26	5.43	241	0.309	22.56	300	0.769	
27	1.54	227	0.097	5.92	264	0.339	
28	15.84	184	0.770	28.84	224	0.978	
29	8.40	143	0.439	12.86	149	0.749	
30	3.37	181	0.413	9.09	166	0.376	
31	3.59	127	0.284	5.09	202	0.297	
32	3.50	221	0.429	---	---	---	Fuel 13A excluded, No Inst. 3 data

Table B-10. Liner Temperature Correlation with Hydrogen Content (Thermocouple No. 7).

(a) Data Correction and Engine Conditions.

| Fuel Number | (T_L-T_3), Inner Liner Temperature Rise, K (From Table B-7 at Test Points Indicated) | | | | | | | | (T_L-T_3), Inner Liner Temperature Rise, K (Average of Two Readings) | | | |
| | Idle | | Cruise | | Takeoff | | Dash | | Idle | Cruise | Takeoff | Dash |
	2	3	4	5	6	7	8	9				
2A1	78	66	154	130	317	374	302	317	72	142	346	310
1A	90	88	155	148	278	294	295	303	89	152	286	299
6A	84	63	205	195	344	348	359	357	74	200	346	358
5A	78	98	276	239	336	328	335	325	88	258	332	330
11A	91	105	191	203	317	327	339	358	98	197	322	349
1AR	88	70	123	92	299	290	296	303	79	108	295	300
13A1	69	75	227	192	324	321	340	354	72	210	323	347
10A	109	98	185	155	309	299	363	362	104	170	304	363
12A	84	95	172	155	303	283	339	307	90	164	293	323
9A	114	110	196	161	289	303	350	372	112	179	296	361
8A	121	146	289	269	333	346	371	354	134	279	340	363
4A	106	98	270	220	352	356	386	390	102	245	354	388
7A	98	106	283	197	348	351	350	377	102	240	350	364
3A	89	86	232	192	316	371	344	342	88	212	344	343

(b) Data Correlation With Fuel Hydrogen Content.

$$(T_L-T_3) = b + m\ (14.5-H)$$

Engine Power Level	Idle	Cruise	Takeoff	Dash
b, Intercept	80.5	147.8	304.9	306.6
m, Slope	9.0	35.2	13.0	25.9
r, Correlation Coefficient	0.481	0.674	0.491	0.892

Table B-11. Flame Radiation Data Correlation.

(a) Correlation with Combustor Operating Conditions:

$$\dot{q}_R = m\, S_R + b$$

where

$$S_R = \exp\left[\left(\frac{P_3 - 1.359}{34.6}\right) + \left(\frac{T_3 - 664}{735}\right)\right]$$

Fuel Number	Number of Data Points	m, Slope, kW/m^2	b, Intercept, kW/m^2	r, Correlation Coefficient	Q_r, Radiant Heat Flux, kW/m^2 (Calculated From Operating Conditions Correlation at S_r = 0.696, 0.845, 1.000 and 1.180)			
					Idle (0.696)	Cruise (0.845)	Takeoff (1.000)	Dash (1.180)
10A	8	113	5	0.984	83.9	100.7	118.2	138.6
12A	8	102	10	0.977	80.9	96.0	111.8	130.1
9A	7	83	23	0.931	80.8	93.1	105.9	120.8
8A	8	87	25	0.992	85.9	98.9	112.4	128.2
4A	8	79	29	0.994	84.3	96.0	108.3	122.5
7A	8	76	34	0.988	87.1	98.5	110.3	124.0
3A	8	62	44	0.953	86.8	96.0	105.6	116.8

(b) Data Correlation with Fuel Hydrogen Content:

$$\dot{q}_R = b + m\,(14.5 - H)$$

Engine Power Level	Idle	Cruise	Takeoff	Dash
b, Intercept	83.2	94.8	106.9	120.9
m, slope	0.60	1.32	2.05	2.93
r, correlation coefficient	0.208	0.470	0.421	0.366

Table B-12. Combustor Exit Temperature Profile Data.

Fuel Number	Reading Number	Temperature Rise Ratio, $\Delta T_{Local}/\Delta T_{Avg}$									
		Average Profile					Peak Profile				
		1 (Outer)	2	3	4	5 (Inner)	1 (Outer)	2	3	4	5 (Inner)
2A	1	0.698	0.929	1.093	1.158	1.122	0.949	1.143	1.253	1.395	1.331
	2	0.682	0.929	1.066	1.178	1.145	0.942	1.168	1.189	1.415	1.353
	3	0.703	0.947	1.091	1.158	1.101	0.940	1.107	1.219	1.340	1.241
	4	0.735	1.003	1.083	1.109	1.070	0.989	1.283	1.303	1.330	1.229
	5	0.736	0.945	1.100	1.137	1.082	0.933	1.174	1.304	1.356	1.286
	6	0.764	0.959	1.091	1.120	1.068	0.934	1.199	1.314	1.349	1.270
	7	0.758	0.910	1.087	1.150	1.093	0.900	1.099	1.361	1.351	1.323
	8	0.778	0.922	1.034	1.156	1.109	0.907	1.109	---	1.357	1.327
1A	9	0.757	0.913	1.063	1.160	1.107	0.881	1.099	---	1.365	1.336
	10	0.770	0.941	1.027	1.154	1.108	0.892	1.111	---	1.362	1.327
	11	0.749	0.917	1.075	1.150	1.109	0.915	1.094	---	1.341	1.302
	12	0.761	0.960	1.037	1.144	1.099	0.898	1.076	---	1.349	1.292
	13	0.640	0.865	1.078	1.192	1.226	0.953	1.213	---	1.352	1.418
	14	0.712	0.959	1.033	1.142	1.154	0.977	1.199	---	1.339	1.300
	15	0.675	0.939	1.041	1.174	1.173	0.963	1.534	---	1.343	1.351
	16	0.696	0.925	1.022	1.180	1.177	0.928	1.422	---	1.388	1.365
6A	17	0.794	0.928	1.060	1.100	1.118	1.052	1.181	1.337	1.317	1.312
	18	0.803	0.930	1.063	1.097	1.107	1.111	1.190	1.318	1.287	1.324
	19	0.811	0.960	1.064	1.097	1.079	1.083	1.167	1.282	1.266	1.238
	20	0.830	0.981	1.072	1.082	1.034	1.098	1.180	1.262	1.226	1.171
	21	0.802	0.956	1.069	1.105	1.068	1.077	1.206	1.318	1.265	1.275
	22	0.809	0.966	1.066	1.099	1.060	1.101	1.210	1.311	1.296	1.245
	23	0.800	0.953	1.065	1.108	1.073	1.070	1.168	1.283	1.301	1.311
	24	0.811	0.964	1.044	1.106	1.075	1.100	1.192	1.300	1.316	1.305
5A	25	0.778	0.956	1.044	1.109	1.106	0.926	1.190	1.293	1.289	1.329
	26	0.770	0.937	1.070	1.121	1.109	1.074	1.191	1.307	1.275	1.345
	27	0.769	0.942	1.062	1.130	1.105	1.049	1.199	1.301	1.264	1.279
	28	0.807	0.967	0.980	1.135	1.111	1.056	1.203	1.301	1.291	1.298
	29	0.750	0.956	1.059	1.091	1.145	1.031	1.173	1.269	1.248	1.284
	30	0.764	0.934	1.062	1.075	1.164	1.012	1.153	1.277	1.257	1.321
	31	0.744	0.934	1.060	1.055	1.208	0.980	1.213	1.243	1.311	1.334
	32	0.725	0.907	1.049	1.106	1.212	0.921	1.191	1.216	1.324	1.442
11A	33	0.792	0.972	1.033	1.103	1.093	1.086	1.186	1.294	1.285	1.331
	34	0.803	0.972	1.046	1.098	1.080	1.087	1.204	1.296	1.277	1.312
	35	0.781	0.941	1.057	1.117	1.105	1.006	1.147	1.267	1.244	1.261
	36	0.789	0.948	1.060	1.107	1.100	1.031	1.174	1.282	1.263	1.271
	37	0.742	0.922	1.053	1.109	1.173	0.943	1.147	.210	1.251	1.355
	38	0.778	0.938	1.049	1.107	1.127	1.000	1.124	.218	1.241	1.241
	39	0.716	0.909	1.054	1.097	1.225	0.927	1.071	1.222	1.339	1.380
	40	0.750	0.931	1.068	1.079	1.172	0.959	1.203	1.230	1.310	1.341
1AR	41	0.796	0.961	1.025	1.101	1.118	1.029	1.168	1.303	1.293	1.298
	42	0.796	0.966	1.037	1.100	1.101	1.073	1.200	1.300	1.296	1.307
	43	0.872	0.972	1.053	1.095	1.059	1.117	1.222	1.319	1.278	1.290
	44	0.838	0.992	1.064	1.079	1.026	1.164	1.262	1.336	1.266	1.243
	45	0.833	0.964	1.076	1.093	1.043	1.136	1.267	1.353	1.297	1.267
	46	0.748	0.965	1.074	1.110	1.052	1.139	1.261	1.366	1.311	1.285
	47	0.785	0.960	1.085	1.111	1.059	1.119	1.237	1.353	1.334	1.332
	48	0.810	0.964	1.083	1.099	1.043	1.133	1.253	1.351	1.317	1.312
13A1	49	0.791	0.934	1.066	1.115	1.095	0.996	1.219	1.226	1.291	1.265
	50	0.787	0.941	1.062	1.105	1.104	0.999	1.216	1.226	1.297	1.290
	51	0.869	0.924	1.084	1.090	1.033	1.125		1.241	1.242	1.153
	52	0.785	0.969	1.137	1.086	1.022	1.107	1.212	1.300	1.237	1.154
	53	0.853	0.930	1.094	1.091	1.033	1.031	1.143	1.288	1.262	1.188
	54	0.859	0.931	1.104	1.086	1.020	1.059	1.133	1.265	1.237	1.146
	55	0.812	0.928	1.076	1.113	1.071	0.973	1.120	1.273	1.284	1.267
	56	0.827	0.927	1.073	1.109	1.064	0.986	1.079	1.280	1.294	1.266

Table B-12. Combustor Exit Temperature Profile Data (Concluded).

Fuel Number	Reading Number	Temperature Rise Ratio, $\Delta T_{Local}/\Delta T_{Avg}$									
		Average Profile					Peak Profile				
		1 (Outer)	2	3	4	5 (Inner)	1 (Outer)	2	3	4	5 (Inner)
10A	57	0.810	0.990	1.042	1.133	1.026	1.040	1.351	1.447	1.283	1.140
	58	0.784	0.981	1.094	1.110	1.031	0.959	1.219	1.319	1.277	1.219
	59	0.866	0.995	1.101	1.070	0.968	0.935	1.180	1.243	1.196	1.110
	60	0.879	1.023	1.112	1.046	0.940	0.977	1.201	1.300	1.187	1.089
	61	0.874	1.002	1.095	1.067	0.963	1.020	1.127	1.206	1.263	1.177
	62	0.885	1.013	1.098	1.057	0.947	1.034	1.125	1.211	1.259	1.160
	63	0.913	0.974	1.076	1.064	0.972	0.983	1.108	1.159	1.223	1.168
	64	0.866	0.981	1.078	1.078	0.998	0.985	1.119	1.060	1.248	1.205
12A	65	0.860	0.986	1.085	1.076	0.993	0.978	1.118	1.161	1.231	1.186
	66	0.867	0.993	1.085	1.071	0.985	0.981	1.120	1.185	1.246	1.194
	67	0.850	0.995	1.089	1.077	0.989	0.932	1.135	1.165	1.225	1.166
	68	0.868	1.013	1.090	1.065	0.963	0.964	1.157	1.181	1.227	1.138
	69	0.793	1.003	1.063	1.089	1.053	0.937	1.189	1.258	1.221	1.202
	70	0.830	0.993	1.092	1.073	1.013	0.958	1.173	1.228	1.179	1.111
	71	0.767	0.956	1.077	1.118	1.082	0.904	1.267	1.362	1.322	1.359
	72	0.748	0.961	1.088	1.122	1.082	0.906	1.236	1.363	1.286	1.294
9A	73	0.791	0.969	1.077	1.097	1.066	0.866	1.181	1.311	1.223	1.201
	74	0.819	0.983	1.067	1.088	1.044	0.940	1.276	1.256	1.202	1.131
	75	0.856	1.033	1.094	1.058	0.958	0.959	1.244	1.264	1.181	1.089
	76	0.910	1.015	1.109	1.041	0.926	1.120	1.276	1.276	1.188	1.035
	77	0.857	1.019	1.094	1.068	0.963	0.977	1.099	1.208	1.210	1.132
	78	0.884	1.036	1.097	1.048	0.935	1.031	1.075	1.213	1.210	1.082
	79	0.861	1.012	1.078	1.068	0.982	0.957	1.074	1.181	1.213	1.130
	80	0.874	1.018	1.076	1.058	0.975	0.981	1.088	1.182	1.215	1.151
8A	81	0.871	1.013	1.072	1.063	0.981	1.016	1.170	1.262	1.263	1.171
	82	0.880	1.020	1.070	1.058	0.973	1.043	1.210	1.277	1.278	1.190
	83	0.859	1.019	1.082	1.062	0.977	0.975	1.091	1.185	1.197	1.118
	84	0.858	1.017	1.083	1.063	0.979	0.986	1.092	1.186	1.208	1.128
	85	0.834	1.011	1.080	1.064	1.011	0.969	1.155	1.194	1.138	1.108
	86	0.805	0.994	1.080	1.085	1.036	0.927	1.162	1.221	1.155	1.144
	87	0.821	1.010	1.084	1.073	1.012	0.914	1.184	1.237	1.170	1.117
	88	0.821	1.003	1.093	1.071	1.012	0.887	1.185	1.246	1.183	1.088
4A	89	0.844	1.005	1.063	1.073	1.016	0.945	1.151	1.214	1.182	1.136
	90	0.836	0.999	1.069	1.074	1.024	0.909	1.173	1.234	1.171	1.136
	91	0.907	1.027	1.068	1.041	0.957	0.994	1.186	1.186	1.170	1.059
	92	0.911	1.031	1.068	1.034	0.956	1.054	1.173	1.187	1.142	1.076
	93	0.879	1.025	1.080	1.084	1.022	0.983	1.179	1.228	1.237	1.217
	94	0.862	1.016	1.065	1.064	0.994	0.958	1.129	1.180	1.197	1.160
	95	0.855	1.017	1.062	1.062	1.004	1.052	1.230	1.280	1.280	1.223
	96	0.861	1.015	1.065	1.060	0.999	1.053	1.228	1.279	1.276	1.218
7A	97	0.844	1.006	1.063	1.062	1.002	1.029	1.206	1.277	1.288	1.238
	98	0.839	1.011	1.066	1.070	1.014	1.045	1.242	1.285	1.293	1.232
	99	0.863	1.011	1.069	1.062	0.994	1.029	1.162	1.222	1.243	1.210
	100	0.862	1.008	1.065	1.063	1.005	1.020	1.171	1.221	1.240	1.208
	101	0.796	0.924	1.091	1.105	1.084	0.892	1.124	1.193	1.195	1.192
	102	0.863	0.970	1.077	1.064	1.026	0.940	1.092	1.145	1.176	1.205
	103	0.803	0.909	1.102	1.104	1.082	0.872	1.096	1.224	1.193	1.226
	104	0.785	0.932	1.124	1.086	1.073	0.910	1.141	1.489	1.183	1.274
3A	105	0.883	1.014	1.062	1.053	0.987	1.024	1.193	1.246	1.245	1.221
	106	0.862	1.021	1.062	1.062	0.994	1.050	1.215	1.260	1.270	1.230
	107	0.853	0.999	1.068	1.072	1.010	0.958	1.165	1.214	1.223	1.194
	108	0.862	1.012	1.066	1.066	0.994	0.996	1.157	1.208	1.224	1.191
	109	0.779	0.980	1.089	1.092	1.059	0.843	1.020	1.179	1.166	1.178
	110	0.843	1.019	1.077	1.060	1.001	0.901	1.122	1.157	1.157	1.119
	111	0.789	0.973	1.115	1.083	1.041	0.897	1.188	1.330	1.173	1.159
	112	0.801	0.978	1 136	1.073	1.012	0.881	1.187	1.536	1.151	1.133

Table B-13. Pattern Factor Test Data Correlation.

Correlation with Combustor Operating Conditions

$$PF = m \ S_{PF} + b$$

where:

$$S_{PF} = \left(\frac{\Delta T}{686}\right)^{-0.25} \left(\frac{W_c \sqrt{T_3/P_3}}{118.89}\right)^{-0.50}$$

Fuel Number	Number of Data Points	m, Slope	b, Intercept	r, Correlation Coefficient	PF Calculated from Operating Conditions (Conditions Correlation at S_{PF} =)			
					Idle (1.178)	Cruise (1.053)	Takeoff (1.000)	Dash (1.005)
1A	8	0.7159	-0.377	0.634	0.467	0.377	0.339	0.343
1AR	8	-0.2099	+0.561	0.608	0.314	0.340	0.352	0.350
2A	8	0.3630	-0.024	0.958	0.403	0.358	0.339	0.341
3A	8	1.5554	-1.402	0.918	0.431	0.236	0.154	0.162
4A	8	0.0848	+0.132	0.183	0.233	0.222	0.217	0.218
5A	8	0.3873	-0.084	0.552	0.372	0.323	0.303	0.305
6A	8	0.2492	+0.041	0.775	0.335	0.304	0.291	0.292
7A	8	0.9615	-0.776	0.773	0.356	0.236	0.185	0.190
8A	8	0.1376	+0.083	0.327	0.245	0.228	0.221	0.221
9A	8	0.2556	-0.029	0.592	0.272	0.240	0.226	0.228
10A	8	0.6470	-0.417	0.748	0.345	0.264	0.230	0.233
11A	8	0.4498	-0.171	0.752	0.359	0.303	0.279	0.281
12A	8	0.6522	-0.446	0.879	0.322	0.240	0.206	0.209
13A	8	0.0000	+0.281	0.296	0.281	0.281	0.281	0.281

APPENDIX C

CARBON DEPOSITION/EMISSION DATA

Two 24 hours tests were conducted to establish the carbon deposition tendencies of the J79-17C combustor. Fuels 1A (Repeat JP-4) and 13A1 (diesel) were used in these tests to represent the range of expected carbon deposition severity. Both tests were begun with clean combustors and fuel nozzles. After each test, the combustor and fuel nozzles were visually inspected and the fuel nozzle was flow calibrated. No changes in the fuel nozzle flow characteristics were detected after either test. The visual assessments of the combustor after each test are presented in Table 14. Figures C-1 through C-4 present the posttest photos of the combustor liner and fuel nozzle. Limited repeat performance data was obtained during the endurance portion of these tests and a summary of pattern factor during this testing is presented in Table C-1.

Table C-2 presents the detailed results from the cascade impactor measurements on Fuels 4A and 10A.
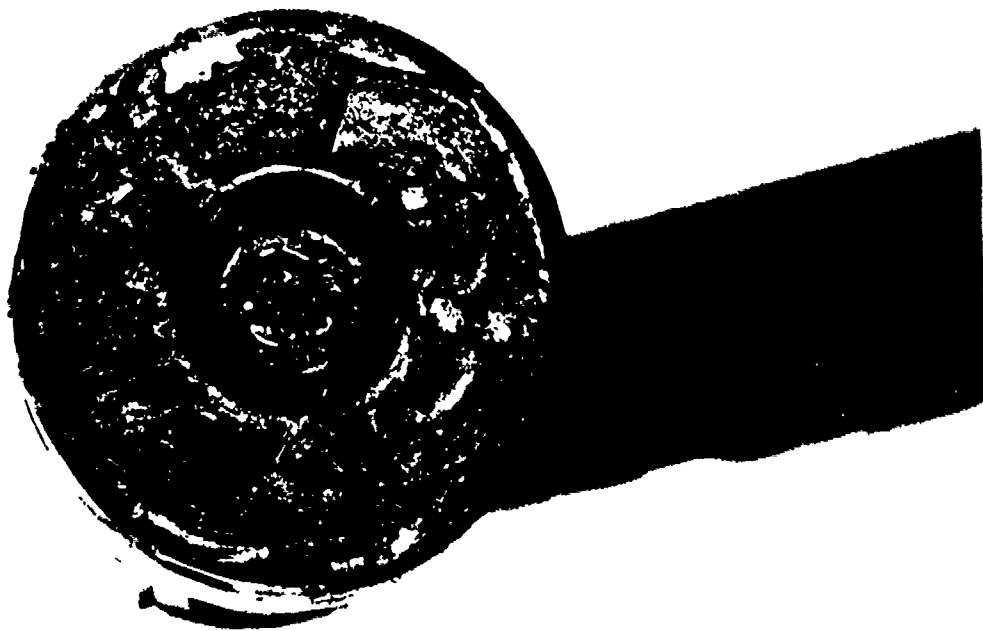
Fig. C... Engine... after 3... of Freon A... 24-hour Test... Fuel 1%.
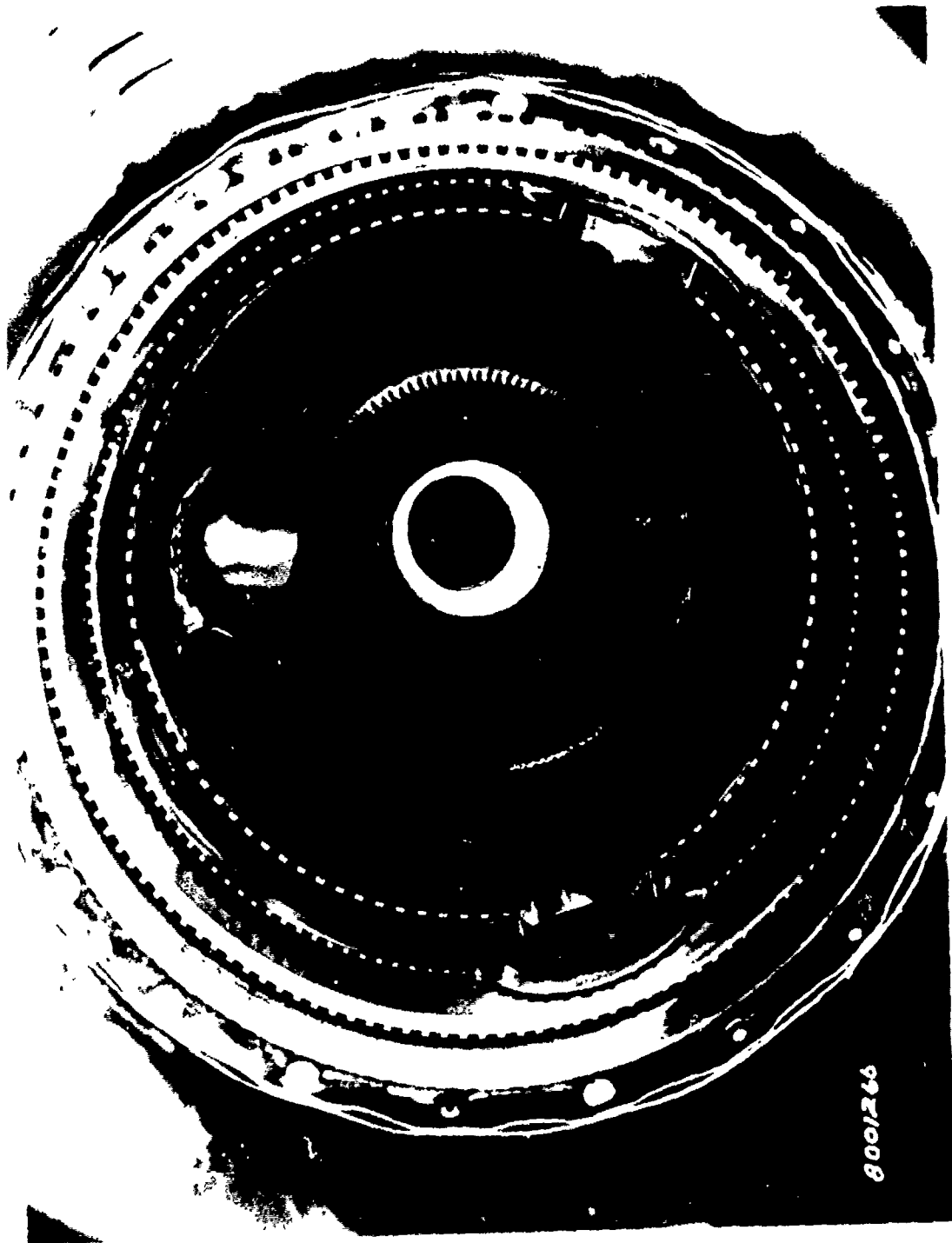
Figure C-3. Post-test Photograph of Liner After 24 Hour Test of Fuel 13 A1.

Figure C-3. Photographic Micrograph of Fuel Nozzle After 24-Hour Test of Fuel 4A.

Table C-1. Pattern Factor During 24 Hour
Tests.

Fuel	Test Point	Test Time, hr	ΔT, K	$\dfrac{W_C \sqrt{T_3}}{P_3}$	PF
1A (Repeat)	2	2.2	298	128	0.303
	3	2.9	375	129	0.320
	4	4.2	536	121	0.319
	5	5.7	678	124	0.336
	7	7.8	591	117	0.353
	6	8.8	524	118	0.366
	8	10.8	452	134	0.353
	9	11.3	523	131	0.351
	8	12.0	434	132	0.376
	8	13.0	438	132	0.356
	8	14.0	420	132	0.409
	7	15.0	539	118	0.371
	7	16.0	542	117	0.387
	6	17.0	512	117	0.372
	6	18.0	508	118	0.378
	5	19.0	644	123	0.292
	5	20.0	641	122	0.317
	4	21.5	487	126	0.288
	3	23.0	344	126	0.355
13A	3	3.4	358	122	0.291
	2	4.0	276	126	0.297
	4	5.2	513	124	0.242
	5	6.8	636	125	0.300
	6	8.6	510	121	0.288
	7	9.5	566	120	0.265
	8	11.6	436	130	0.284
	9	11.9	444	130	0.294
	9	12.9	452	130	0.266
	9	13.8	468	129	0.317
	7	15.2	566	120	0.292
	5	16.0	727	122	0.173
	5	17.6	686	123	0.225
	4	18.1	496	127	0.212
	4	19.3	501	127	0.202
	3	22.6	291	129	0.349
	2	22.8	222	132	0.251

Table C-2. Detailed Cascade Impactor Carbon Particle Size Data.

Fuel	Test Reading	Test Point	Total Gas Flow Through Impactor, kg	Stage	Particle 50% Cut Diameter, microns	Absolute Emission, mg carbon	Cumulative % Undersize
4A	91	4	0.874	Pre-Impactor	>19.00	2.16	---
				0	19.00	1.04	81.2
				1	12.50	1.71	70.9
				2	8.40	0.78	66.3
				3	5.70	0.06	65.9
				4	3.70	0.76	61.4
				5	1.80	0.84	56.4
				6	1.20	1.28	18.8
				7	0.78	0.89	13.6
				8	<0.78	7.35	---
				Total	---	16.87	---
10A	59	4	0.958	Pre-Impactor	>19.00	1.94	---
				0	19.00	0	83.2
				1	12.50	2.17	64.4
				2	8.40	1.14	54.5
				3	5.70	0.83	47.3
				4	3.70	0.93	39.3
				5	1.80	0	39.3
				6	1.20	0	39.3
				7	0.78	0	39.3
				8	<0.78	4.53	---
				Total	---	11.54	---

159

APPENDIX D

LOW PRESSURE TEST DATA

Two types of tests were conducted in the low pressure combustor test rig: altitude relight tests and cold-day ground start tests. Apparatus and procedures which were used are described in Section V-B.

Detailed results for the altitude relight tests are presented in Tables D-1 through D-7. The combustor operating conditions are listed from which the simulated flight conditions were determined, and in the remarks column, the type of data point is indicated (LIGHT = maximum altitude relight capability at normal minimum fuel flow rate, PBO = pressure blowout, LLO = lean lightoff, LBO = lean blowout).

Detailed results of the cold-day ground start tests are listed in Tables D-8 through D-11. At each combustor operating condition shown, lean lightoff and lean blowout fuel/air ratios were determined which are listed. All lightoff attempts were successful, so each test was terminated only after the planned minimum temperature (239 K) was reached.

Table D-1. Altitude Relight Test Results, Fuel No. 1A.

Fuel Number	Simulated Flight Condition		Combustor Operating Conditions								Remarks			
	Alt km	M_p	T_F K	T_3 K	P_3 kPa	W_c (engine) kg/s	$\frac{\Delta P}{P}$ %	V_r m/s	W_F (engine) g/s	f g/kg	Light	PBO	LLO	LBO
1A	6.7	0.43	244.3	244.3	46.9	2.267	3.53	9.2	64.9	28.60	Yes	x		
	7.8	0.48	244.3	244.3	40.8	2.267	4.06	10.6	64.9	28.60			x	
	6.7	0.43	244.3	244.3	46.9	2.267	3.53	9.2	32.3	14.20				x
	6.7	0.43	244.3	244.3	46.9	2.267	3.53	9.2	15.2	6.70	Yes	x		
	4.6	0.55	277.6	277.6	66.2	4.082	6.51	13.3	64.9	15.90			x	
	8.7	0.74	277.6	277.6	46.6	4.082	9.25	18.9	64.9	15.90				
	4.6	0.55	277.6	277.6	66.2	4.082	6.51	13.3	40.7	10.00	Yes	x		
	4.6	0.55	277.6	277.6	66.2	4.082	6.51	13.3	20.9	5.12				x
	5.2	0.65	288.7	283.7	67.4	4.990	5.62	13.4	64.9	13.00			x	
	6.7	0.72	288.7	283.7	60.3	4.990	6.28	15.0	64.9	13.00	Yes	x		
	5.2	0.65	288.7	283.7	67.4	4.990	5.62	13.4	51.3	10.30				
	5.2	0.65	288.7	283.7	67.4	4.990	5.62	13.4	30.0	6.01				x
	4.8	0.84	287.6	281.5	102.0	9.072	13.30	19.5	64.9	7.15	No			
1A (R)	7.3	0.46	244.3	244.3	43.5	2.267	3.41	9.9	64.9	28.60	Yes	x		
	8.4	0.51	244.3	244.3	38.1	2.267	3.89	11.3	64.9	28.60			x	
	7.3	0.46	244.3	244.3	43.5	2.267	3.41	9.9	27.5	12.10				x
	7.3	0.46	244.3	244.3	43.5	2.267	3.41	9.9	15.0	6.62	Yes	x		
	6.1	0.62	277.6	277.6	57.7	4.082	5.43	15.3	64.9	15.90			x	
	8.4	0.73	277.6	277.6	47.6	4.082	6.58	18.5	64.9	15.90				
	6.1	0.62	277.6	277.6	57.7	4.082	5.43	15.3	45.9	11.20	Yes	x		
	6.1	0.62	277.6	277.6	57.7	4.082	5.43	15.3	20.5	5.02				x
	6.1	0.69	284.3	284.3	63.2	4.990	4.92	17.5	64.9	13.00			x	
	8.0	3.78	282.0	284.3	55.4	4.990	5.61	20.0	64.9	13.00	Yes	x		
	6.1	0.69	282.0	284.3	63.2	4.990	4.92	17.5	34.7	6.95				
	6.1	0.69	282.0	284.3	63.2	4.990	4.92	17.5	26.8	2.95				x
	5.1	0.86	282.6	281.5	100.1	9.072	13.40	19.9	135.0	14.90	No			

Table D-2. Altitude Relight Test Results, Fuel No. 2A and 3A.

Fuel Number	Alt km	M_p	T_F K	T_3 K	P_3 kPa	W_c (engine) kg/s	$\Delta P/P$ %	V_r m/s	W_F (engine) g/s	f g/kg	Light	PBO	LLO	LBO
2A	4.3	0.36	244.3	244.3	61.6	2.267	2.40	7.0	64.9	28.60	Yes			
	6.9	0.44	244.3	244.3	45.7	2.267	3.23	9.4	64.9	28.60		X	X	X
	4.3	0.36	244.3	244.3	61.6	2.267	2.40	7.0	35.5	15.70				
	4.3	0.36	244.3	244.3	61.6	2.267	2.40	7.0	28.7	12.70	Yes			
	5.9	0.61	277.6	277.6	58.7	4.082	5.42	15.0	64.9	15.90				
	7.5	0.69	277.6	277.6	50.9	4.082	6.25	17.3	64.9	15.90		X	X	X
	5.9	0.61	277.6	277.6	58.7	4.082	5.42	15.0	57.7	14.10				
	5.9	0.61	277.6	277.6	58.7	4.082	5.42	15.0	26.8	6.60	Yes			
	4.6	0.62	288.2	283.7	71.2	4.990	5.69	15.5	64.9	13.00				
	7.3	0.75	288.2	283.7	58.0	4.990	6.98	19.0	64.9	13.00		X	X	X
	4.6	0.62	288.2	283.7	71.2	4.990	5.69	15.5	49.4	9.90				
	4.6	0.62	288.2	283.7	71.2	4.990	5.69	15.5	37.5	7.50	No			
	5.1	0.86	287.0	283.7	100.0	9.072	13.40	20.1	135.0	14.90				X
3A	5.2	0.39	245.9	244.3	55.4	2.267	3.24	7.8	64.9	28.60	Yes			
	7.7	0.48	245.4	243.7	41.6	2.267	4.33	10.3	64.9	28.60		X	X	X
	5.2	0.39	245.4	243.7	55.4	2.267	3.24	7.8	41.6	18.30				
	5.2	0.39	244.3	243.7	55.4	2.267	3.24	7.8	32.8	14.50				
	5.8	0.61	277.6	278.2	58.8	4.082	5.75	15.1	64.9	15.90	Yes			
	7.3	0.68	276.5	278.7	51.0	4.082	6.62	17.4	64.9	15.90		X	X	X
	5.8	0.61	276.5	278.7	58.8	4.082	5.75	15.1	47.9	11.70				
	5.8	0.61	277.6	279.3	58.8	4.082	5.75	15.1	17.9	4.38				
	6.3	0.70	281.5	284.6	62.2	4.990	5.35	17.8	64.9	13.00	Yes			
	7.8	0.77	280.9	284.6	56.1	4.990	5.93	19.7	64.9	13.00		X	X	X
	6.3	0.70	280.9	283.7	62.2	4.990	5.35	17.7	57.9	11.60				
	6.3	0.89	285.4	281.5	83.0	7.938	5.35	13.2	19.4	3.89	No			
	6.9	0.78	284.8	280.9	98.9	7.938	7.24	11.0	64.9	8.18	Yes			
	3.1	1.00	284.3	280.4	78.9	7.938	4.54	13.8	64.9	8.18				
	9.3	0.78	284.3	280.4	98.9	7.938	5.68	11.0	64.9	8.18		X		
	3.1	0.78	284.3	280.4	98.9	7.938	4.54	11.0	83.9	10.60	Yes			
	8.7	1.05	283.2	282.0	87.7	8.414		22.7	64.9	7.71				
	5.3	0.87	283.7	280.9	98.9	9.072	7.02	20.1	47.0	5.18				X

Velocity Blowout

Table D-3. Altitude Relight Test Results, Fuel No. 4A and 5A.

Fuel Number	Simulated Flight Condition		Combustor Operating Conditions								Remarks			
	Alt km	M_p —	T_F K	T_3 K	P_3 kPa	W_c (engine) kg/s	$\frac{\Delta P}{P}$ %	V_r m/s	W_F (engine) g/s	f g/kg	Light	PBO	LLO	LBO
4A	2.4	0.33	243.7	243.7	75.3	2.267	2.18	5.7	64.9	28.60	Yes			
	7.3	0.46	243.7	243.7	43.5	2.267	3.77	9.9	64.9	28.60		x	x	x
	2.4	0.33	243.7	243.7	75.3	2.267	2.18	5.7	51.4	22.70				
	2.4	0.33	243.7	243.7	75.3	2.267	2.18	5.7	29.0	12.80	Yes			
	5.3	0.58	277.5	276.5	61.8	4.082	5.54	14.2	64.9	15.90				
	7.6	0.69	277.5	276.5	50.6	4.082	6.76	17.4	64.9	15.90		x	x	x
	5.3	0.58	277.5	276.5	61.8	4.082	5.54	14.2	63.3	15.50				
	5.3	0.58	277.5	276.5	61.8	4.082	5.54	14.2	32.3	7.91	Yes			
	4.5	0.62	290.4	290.9	72.0	4.990	4.49	15.7	64.9	13.00				
	7.6	0.76	290.4	290.9	56.7	4.990	5.71	19.9	64.9	13.00		x	x	x
	4.5	0.62	290.4	290.9	72.0	4.990	4.49	15.7	59.2	11.90				
	4.5	0.62	290.4	290.9	72.0	4.990	4.49	15.7	31.5	6.31	Yes			
	5.0	0.85	288.7	292.0	100.7	9.072	8.40	20.5	12.6	13.90	No			
5A	6.4	0.42	244.3	244.3	48.5	2.267	2.95	8.9	64.9	28.60	Yes			
	6.8	0.44	244.3	244.3	46.1	2.267	3.11	9.4	64.9	28.60		x	x	x
	6.4	0.42	244.3	244.3	48.5	2.267	2.95	8.9	55.3	24.40				
	6.4	0.42	244.3	244.3	48.5	2.267	2.95	8.9	23.3	10.30	Yes			
	5.8	0.60	277.6	277.6	59.3	4.082	4.96	14.9	64.9	15.90				
	7.9	0.70	277.6	277.6	49.5	4.082	5.94	17.8	64.9	15.90		x	x	x
	5.8	0.60	277.6	277.6	59.3	4.082	4.96	14.9	63.1	15.50				
	5.8	0.60	277.6	277.6	59.3	4.082	4.96	14.9	24.8	6.08	Yes			
	4.6	0.62	287.0	292.6	71.0	4.990	4.15	16.0	64.9	13.00				
	8.0	0.78	287.0	292.6	55.3	4.990	5.34	20.6	64.9	13.00		x	x	x
	4.6	0.62	287.0	292.6	71.0	4.990	4.15	16.0	46.4	9.30				
	4.6	0.62	287.0	292.6	71.0	4.990	4.15	16.0	26.2	5.25	Yes			
	5.4	0.87	288.1	289.8	98.6	9.072	13.70	20.8	135.0	14.90	No			

Table D-4. Altitude Relight Test Results, Fuel No. 6A and 7A.

Fuel Number	Simulated Flight Condition		Combustor Operating Conditions								Remarks			
	Alt km	M_p -	T_F K	T_3 K	P_3 kPa	W_c (engine) kg/s	$\frac{\Delta F}{P}$ %	V_r m/s	W_F (engine) g/s	f g/kg	Light	PBO	LLO	LBO
6A	6.0	0.41	244.3	244.3	50.45	2.267	2.87	8.6	64.9	28.60	Yes			
	8.3	0.51	244.3	244.3	38.60	2.267	3.75	11.2	64.9	28.60		X		
	6.0	0.41	244.3	244.3	50.45	2.267	2.87	8.6	31.2	13.80			X	X
	6.0	0.41	244.3	244.3	50.45	2.267	2.87	8.6	18.6	8.20				
	5.6	0.60	277.6	277.6	59.9	4.082	5.17	14.7	64.9	15.90	Yes			
	7.2	0.67	277.6	277.6	52.2	4.082	5.94	16.9	64.9	15.90		X		
	5.6	0.60	277.6	277.6	59.9	4.082	5.17	14.7	64.3	15.80			X	X
	5.6	0.60	277.6	277.6	59.9	4.082	5.17	14.7	24.6	6.03				
	4.0	0.60	285.4	287.0	74.8	4.990	5.56	14.9	64.9	13.00	Yes			
	7.1	0.74	285.4	287.0	58.5	4.990	7.11	19.1	64.9	13.00		X		
	4.0	0.60	285.4	287.0	74.8	4.990	5.56	14.9	54.9	11.00			X	X
	4.0	0.60	285.4	287.0	74.8	4.990	5.56	14.9	36.3	7.27				
	5.0	0.86	285.4	285.4	100.5	9.072	13.50	20.1	135.0	14.90	No			
7A	5.0	0.38	245.4	244.8	57.2	2.267	2.19	7.6	64.9	28.60	Yes			
	7.0	0.45	245.4	244.8	45.3	2.267	2.77	9.5	64.9	28.60		X		
	5.0	0.38	245.4	243.7	57.2	2.267	2.19	7.5	36.4	16.10			X	X
	5.0	0.38	244.8	243.7	57.2	2.267	2.19	7.5	34.2	15.10				
	5.7	0.60	277.6	277.6	59.6	4.082	4.99	14.8	64.9	15.90	Yes			
	7.9	0.70	278.7	278.7	49.4	4.082	6.02	17.9	64.9	15.90		X		
	5.7	0.60	278.7	278.7	59.6	4.082	4.99	14.9	53.7	15.20			X	X
	5.7	0.60	278.7	279.3	59.6	4.082	4.99	14.9	20.0	4.90				
	6.3	0.78	284.8	287.0	62.3	4.990	4.86	17.9	64.9	13.00	Yes			
	6.5	0.70	284.8	287.6	55.5	4.990	5.45	20.1	64.0	12.80		X		
	6.3	0.70	285.4	287.0	62.3	4.990	4.86	17.9	26.2	5.25			X	X
	5.6	0.89	285.4	281.5	97.2	9.072	19.20	20.5	126.0	13.90	No			

Table D-5. Altitude Relight Test Results, Fuel No. 8A and 9A.

Fuel Number	Simulated Flight Condition		Combustor Operating Conditions								Remarks			
	Alt km	M_p	T_F K	T_3 K	P_3 kPa	W_c (engine) kg/s	$\frac{\Delta P}{P}$ %	V_r m/s	W_F (engine) g/s	f g/kg	Light	PBO	LLO	LBO
8A	6.6	0.43	242.6	243.7	47.2	2.267	3.36	9.1	64.9	28.60	Yes			
	9.1	0.55	244.8	242.6	35.3	2.267	4.50	12.1	64.9	28.60		X	X	X
	6.6	0.43	243.7	243.7	47.2	2.267	3.36	9.1	26.2	11.60				
	6.6	0.43	243.7	244.8	47.2	2.267	3.36	9.2	17.5	7.72				
	7.1	0.67	276.5	276.5	52.6	4.082	5.87	16.7	64.9	15.90	Yes			
	8.0	0.71	277.5	277.0	43.9	4.082	6.32	18.0	64.9	15.90		X	X	X
	7.1	0.67	278.2	277.0	52.6	4.082	5.87	16.7	43.8	10.70				
	7.1	0.67	278.2	278.2	52.6	4.082	5.87	16.8	20.2	4.95	Yes			
	5.7	0.67	278.2	284.8	65.1	4.990	4.34	17.0	64.9	13.00				
	7.8	0.77	278.7	284.3	56.0	4.990	5.05	19.7	64.9	13.00		X	X	X
	5.7	0:67	279.3	284.3	65.1	4.990	4.34	17.0	46.6	9.34				
	5.7	0.67	278.2	284.8	65.1	4.990	4.34	17.0	22.7	4.55				
	5.6	0.88	279.8	284.8	97.6	9.072	14.40	20.6	126.0	13.90	No			
9A	6.6	0.43	245.4	243.7	47.3	2.267	3.37	9.1	64.9	28.60	Yes			
	8.3	0.50	244.8	243.7	38.8	2.267	4.10	11.1	64.9	28.60		X	X	X
	6.6	0.43	243.7	243.7	47.3	2.267	3.37	9.1	25.2	11.10				
	6.6	0.43	243.7	243.7	47.3	2.267	3.37	9.1	16.9	7.45				
	7.9	0.70	278.7	278.7	49.6	4.082	6.49	17.9	64.9	15.90	Yes			
	8.9	0.75	278.2	278.7	45.9	4.082	7.02	19.3	64.9	15.90		X	X	X
	7.9	0.70	278.2	278.7	49.6	4.082	6.49	17.9	42.8	10.50				
	7.9	0.70	279.3	278.2	49.6	4.082	6.49	17.8	25.2	6.17	Yes			
	6.3	0.70	285.9	289.8	62.2	4.990	5.07	18.1	64.9	13.00				
	7.5	0.75	285.9	290.4	58.1	4.990	5.42	19.4	64.9	13.00		X	X	X
	6.3	0.70	285.4	289.8	62.6	4.990	5.07	18.1	45.7	9.16				
	6.3	0.70	285.9	289.8	62.6	4.990	5.07	18.1	25.2	5.05				
	5.2	0.86	287.6	288.7	99.8	9.072	13.80	20.4	126.0	13.90	No			

165

Table D-6. Altitude Relight Test Results, Fuel No. 10A and 11A.

Fuel Number	Simulated Flight Condition Alt km	M_p	T_F K	T_3 K	P_3 kPa	W_c (engine) kg/s	$\frac{\Delta P}{P}$ %	V_r m/s	W_F (engine) g/s	f g/kg	Remarks Light	PBO	LLO	LBO
10A	6.2	0.42	243.2	244.8	49.4	2.267	3.06	8.8	64.9	28.6	Yes	X		
	8.2	0.50	243.7	244.8	39.2	2.267	3.85	11.0	64.9	28.6			X	X
	6.2	0.42	242.6	243.7	49.4	2.267	3.06	8.7	24.3	10.7				
	6.2	0.42	243.7	243.7	49.4	2.267	3.06	8.7	15.1	6.67				
	6.4	0.62	278.2	277.0	56.9	4.082	5.65	15.5	64.9	15.9	Yes	X		
	8.1	0.71	278.7	277.0	48.4	4.082	6.64	18.2	64.9	15.9			X	X
	6.4	0.62	278.7	277.0	56.9	4.082	5.65	15.5	33.1	8.12				
	6.4	0.62	278.7	278.2	56.9	4.082	5.65	15.5	17.3	4.23				
	6.3	0.70	288.2	288.7	62.3	4.990	6.51	18.0	64.9	13.0	Yes	X		
	8.6	0.81	288.2	289.3	53.5	4.990	7.54	21.0	64.9	13.0			X	X
	6.3	0.70	287.6	289.3	62.3	4.990	6.51	18.0	39.1	7.83				
	6.3	0.70	288.2	289.3	62.3	4.990	6.51	18.0	24.2	4.85	No			
	7.5	0.93	282.6	291.5	81.2	7.938	10.6	14.0	64.9	8.18	No			
	7.6	0.93	282.6	291.5	81.2	7.938	10.6	14.0	126.0	15.9	Yes			
	3.6	0.76	282.6	291.5	97.1	7.938	6.45	11.7	64.9	8.18				X
	3.6	0.76	283.7	290.9	97.1	7.938	6.45	11.6	42.8	5.40				
	8.8	0.97	284.3	290.9	80.2	7.938	7.82	14.1	64.9	8.18		X		
	5.3	0.87	288.7	284.3	98.8	9.072	19.4	20.3	126.0	13.9	No			
	7.8	1.14	282.6	291.5	91.3	9.072	11.3	22.6	35.5	3.92		X		X
	12.9	1.17	282.6	291.5	86.6	9.072	11.9	23.8	64.9	7.15				
11A	6.7	3.44	244.3	244.3	46.5	2.267	3.26	9.3	64.9	28.6	Yes	X		
	7.7	0.48	244.3	244.3	41.4	2.267	3.66	10.4	64.9	28.6			X	X
	6.7	0.44	244.3	244.3	46.5	2.267	3.26	9.3	25.6	11.3				
	6.7	0.44	244.3	244.3	46.5	2.267	3.26	9.3	16.3	7.20				
	6.9	0.66	277.6	277.6	53.6	4.082	5.85	16.5	64.9	15.9	Yes	X		
	7.9	0.70	277.6	277.6	49.5	4.082	6.33	17.8	64.9	15.9			X	X
	6.9	0.66	277.6	277.6	53.6	4.082	5.85	16.5	51.5	12.6				
	7.9	0.66	277.6	277.6	53.6	4.082	5.85	16.5	22.7	5.56				
	6.9	0.73	295.4	299.8	59.0	4.990	5.51	19.8	64.9	13.0	Yes	X		
	8.2	0.79	295.4	299.8	54.6	4.990	5.74	21.3	64.9	13.0			X	X
	6.9	0.73	295.4	299.8	59.0	4.990	5.31	19.8	51.7	10.4				
	6.9	0.73	295.4	299.8	59.0	4.990	5.31	19.8	29.1	5.83				
	4.9	0.84	295.9	300.4	101.7	9.072	13.3	20.9	64.9	7.15	No			
	4.9	0.84	295.9	300.4	101.7	9.072	13.3	20.9	68.4	7.54	Yes			
	13.7	1.19	295.9	300.4	82.7	9.072	16.4	25.7	68.4	7.54		X	X	
	4.9	0.84	295.9	300.4	101.7	9.072	13.3	20.9	68.4	7.54	Yes			
	4.9	0.84	295.9	300.4	101.7	9.072	13.3	20.9	50.6	5.58	Yes			X

Table D-7. Altitude Relight Test Results, Fuel No. 12A and 13A.

Fuel Number	Simulated Flight Condition		Combustor Operating Conditions								Remarks			
	Alt km	M_p	T_F K	T_3 K	P_3 kPa	W_c (engine) kg/s	$\frac{\Delta P}{P}$ %	v_r m/s	W_F (engine) g/s	f g/kg	Light	PBO	LLO	LBO
12A	6.4	0.43	244.3	244.3	48.6	2.267	3.10	8.9	64.9	28.6	Yes			
	7.8	0.48	244.3	244.3	40.8	2.267	3.69	10.6	64.9	23.6		X		
	6.4	0.43	244.3	244.3	48.6	2.267	3.10	8.9	27.8	12.3			X	
	6.4	0.43	244.3	244.3	48.6	2.267	3.10	8.9	17.5	7.72				X
	7.0	0.66	277.6	277.6	53.2	4.082	5.81	16.6	64.9	28.6	Yes			
	8.4	0.73	277.6	277.5	47.6	4.082	6.49	18.5	64.9	28.6		X		
	7.0	0.66	277.6	277.6	53.2	4.082	5.81	16.6	35.5	8.70			X	
	7.0	0.66	277.6	277.6	53.2	4.082	5.81	16.6	22.4	5.49				X
	6.3	0.70	287.0	287.6	62.2	4.990	6.69	18.0	64.9	28.6	Yes			
	7.5	0.76	287.0	287.6	57.1	4.990	7.28	19.6	64.9	28.6		X		
	6.3	0.70	287.0	287.6	62.2	4.990	6.69	18.0	52.3	10.5			X	
	6.3	0.70	287.0	287.6	52.2	4.990	6.69	18.0	33.6	6.73				X
	5.0	0.85	285.9	284.8	100.8	9.072	13.4	20.0	135.0	14.9	No			
13A	4.6	0.37	244.3	244.3	59.6	2.267	2.99	7.2	64.9	28.6	Yes			
	5.8	0.40	244.3	244.3	51.8	2.267	3.44	8.3	64.9	28.6		X		
	4.6	0.37	244.3	244.3	59.6	2.267	2.99	7.2	48.9	21.6			X	
	4.6	0.37	244.3	244.3	59.6	2.267	2.99	7.2	32.0	14.1				X
	3.9	0.53	277.6	277.6	70.1	4.082	4.97	12.6	64.9	15.9	Yes			
	6.4	0.63	277.6	277.6	55.8	4.082	6.24	15.8	64.9	15.9		X		
	3.9	0.53	277.6	277.6	70.1	4.082	4.97	12.6	59.2	14.5			X	
	3.9	0.53	277.6	277.6	70.1	4.082	4.97	12.6	34.4	8.43				X
	6.5	0.71	292.6	293.7	61.3	4.990	6.83	18.6	64.9	13.0	Yes			
	7.8	0.77	292.6	293.7	56.2	4.990	7.44	20.3	64.9	13.0		X		
	5.5	0.71	292.6	293.7	61.3	4.990	6.83	18.6	60.0	12.0			X	
	6.3	0.71	292.6	293.7	61.3	4.990	6.83	18.6	54.3	10.9				X
	5.0	0.85	292.6	293.7	100.9	9.072	13.4	20.6	135.0	14.9	No			

Table D-8. Ground Start Test Results, Fuel Numbers 1A Through 3A.

Fuel No.	Combustor Operating Conditions					Lean Blowout		Lean Lightoff	
	T_F K	T_3 K	P_3 kPa	W_c (engine) kg/s	$\frac{\Delta P}{P}$ %	W_f (engine) g/s	f g/kg	W_f (engine) g/s	f g/kg
1A	227.5	227.5	101.8	3.175	0.90	8.8	2.77	21.2	6.67
	272.0	272.0	101.8	3.175	0.90	9.5	2.99	22.4	7.04
	266.4	266.4	101.7	3.175	0.88	10.5	3.30	21.2	6.67
	260.8	260.8	101.7	3.175	0.88	10.5	3.30	19.5	6.13
	255.3	255.3	101.7	3.175	0.84	10.5	3.30	22.9	7.20
	249.7	249.7	101.6	3.175	0.80	11.1	3.49	21.7	6.82
	244.2	244.2	101.5	3.175	0.77	11.1	3.49	21.7	6.82
	238.6	238.6	101.5	3.175	0.72	11.6	3.65	22.4	7.04
1A(R)	277.5	277.5	102.1	3.175	0.66	8.6	2.70	20.9	6.57
	272.0	272.0	102.1	3.175	0.65	9.2	2.89	21.4	6.73
	266.4	266.4	102.1	3.175	0.63	9.8	3.08	20.9	6.57
	260.8	260.8	102.0	3.175	0.60	10.1	3.18	19.2	6.04
	255.3	255.3	102.0	3.175	0.57	10.2	3.21	22.4	7.04
	249.7	249.7	101.9	3.175	0.52	10.8	3.40	23.1	7.26
	244.2	244.2	101.9	3.175	0.50	11.5	3.62	24.1	7.58
	238.6	238.6	101.8	3.175	0.45	11.7	3.68	25.3	7.96
2A	277.5	277.5	103.2	3.175	0.63	17.1	5.38	24.2	7.61
	272.0	272.0	103.2	3.175	0.62	18.3	5.75	23.3	7.33
	266.4	266.4	103.2	3.175	0.62	19.4	6.10	27.7	8.71
	260.8	260.8	103.2	3.175	0.55	21.2	6.67	25.2	7.92
	255.3	255.3	103.1	3.175	0.57	24.3	7.64	29.4	9.25
	249.7	249.7	103.1	3.175	0.53	25.6	8.05	33.1	10.41
	244.2	244.2	103.1	3.175	0.60	28.5	8.96	35.5	11.16
	238.6	238.6	103.0	3.175	0.54	26.5	8.33	33.1	10.41
3A	277.5	278.2	101.8	3.175	0.68	15.6	4.91	24.3	7.65
	270.4	272.0	101.8	3.175	0.64	22.4	7.05	25.0	7.86
	265.9	267.6	101.8	3.175	0.62	22.1	6.93	25.2	7.92
	261.5	261.5	101.7	3.175	0.61	23.1	7.25	26.5	8.32
	257.0	256.5	101.7	3.175	0.60	27.3	8.60	32.8	10.30
	249.7	249.7	101.7	3.175	0.59	27.6	8.68	33.6	10.60
	245.4	245.4	101.7	3.175	0.55	32.8	10.30	45.4	14.30
	239.8	237.6	101.7	3.175	0.54	39.6	12.40	75.9	23.90

Table D-9. Ground Start Test Results, Fuel Numbers 4A Through 7A.

Fuel No.	Combustor Operating Conditions					Lean Blowout		Lean Lightoff	
	T_F K	T_3 K	P_3 kPa	W_c (engine) kg/s	$\frac{\Delta P}{P}$ %	W_f (engine) g/s	f g/kg	W_f (engine) g/s	f g/kg
4A	277.5	277.0	101.1	3.175	0.68	18.3	5.75	29.9	9.40
	272.6	271.5	101.1	3.175	0.65	17.3	5.44	27.6	8.68
	266.4	266.4	101.1	3.175	0.62	19.0	5.97	29.2	9.18
	260.4	260.8	101.0	3.175	0.62	21.0	6.60	31.1	9.78
	254.8	255.3	101.0	3.175	0.60	23.3	7.33	30.5	9.59
	249.6	249.7	101.0	3.175	0.59	29.5	9.28	41.8	13.14
	244.8	244.2	101.0	3.175	0.57	28.7	9.03	33.5	10.53
	239.3	239.3	101.0	3.175	0.51	32.8	10.31	46.0	14.47
5A	277.5	277.5	101.8	3.175	0.63	15.8	4.97	23.3	7.33
	272.0	272.0	101.8	3.175	0.61	17.6	5.53	23.1	7.26
	266.4	266.4	101.8	3.175	0.60	18.3	5.75	23.3	7.33
	260.8	260.8	101.7	3.175	0.60	20.2	6.35	23.4	7.36
	255.3	255.3	101.7	3.175	0.58	20.8	6.54	24.3	7.64
	249.7	249.7	101.6	3.175	0.49	21.2	6.67	26.7	8.40
	244.2	244.2	101.6	3.175	0.59	22.4	7.04	28.4	8.93
	238.6	238.6	101.6	3.175	0.56	23.2	7.30	29.7	9.34
6A	277.5	277.5	101.4	3.175	0.62	13.7	4.31	20.9	6.57
	272.0	272.0	101.4	3.175	0.60	14.5	4.56	20.8	6.54
	266.4	266.4	101.4	3.175	0.59	14.9	4.69	22.3	7.01
	260.8	260.8	101.4	3.175	0.59	15.4	4.84	22.6	7.11
	255.3	255.3	101.4	3.175	0.58	17.4	5.47	22.8	7.17
	249.7	249.7	101.4	3.175	0.58	18.3	5.75	25.3	7.96
	244.2	244.2	101.3	3.175	0.62	20.4	6.42	26.3	8.27
	238.6	238.6	101.3	3.175	0.48	21.8	6.86	27.2	8.55
7A	277.5	279.3	101.0	3.175	0.63	20.2	6.35	26.6	8.36
	270.4	273.2	100.9	3.175	0.60	18.3	5.75	27.3	8.58
	266.4	266.4	100.9	3.175	0.58	20.9	6.57	26.7	8.40
	260.8	262.0	100.9	3.175	0.58	22.7	7.14	27.8	8.74
	254.8	254.3	100.9	3.175	0.57	25.2	7.92	29.0	9.12
	249.7	248.7	100.9	3.175	0.57	25.2	7.92	36.4	11.40
	244.8	243.7	100.8	3.175	0.54	27.7	8.71	37.0	11.60
	239.8	237.6	100.8	3.175	0.52	28.0	8.81	37.8	11.90

Table D-10. Ground Start Test Results, Fuel Numbers 8A Through 11A.

Fuel No.	Combustor Operating Conditions					Lean Blowout		Lean Lightoff	
	T_F K	T_3 K	P_3 kPa	W_c (engine) kg/s	$\frac{\Delta P}{P}$ %	W_f (engine) g/s	f g/kg	W_f (engine) g/s	f g/kg
8A	278.8	277.5	101.1	3.175	0.66	9.8	3.08	22.7	7.14
	272.6	272.6	101.1	3.175	0.65	8.1	2.55	23.6	7.42
	266.7	265.9	101.1	3.175	0.63	10.7	3.36	22.7	7.14
	260.3	261.7	101.0	3.175	0.62	10.1	3.18	22.7	7.14
	254.8	255.3	101.0	3.175	0.61	13.4	4.21	21.4	6.73
	249.7	250.0	101.0	3.175	0.57	13.9	4.37	21.5	6.76
	243.7	243.2	101.0	3.175	0.55	16.4	5.16	21.7	6.82
	238.1	237.6	100.9	3.175	0.54	17.0	5.35	22.1	6.95
9A	276.8	277.3	101.0	3.175	0.66	9.8	3.08	21.7	6.82
	271.0	272.1	101.0	3.175	0.65	8.1	2.55	21.4	6.73
	266.8	267.1	101.0	3.175	0.63	10.7	3.36	22.2	6.98
	261.2	261.2	101.0	3.175	0.61	10.1	3.18	23.7	7.45
	254.8	254.8	101.0	3.175	0.60	13.4	4.21	29.0	9.12
	249.2	248.8	100.9	3.175	0.60	13.9	4.37	27.7	8.71
	245.4	243.7	100.9	3.175	0.57	16.4	5.16	28.7	9.03
	238.4	238.4	100.9	3.175	0.55	17.0	5.35	29.4	9.25
10A	277.5	279.3	99.9	3.175	0.69	8.9	2.81	21.9	6.89
	271.5	270.9	99.9	3.175	0.67	9.2	2.89	22.8	7.17
	266.4	268.2	99.9	3.175	0.65	10.2	3.21	21.3	6.70
	261.5	262.6	99.8	3.175	0.63	11.0	3.45	23.9	7.53
	255.3	253.7	99.8	3.175	0.62	11.8	3.72	22.8	7.17
	249.7	248.7	99.8	3.175	0.59	12.2	3.84	22.3	7.01
	243.7	243.2	99.7	3.175	0.57	12.5	3.92	21.4	6.74
	237.0	237.6	99.7	3.175	0.57	12.6	3.96	22.8	7.17
11A	277.5	277.5	101.7	3.175	0.66	8.9	2.79	19.0	5.97
	272.0	272.0	101.7	3.175	0.64	9.1	2.86	20.3	6.38
	2).4	266.4	101.6	3.175	0.63	9.8	3.08	22.4	7.04
	260.8	260.8	102.8	3.175	0.61	10.1	3.18	23.7	7.45
	255.3	255.3	102.8	3.175	0.59	10.1	3.18	22.3	7.01
	249.7	249.7	102.8	3.175	0.59	12.0	3.77	23.3	7.33
	244.2	244.2	102.7	3.175	0.58	12.3	3.87	21.8	6.86
	238.6	238.6	102.7	3.175	0.54	13.1	4.12	20.8	6.54

Table D-11. Ground Start Test Results, Fuel Numbers 12A Through 13A.

Fuel No.	Combustor Operating Conditions					Lean Blowout		Lean Lightoff	
	T_F K	T_3 K	P_3 kPa	W_c (engine) kg/s	$\frac{\Delta P}{P}$ %	W_f (engine) g/s	f g/kg	W_f (engine) g/s	f g/kg
12A	277.5	277.5	101.7	3.175	0.67	9.8	3.08	19.7	6.19
	272.0	272.0	101.7	3.175	0.64	10.2	3.21	18.9	5.94
	266.4	266.4	101.6	3.175	0.63	10.2	3.21	20.3	6.38
	260.8	260.8	101.6	3.175	0.65	10.5	3.30	21.4	6.73
	255.3	255.3	101.6	3.175	0.60	11.2	3.52	21.0	6.60
	249.7	249.7	101.6	3.175	0.63	12.0	3.77	21.4	6.73
	244.2	244.2	101.5	3.175	0.57	13.1	4.12	22.4	7.04
	238.6	238.6	101.5	3.175	0.58	14.0	4.40	22.9	7.20
13A	277.5	277.5	102.5	3.175	0.73	21.3	6.70	31.0	9.75
	272.0	272.0	102.5	3.175	0.63	25.6	8.05	31.2	9.81
	266.4	266.4	102.5	3.175	0.60	27.1	8.52	31.9	10.00
	260.8	260.8	102.5	3.175	0.60	27.0	8.49	41.3	13.00
	255.3	255.3	102.5	3.175	0.61	29.4	9.25	56.8	17.90
	249.7	249.7	102.5	3.175	0.57	24.6	7.74	66.4	20.90
	244.2	244.2	102.4	3.175	0.54	25.8	8.11	59.1	18.60
	238.6	238.6	102.4	3.175	0.30	27.1	8.52	117.6	37.00

APPENDIX E

FUEL NOZZLE FOULING TEST DATA

Fuel nozzle fouling tests were conducted in a small flame tunnel rig using apparatus and procedures described in Section V-C. Primary results were periodic bench flow calibrations of the fuel nozzles to detect orifice plugging and/or flow divider valve seizure. These periodic flow calibration data, ordered by fuel type, nozzle inlet fuel temperature and accrued time are presented in Table E-1.

Table E-1. J79-17C Fuel Nozzle Fouling Test Results.

Table E-1. J79-17C Fuel Nozzle Fouling Test Results (Concluded).

Fuel Type	Fuel Temperature, K	Run Number	Fuel Nozzle S/N	Test Hours	Flow Rate g/sec at ΔP_f (MPa) 0.552	0.862	1.378	2.068	2.758	2.068	1.378	0.862	0.552	Flow Rate/Pretest Flow Rate at ΔP_f (MPa) 0.552	0.862	1.378	2.068	2.758	2.068	1.378	0.862	0.552	Ascending Flow Rate / Descending Flow Rate at ΔP_f (MPa) 0.552	0.862	1.378	2.068
13A1	469	3	180273	0	3.12	10.5	59.5	133.3	220.0	134.6	59.2	11.0	3.01	1.000	0.913	1.000	0.969	1.000	0.986	1.000	0.909	1.000	1.038	0.954	1.005	0.991
				3	3.04	11.5	59.5	137.6	212.6	136.5	58.8	12.1	2.96	0.972	1.000	0.991	1.000	0.994	1.000	0.994	1.000	0.983	1.026	0.952	1.003	1.008
				6	2.92	11.3	58.3	137.2	219.4	136.2	58.2	11.2	2.96	0.935	0.983	0.980	0.997	0.997	0.998	0.983	0.926	0.983	0.987	1.016	1.002	1.007
				9	2.11	8.87	57.6	138.3	220.0	137.1	57.0	10.2	3.04	0.946	0.771	0.963	1.004	0.997	0.998	0.962	0.863	0.979	1.035	0.972	1.011	1.009
				12	2.94	9.30	58.0	138.2	219.4	136.8	57.3	10.1	2.95	0.948	0.809	0.975	1.005	0.997	1.002	0.965	0.835	0.975	1.004	0.925	1.012	1.010
				18	2.89	8.10	58.2	139.3	215.1	135.6	55.9	8.74	2.80	0.923	0.704	0.978	1.004	0.978	1.002	0.945	0.722	0.929	1.032	0.923	1.012	1.025
				24	2.82	7.50	56.3	139.0	210.4	136.8	55.4	7.80	2.80	0.903	0.652	0.936	1.010	0.956	1.002	0.934	0.645	0.929	1.009	0.961	1.016	1.016
				30	2.91	7.50	55.7	138.3	208.2	137.6	55.3	7.42	2.76	0.931	0.652	0.936	1.012	0.944	1.008	0.934	0.613	0.916	1.055	1.010	1.007	1.013
				36	2.80	3.36	50.0	138.1	204.9	136.8	59.9	11.5	2.75	0.895	0.292	0.840	1.004	0.931	1.004	0.934	0.950	0.412	1.018	0.293	0.835	0.987
				42	2.66	6.62	58.8	139.6	200.0	139.9	59.2	7.48	2.81	0.850	0.576	0.988	1.015	0.909	1.023	0.988	0.618	0.933	0.944	0.879	0.993	1.006
				48	2.62	4.62	57.1	138.3	193.7	134.5	59.1	6.50	2.99	0.839	0.402	0.960	1.063	0.880	1.000	0.998	0.537	0.958	0.904	0.711	0.944	1.014
				54	5.46	8.42	65.3	140.6	194.4	138.6	64.8	8.42	5.20	1.748	0.732	1.097	1.022	0.883	1.015	1.094	0.696	1.728	1.050	1.000	1.008	1.014
13A2	478	6	180272	0	3.24	12.8	58.0	135.7	213.2	137.0	58.3	12.8	3.12	1.000	1.000	1.000	1.000	1.000	1.000	1.000	1.000	1.000	1.034	1.001	0.994	0.996
				6	3.14	11.1	57.3	137.5	213.8	136.7	58.1	12.5	3.02	0.969	0.865	0.988	1.013	1.003	0.950	0.989	0.972	0.968	1.038	0.891	0.987	1.007
				12	3.16	10.1	56.6	145.6	217.5	144.6	57.2	11.0	3.09	0.977	0.784	0.976	1.013	1.020	1.051	0.855	0.855	0.988	1.024	0.917	0.999	1.007
				19	2.95	8.47	58.0	144.8	215.0	144.5	57.2	9.77	3.04	0.911	0.640	1.000	1.083	1.008	1.065	0.982	0.762	0.972	0.971	0.867	1.013	1.002
				26	2.90	6.30	55.6	146.3	206.1	165.8	57.3	8.40	3.06	0.895	0.491	0.959	1.097	0.967	1.040	0.983	0.654	0.990	0.967	0.750	1.017	0.996
				33	2.82	3.58	55.1	165.2	201.2	165.8	57.8	6.65	3.04	0.872	0.279	0.950	1.070	0.944	1.060	0.991	0.519	0.972	0.929	0.538	0.952	0.996
				40	2.77	3.40	55.7	162.4	193.3	143.0	58.5	5.44	2.97	0.856	0.265	0.961	1.049	0.908	1.039	1.002	0.426	0.952	0.932	0.626	0.953	0.996
13A2	491	4	180271	0	3.10	11.8	55.1	133.3	211.3	133.3	55.1	12.0	3.07	1.000	1.000	1.000	0.984	0.980	0.976	0.963	1.000	1.000	1.008	0.991	1.000	1.000
				3	3.21	7.65	47.5	135.5	215.6	134.6	57.2	11.8	3.04	1.035	0.649	0.862	1.000	1.000	1.000	1.000	0.988	0.988	1.058	0.650	0.830	0.992
				6	3.05	6.38	48.1	135.8	215.4	135.8	56.2	10.3	2.94	0.984	0.697	0.874	1.002	0.999	0.941	0.983	0.882	0.955	1.039	0.783	0.837	1.000
				12	2.86	6.12	51.7	140.4	215.4	138.7	55.3	6.78	2.95	0.923	0.538	0.938	1.034	1.000	1.015	0.967	0.734	0.959	0.970	0.227	0.934	1.012
				18	2.82	6.12	53.0	141.1	206.8	160.5	52.9	8.07	2.99	0.910	0.217	0.943	1.041	0.930	1.029	0.923	0.509	0.971	0.945	1.008	1.002	1.004
				24	2.56	3.21	35.4	161.2	202.1	162.5	54.3	5.16	2.86	0.825	0.271	0.843	1.042	0.937	1.043	0.949	0.429	0.930	0.894	0.125	0.652	0.996
				30	2.55	3.11	48.1	139.2	196.3	139.6	52.9	4.57	2.64	0.821	0.263	0.876	1.027	0.910	1.022	0.925	0.383	0.922	0.897	0.680	0.910	0.997

174

APPENDIX F

SMOKE DATA CALCULATION

In this program, combustor component rig tests were conducted in which smoke emission levels were measured at the combustor exit plane by the method specified in Reference 6. The result is a Smoke Number (SN) which expresses the opacity of filter paper that has been stained by the exhaust gases. SN is therefore, not a true thermodynamic property of the exhaust gas. A relationship between SN and carbon weight fraction (X_c), which is a thermodynamic property, is presented in Reference 16. This relationship is reproduced in Figure F-1.

When combustor exhaust gases are diluted by turbine cooling air as they are in the J79 engine, both SN and Xc are reduced. Smoke emission index (EI_s) g carbon/kg fuel, however, remains constant. EI_s is calculated by the relationship:

$$EI_s = (x_{ci}) \left(\frac{1000 + f_i}{f_i} \right) (10^{-3})$$

where:

i = engine station where sample is taken

f = fuel/air weight ratio (g fuel/kg air)

Therefore, engine smoke level, which would be measured at engine Plane 8, can be calculated from combustor rig measurements, taken at simulated engine Plane 4, by the following procedure:

1. Measured (SN_4) and (f_4) at simulated engine test conditions

2. $SN_4 \rightarrow (X_{c4})$ (from Figure F-1)

3. $EI_s = (X_{c4}) \left(\frac{1000 + f_4}{f_4} \right) (10^{-3})$

4. Cycle data $\rightarrow f_8$ at simulated engine test condition

5. $X_{c8} = EI_s \left(\frac{f_8}{1000 + f_8} \right) (10^{-3})$

6. $X_{c8} \rightarrow SN_8$ (from Figure F-1)

For the J79-17C engine, f8/f4 = 0.838 at non-afterburning operating conditions. In the test data summary, SN_4, X_{c8}, EI_s, and SN_8 are all tabulted in Tables B-1 and B-2 for possible future use.
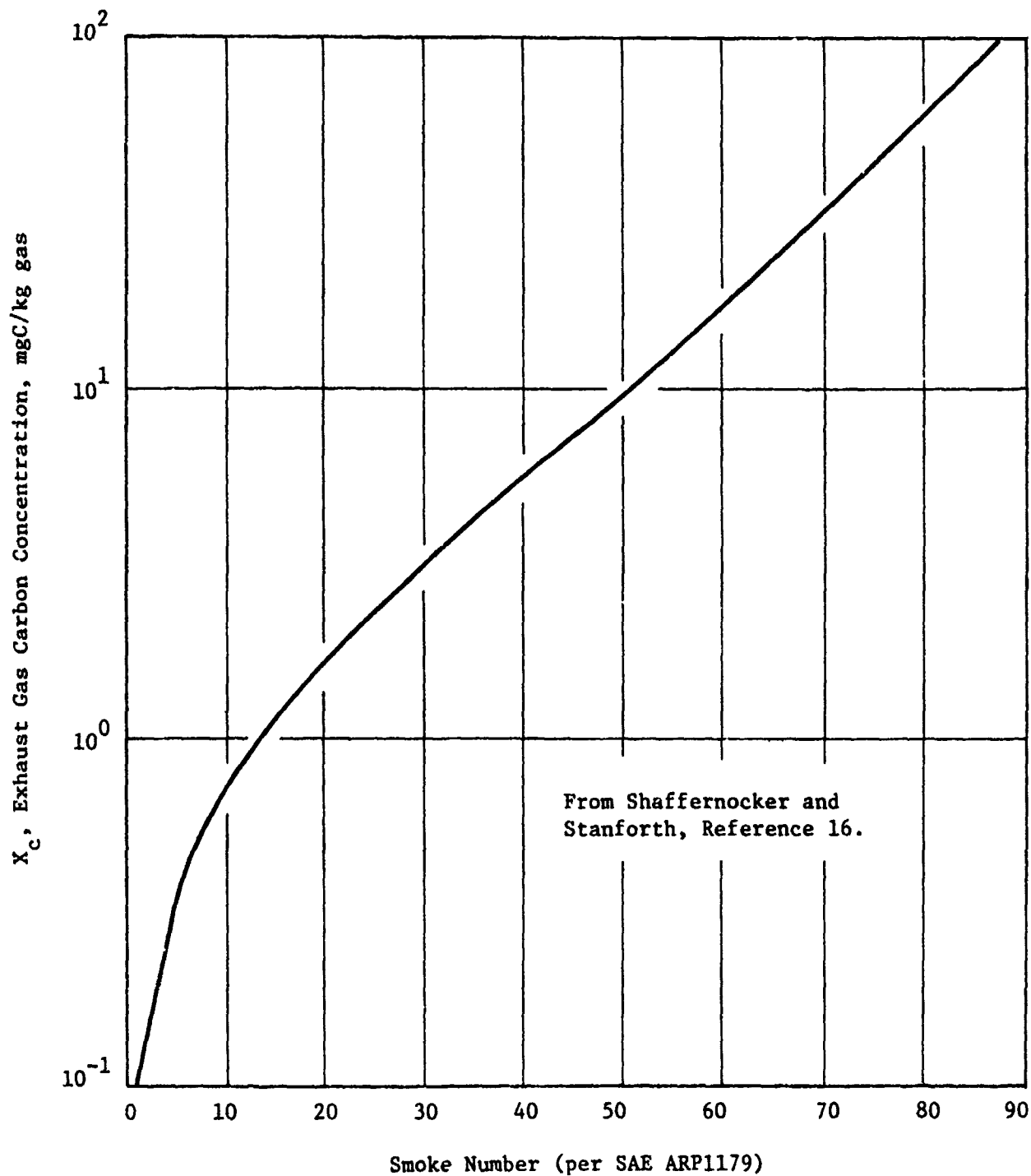
Figure F-1. Experimental Relationship Between Smoke Number and Exhaust Gas Carbon Concentration.

REFERENCES

1. Gleason, C.C., et al, "Evaluation of Fuel Character Effects on J79 Engine Combustion System," AFAPL-TR-79-2015, GE79AEG321, June 1979.

2. Gleason, C.C., et al, "Evaluation of Fuel Character Effects on F101 Engine Combustion System," AFAPL-TR-79-2018, GE79AEG405, June 1979.

3. Verdouw, A.J., "Fuel Character Effects on the Stoichiometric Combustor," AFAPL-TR-78-12, DDA EDR9356, October 1978, Confidential.

4. Jackson, T.A., "Fuel Character Effects on the J79 and F101 Engine Combustion Systems," NASA Symposium on Aircraft Research and Technology for Future Fuels, Cleveland, Ohio, April 16-17, 1980, Paper No. 12, CP2146, July 1980.

5. Longwell, J.P., Ed., "Jet Aircraft Hydrocarbon Fuels Technology," NASA CP-2033, January 1978.

6. "Aircraft Gas Turbine Engine Exhaust Smoke Measurement," Aerospace Recommended Practice 1179, SAE, 1970.

7. "Procedure for the Continuous Sampling and Measurement of Gaseous Emissions from Aircraft Turbine Engines," Aerospace Recommended Practice 1256, SAE, 1971.

8. Covey, M.W., "Final Report on Phase II of the Model J79-GE-10 Smoke Reduction/Improved Life Engine Flight Evaluation," NATC SA-44R-79, August 1979.

9. Gleason, C.C., and Bahr, D.W., "Experimental Clean Combustor Program Alternate Fuels Addendum, Phase II Final Report," NASA CR-134972, January 1976.

10. Moses, C.A., and Naegeli, D.W., "Effects of High Availability Fuels on Combustor Properties," AFAPL-101, January 1978.

11. Blazowski, W.S., and Jackson, T.A., "Evaluation of Future Jet Fuel Combustion Characteristics," AFAPL-TR-77-93, July 1978.

12. "Aircraft Engine Emissions Catalog," Naval Environmental Protection Support Service Report No. AESO101-Revision 4, July 1975.

13. Topicz, A., "Low Smoke Long Life Combustion System," General Electric Engineering Change Proposal No. 79U190, August 1974.

14. Colley, W.D., et al, "Development of Emissions Measurement Technique for Afterburning Turbine Engines: Supplement 2 - Afterburner Plume Computer Program User's Manual," AFAPL-TR-75-52, Supplement 2, October 1975.

15. El-Shanawany, M.S., and Lefebvre, A.H., "Airblast Atomization: The Effect of Linear Scale on Mean Droplet Size," ASME paper No. 80-GT-74, March 1980.

16. Shaffernocker, W.M., and Stanforth, C.M., "Smoke Measurement Techniques," SAE Paper No. 680346, April 1968.